Experimental Study of Soil Anisotropy Using Hollow Cylinder Testing

By

Lintao Yang

M.Sc., B.Eng.

Thesis submitted to the University of Nottingham for the degree of Doctor of Philosophy

September 2013

The University of Nottingham

UNITED KINGDOM · CHINA · MALAYSIA

DECLARATION OF ORIGINALITY

Title of Thesis: *Experimental Study of Soil Anisotropy Using Hollow Cylinder Testing*

I declare that the thesis hereby submitted for the degree of Doctor of Philosophy at the University of Nottingham is my own work except as cited in the references and has not been previously submitted for any degree.

Name : LINTAO YANG

Signature : 

Date : 10/09/2013

Abstract

Most sedimentary deposits are inherently anisotropic due to their natural deposition in horizontal layers. This inherent anisotropy highlights the fact that the response of soils to loading is depending on both stress magnitude and its direction. Most of the field problems in geotechnical engineering are three-dimensional, and a soil is more likely to subject an anisotropic stress state ($\sigma_1 \neq \sigma_2 \neq \sigma_3$), together with rotation of the principal axes. It is therefore essential that the soil behaviour under such realistic and general loading conditions is to be well understood, so that engineers can devise appropriate geotechnical design and analysis in practical situations.

The Small-Strain Hollow Cylinder Apparatus (SS-HCA), developed by GDS Instruments Ltd. has been used to study drained anisotropic behaviour of sand under generalized stress conditions. In particular, the anisotropic stress-strain-strength characteristics, volume change behaviour, non-coaxiality and combined effects of α and b are studied. Three testing programs composed of two main types of stress paths (e.g. monotonic loading with different inclinations of the major principal stress and cyclic rotation of principal stress axes) were conducted.

Inherently anisotropic behaviour of sands is clearly illustrated by deformation response that is strongly dependent on the loading direction in the monotonic shear tests. For a given loading direction, the mechanical response of sands is affected by the material density, the particle properties and the loading history. Non-coincidence of principal directions of stress and strain increment is observed and shear band inclinations in hollow cylindrical specimens follow the theoretical predictions. Results

also clearly show the effects of intermediate principal stress on the deformation response of sand. This is seen in variation of stress-strain response and peak friction angle with differing *b*-values.

A significant plastic deformation is induced during rotational shear despite the magnitudes of principal stresses remaining constant. Volumetric strain during rotational shear is mainly contractive and the amount of the volumetric strain increases with the increase in the stress ratio. Most of the contractive volumetric strain occurred during the first 20 cycles and its accumulation rate tended to decrease as the number of cycles increases. When principal stress rotation continues, the sand samples appear to be stabilized and the strain trajectory in the deviatoric plane approaches an ellipse. The test results also demonstrate that the mechanical behaviour of sand under rotational shear is generally non-coaxial, and the stress ratio has a significant effect on the non-coaxiality. The larger the stress ratio, the lower degree of non-coaxiality is induced. It was also observed that parameter *b* is not a negligible factor for the sand deformation during rotational shear, but has significant impact. The larger the *b*-value, the more the volumetric strain is accumulated.

Acknowledgements

I wish to thank, first and foremost, my supervisor Professor Hai-Sui Yu, for his supervision, guidance and financial support throughout this research. Moreover, his profound knowledge, persistent pursuit and continuing curiosity of geotechnical engineering have been and always will be a great inspiration to me.

I would like to express my hearty gratitude to my co-supervisor, Dr. Dariusz Wanatowski, for providing me meticulous guidance, essential support and valuable suggestions at every phase of this project. This thesis would not have been possible without his constant assistance and endless patience. Special and sincere thanks are also due to Dr. Xia Li, for sparking my interest and sharing with me her findings and experiences in this research topic. Her continuous presence has been precious throughout this project.

Sincere thanks are extended to all the technicians in the School of Civil Engineering for their assistance and help with experimentation, in particular, Ian Richardson, Michael Langford and Andrew Maddison. I would also like to thank Dr. Yanyan Cai, Dr. Amanullah Marri and Dr. Salah Ud-Din for their kind help in the HCA test at the beginning of this research.

I would like to thank all my friends in the Nottingham Centre for Geomechanics (NCG) for making this place so special and wonderful. Working at NCG will no doubly be one of the most thoughtful and rewarding experiences in my life.

Last but by no means least, I would like to extend my deepest gratitude to my parents and my brother. Your dedication, care, encouragement and support have always been

a great inspiration for me to endure these tough years. I firmly believe that your endless love will drive me to continue moving forward in the challenging future.

Contents

Chapter 1 Introduction

1.1 Background

It is well known that natural soils are often deposited in horizontal layers and then subjected to anisotropic stress leading to preferred orientation of the particles. As a consequence, most natural soil deposits possess an inherently anisotropic structure which causes variation in deformation-strength characteristics as the loading direction changes. The awareness of soil anisotropy, and of its relevance to geotechnical engineering, is a consequence of considerable research effort made earlier in the laboratory and the field analysis. Among many others, the classical studies by Arthur and his co-workers (e.g. Arthur and Menzies, 1972, Arthur and Phillips, 1975, Arthur et al., 1977 and 1980) and the microscopic observation by Oda (1972a and 1972b) on sand fabric are often quoted as the beginning of the continuous and intensive laboratory investigation of soil anisotropy worldwide, which had been rather sporadic before the early 1970s.

Extensive experimental studies on the mechanical behaviour of soils have been made as a response to the increasing awareness of significance of soil anisotropy in many aspects of geotechnical problems. For example, the effects of anisotropy on the stress-strain behaviour of soils (e.g. Surachat 1977; Tatsuoka, 1980; Donald 1985; Kurukulasuriya et al. 1999; Reinaldo 2003; Yin and Kumruzzaman 2008); the influence of anisotropy on failure characteristics of granular soils (e.g. Yamada and Ishihara 1979; Matsuoka and Ishizaki 1981; Ochiai and Lade 1983; Kirkgard and Lade 1993); deformation-strength characteristics of anisotropic sand during the

rotation of principal stress axes (e.g. Arthur et al.1980; Ishihara and Towhata, 1983; Symes et al. 1983 and 1984; Gutierrez et al. 1991; Menkiti 1995; Albert et al. 2003).

Micromechanics-based approaches based on discrete element method (DEM) have also evolved, as an important role to gain fundamental understanding of the internal fabric that is directly responsible for the anisotropic stress-strain behaviour observed in the laboratory. For example, Cundall et al. (1982) and Rothenburg and Bathurst (1989) have applied the DEM to study the evolution of material fabric and its relationship with the stress-strain behaviour of granular assembly under biaxial loading conditions. Cambou et al. (1995) analysed anisotropic elastic behaviour of granular materials with the integration of statistic homogenization process, DEM and contact dynamics method. Li and Yu (2009) investigated the effect of material anisotropy produced during sample preparation and the influence of loading direction on the behaviour of granular materials with the application of DEM.

The findings from both laboratory and numerical studies have been crystallized as anisotropic soil constitutive models and fed-back into analysis. Their application to real problems not only accurately reproduced observed phenomena, but also led to a more profound understanding of anisotropic ground responses. In conclusion, the mechanical properties of granular geomaterials are potentially influenced by their anisotropic behaviour. Incorporating soil anisotropy into geotechnical characterization, analysis and design is one of the most important steps forward for geotechnical engineering.

1.2 Aims and objectives of the research

Lack of knowledge and understanding regarding anisotropic behaviour of sand under generalized stress space led to the evolution of the main theme of this research. The aim of this study is to experimentally investigate the anisotropic behaviour of granular soil subjected to general stress states using Hollow Cylinder Apparatus. As such, comprehensive investigation on the drained behaviour of sand under monotonic shear with different inclinations of the major principal stress axis and rotational shear with continuous rotation of principal stress axes is carried out. A better understanding of the soil anisotropy and its effects on the stress-strain behaviour, failure characteristics and non-coaxiality of granular geomaterials is obtained as a result of this research.

To achieve this aim, the following objectives were pursued:

- To carry out a few series of tests in the Hollow Cylinder Apparatus with various stress paths. This is to generate a basic understanding of the stress-strain behaviour of related materials and it also allows the evaluation of the reliability and repeatability of the test results.

- To quantify the mechanical behaviour of sand in drained monotonic shear with different inclinations of the major principal stress to the vertical axis. A systematic investigation of the effects of particle shape, material density and preshearing on the stress-strain and volume change behaviour, failure characteristics and noncoaxiality of sands was undertaken.

- To investigate the anisotropic behaviour of saturated sand in drained rotational shear. In the tests, samples were subjected to cyclic rotation of principal stress axes while the magnitudes of principal stresses were maintained constant. A

special attention in the investigation was placed on the stress-strain behaviour, deformation characteristics and noncoaxiality of sand tested at different effective stress ratios. Meanwhile, the effects of particle shape and material density has also been investigated.

- To investigate the influence of the relative magnitude of the intermediate principal stress, characterized by the different *b*-values, on the mechanical response of saturated sand in both monotonic and rotational shear under drained conditions. In the tests, specimens were subjected to a series of stress states with various values of the intermediate principal stress in order to assess its anisotropic properties in a more general stress space.

1.3 Outline of the Thesis

The thesis consists of seven chapters. Following this introductory section (**Chapter 1**) **Chapter 2** describes a general review on the anisotropic behaviour of granular soils, including the definition of the soil anisotropy as well as the conceptual and experimental evidences in support of anisotropic nature of granular soils. Non-coaxiality as an important aspect of anisotropy of granular soils is also involved. Important findings and conclusions from previous investigations related to the objectives of this thesis are then critically reviewed. This chapter also presents a brief introduction to the currently available stress path testing devices, emphasizing their capabilities and limitations. This is intended to put the Hollow Cylinder Apparatus in a proper perspective in its potential as a general stress path testing device.

Chapter 3 introduces the basic principles of the testing system (GDS 10kN/200Nm Small-Strain Hollow Cylinder Apparatus), this including the details of the

instrumentation used for the generation and measurement of loads, pressures, stresses and strains, as well as the software system for data acquisition and test control. It also describes the physical properties of the materials used for this research. The sample preparation techniques adopted and the testing procedures are also outlined. The chapter finally presents the validation on the repeatability and reproducibility of the test results.

Chapter 4 describes the results of drained monotonic shear tests. The effects of particle shape, material density and preshearing on the stress-strain and volume change behaviour, failure characteristics and noncoaxiality of saturated sands under monotonic shear with different inclinations of the major principal stress axis are discussed in a systematic manner. Observations on the shear banding are also presented.

Chapter 5 focuses on the results of the drained rotational shear tests. The variation of the strain components, development of volumetric strain, shear stress-strain relationship, evolution of strain paths and noncoaxiality of saturated sands subjected to rotational shear at different stress ratios is described in detail. The investigation of the effects of particle shape and material density on soil response in drained rotational shear is also presented.

Chapter 6 includes a presentation and discussion of the results obtained from the monotonic and rotational shear tests with different *b*-values. The influence of the intermediate principal stress parameter *b* on the mechanical response of granular soils under the two particular general stress states has been discussed in detail in this chapter.

Chapter 7 summarizes the relevant conclusions presented in previous chapters. Limitations of this research and suggestions for future studies are also listed in this chapter.

Chapter 2 Literature Review

2.1 Introduction

This literature review first gives an introduction to the anisotropic behaviour of granular soils, including the definition of two types of anisotropy (i.e., inherent anisotropy and induced anisotropy) as well as the conceptual and experimental evidences in support of anisotropic nature of granular soils. Non-coaxiality as an important aspect of anisotropy of granular soils is also involved.

Following above introduction this chapter summarises previous investigations into the effects of principal stress direction, the intermediate principal stress and rotational shear on soil response. Areas of research which have not yet addressed are pointed out.

Finally the chapter reviews the common devices that are used for investigating the effects of soil anisotropy. A fundamental principle of stress and strain calculations for Hollow Cylinder Apparatus is explained in detail, followed by a section regarding the stress non-uniformities in hollow cylinder specimens. A brief description of membrane penetration errors is also included.

2.2 Anisotropic Soil Behaviour

2.2.1 Introduction

The term soil anisotropy refers to any directional-dependence in mechanic properties such as dialtancy, strength and stiffness of soil mass. It is believed that the micro-

structure characteristics of soils, including their particle shapes, sizes, arrangements, void distributions and the nature contact between the particles is the ultimate cause of soil anisotropy. However the environmental and geological conditions during the deposition of the soils are the external conditions constituting the natural anisotropy of soils (Zhang et al. 2003). Because the particles of soil sediments experienced gravitational force, the resulted particle contacts are directionally dependent and the fabric of the soil may later be disturbed with application of loads. Casagrande and Carrillo (1944) first pointed out the importance of anisotropy in soil mechanics, and distinguished two types of anisotropy, i.e., the inherent anisotropy and the induced anisotropy. The impact of anisotropy on the mechanical behaviour of granular geometerials always remains a subject of great interest and it goes throughout the entire developmental process of soil mechanics.

2.2.2 Inherent anisotropy

Inherent anisotropy was defined by Casagrande and Carrillo (1944) as ‘a physical characteristic inherent in the material and entirely independent of the applied stresses and strains’. It is attributed to the initial spatial arrangement of particles, voids, and associated contacts. This is generally initiated during the deposition process so that the soil particles may move under gravity to adopt a stable structure by preferred directions of particle orientation and contacts normal. Such initially-generated inherent anisotropy in the soil structure eventually affects engineering properties of the granular soils, such as shear strength and deformational characteristics. Therefore the study of inherent anisotropy has been one of research hotspots in soil mechanics for the last few decades.

Extensive experimental and numerical investigations have been carried out to understand the inherently anisotropic nature of granular geometerials since Darwin (1918) first implied that laboratory prepared samples of poured sand were layered normal to the direction of deposition. More recently, the geometrical anisotropy of grain orientation has been studied by Parkin et al. (1968). They impregnated the triaxial sand samples with resin after hydrostatic compression tests and by using photographic enlargements they found that the long axes of the grains tended to be aligned in the horizontal plane and was symmetrically disposed about the vertical axis. Similar observations have also been reported from 2D DEM simulations by Hosseininia (2012) who tested irregular convex-polygonal particles under biaxial compression and found that the long axes of particles tended to be inclined perpendicular to the loading axis, which results in generating more stable column-like microstructures in order to transfer the applied load.

However, inherent anisotropy does not only present in assembly of irregular shaped particles but also in spherical particles. Kallstenius and Bergau (1961) investigated the fabric of assemblies of glass spheres which were allowed to fall freely under action of gravity through air. They showed that the number of grains in contact with vertical area is different from the number of grains in contact with horizontal area. That means even spherical grains may develop an anisotropic structure in their particle contacts. This observation is further supported by the work of Oda (1981) who carried out plane strain tests on uniform-anisotropic, uniform-pseudo isotropic, layered-anisotropic, and layered-pseudo isotropic samples and found that the anisotropic strength response, caused by the anisotropic distribution of contact normal should be expected even in a uniform mass of spheres. Furthermore, Oda and Iwashita (1999)

recognized that there exist two forms of inherent anisotropy from the micro-fabric point of view:

a) By preferred orientation of non-spherical particles

b) By preferred orientation of unit vectors normal to contact surfaces

The evidence of the two forms of inherent anisotropy has been widely documented in the literature. Yang et al. (2008) examined the inherent fabrics of Toyoura sand specimen prepared using dry deposition method. After sample preparation, a modified traditional triaxial cell was used to forcing epoxy resin into the soil specimen under a low differential pressure. The hardened specimen was then cut into small patches along different locations of vertical section for image analysis by scanning electron microscope (SEM). The angles of the long axes of the grains with respect to the bedding plane in the rose diagram representations are shown in Figure 2-1. It is clear that the preferential particle orientation for the specimen is in the horizontal direction.

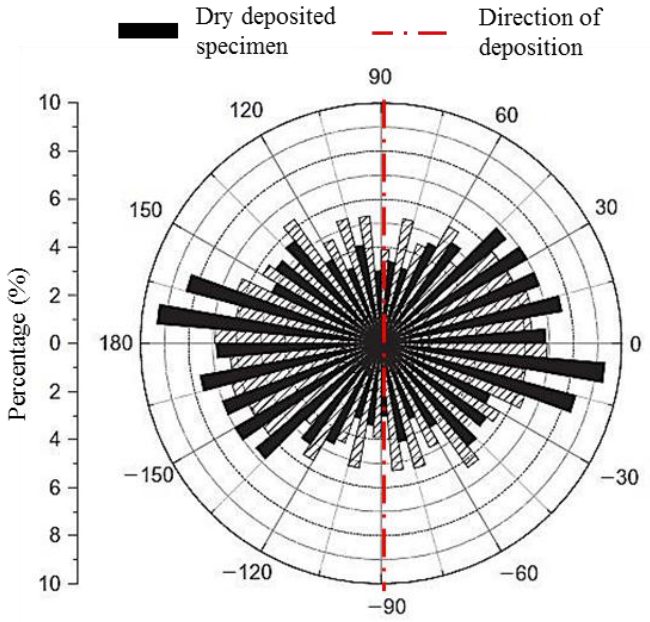

Figure 2-1: Characterization of inherent fabric anisotropy of Toyoura sand with preferred particle orientations for vertical sections (Yang et al. 2008).

Li and Yu (2009) carried out a 2D DEM simulation to investigate the anisotropic distribution of normal contact force produced during sample preparation. The particle was formed by clumping two equal-sized disks together and the specimen was prepared using a deposition method which is similar to that generated using the dry deposition method in laboratory. Figure 2-2 shows the result of directional distribution of normal contact force from their simulation. In the figure a_c characterizes the degree of anisotropy and $a_c/2\pi$ denotes the density of contact normal. As a clear evidence of the anisotropic structure produced during particle deposition we can see that the major principal direction of contact normal was coincident with the direction of deposition.

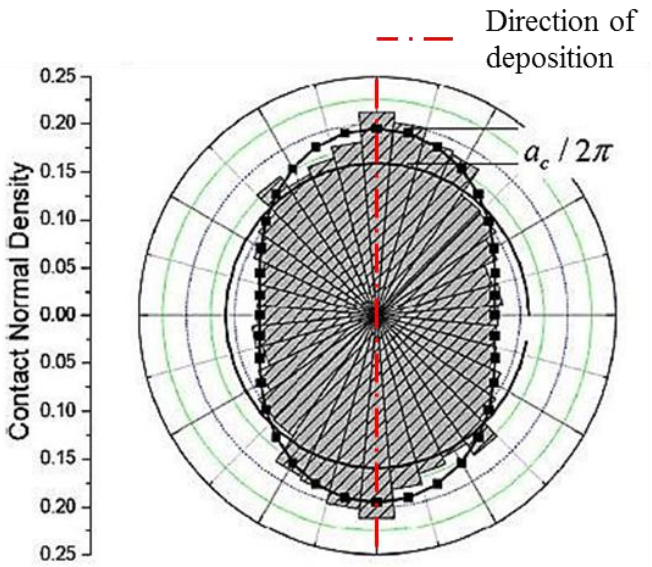

Figure 2-2: Directional distribution of contact normal (Li and Yu 2009).

The differences in the inherent anisotropic conditions of the samples either by preferred orientation of particles or contact normal could certainly affect the mechanical behaviour of soil mass. Studying the mechanical behaviour of inherently anisotropic granular soils has been the subject of many laboratory researches.

Different test methods including direct shear tests (Phillips and May 1967; Oda and Konishi 1974), true triaxial tests (Arthur and Menzies 1972; Yamada and Ishihara 1979; Miura and Toki 1984), conventional triaxial tests (Oda 1972a), hollow cylinder tests (Hight et al. 1983; Symes et al. 1984; Miura et al. 1986; Gutierrez et al. 1991; Lade et al. 2008) have been used to investigate characteristics of inherently anisotropic sand fabrics. Apart from the efforts made in laboratory researches, numerical studies based on discrete element method (DEM) have also been carried out (Li and Yu 2009; Sazzad and Suzuki 2010; Mahmood and Iwashita 2010; Hosseininia 2012). The outcome of all these tests indicates that shear strength and deformability of granular soils is highly dependent on the initial fabric condition of the soil mass. In other words, the stress-strain behaviour of such soils significantly varies with the direction of applied loading or stresses with respect to the bedding plane.

The state of stress for a three-dimensional point can be defined by the stress tensor:

$$\sigma_{ij} = \begin{bmatrix} \sigma_{xx} & \sigma_{xy} & \sigma_{xz} \\ \sigma_{yx} & \sigma_{yy} & \sigma_{yz} \\ \sigma_{zx} & \sigma_{zy} & \sigma_{zz} \end{bmatrix} \tag{2-1}$$

The stress tensor in terms of the principal stresses takes the form:

$$\sigma_{ij} = \begin{bmatrix} \sigma_1 & 0 & 0 \\ 0 & \sigma_2 & 0 \\ 0 & 0 & \sigma_3 \end{bmatrix} \tag{2-2}$$

In order to know the full stress states, the angles that define their directions (α, β and γ) are needed (Figure 2-3).

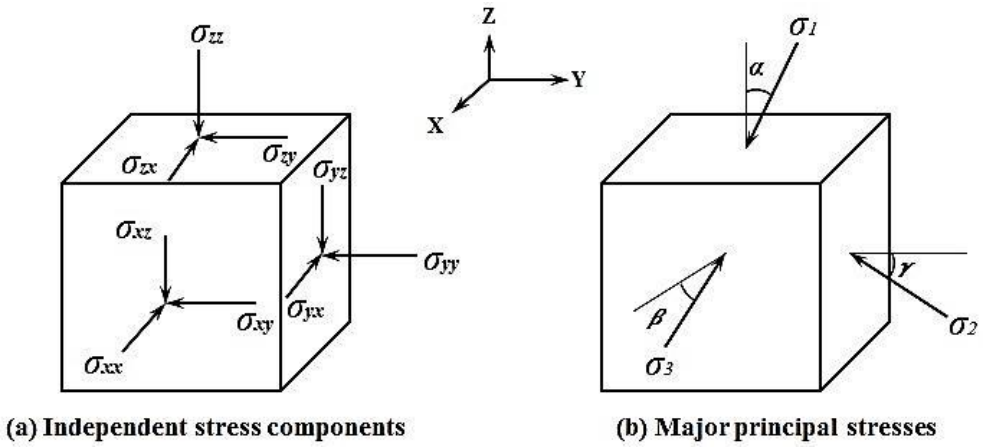

Figure 2-3: Stress components acting on a soil element.

A representative example can be seen from the laboratory study carried out by Nakata et al. (1997) who tested carbonate sand under fixed principal stress directions using hollow cylinder torsional shear apparatus. Samples were prepared using water sedimentation method and the initial conditions are the same for all the samples. The failure point corresponding to the peak shear stress obtained in each test is plotted in the *X*-*Y* stress space (where $X = \sigma_{z\theta}$ and $Y = (\sigma_z - \sigma_\theta)/2$) in Figure 2-4. In the plane, a vector from the origin has a length proportional to the shear stress $\tau = X^2 + Y^2 = \sqrt{(\sigma_Z - \sigma_\theta)/4 + \sigma_{Z\theta}{}^2}$ and makes an angle of $2\alpha_\sigma$, which is twice the angle of the major principal stress σ_1 makes with the vertical axis (Gutierrez et al. 1991). The effect of the direction of loading on the strength of the sand is clearly manifested in this figure. The failure points are not equidistant from the origin of the stress space and as can be seen, the sand samples fail at lower values of shear stress when the direction of major principal stress deviates from the deposition direction.

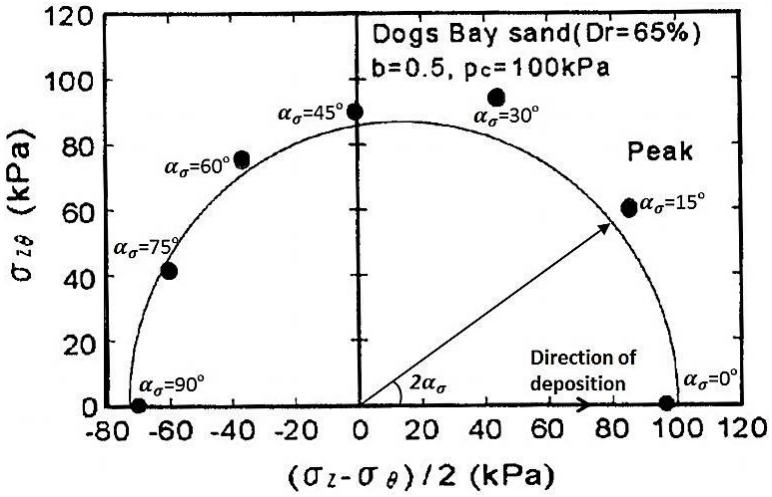

Figure 2-4: Failure envelop in *X*-*Y* stress space (Nakata et al. 1997).

However, extreme stress changes that cause particle sliding, mixing or crushing could disturb and breaking the nature of contact normals and the microstructure of the soil mass. According to Oda et al. (1985), after peak stress was reached, the contacts between the particles and structure of the voids could radically change which would destroy the inherent anisotropy. More recently, Sadrekarimi and Olson (2012) similarly showed that the inherent anisotropy do not affect the critical states at which particle rearrangement is complete and the initial sand fabric would completely erased as the sand sample approaches the critical state.

2.2.3 Induced anisotropy

After sedimentation the particles may move under load to form a stable structure in relation to the forces acting upon them, developing an induced anisotropy. It was defined as a 'physical characteristic due exclusively to the strain associated with an applied stress' (Casagrande and Carrillo 1944). Regardless of the initial particle and contact arrangement, induced anisotropy is directly related to the directional redistribution of particles and interparticle contacts during shearing and plastic

deformation. It can develop in an originally isotropic material or change any pre-existing condition of the internal microstructural. This systematic alteration is responsible for the anisotropic stress-strain-strength response of the soil mass (Reinaldo 2003).

Based on laboratory testing, various investigators (Arthur1972; Arthur et al. 1977; Oda 1972a; Oda et al. 1985; Wong and Arthur 1985; Wong 2003) reported that initially isotropic or anisotropic granular materials exhibit stress-induced anisotropy during loading, unloading, and reloading. Using the Directional Shear Cell (DSC), Wong and Arthur (1985) investigated the effect of induced anisotropy on the mechanical response of dense Leighton Buzzard sand. A separation of the effects of inherent and induced anisotropy was achieved by pouring the sand in the direction normal to the plane of strain (Figure 2-5). They experimentally proved that there is no directional dependence of mechanical properties on this plane. As a result, we can characterize this plane as an 'initially isotropic plane'.

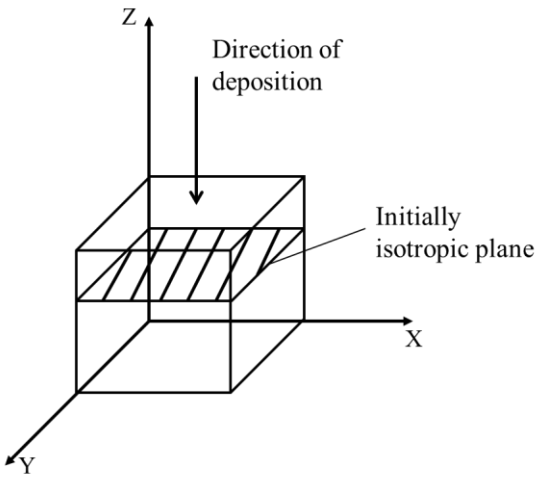

Figure 2-5: Explanation of initially isotropy plane (Wong and Arthur 1985).

Samples were made in this way and then sheared under drained conditions in the initially isotropic plane to explore how anisotropy could be induced. After an

isotropic consolidation, samples were subjected to a two-stage loading scheme (i.e. stress path A precedes stress path B), as shown in Figure 2-5. In stage A all the four samples were loaded to a predetermined effective stress ratio σ_1' / σ_3' and then unloaded back to isotropic stress state with $\sigma_1' / \sigma_3' = 1$. During stage B the samples were reloaded with the major principal stress rotated to a direction $\Delta\psi$ different to that of stage A. Figure 2-6 and 2-7 show the stress-strain relationship and dilatancy from these tests, the soil response depended strongly on the loading direction. With the reloading direction deviates from the preloading direction, the samples tended contract more and response less stiff, nevertheless, the effective stress ratios at failure remained approximately constant. These results clearly demonstrate that the effects of induced anisotropy are quite pronounced on the subsequent mechanical response of granular soils. By comparing the results of the tests on initially isotropic plane and inherently anisotropic plane, Wong and Arthur further found that the magnitude of the induced anisotropy could be even larger than the magnitude of inherent anisotropy. Hence the effect of induced anisotropy on the mechanical behaviour of granular soils cannot be simply ignored.

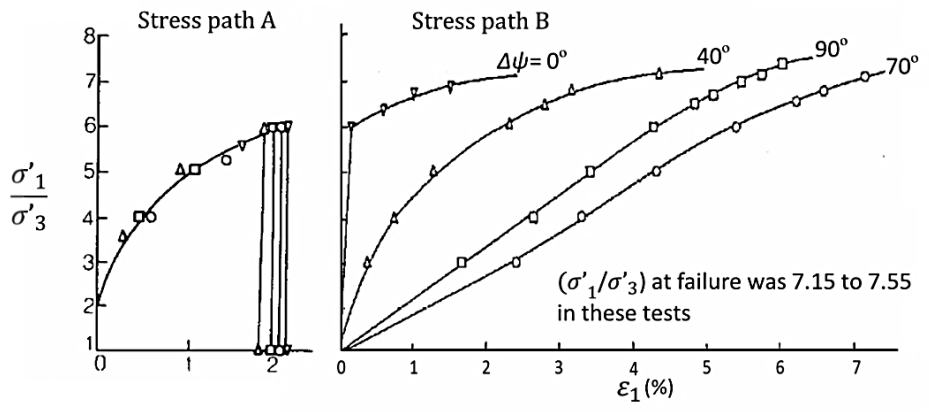

Figure 2-6: Characterization stress-strain response of stress path A-B on initially isotropic samples (Wong and Arthur, 1985).

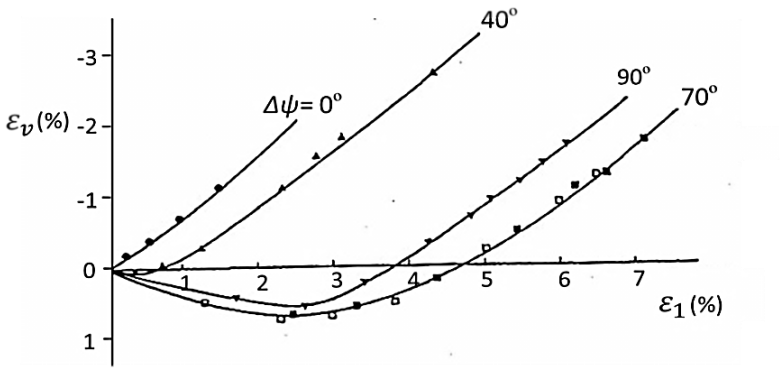

Figure 2-7: Characterization of volumetric strains of stress path B (Wong and Arthur, 1985).

From microscopic view, Oda (1972b) suggested that the soil fabric continuously changes during the shearing process and further anisotropy was induced in the soil structure to resist the loads applied. He mentioned that the particle contact normals tend to align themselves parallel to the direction of the major principal stress while the contact normals in the perpendicular direction are reduced. In fact it is this very redistribution of contacts that leads to induced anisotropy and determines the subsequent stress-strain behaviour. The observations from the 2D DEM simulations carried out by Li and Yu (2009) further supported Oda's studies. In the simulation, as mentioned in section 2.2.2, the initially anisotropic sample was prepared using a deposition method and the pre-loaded sample was obtained by shearing the initially anisotropic specimen in the deposition direction and then unloading it to the isotropic stress state using strain control. Figure 2-8 shows the result of directional distribution of normal contact force. It can be seen clearly that contact points with normals that coincide with the major principal strain axis are created, while those with normals perpendicular to the axis are lost after pre-loading.

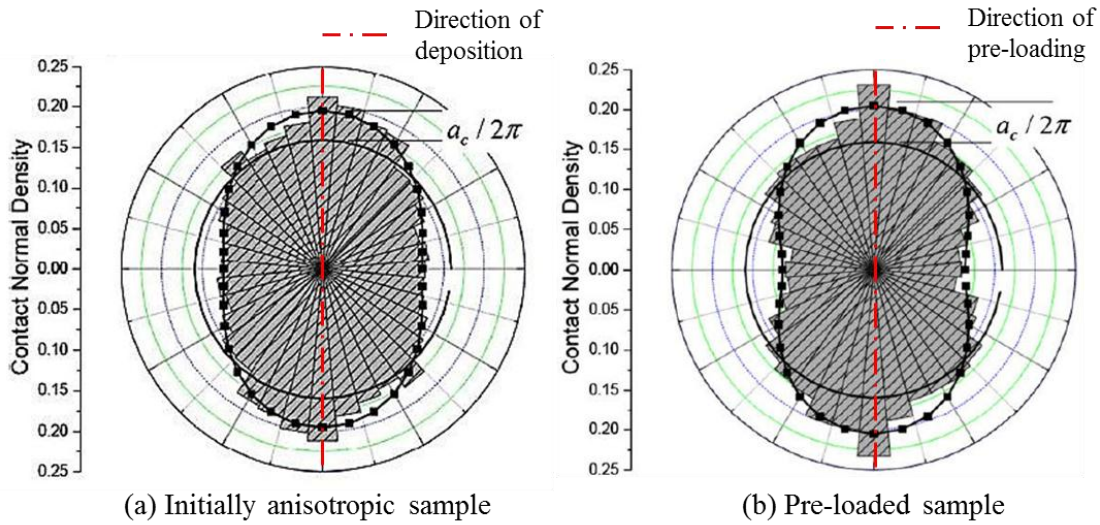

Figure 2-8: Directional distribution of contact normal (Li and Yu 2009).

However as pointed out by Oda (1972b), the soil fabric is constantly changing and reorienting itself during the shearing process, and, in a way, particle contact normals as well as the voids between the grains formed load resisting columns. When the peak stress was achieved, the void and contact normal columns started breaking down and the soil fabric was altered. It is therefore suggested that induced anisotropy is unlikely to have a significant effect on the internal friction angle of the soil. Subsequent torsional shear testing on medium-loose Ham River Sand has shown that for a given loading direction, the friction angle is relatively unaffected by previous stress rotation (Symes et al. 1984), providing confirmation of Oda's theory with respect to peak shear strength. However, the induced anisotropy does have a significant effect on the strain required to achieve a given stress ratio (Arthur et al. 1977).

2.2.4 Non-coaxial behaviour

Non-coaxiality, as an important aspect of anisotropy of granular materials, refers to the non-coincidence of principal stress directions and corresponding principal plastic

strain rate directions during plastic deformation (Yu 2008). In conventional plasticity theory, the stress and the plastic strain rate are assumed to be coaxial. The assumption of coaxiality was first made by Saint Venant when he applied Tresca's yield criterion to a problem in metal plasticity (Cai 2010). A theory of plasticity based on this fundamental coaxial assumption is termed as coaxial plasticity and most soil models currently in use in geotechnical practice are based on the plastic potential theory which often predicts coaxiality (Yu 2006). However, extensive experimental data obtained from different tests along various stress paths has clearly demonstrated that soil behaviour is generally non-coaxial (Roscoe et al. 1967; Drescher and De Jong 1972; Drescher 1976; Arthur et al. 1977, 1980; Symes et al. 1984, 1988; Miura et al. 1986; Gutierrez et al. 1991; Gutierrez and Ishihara 2000; Lade et al. 2009; Tong et al. 2010).

Yu et al. (2005) Yu and Yuan (2005, 2006) and Yang and Yu (2006) made the first attempts to extensively investigate the influences of the non-coaxial soil models on the stress–strain responses of soils. In the study by Yu et al. (2005) and Yang and Yu (2006), the original yield vertex non-coaxial theory by Rudnicki and Rice (1975) was employed. They also numerically integrated the non-coaxial models and implemented it into a finite element software ABAQUS. They used the non-coaxial models to simulate the behaviour of shallow foundations, under various initial conditions and loading conditions. Their comprehensive predictions indicated that the use of the non-coaxial models usually gave softer responses than with coaxial models when the soil is subject to principal stress rotations. Therefore, they argued that ignoring non-coaxial behaviour will under-predict deformation for a given applied load. As a result, failure to account for non-coaxial soil behaviour would lead to an unsafe design in geotechnical practice.

The result from simple shear tests in sand reported by Roscoe et al. (1967) represents one of the earliest evidence of non-coaxial behaviour of granular materials. As shown in Figure 2-9, the experimental results show clearly that when the principal stress direction θ_σ changes, the direction of the corresponding principal strain rate $\theta_{\dot{\varepsilon}}$ does not follow. It needs to be noted that as elastic strain increment takes much smaller proportion in the total strain increment than the plastic strain increment (Gutierrez et al. 1991), the total strain increment instead of the plastic strain increment is used in their analysis. As can be seen in Figure 2-9, the difference of the stress and strain rate directions is the largest when shear strain is small and it gradually reduces when shear strain increases. The direction of the principal stress and that of the principal strain rate becomes identical at critical state when shear strain becomes very large.

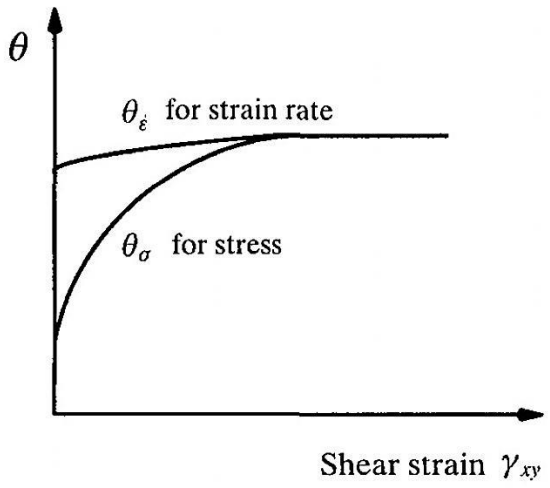

Figure 2-9: Measured non-coaxiality between the directions of stress and strain increment in simple shear test (Roscoe 1967).

Using the Directional Shear Cell (DSC), Wong and Arthur (1985) also observed the non-coincidence of the major principal stress and strain increment directions. As mentioned in section 2.2.3, samples were subjected to a two-stage loading scheme under drained conditions in the initially isotropic plane. Presented in Figure 2-10, is the measured degree of non-coaxiality ξ against stress ratio relationships at different

reloading directions. It can be seen that the sand behaves almost coaxial when the samples were reloaded with the direction of major principal stress coincides with ($\Delta\psi$ = 0°) or perpendicular to ($\Delta\psi$ = 90°) that of pre-loading. And, an obvious non-coaxiality was observed when $\Delta\psi$ = 40° and 70°. Once again, the data shows that the degree of non-coaxiality gradually reduces with increasing stress ratios and specimens were nearly coaxial when close to failure.

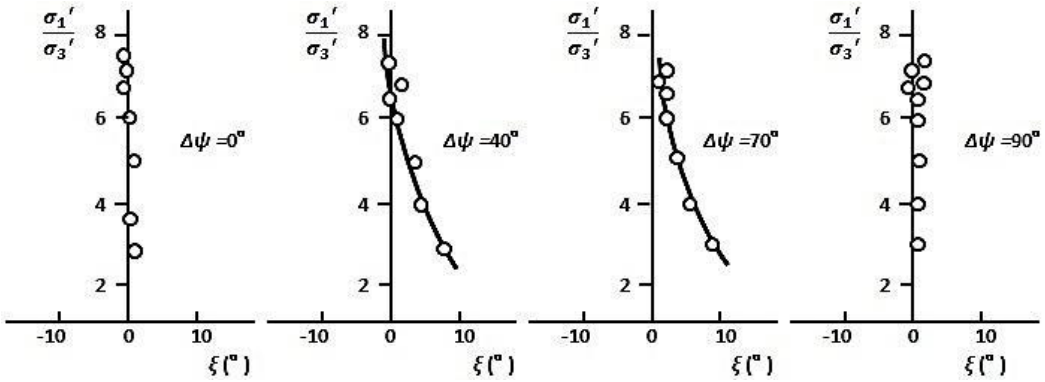

Figure 2-10: Measured non-coaxiality in directional shear test (Wong and Arthur 1985).

More recently, Ibraim and his colleagues (2010) performed a series of strain controlled tests on a two-dimensional analogue granular material, in a special laboratory apparatus which permits full control of plane deformations, including rotation of principal axes. The test path was controlled by the principal strain increment direction ξ and by the imposed dilation angle v. The evolution of the difference between the principal directions of stain and stress (ξ - α) is shown in Figure 2-11. The tests are differentiated by the values of ξ and v, for example, A-T9(15.4d) is a test with ξ = 9° and imposed dilation angle v = 15.4 °. The letter *c* or *d* indicates compression or dilation respectively. It can be seen that the degree of non-coaxiality as measured by the difference of the two principal directions becomes progressively smaller as straining continues, and finally almost attains coaxiality as

the stress state approaches the asymptotic state. The data also shows that the higher the inclination angle of the major principal strain increment to the vertical axis, the faster the principal axes of stress rotate.

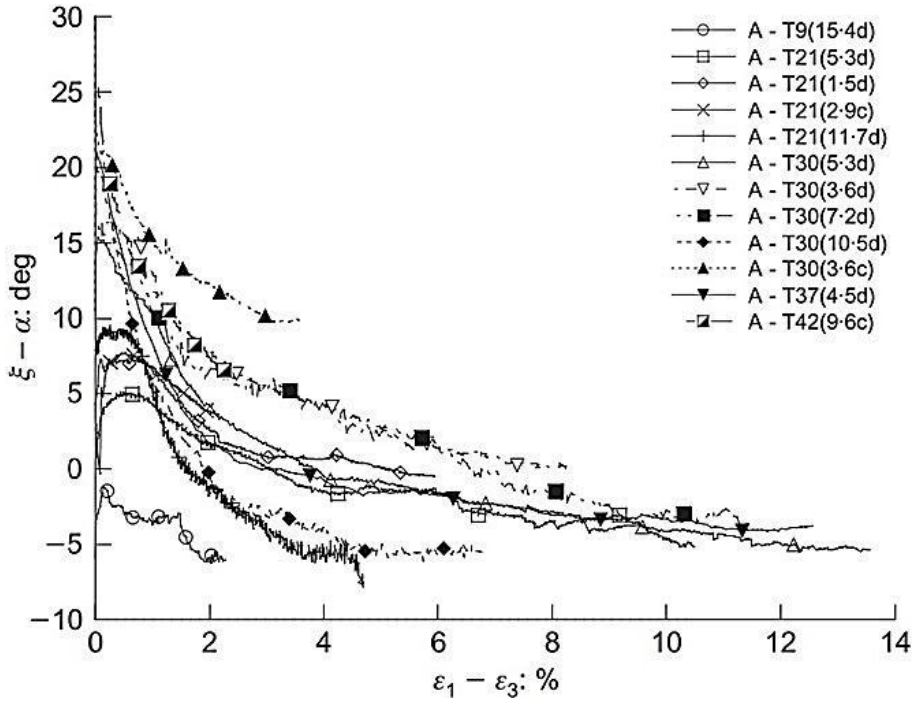

Figure 2-11 Difference between the direction of the major principal strain increment, ξ, and the direction of the major principal stress, α, with the straining process for all the tests with fixed rotation of principal axes (Ibraim et al. 2010).

The non-coaxial behaviour of sand was also observed in hollow cylinder apparatus (HCA) by many researchers (e.g. Hight et al. 1983; Symes et al. 1984; Miura 1986; Gutierrez et al. 1991). Details of the apparatus will be introduced in section 2.4. As reported by Gutierrez et al. (1991), Figure 2-12 shows the plastic strain increment directions obtained during monotonic tests along different fixed principal stress directions. In general, the soil behaviour is non-coaxial, where the unit plastic strain increment vectors were deviated from the radial stress paths especially at low shear stress level. However, the deviations are very small and may be neglected when close to the failure surface. It is also noted that elastic strain increment takes much smaller proportion in the total strain increment than the plastic strain increment. Figure 2-13

shows the plastic strain increment directions obtained during pure principal stress rotation tests at different shear stress levels. Comparing the measured non-coaxiality with the monotonic fixed direction tests, the deviation between the principal plastic strain increment and the principal stress directions are more significant.

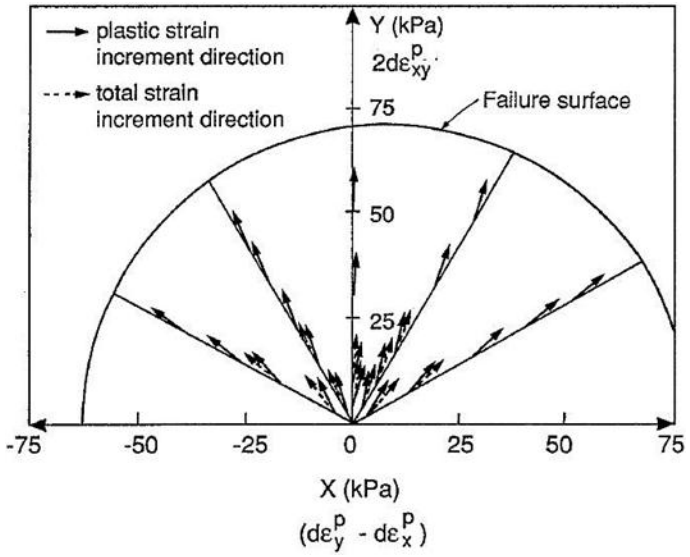

Figure 2-12: Measured non-coaxiality in monotonic tests along different fixed principal stress directions (Gutierrez et al. 1991).

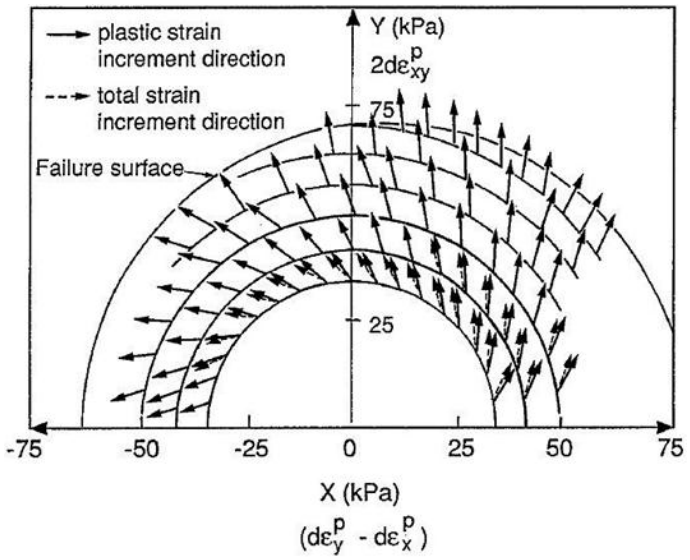

Figure 2-13: Measured non-coaxiality in pure principal stress rotation tests at different levels of mobilized friction angle (Gutierrez et al. 1991).

Micromechanics-based approaches, particularly those based on the Discrete Element Method (DEM), have proven useful information to advance understanding of non-coaxial behaviour of granular materials. Li and Yu (2009) investigated the non-

coaxial behaviour of pre-loaded sample under monotonic shearing in various loading directions using 2D DEM. In their simulation, samples made of two equal sized clumps were first deposited and preloaded in the vertical direction. After unloading to an isotropic stress state, samples were then sheared along different fixed principal strain incremental directions from vertical (α = 90°) to horizontal (α = 0°) with 15° intervals. Figure 2-14 presents the measured non-coaxiality for the tests. The results have confirmed the observations obtained earlier by Wong and Arthur (1985) in that the sand behaves almost coaxial when the samples were reloaded with the direction of major principal stress coincides with or perpendicular to that of pre-loading. However, non-coaxiality was observed to be large when the loading direction deviated away from the direction of preloading.

As pointed by Yu (2008), soil fabric and its evolution are the main reasons for its non-coaxial behaviour. Hence, the microscopic information characterized by principal directions of contact normal and contact force was analyzed by Li and Yu (2009) in order to explore the underlying mechanisms of non-coaxiality. The micro-structural expression of the stress tensor in terms of its micro counterpart, contact forces, and geometrical variables, contact vectors is shown as follow:

$$\bar{\sigma}_{ij} = \frac{1}{V}\sum_{C\in V} v_i^c f_j^c \tag{2-3}$$

in which $\bar{\sigma}_{ij}$ stands for the average stress over volume *V*. The equation expresses the macro-scale stress tensor as the volumetric average of the tensor product of micro-scale contact forces f_j^c and contact vectors v_i^c.

It is clear from the above expression that the stress tensor is dependent of contact force as well as contact normal between particles. As shown in Figure 2-15 (a), the

principal contact force direction is more or less coincident with the loading direction throughout the reloading stage. Figure 2-15 (b) shows the principal directions of contact normal. At the beginning of tests the major principal directions of contact normal was coincident with the direction of deposition. For test with loading direction parallel to the pre-loading direction (α = 90°), the principal direction of contact normal was coincident with loading direction throughout the test. For test with loading direction perpendicular to the preloading direction (α = 0°), contacts with contact normals parallel to the loading direction were created suddenly at the initial stage of test. However, for test with loading direction fixed at α = 75°, 60°, 45°, 30° and 15°, the principal directions of contact normal were gradually rotated in such a manner that they finally pointed in the loading direction at large strain levels. A similar observation was reported by Oda et al. (1985) from their laboratory investigation on two-dimensional assemblies of photoelastic rods. As the principal contact force direction is more or less coincident with the loading direction, non-coaxiality is hence the result of the principal directions of contact normal being deviated from the loading direction (Li and Yu 2009).

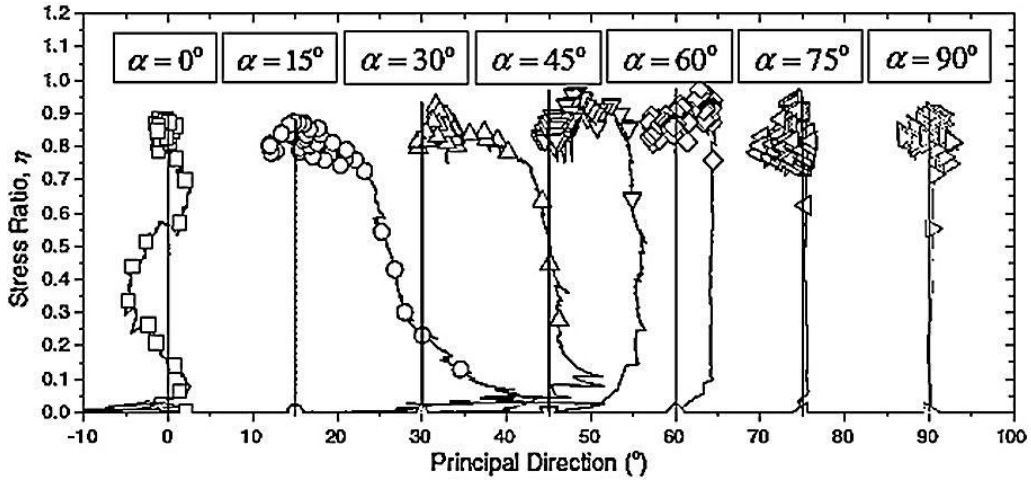

Figure 2-14: Measured non-coaxiality in monotonic tests along different fixed principal strain incremental directions (Li and Yu 2009).

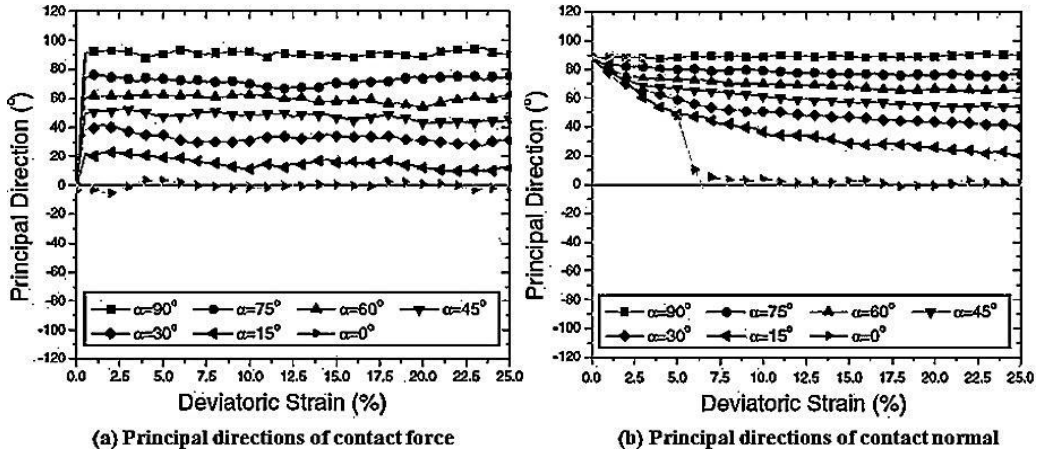

Figure 2-15: Principal directions of: (a) contact force and (b) contact normal (Li and Yu 2009).

2.3 Effects of Principal Stress Direction and Intermediate Principal Stress on Soil Response

2.3.1 Introduction

Triaxial tests are usually employed to evaluate the mechanical response of geomaterials. In conventional triaxial testing where a cylindrical specimen is tested, the state of stress is axisymmetric. The intermediate principal stress is always equal to the major or minor principal stresses and the direction of the major principal stress is always parallel or normal to the vertical. However, most of the field problems in geotechnical engineering are three-dimensional, and a soil is more likely to subject an anisotropic stress state ($\sigma_1 \neq \sigma_2 \neq \sigma_3$), together with rotation of the principal axes. It is essential that the soil behaviour under such realistic and general loading conditions is well understood, so that engineers can devise appropriate geotechnical design and analysis in practical situations. Intense research efforts have been made to understand the effects of principal stress direction and intermediate principal stress on soil behaviour for the last few decades. Results from the studies have shown clearly that

variations in the principal stress inclination and the intermediate principal stress can significantly affect the stress-strain or strength-deformation behaviour of granular soils.

2.3.2 Effects of principal stress direction

In geological environments where sedimentation occurs in the direction of gravity, it is expected that the angles $\alpha = \beta = \gamma = 0°$ (see Figure 2-3(b)). However, most forms of geotechnical construction activity will invariably lead to principal stress axes rotation taking place in the field. Embankment loading is a typical example where rotation of the principal stresses occurs. Figure 2-16 shows a potential slip surface through the side slope of an embankment with the stress state at four locations on the slip surface. Between Locations A and D a gradual rotation of the principal stresses occurs. The major and minor principal stresses rotate through an angle α from the vertical and horizontal respectively, while the intermediate principal stress is assumed continually acting into the plane. Location B in Figure 2-16 shows a typical stress state where the principal stresses are different from the bedding plane. In this case, it is not possible to determine the strength and deformation characteristics of the soil using conventional triaxial testing methods. Thus the measurement and study of the stress-strain-strength behaviour of soils in general stress states involving the change of magnitudes and direction of the principal stresses are necessary and important.

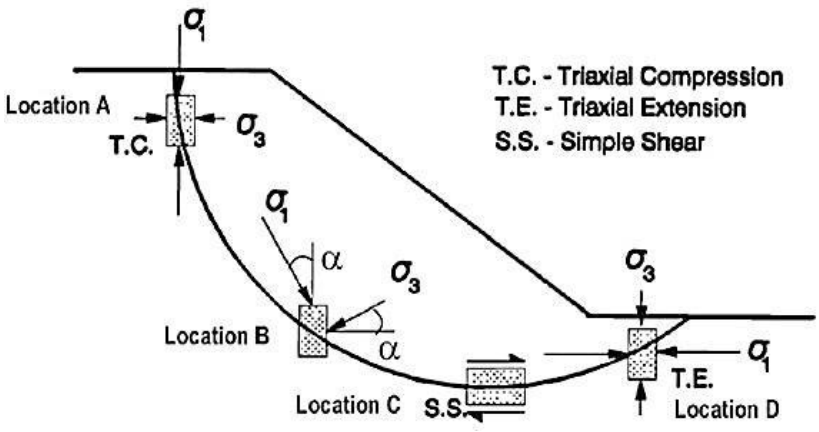

Figure 2-16: Limiting equilibrium stress states underneath an embankment (Uthayakumar and Vaid, 1998).

Miura et al. (1986) carried out drained tests on dense Toyoura sand, in a hollow cylinder apparatus (200 mm height, 150 mm OD and 314 mm ID). Samples were isotropically consolidated to a mean effective stress p' = 98 kPa, with a back pressure of 196 kPa to ensure sufficient saturation. Monotonic loading with fixed principal stress directions (α = 0°,15°, 30°, 60°, 75°, 90°) was then applied on the specimens with drained condition. Effective mean stress p' = 98 kPa and the intermediate principal stress parameter b = 0.5 were maintained constant throughout the test.

Figure 2-17 presents the stress-strain relationships for the tests conducted by Miura et al. as described above. If a specimen is isotropic in its mechanical properties, the deformation behaviour does not depend on the direction of principal stress axes during shear. It can be observed from the results that the shear deformation response depended strongly on the principal stress direction. The stiffest response is seen for loading in the vertical (α = 0°) deposition direction. In general, the strain response becomes softer with increasing values of α. Stress ratios at peak reduced dramatically as the direction of the major principal stress was rotated from the vertical.

It should be pointed out that all the stress-strain curves obtained by Miura et al. are ceased at the peak stress. This is because the shearing was carried out using stress controlled loading mode, and therefore the behaviour of sand at large strains was uncertain.

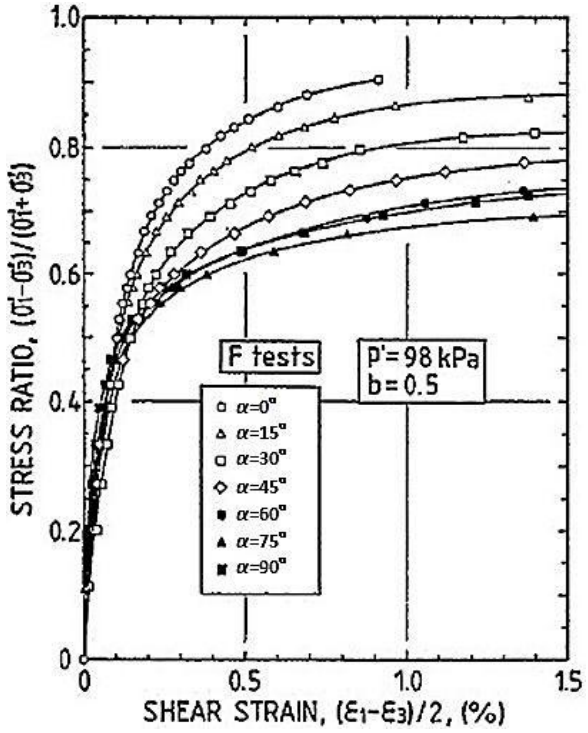

Figure 2-17: Stress ratio versus shear strain from HCA tests on isotropically consolidated, dense Toyoura sand (Miura et al. 1986).

Figure 2-18 shows the relationships between the peak deviator stress and associated major principal stress directions. For α = 0° to 30° and α = 60° to 90°, the change of the peak deviator stress was not very significant, while a clear change occurred between α = 30° to 60°, with a sharp drop from α = 30° to 45°. The maximum peak stress ratio existed at α = 0° and kept dropping until the minimum value was achieved at α = 60°, then the specimen strength reverted slightly at α = 90°. Miura et al. explained this observation using the concept of mobilized planes of Matsuoka (1974). It was suggested that the maximum deformability occurs when the mobilized planes

(i.e. plane of maximum stress obliquity) and the bedding plane are coincident. Figure 2-19 is the schematic explanation for the planes. At pre-failure state (stress ratio $R \approx 0.5$), the mobilized plane is inclined to the major principal stress direction by approximately 30°. As such, when the inclination of the major principal stress is 60° to the vertical, the mobilized plane would make an angle of about 90° with the vertical. This indicates approximate coincidence of bedding and mobilized planes, and thus affirming the lowest strength observed at $\alpha = 60°$.

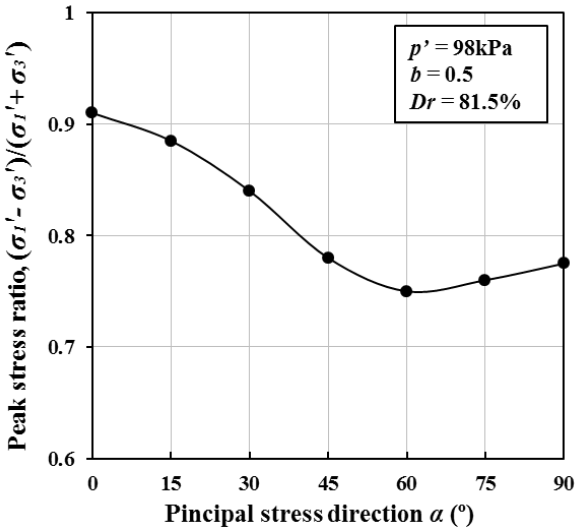

Figure 2-18: Dependence of peak stress ratio on the direction of principal stress axes (Miura et al. 1986).

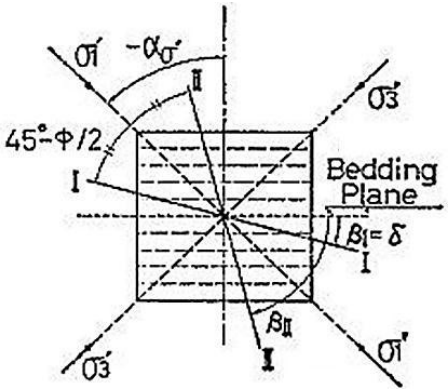

Figure 2-19: Schematic explanation for Mobilized planes I and II.

The plane strain tests carried out by Oda et al. (1978) showed similar results to those of Miura et al. (1986) described above. In their tests, the dense samples of Toyoura

sand were prepared in a tilting mould to give different directions of sample deposition with respect to the principal stress axes. Samples were isotropically consolidated to mean pressures of 50, 100, 200 and 400 kPa, and then sheared by increasing the vertical stress until failure, while keeping σ_3' constant and controlling σ_2' to maintain plane strain conditions ($b \approx 0.2$-0.3). Because of limitations of the testing device the tests were limited to a maximum vertical strain of 6%.

Figure 2-20 shows the stress-strain relations in the plane strain tests for the case of σ_3' = 200 kPa. The stiffness from these tests was also observed to decrease with increasing α and the volumetric strains are seen to be less dilatant for higher values of α. The similar trends in the stress-strain responses were observed for the samples sheared at other stress levels.

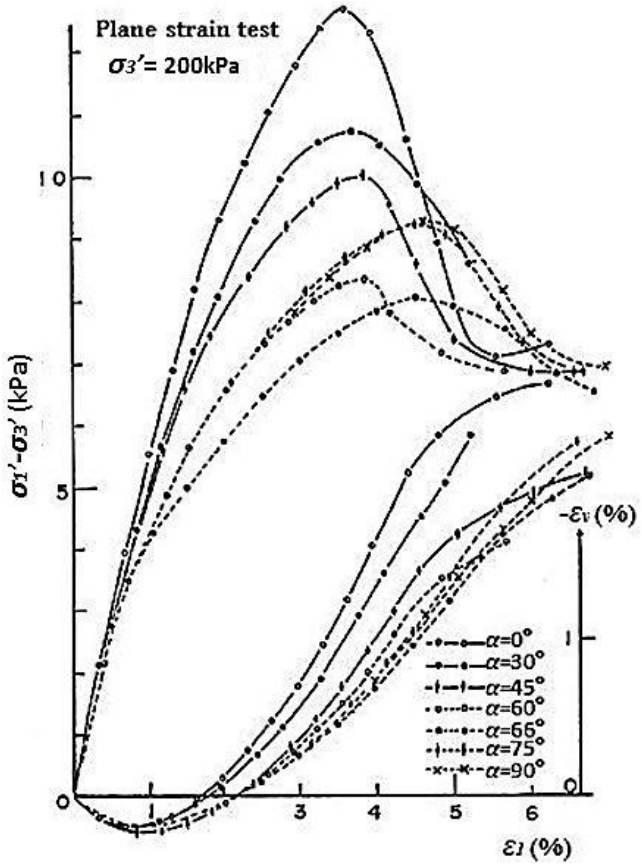

Figure 2-20: Stress-strain relations in the plane strain tests on isotropically consolidated dense Toyoura sand (Oda et al. 1978).

Figure 2-21 shows the dependence of peak stress ratio on the direction of principal stress axes at different stress levels. The results illustrate that the lowest strength was achieved between α = 60° and 75° and the specimen strength also showed slight reversion at α = 90°. This tendency agrees well with the results reported by Miura et al. (1986).

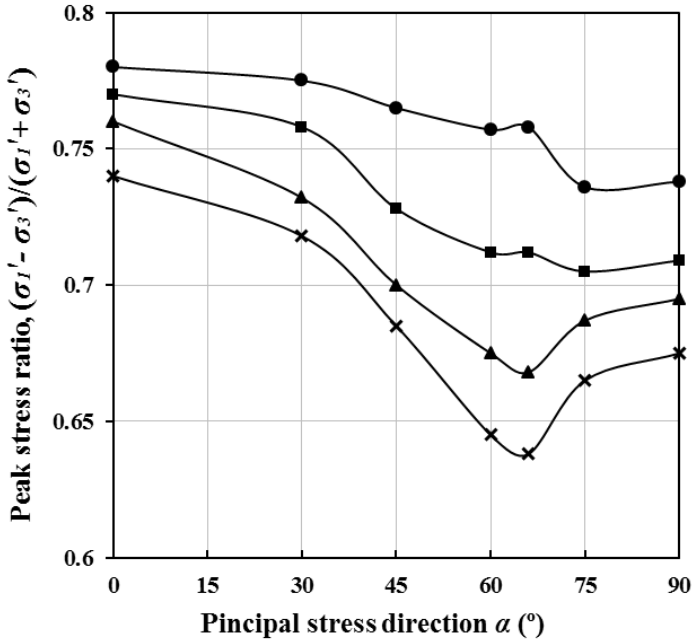

Figure 2-21: Dependence of peak stress ratio on the direction of principal stress axes (reproduction from Oda et al. 1978).

Results in support of the general increase in deformability of sand with increasing α have also been reported by Arthur and Menzies (1972) in cubical triaxial tests on tilted samples, Oda et al. (1978) in triaxial compression tests, Arthur et al. (1981) in directional shear cell tests, Symes (1983) in HCA tests and Nakata et al. (1997) in HCA tests. However due to the limitations of the testing device all the tests described above were limited to small strains and deformations. Therefore, a device that is capable of performing large strain test and with the ability to monitor and independently control the direction of the major principal stress is required.

2.3.3 Effects of Intermediate principal stress

The intermediate principal stress parameter *b*, as shown in Equation 2.4, are commonly used in the investigation on the effects of intermediate principal stress on the soil behaviour.

$$b = \frac{\sigma_2 - \sigma_3}{\sigma_1 - \sigma_2} \tag{2-4}$$

This parameter was first introduced by Habib (1953) in investigating the strength characteristics of clays and sands in torsional triaxial tests. It directly describes the relative magnitude of the intermediate principal stress as compared to the major and minor principal stresses. The *b*-value has a fixed range of variation (0~1) and in conventional triaxial compression $b = 0$, whereas in triaxial extension $b = 1$. As suggested by Bishop (1966), the influence of intermediate principal stress σ_2 on soil response can be more readily appreciated in terms of *b* rather that σ_2 itself.

The conventional triaxial compression testing ($b = 0$) is invariably used to determine practical soil parameters for design purposes in geotechnical engineering. However, experimental results suggest that in many field situations, the deformation more closely approximate plane strain conditions ($b \approx 0.2$-0.3). The investigation of the differences between triaxial and plane strain behaviour of soils has received considerable attention in the past for studying the failure conditions in soils. As shown in Figure 2-22, the shear strength of dry sands in plane strain compassion test is compared with shear strength in triaxial compression test by Nabil (1976). It can be seen that the maximum stress ratio is greater in the plane strain test than in the triaxial test and the maximum stress ratio was obtained at a smaller axial strain in the plane strain test than in the triaxial test. Similar observations were also reported by many

other researchers (e.g. Bjerrum and Kummeneje 1961; Cornforth 1964; Vaid and Campanella 1974). The large discrepancy between the results in triaxial and plane strain test suggests that, in general, the intermediate principal stress σ_2 would have profound effects on the mechanical behaviour of soils.

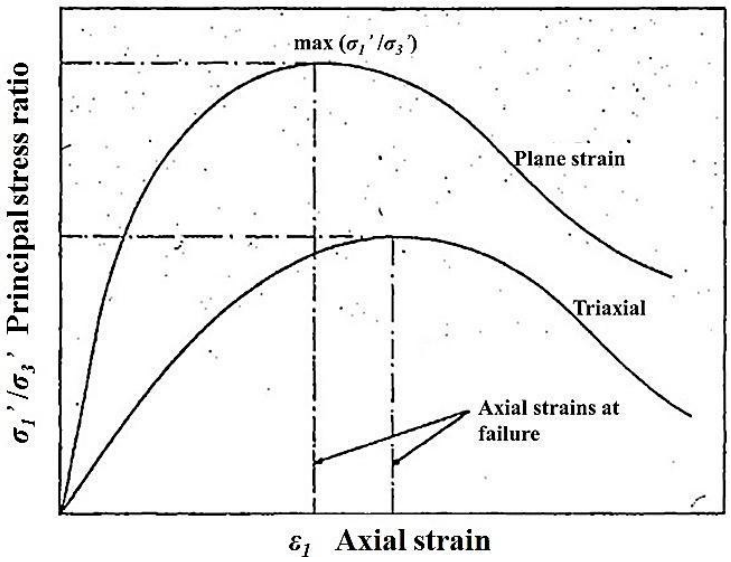

Figure 2-22: Representation stress-strain curves for plane strain and triaxial test (Nabil 1976).

As a response to the raising awareness about the importance of effects of *b* value on soil behaviour, several types of true triaxial test apparatuses were developed (e.g. Ko and Scott 1967; Hambly and Roscoe 1969; Lade and Duncan 1973; Desai et al. 1982). The advantages and disadvantages of different boundary conditions used in various true triaxial devices were summarized by Mould (1979). Unlike conventional triaxial apparatus, all three principal stresses can be controlled independently, rather than just two in a conventional triaxial system. This allows varying the value of *b* over its full range between 0 and 1.

Lade and Duncan (1973) designed a cubical triaxial tester with a combination of flexible and rigid boundaries to investigate the effects of *b* value on the stress-strain

and strength characteristics of Monterey sand. The results presented in Figure 2-23 (a) and (b) showed that for both dense and loose specimens the slop of the stress-strain curve increased, the strain-to-failure decreased, and the rate of dilation increased with increasing *b* value. The *φ'-b* diagram is widely used to represent the variation of peak strength under three dimensional stress conditions, where the friction angle *φ'* = arcsin $[(\sigma_1 - \sigma_3)/(\sigma_1 + \sigma_3)]$. As shown in Figure 2-24 the angle *φ'* increased significantly from axisymmetric ($b = 0$) to plane strain conditions ($b \approx 0.2$-0.3). As *b* increased further, *φ'* began to increase again, and it reached its highest value near $b = 0.8$ from which it decreased as *b* increases to unity. It was also observed from the results that a given increment in *b* had a greater effect on both the stress-strain and the strength characteristics at small *b* values than at high *b* values.

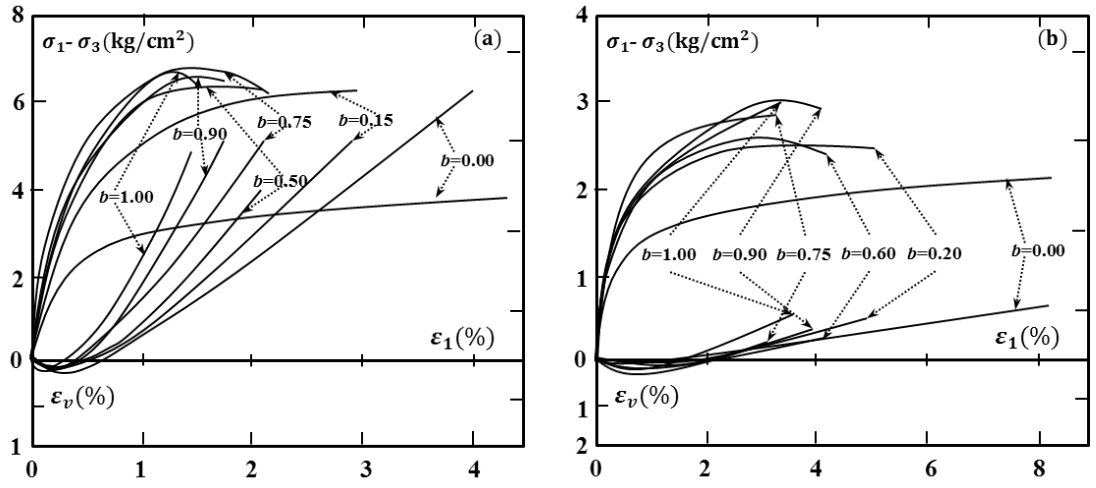

Figure 2-23: Stress-strain and volume change characteristics obtained in cubical triaxial tests on: (a) dense Monterey sand and (b) loose Monterey sand (reproduction from Lade and Duncan, 1973).

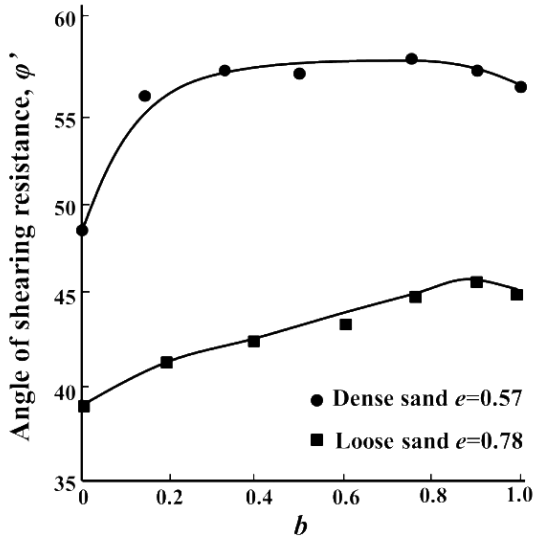

Figure 2-24: Variation in the angle of shearing resistance *φ'* with intermediate principal stress parameter *b* (Lade and Duncan, 1973).

Symes (1983) carried out series of tests using hollow cylinder apparatus to investigate the effects of b value on the drained behaviour of medium-loose Ham River sand. Tests were performed with b = 0, 0.14, 0.5 and 1.0, while α was set at 45° during shearing. The stress ratio versus octahedral shear strain curves obtained from tests is shown in Figure 2-25. The diagram shows that tests with b = 0.14 and 0.5 had the least strains to failure and presented the highest initial stiffness and strength. These two tests also exhibited the least volumetric strains to failure. The resulting angles of shearing resistance obtained at the failure points are shown in the Figure 2-26. The highest strength and stiffness are observed when shearing with conditions that are closer to plane strain ($b \approx 0.2$-0.3). The softest response and the lowest strength were obtained when b = 1.0. Similar results were also found by Sayao and Vaid (1997) on medium-loose Ottawa sand tested in a hollow cylinder apparatus. However, this is inconsistent with the observations by Lade and Duncan (1973) described above. Possible causes for this inconsistency will be discussed later.

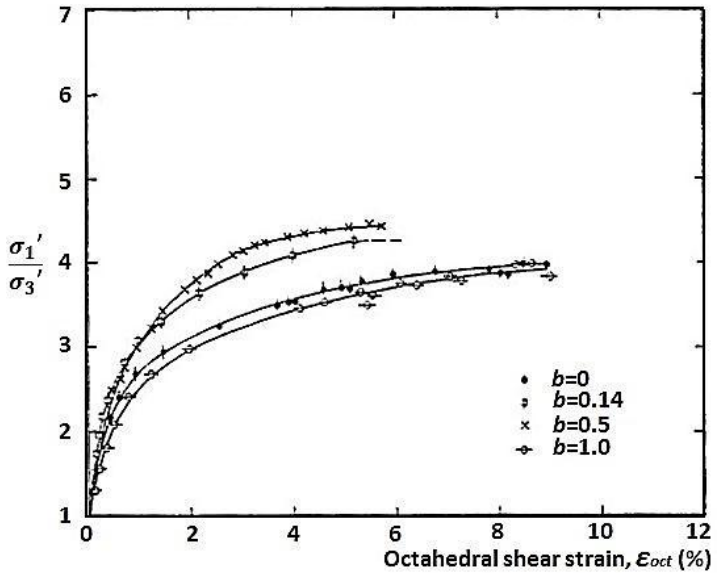

Figure 2-25: Stress-strain and volume change characteristics obtained in HCA tests on medium-loose Ham River sand (Symes, 1983).

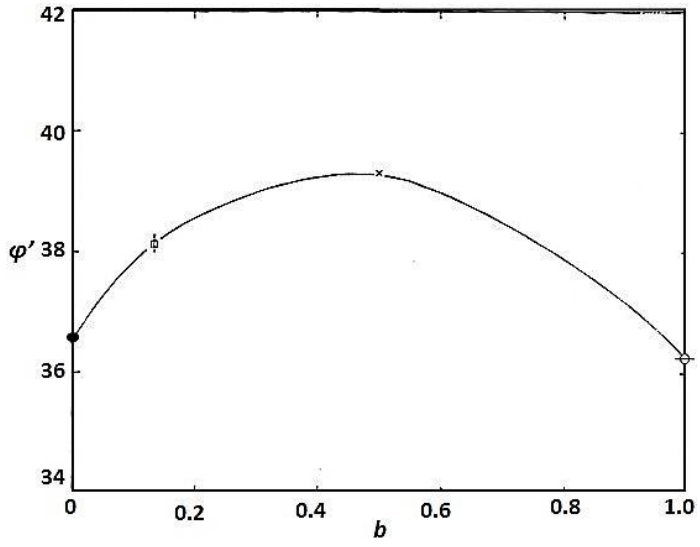

Figure 2-26: Variation in the angle of shearing resistance *φ'* with intermediate principal stress parameter *b* (Symes, 1983).

Representative *φ'*-*b* relationships obtained for sands in various studies are summarized and compared by Lade (2006). As demonstrated in Figure 2-27, the relationships have been sorted such that those with similar shapes are shown on the same diagram. It can be observed that most studies seem to indicate that the friction angle *φ'* increases from axisymmetric ($b = 0$) to plane strain conditions ($b \approx 0.2$-0.3).

However, for larger values of *b*, considerable disarray appears to be present. The conflicting results between the three groups are probably due to several factors that affecting individually measured strengths under three dimensional stress conditions, such as the major principal stress direction (vertical or horizontal); variations in mean effective stress; effects of shear band occurrence in hardening regime; effects of boundary restraints and stress or strain nonuniformities (Ergun 1981; Sayao and Vaid, 1996; Wang and Lade, 2001). Consequently, more experimental evidence is still needed to provide a better understanding of the effects of intermediate principal stress on soil behaviour.

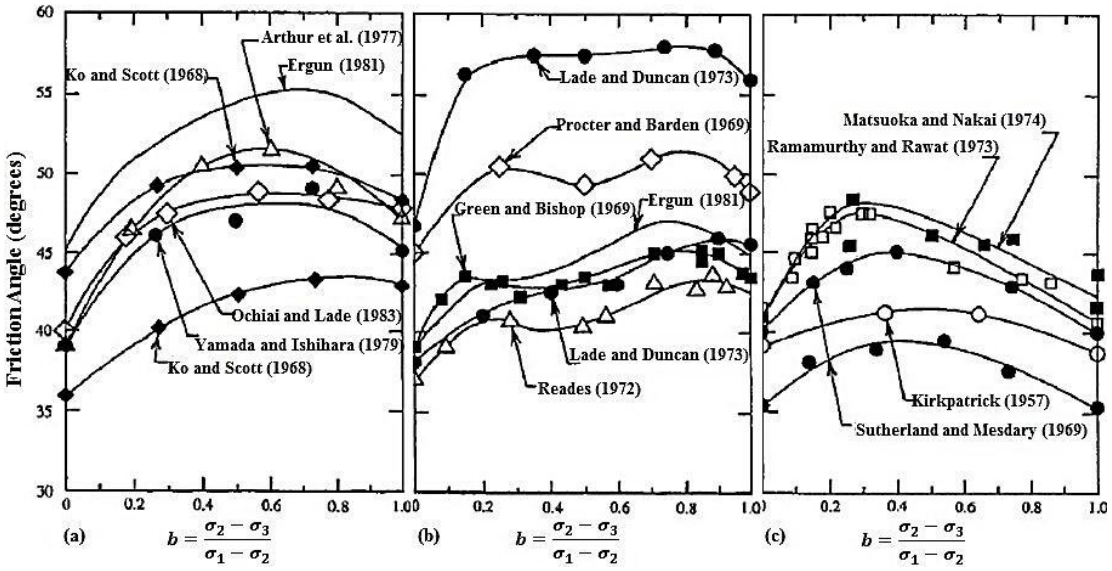

Figure 2-27: Three groups of *φ'-b* relationships from true triaxial tests on sand Lade (2006).

2.4 Effects of Rotational Shear on Soil Response

2.4.1 Introduction

As mentioned in section 2.2 that most sedimentary deposits are inherently anisotropic due to their common natural deposition in horizontal layers. This inherent anisotropy

highlights the fact that the response of soils to loading is depending on both stress magnitude and direction. Rotational shear, also known in the literature as continuous rotation of principal stress axes, is a pattern of loading in which the continuous rotation of principal stress axes takes place under a constant amount of deviatoric stress. Many loading situations such as those induced by earth quakes, traffic loadings and sea waves are common examples of the rotational shear. Figure 2-28 shows the stress path of the rotational shear in *X*-*Y* stress space.

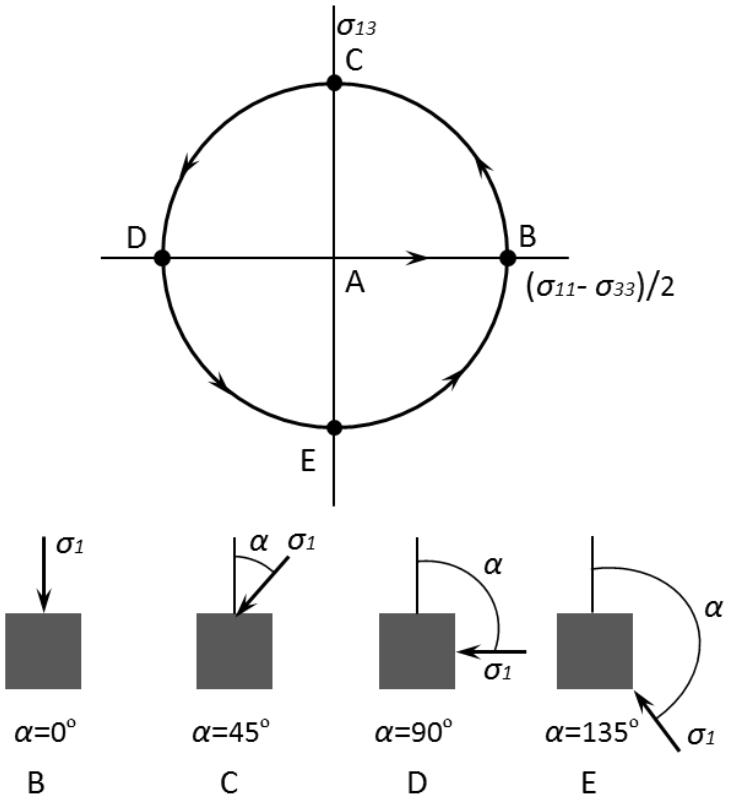

Figure 2-28: Stress path of rotational shear in *X*-*Y* stress space.

Extensive experimental studies of rotational shear have been made on granular soils over the past few decades in order to develop constitutive models accurately accounting for the effects of rotational shear and to reliably predict the soil behaviour in the field.

2.4.2 Undrained response

Undrained conditions can prevail in the presence of relatively fast loading conditions and there are several situations in which the stress axes rotate continuously and sand is quite susceptible to liquefaction. Among them is the cyclic loading condition during earthquakes. However, the most critical situation is found in the seabed deposit during a storm period (Towhata and Ishihara 1985). Because of the practical importance of this phenomenon, the effects of undrained anisotropy and principal stress rotation in saturated sand are of great interest.

Using a torsional shear apparatus, Broms and Casbarian (1965) first investigated the effects of the rotation of principal stress axes on the shear strength and pore pressure development in isotropically consolidated kaolin clay. They found that the continuous rotation of principal stress axes increases the rate of pore water pressure generation and reduces the undrained strength of the saturated clay. Using the Directional Shear Cell (DSC) Arthur et al. (1980, 1981) carried out more comprehensive studies on this subject. The results showed that the undrained deformation and strength characteristics of the Leighton Buzzard sand under monotonic loading conditions are influenced significantly by the previous rotation of the principal stress directions (α rotated through an angle of 70°). Symes et al (1984) performed a series of undrained torsion shear tests on Ham river sand. In support of the findings from Broms and Casbarian (1965), the results showed that excess pore water pressure was generated under the cyclic rotation of principal stress axes (α varied from 0° to 24.5° and back to 0°).

However, due to the limitation of the testing apparatus, the rotation of principal stress axes was restricted to a narrow range in the studies described above. In an effort to

simulate the complete rotation of principal stress directions induced in a seabed deposit as a result of traveling waves, Ishihara and Towhata (1983) carried out a series of cyclic undrained tests on saturated loose Toyoura sand using a triaxial torsion shear apparatus. A continuous principal stress axes rotation over the full range of 90° was achieved in their study. The major finding they reported was that even though the magnitude of applied shear stress is kept unchanged, the rotation of the principal stress axes always results in pore pressure build up, and can eventually lead to liquefaction. They therefore pointed out that the plastic irrecoverable deformation can occur in the sand in any loading scheme involving rotation of the principal stress directions. Similar results on Toyoura sand were also reported by Towhata and Ishihara (1985) in a triaxial torsion shear apparatus.

Furthermore, Ishihara and Towhata (1983) demonstrated that the behaviour of sand during rotational shear is generally non-coaxial. As schematically illustrated in Figure 2-29 when the increments of the deviator strain, $d(\varepsilon_z - \varepsilon_\theta)$ and shear strain, $d\gamma_{\theta z}$, are represented superimposed on the stress space employing $\sigma_z - \sigma_\theta$ and $2\tau_{\theta z}$ as coordinates, then a stress increment vector with components, $d(\sigma_z - \sigma_\theta)$ and $d2\tau_{\theta z}$ is oriented in the same direction as the strain increment vector formed by $d(\varepsilon_z - \varepsilon_\theta)$ and $d\gamma_{\theta z}$. Therefore, the deformation which is elastic in nature is characterized by the parallelism of the strain increment vector and stress increment vector. In contrast to this, if the deformation is perfectly plastic, the shear strain increment vector is oriented in the same direction as the vector of the existing shear stress (Ishihara and Towhata 1983).

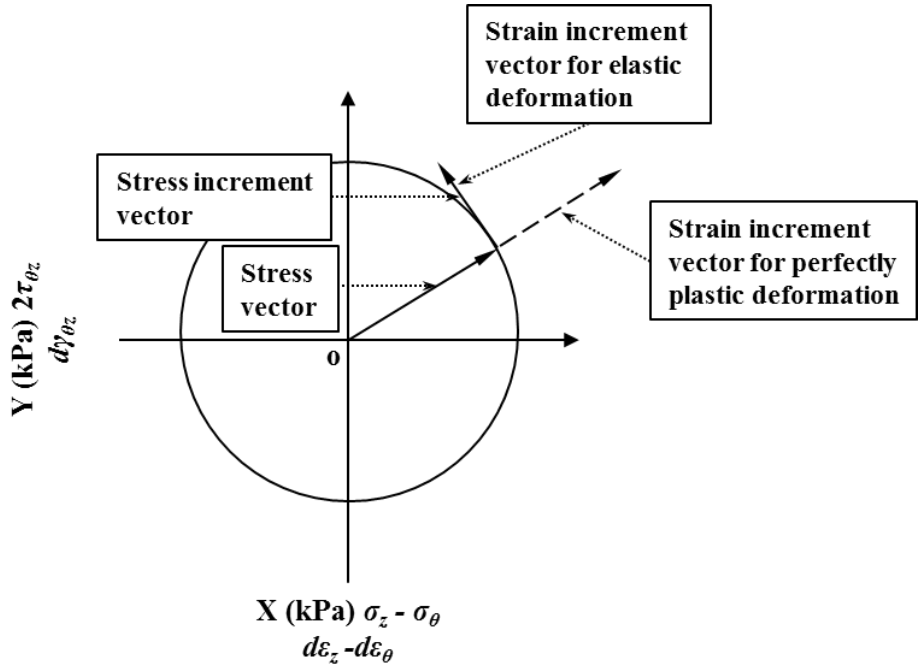

Figure 2-29: Illustration of strain increment vectors in relation the stress vector and stress increment vector (Ishihara and Towhata 1983).

Figure 2-30 shows the strain increment vectors superimposed on the stress space. It can be seen that the vectors of strain increment are neither parallel to the vectors of stress increment nor current stress. As the loading proceeds, the strain increment vectors tend to deviate outwardly from the stress increment vectors and finally they are almost coincides with the current stress vectors. Consequently, the deformation of the sand during rotational shear contains both elastic and plastic components. The elastic component dominated at the early stage and reduced as loading proceeds, and then the plastic part of deformation became dominant.

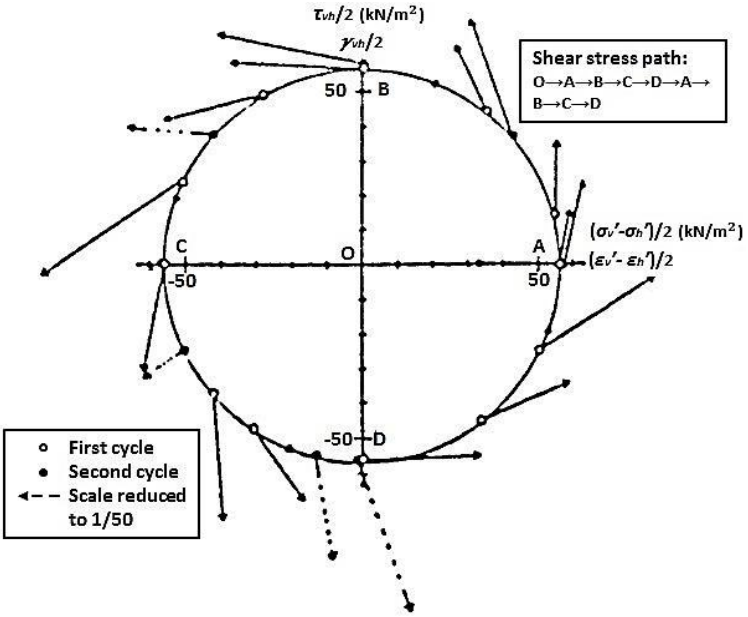

Figure 2-30: Strain increment vectors superimposed on the stress space (Ishihara and Towhata, 1983).

However, Shibuya et al. (1985) pointed out that, the tests done by Ishihara and Towhata (1983) suffered from limitations in that the inner and outer cell pressures could not be independently controlled. The limitations resulted in the intermediate principal stress parameter, measured by $b = (\sigma_2 - \sigma_3)/(\sigma_1 - \sigma_3)$, and the mean total stress, measured by $p = (\sigma_1 + \sigma_2 + \sigma_3)/3$, changing contemporaneously with the rotation of principal stress axes. They emphasised that the rotational shear tests should be carried out under conditions in which the deviatoric stress *q*, intermediate principal stress parameter *b* and mean stress *p* are maintained during the rotation of the principal stress axes.

Cyclic rotation of the principal stress axes while maintaining conditions of constant *b* =0 and *p* = 100kPa was successfully achieved by Nakata et al. (1998) using a hollow cylinder apparatus (200 mm H, 100 mm OD and 60 mm ID). The undrained response of saturated Toyoura sand at various densities (*Dr* = 30% to 90%) subjected to rotation of the principal stress directions were investigated in their study. Figure 2-31

shows the variation of pore pressure and strain components against the number of cycles for a dense sample with relative density D_r = 90%. It is clear that pore pressures and strains are accumulated despite the deviatoric stress q remaining constant. Significant pore pressure build up was observed in the first few cycles and the magnitude of generated strains increases continuously with the increase in the number of cycles.

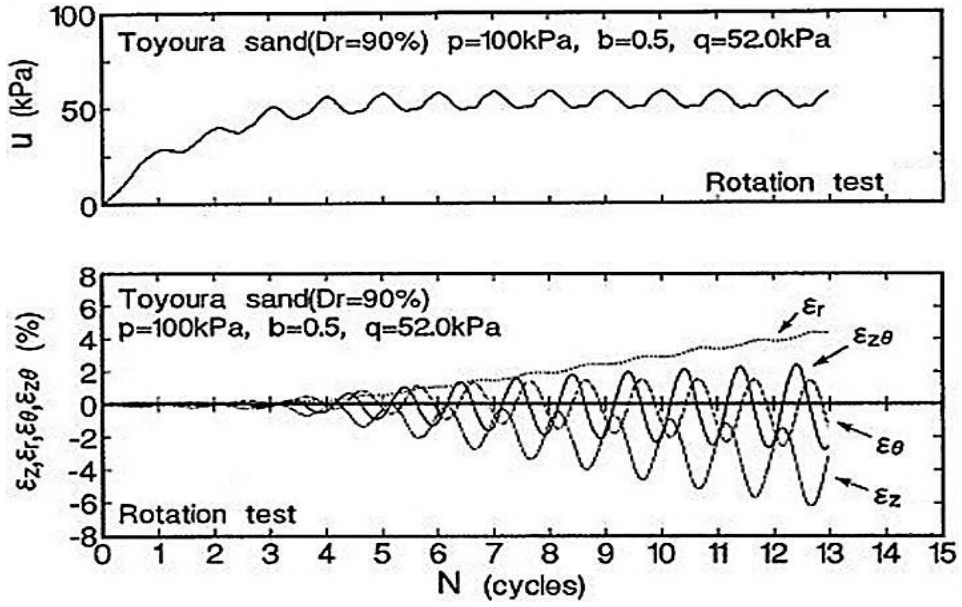

Figure 2-31: Pore pressure and strain components against number of cycles (Nakata et al., 1998).

By compare the test results from samples with different relative density and stress level, the authors also found that the flow deformation could occur when the effective stress state of a sample attained the critical stress state. And the form of deformation could be classified into non-flow, limited flow or full flow deformation and it is dependent on both the relative density of the sand and the level of deviatoric stress.

More recently, Yang et al. (2007) studied the influence of the relative magnitude of the intermediate principal stress on the pore pressure response and deformation characteristics of Toyoura sands during cyclic rotation of principal stress axes. The

investigation was conducted in an automated hollow cylinder apparatus (314 mm H, 200 mm OD and 150 mm ID). A total of 12 undrained tests were conducted under various conditions (D_r = 70% and 90%; q = 34.65kPa and 51.96kPa) with b = 0, 0.5, 1.0. During the tests, samples were first anisotropically consolidated to a specified stress state with effective mean stress p' = 100kPa. The cyclic rotation of principal stress axis was then commenced under otherwise identical conditions.

Figure 2-32 presents the pore water pressures generated in rotational shear at different b values for dense samples with relative density D_r = 70%. Consistent with previous studies described above, pore water pressure was generated despite that the magnitudes of principal stresses are maintained constant. Comparing tests with different b values, it is evident that the pattern of pore water pressure generation was dependent on the value of b, the rate of pore pressure generation under the condition b = 0 was much slower than that under the conditions b = 0.5 and b = 1.0. This observation suggests that the soil sheared under the condition of lower b value has a much stronger resistance to pore pressure build-up. Thus, the relative magnitude of the intermediate principal stress was not a negligible factor for the pore pressure response during rotational shear, but had significant impact.

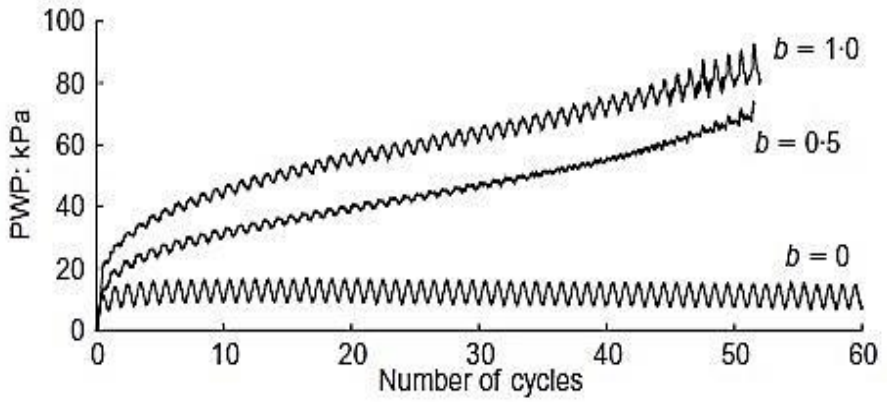

Figure 2-32: Pore water pressures generated in rotational shear (Yang et al. 2007).

Figure 2-33 shows the stress paths in $(\sigma_z - \sigma_\theta)/2p'$ space at different b values for dense samples with relative density D_r = 70% and deviatoric stress q = 34.65kPa. It is clear that the intermediate principal stress parameter b had a substantial impact on the deformation behaviour of sands under cyclic rotation of principal stress axes. The effective mean normal stress in the tests at b = 0.5 and b = 1.0 was reduced significantly such that the soil specimens failed in both cases, whereas the specimen tested at b = 0 showed a limited reduction of the effective mean normal stress, and no sign of failure was observed.

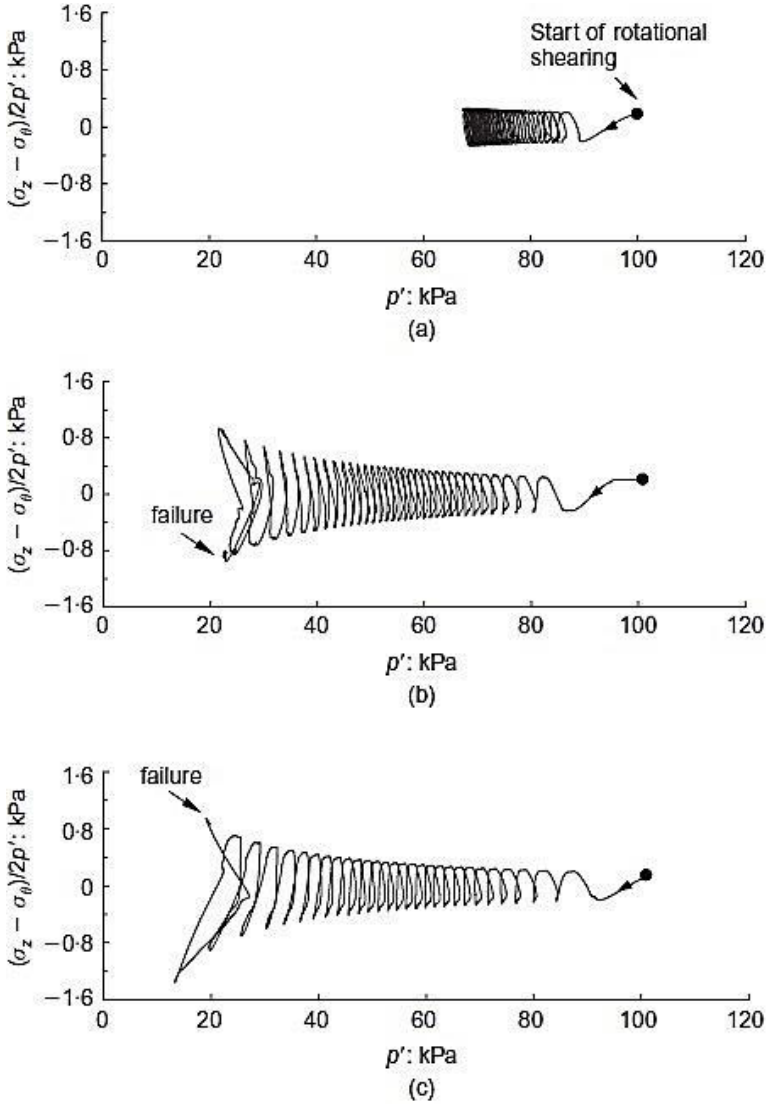

Figure 2-33: Stress paths in $(\sigma_z$-$\sigma_\theta)/2p'$ space for test with (a) b = 0; (b) b = 0.5; (c) b = 1 (Yang et al. 2007).

In support of the findings from Nakata et al. (1998), the authors also found that the magnitude of the deviatoric stress has a significant effect on the pore pressure response and deformation characteristics during undrained rotational shear: the larger the deviatoric stress, the faster was the pore pressure build-up, and the more likely the soil was to fail. Under otherwise identical conditions, the pore pressure was generated more rapidly in relatively loose samples. However, compared with the effect due to the change of the deviatoric stress magnitude, the influence of the soil density appeared to be less pronounced in undrained rotational shear.

2.4.3 Drained response

Compared with undrained tests, since the effective stress paths can be positively controlled in drained tests, the stress-strain relationship and deformation mechanism can be better established by performing drained experiments (Tong et al. 2010). Drained experiments where principal stress axes rotated with other stress parameters including the deviatoric stress q, effective mean stress p' and intermediate principal stress parameter b remaining constant, were performed successfully by Miura et al. (1986), Symes et al. (1982, 1988), Sayao (1989), Vaid et al. (1990), Gutierrez et al. (1991), Wijewickreme and Vaid (1993), Joer et al. (1998). The variables investigated in these studies included the relative density, the initial major principal stress direction, the rotation direction of principal stress axes and the deviatoric stress level. The main findings from these studies can be concluded as follows:

a) Despite the values of the magnitudes of effective principal stresses kept constant, accumulation of both volumetric contractions and shear distortions can be induced by the rotation of principal stress axes alone.

b) The relative density, the effective mean normal stress, and the deviatoric stress ratio have significant effects on the deformation behaviour of sands under the rotation of principal stress axes. In general, the deformation generates more rapidly in relatively loose samples. Similarly, for a given density, larger deformations result at higher levels of deviatoric stress and effective mean normal stress.

c) The magnitude of the deformation depended highly on the initial major principal stress direction and the rotation direction, which indicates that the effects of the initial fabric of specimen on the deformation characteristics under the principal stress axes rotation are significant.

d) The flow of sands under principal stress axes' rotation is depended on the stress increment direction as well as on the shear stress level. The mechanical behaviour of granular soil is generally non-coaxial under principal stress rotation. The shear stress level has a significant effect on the non-coaxiality. The higher the shear stress level, the lower the degree of non-coaxiality could be induced.

However, the rotation of principal stress axes was restricted to a narrow range in the above studies. Cyclic drained rotational shear test with complete rotation over the full range of 90° was successfully performed by Miura et al. (1986) in a hollow cylinder apparatus (200 mm H, 100 mm OD and 60 mm ID). The dense Toyoura sand sample was prepared by Multiple Sieving Pluviation method. After isotropically consolidation, drained rotational shear test with b = 0.5 and p' = 98kPa was performed on sands at stress ratio of 0.5. In the test, specimens were subjected to 7 cycles rotations.

Figure 2-34 shows the evolutions of the volumetric strain ε_v at different number of cycles for rotational shear test. A positive value along the vertical axis indicates contraction and the negative indicates dilation. Consistent with the results of previous studies reported, contractive volumetric strain was accumulated due to the rotation of principal stress axis and significant volumetric strain occurs during the first cycle and its accumulation rate tends to decrease as the number of cycles increases.

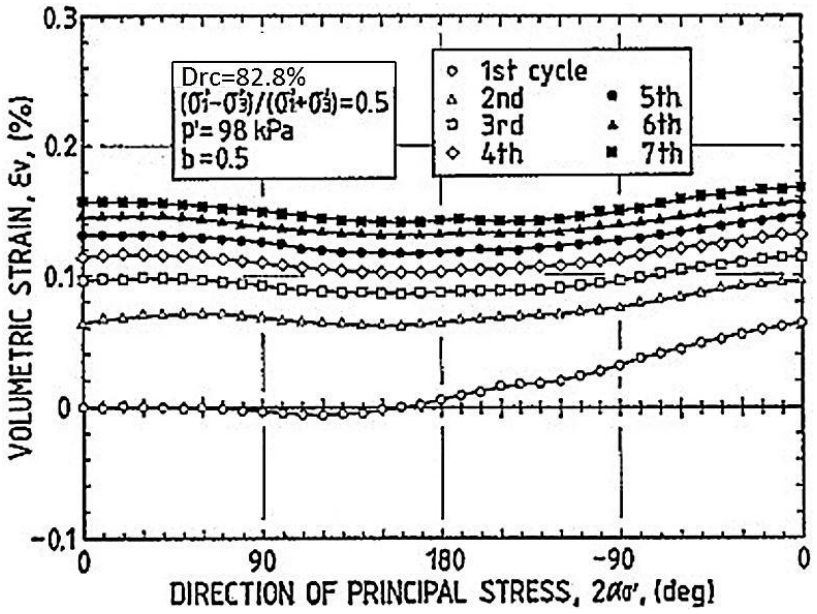

Figure 2-34: Volume change characteristics under the rotation of principal stress axes (Miura et al. 1986).

Shown in Figure 2-35 are the strain increment vectors superimposed on the stress space for the rotational shear test at the first cycle and the magnitude of strain increment at different number of cycle is shown in Figure 2-36. Similar to the results reported from undrained rotational shear test by Ishihara and Towhata (1983) apparent non-coaxiality between the directions of strain increment and stress can be observed in Figure 2-35. Moreover, from Figure 2-36, it can be seen that the magnitude of strain increment has two peaks appear at $2\alpha_\sigma$ = 60° and -150° respectively and a common manner of variation can be observed at different number

of cycle's rotation. The author thus concluded that the initial fabric formed during deposition has a profound influence on the deformation characteristics of soils and the effects cannot be erased by the rotation of principal stress axes.

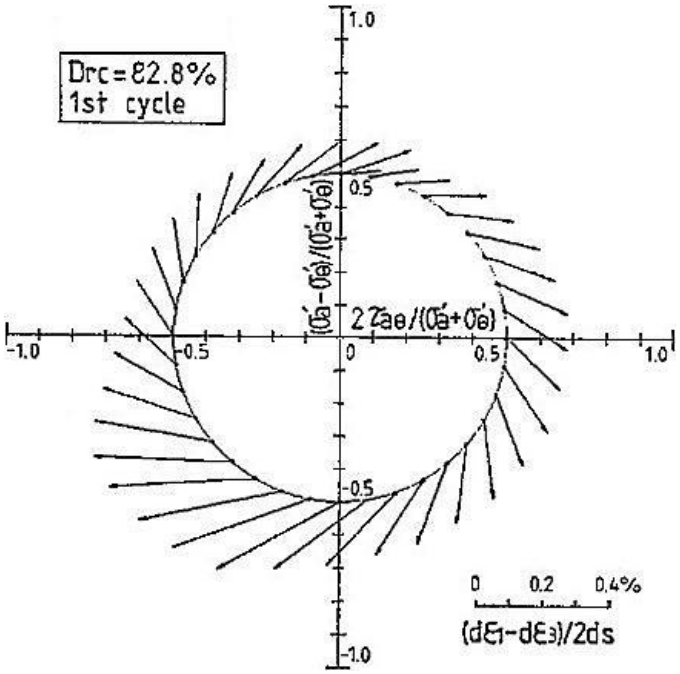

Figure 2-35: Strain increment vectors superimposed on the stress space (Miura et al. 1986).

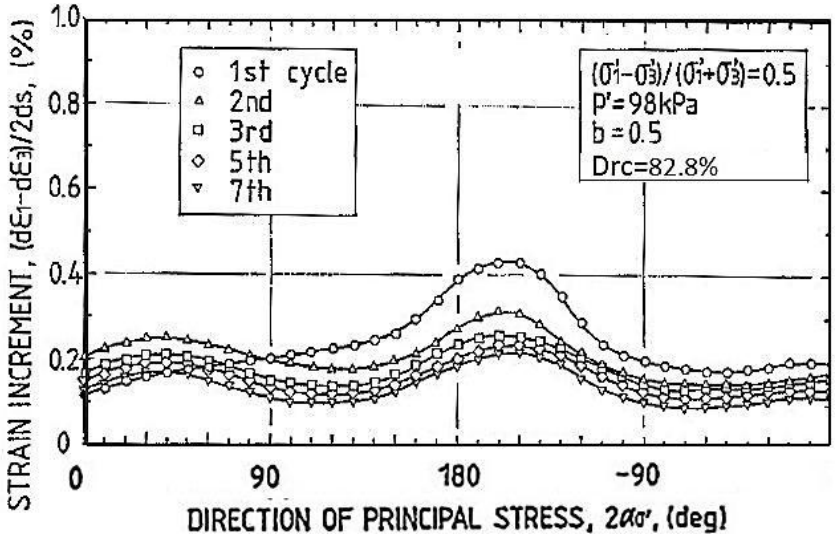

Figure 2-36: Strain increment against the direction of principal stress axes (Miura et al. 1986).

More recently, Tong et al. (2010) carried out a series of tests using a hollow cylinder apparatus (314mm H, 200mm OD and 150mm ID) to investigate the drained behaviour of Toyoura sand, subjected to rotation of the principal stress axes. Samples were formed by air pluviation method and a total of 12 tests were conducted with three b values (b = 0.1, 0.5 and 1.0) at various conditions. The specimens were first isotropically consolidated to p' = 100 kPa and then subjected to cyclic rotation of principal stress axes with fixed value of b, p' and q.

The evolutions of the volumetric strain ε_v with the increasing number of cycles for rotational shear tests are shown in Figure 2-37. Contractive volumetric strain was accumulated with oscillation characteristics. Similar to Miura (1986)'s findings, most of the volumetric strain occurs during the first few cycles and its accumulation rate tends to decrease as the number of cycles increases. Compare tests with different b values, it can be seen clearly that the effects of b on the development of the volumetric strain are significant. The amount of the volumetric strain at the same number of cycles increases with the increase in b and the accumulated volumetric strain under b = 1.0 is much higher than that under b = 0.1. Since the volumetric strain in drained tests is related to the excess porewater pressure in undrained tests, the above results coincide with the experimental findings of Yang et al. (2007) that the rate of pore pressure generation under the condition b = 0 was much slower than that under the conditions b = 0.5 and b = 1.0.

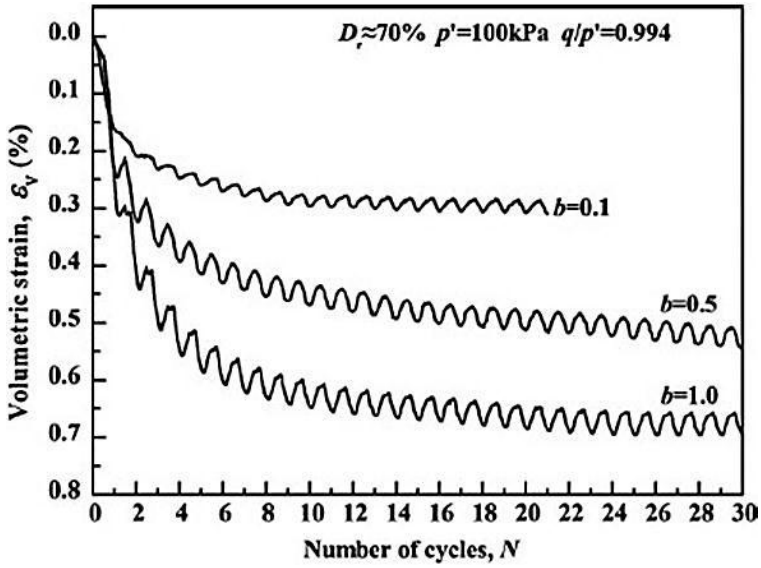

Figure 2-37: Development of the volumetric strain with number of cycles (Tong et al. 2010).

Figure 2-38 presents strain increment vectors superimposed on the stress space for the test at number of cycles $N = 2$ under the value of $b = 0.5$. It can be seen that the strain increment differs significantly in different sections, which is quite different from Miura (1986)'s observations. When the principal stress axes rotate along the stress paths of DE and FC, the amount of shear strain increment is small. The sand sample seems to behave elastically as the strain increment direction almost coincides with the stress increment direction. However, when the principal stress axes rotate along the stress paths of CD and EF, the amount of shear strain increment is large and the obvious noncoaxiality between the directions of the strain increment and stress is induced. However, as it can be seen from the figure, due to the limitation of the testing apparatus the stress paths of DE and CF are not truly circular. It means that constant deviatoric stress was not maintained when the principal stress axis rotated along the stress paths in these two sections.

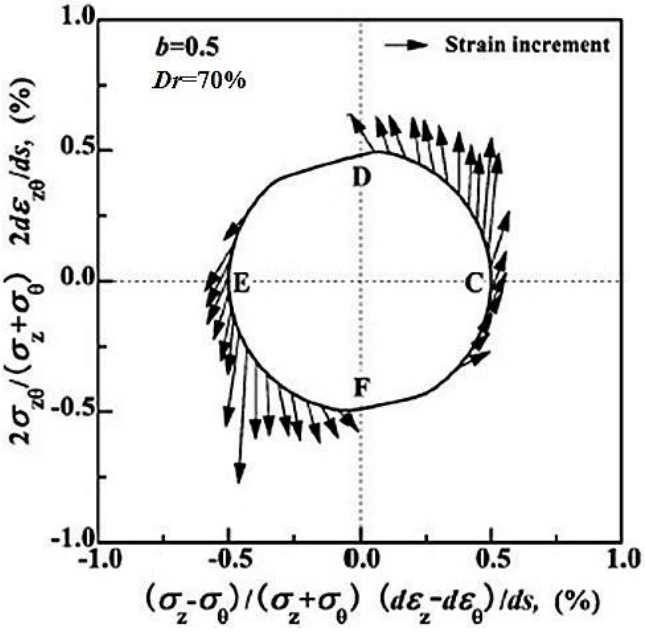

Figure 2-38: Strain increment vectors superimposed on the stress space (Tong et al. 2010).

Figure 2-39 shows the variation of noncoaxiality degree for tests with different b values at second and tenth cycle. It can be found that the angle of noncoaxiality β almost lies in the range of 20° – 40° and tends to decrease when α_σ rotates from 0° to 45° and from 90° to 135°, respectively. Meanwhile, during the first several cycles such as N = 2, β tends to decrease with the increase in b. However, with the increasing number of cycles, the effects of b on β are not significant.

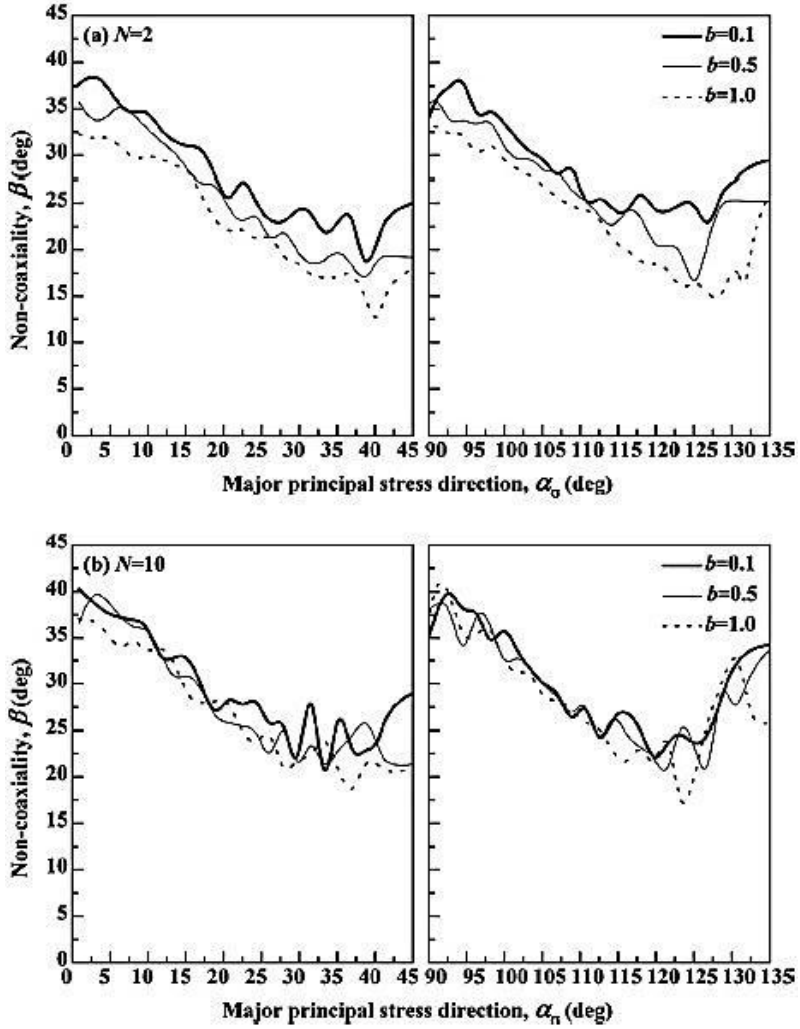

Figure 2-39: Variation in noncoaxiality degree with major principal stress direction for tests with different *b* values at (a): *N* = 2; and (b) *N* = 10 (Tong et al. 2010).

Numerical tests performed by Li and Yu (2009) using 2D discrete element method (DEM) also indicated that principal stress axes' rotation resulted in contraction of granular materials and the material behaviour is more contractive during stress rotation than that in unidirectional shearing. Based on the knowledge of internal structure and its evolution, they found that the internal material structure rotates together with the rotation of principal stress axes, accompanied by the deformation components normal to the stress direction. Hence, the material behaviour is non-coaxial.

2.5 Experimental Devices that have been used to Study Soil Anisotropy

2.5.1 Introduction

The study of soil mechanics relies fundamentally on the assessment of soil behaviour by means of laboratory testing. In order to study the entire anisotropic deformation and strength characteristics of geomaterials, it is necessary to have a device that allows the monitor and independent control not only of the magnitude of the three principal stresses but also of the inclination of the major principal stress axis. Driven by the need to investigate the anisotropic behaviour of granular soils under generalized stress space, different laboratory testing devices (e.g., torsional triaxial device, hollow cylinder triaxial device, simple shear apparatus, directional shear cell (DSC) and hollow cylinder apparatus (HCA)) have been developed throughout the years. However, the only device suitable for general stress path in which four stress components (e.g., σ_1, σ_2, σ_3 and α) can be independently controlled is the HCA. Because of its versatility, HCA are becoming an increasingly popular research tool in conducting fundamental research on soil behaviour under generalized stress conditions.

2.5.2 Devices to study soil anisotropy

In the torsional triaxial devices three-dimensional stress states can be achieved by applying a torsional load T_h to the end platens of standard triaxial specimens. Independent control of axial load, cell pressure and torque about the vertical axis (Figure 2-40) allows loading with different magnitudes of the three principal stresses

(Ishihara and Li, 1972). With this configuration, σ_1 and σ_3 simultaneously rotate in the vertical plane normal to the radial direction. The rotation angle, α, is a direct function of σ_1, σ_2, and σ_3, thus cannot be independently controlled. The main criticism against the use of torsional triaxial devices lies on the non-uniformities of the torsional shear stresses and strains in the horizontal cross section of the specimen.

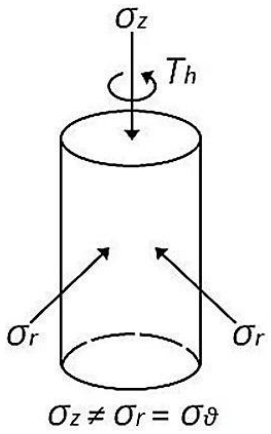

Figure 2-40: Schematic representation of torsional triaxial devices.

The non-uniformities of stresses and strains in torsional triaxial devices can be greatly reduced in a triaxial torsion shear device as shown in Figure 2-41 (Ishihara and Towhata, 1983). However, the stress condition suffered from limitations in that the inner and outer cell pressures could not be independently controlled. For this condition ($p_i = p_o$) it can be shown that the relationship between intermediate principal stress parameter, *b* and the orientation of the major principal stress to the vertical, *a*, is $b = sin^2\alpha$. Consequently, independent control of the four stress parameters (*p*, *q*, *b* and α) cannot be achieved.

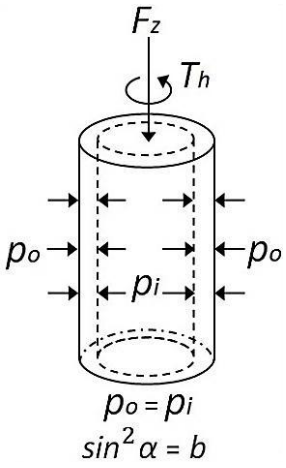

Figure 2-41: Schematic representation of triaxial torsion shear device.

Another shear device that imposes continuous rotation of principal stresses under plane strain conditions is the simple shear apparatus (Figure 2-42). However, it suffers from the lack of compensating shear stress components on the lateral boundaries and nonuniformities in stress and strain distributions (e.g., Saada and Townsend 1981; Pradhan et al. 1988). In addition, principal stress directions and magnitudes are neither known nor controlled. The device is therefore not suitable for fundamental investigations of the effects of principal stress rotations on soil behaviour.

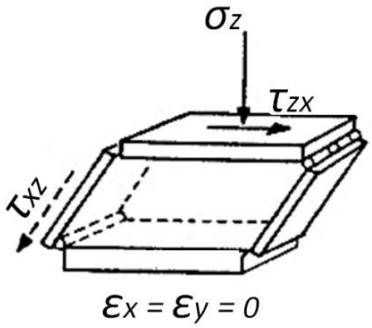

Figure 2-42: Schematic representation of simple shear device.

In an attempt to overcome the limitations of simple shear devices, Arthur et al. (1977) developed the directional shear cell (DSC). In this device, normal and shear stresses can be independently controlled on four faces of a cubical specimen (Figure 2-43).

These stresses are applied through flexible membranes (pressure bags and shear sheets), while nominal plane strain conditions are maintained by having the specimen constrained between smooth rigid end platens on the other two faces. Thus, the distribution of stresses can be expected to be reasonably uniform. However it suffers the problem of low stress level ($\sigma_3' \leq$ 14kPa) due to the limited capacity of the membranes that apply the stresses. At this low confining stress, relatively large dilative volumetric strains and high friction angles can be exerted. In addition, the strain measurements are quite difficult in the DSC, because of the specimen flexible boundaries.

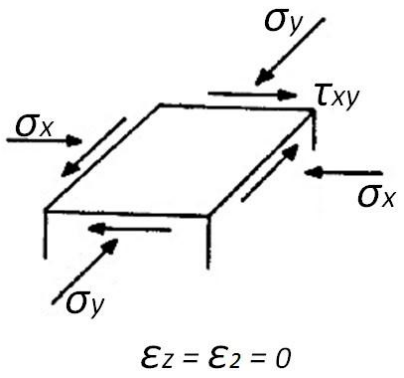

Figure 2-43: Schematic representation of DSC.

Some researchers (Duncan and Seed 1965; Arthur and Phillips 1975; Oda et al. 1978; Wong and Arthur 1985) attempted to simulate the effects of an inclined major principal stress direction relative to bedding plane by preparing specimens in a tilting mould. However, this technique or approach has limitations in apparatuses such as plane strain, true triaxial and simple shear, as the direction of the major principal stress cannot be varied during the test.

Plane strain, simple shear, true triaxial and directional shear cell devices also often have the limitation of not allowing control of the drainage conditions. Tests can be

performed drained on either dry or submerged samples, but undrained tests can only be achieved by rapid shearing of low-draining materials or by simulating constant volume conditions, which is not particularly accurate if small strain stiffness measurements are important.

Hollow cylinder devices (Figure 2-44) allow the independent control of the three principal stresses and the inclination of the major principal stress axis. When each of these stresses can be controlled independently, both the principal stress direction, α, and the relative magnitude of the intermediate principal stress, b, can be controlled. It is also possible to control (or measure) the pore water pressure and apply back pressure, so that drainage conditions can be controlled and both drained and undrained tests can be performed. As a result, the HCA offers an opportunity of extending the stress path approach to include simulation of both principal stress rotation and variation in intermediate principal stress, as well as conducting fundamental research into the effect of principal stress rotation under a reasonably generalized stress state.

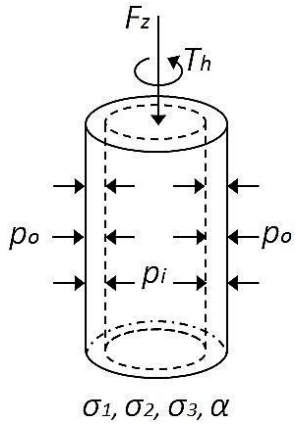

Figure 2-44: Schematic representation of HCA.

The main disadvantages that have been attributed to the HCA are related to stress and strain non-uniformities induced by end-restraint and sample curvature. As suggested

by many researchers (e.g., Hight et al. 1983; Sayao and Vaid 1991; Reinaldo 2003) that these stress non-uniformities can be greatly minimized by a suitable design of specimen dimensions and by avoiding certain stress paths. This subject is analyzed in detail in the next section.

2.5.3 Hollow cylinder apparatus (HCA)

2.5.3.1 Stress and strain calculations

As shown in Figure 2-45a, the loading on the hollow cylindrical specimen consisted of an axial force, *F*, torque, M_T, outer cell pressure, p_o and inner cell pressure, p_i. The magnitudes of these loads are all controlled in an independent manner. The axial force, *F*, develops an axial stress, σ_z; the torque M_T contributes to shear stresses, $\tau_{\theta z}$ and $\tau_{z\theta}$, in vertical and horizontal planes; Differences between p_o and p_i establish a gradient of radial stress, σ_r, across the cylinder wall. The circumferential stress, σ_θ, will then be different from σ_r as shown by the equation for radial equilibrium (Hight et al. 1983),

$$\sigma_\theta - \sigma_r = r\frac{d\sigma_r}{dr} \tag{2-5}$$

where: *r* is the radial distance to a point in the hollow cylinder, $d\sigma_r$ is the radial and stress increment. When $p_i = p_o$, σ_r becomes identical to σ_θ.

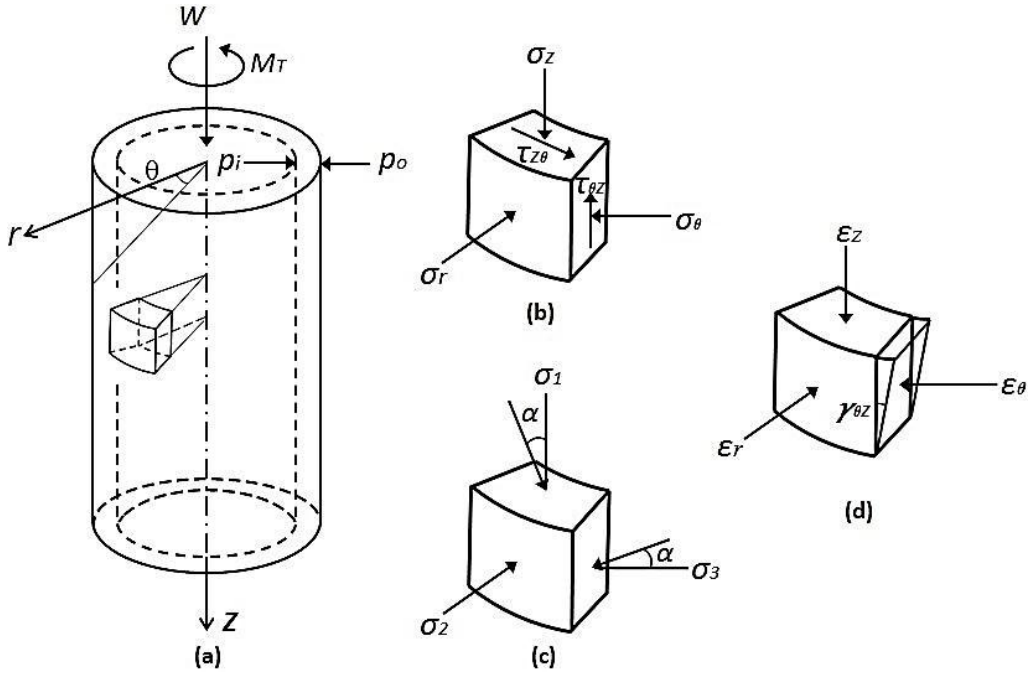

Figure 2-45: Idealized stress and strain components within the HCA: (a) hollow cylinder specimen subjected to axial load, *W*, torque, M_T, internal pressure, P_i, and external pressure, P_o; (b) element component stresses; (c) element component strains; (d) element principal stresses.

Since the stresses are not uniformly distributed across the sample wall especially when unequal inner and outer cell pressures are used, it is necessary to compute average values. The equations used to calculate the average stresses, $\bar{\sigma}_z$, $\bar{\sigma}_r$, $\bar{\sigma}_\theta$, and $\bar{\tau}_{\theta z}$, suggested by Hight (1983) are given as follows,

$$\bar{\sigma}_z = \frac{W}{\pi(r_o^{\,2} - r_i^{\,2})} + \frac{P_0 r_o^{\,2} - P_i r_i^{\,2}}{r_o^{\,2} - r_i^{\,2}} \tag{2-6}$$

$$\bar{\sigma}_r = \frac{P_o r_o + P_i r_i}{r_o + r_i} \tag{2-7}$$

$$\bar{\sigma}_\theta = \frac{P_o r_o - P_i r_i}{r_o - r_i} \tag{2-8}$$

$$\bar{\tau}_{\theta z} = \frac{3M_T}{2\pi(r_o^{\,3} - r_i^{\,3})} \tag{2-9}$$

where: r_o and r_i are the outer and inner radius of the hollow cylindrical specimen.

However, it needs to be noted that only σ_z is not dependent on the material constitutive law and is obtained by equilibrium considerations only. The remaining stress components correspond to the assumption of a linear elastic isotropic material. The expressions for σ_r, σ_θ and $\tau_{\theta z}$ used above are obtained by averaging over the volume of the specimen.

When the four stress components are applied on an element in the wall of the hollow cylindrical specimen, the major principal stress, σ_1, intermediate principal stress, σ_2, and minor principal stress, σ_3, (Figure 2-45c) can thus be derived as follows,

$$\sigma_1 = \frac{\sigma_z + \sigma_\theta}{2} + \sqrt{\left(\frac{\sigma_z - \sigma_\theta}{2}\right)^2 + \tau_{\theta z}^2} \tag{2-10}$$

$$\sigma_2 = \sigma_r \tag{2-11}$$

$$\sigma_3 = \frac{\sigma_z + \sigma_\theta}{2} - \sqrt{\left(\frac{\sigma_z - \sigma_\theta}{2}\right)^2 + \tau_{\theta z}^2} \tag{2-12}$$

Equivalently, the stress state of the specimen can also be expressed by four independent parameters namely: the deviatoric stress, *q*, mean stress, *p*, intermediate principal stress parameter, *b*, and inclination of the major principal stress axis, *α*, as defined in the following equations.

$$p = \frac{\sigma_1 + \sigma_2 + \sigma_3}{3} \tag{2-13}$$

$$q = \sqrt{\frac{1}{2}\left\{(\sigma_1 - \sigma_2)^2 + (\sigma_2 - \sigma_3)^2 + (\sigma_1 - \sigma_3)^2\right\}} \tag{2-14}$$

$$b = \frac{\sigma_2 - \sigma_3}{\sigma_1 - \sigma_3} \tag{2-15}$$

$$\alpha = \frac{1}{2}\tan^{-1}\left(\frac{2\tau_{\theta z}}{\sigma_z - \sigma_\theta}\right) \tag{2-16}$$

Correspondingly, the deformation of a sand element is expressed by axial strain, $\bar{\varepsilon}_z$, radial strain, $\bar{\varepsilon}_r$, circumferential strain, $\bar{\varepsilon}_\theta$, and shear strain, $\bar{\gamma}_{\theta z}$ (Figure 2-45d). The average strains are calculated as follows:

$$\bar{\varepsilon}_z = \frac{w}{H} \tag{2-17}$$

$$\bar{\varepsilon}_r = -\frac{u_0 - u_i}{r_o - r_i} \tag{2-18}$$

$$\bar{\varepsilon}_\theta = -\frac{u_0 + u_i}{r_o + r_i} \tag{2-19}$$

$$\bar{\gamma}_{\theta z} = \frac{2\theta(r_o^{\,3} - r_i^{\,3})}{3H(r_o^{\,2} - r_i^{\,2})} \tag{2-20}$$

where: w is the axial deformation of the reference height H, θ is the circumferential angular deformation (measured in radians), u_o and u_i are the radial deformations of the outer and inner wall with initial radii of r_o and r_i respectively (Figure 2-46).

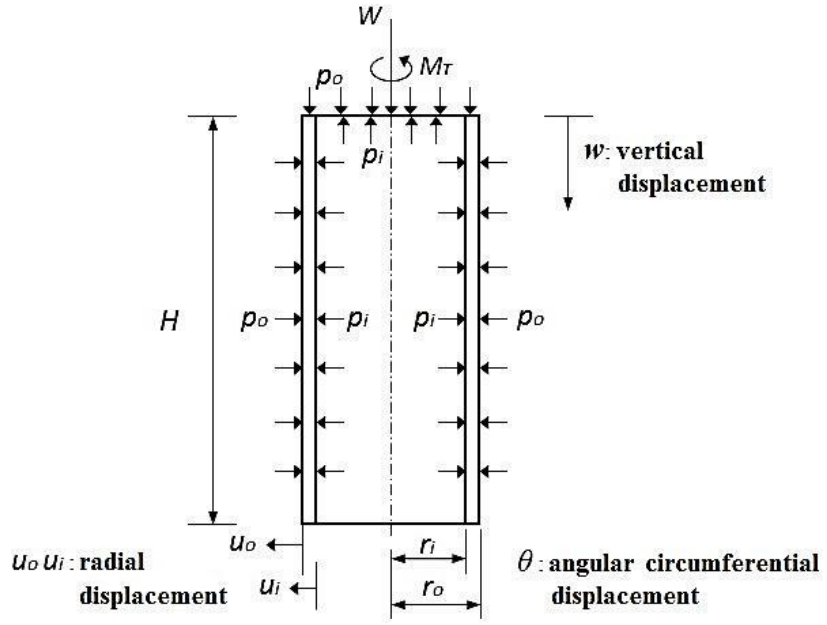

Figure 2-46: Idealized strain conditions in a hollow cylindrical sample (Height, 1983).

It needs to be noted that as mentioned by Height (1983), since the average values of ε_z and $\gamma_{\theta z}$ are based on strain compatibility only. The expressions for the average strains are valid and independent of the constitutive law of the material. The average values of ε_r and ε_θ are based on a linear variation of radial displacement across the wall of the specimen.

The major and minor principal strains can be derived from the average strain components as:

$$\varepsilon_1 = \frac{\overline{\varepsilon_z} + \overline{\varepsilon_\theta}}{2} + \sqrt{\left(\frac{\overline{\varepsilon_z} - \overline{\varepsilon_\theta}}{2}\right)^2 + \left(\frac{\overline{\gamma_{\theta z}}}{2}\right)^2} \tag{2-21}$$

$$\varepsilon_2 = \overline{\varepsilon_r} \tag{2-22}$$

$$\varepsilon_3 = \frac{\overline{\varepsilon_z} + \overline{\varepsilon_\theta}}{2} - \sqrt{\left(\frac{\overline{\varepsilon_z} - \overline{\varepsilon_\theta}}{2}\right)^2 + \left(\frac{\overline{\gamma_{\theta z}}}{2}\right)^2} \tag{2-23}$$

The deformation of the specimen is also described by the volumetric strain ε_v and the deviatoric strain ε_q as given in the following equations.

$$\varepsilon_v = \varepsilon_1 + \varepsilon_2 + \varepsilon_3 \tag{2-24}$$

$$\varepsilon_q = \sqrt{\frac{2}{9}\left\{(\varepsilon_1 - \varepsilon_2)^2 + (\varepsilon_2 - \varepsilon_3)^2 + (\varepsilon_3 - \varepsilon_1)^2\right\}} \tag{2-25}$$

The direction of strain increment $\alpha_{d\varepsilon}$ can be calculated from the incremental strain components

$$\alpha_{d\varepsilon} = \frac{1}{2}\tan^{-1}\left(\frac{d\gamma_{\theta z}}{d\varepsilon_z - d\varepsilon_\theta}\right) \tag{2-26}$$

The degree of non-coaxiality β as measured by the deviation between the major principal stress direction and the principal strain increment direction can therefore be calculated

$$\beta = \alpha - \alpha_{d\varepsilon} \tag{2-27}$$

2.5.3.2 Stress non-uniformities in hollow cylinder specimens

The test specimen, which represents a single point under consideration in the ground, must be subject to a reasonably uniform state of effective stress for accurate interpretations of the experimental data (Naughton and O'Kelly 2007). However, in common with other testing devices for shear strength measurement, the HCA has been criticized (e.g. Saada 1988 and Sayao and Vaid 1991) on account of the stress and strain non-uniformities across the wall of the hollow cylinder sample.

In a hollow cylinder sample the degree of stress nonuniformities in the wall depends on the stress state, specimen dimensions and constitutive law of the material (Sayao 1989). The axial stress σ_z is usually assumed uniform. However, the other three stress components σ_r, σ_θ and $\tau_{\theta z}$ will all vary across the wall for generalized loading conditions when either torque or different internal and external pressures are applied. Torque applied through rigid platens leads to variations in $\tau_{\theta z}$ across the wall, while differences between p_o and p_i give rise to variations of σ_r and σ_θ across the wall. As mentioned by Reinaldo (2003), the sources of these non-uniformities can be summarized as follows:

a) The end restraints generated by the rough end platens.
b) The rigid confinement of the upper and lower boundaries of the specimen.
c) The wall curvature whenever the stress paths require the application of a torque or different inner and outer cell pressures that act across the wall thickness.

By using the two-dimensional axisymmetric models with either linear elastic or strain-hardening Modified Cam-Clay constitutive laws, Hight et al. (1983) investigated stress non-uniformities due to the application of torque and differences in the inner and outer cell pressures. A non-uniform coefficient β_3 as showing in the following expression was defined by the authors in order to quantify the level of non-uniformity across the hollow cylinder wall

$$\beta_3 = \frac{\int_a^b \left| \sigma(r) - \overline{\sigma}^* \right| dr}{(r_o - r_i)\sigma_L} \tag{2-28}$$

where: $\overline{\sigma}^*$ is the true average from the distribution of stress across the wall of the sample, σ_L is a measure of the average stress level, taken as $(|\sigma_r|+|\sigma_\theta|)/2$, $\sigma(r)$ is the distribution of the stress across the wall of the sample, r_i and r_o are the inner and outer radius respectively.

Figure 2-47 shows the definitions used for stress non-uniformity. Combined with the expression 2-28, it can be seen that β_3 is a measure of the average of the absolute values of the differences between the stress distribution and the real average. According to Hight et al., the magnitude of β_3 is dependent on the stress state, specimen dimensions and constitutive law of the material. Similar definitions can be used to evaluate the level of strain non-uniformities.

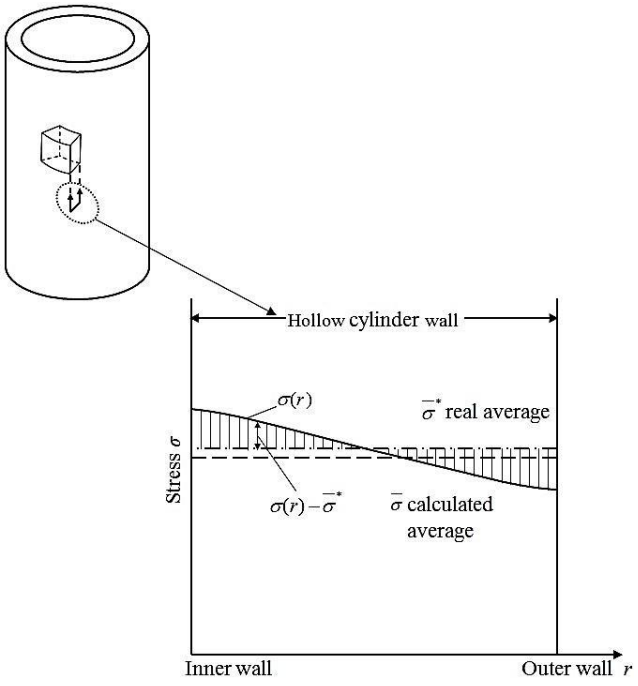

Figure 2-47: Definitions used for stress non-uniformity (Hight et al. 1983).

Hence, Hight et al. defined 'no-go' regions in *q*, *b*, α space within which stress non-uniformities were considered unacceptable. Figure 2-48 shows a schematic

representation of such 'no go' regions. The level of stress non-uniformity was considered acceptable if $\beta_3 < 0.11$. In order to satisfy such criteria, the ratio of outer to inner cell pressures was restricted to the range $0.9 < p_0 / p_i < 1.2$.

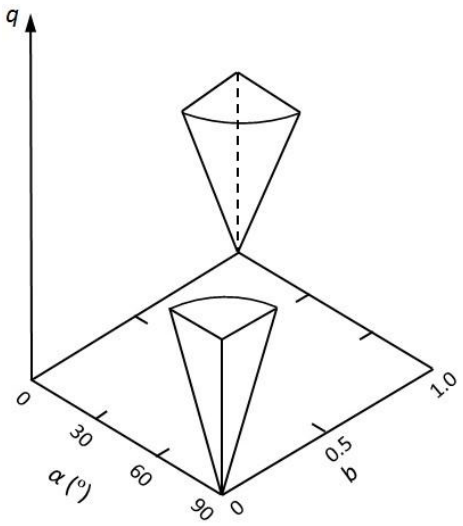

Figure 2-48: Regions where unacceptable stress non-uniformity may arise (Hight et al. 1983).

However, Sayao and Vaid (1991) argued that the approach of acceptable level of non-uniformity in individual stress components without considering the shear stress $\tau_{\theta z}$ is not satisfactory. It can lead to serious and unacceptable non-uniformities in the distribution of stress ratio R ($R = \sigma_1' / \sigma_3'$) across the specimen wall. Hence, a different stress non-uniformity parameter across the wall of the specimen in terms of the stress ratio R was proposed as flows:

$$\beta_R = \frac{R_{max} - R_{\min}}{\overline{R}} \tag{2-29}$$

where: R_{max} and R_{min} are the maximum and minimum stress ratio respectively and $\overline{R}$ is the average value of stress ratios.

Figure 2-49 shows a comparison of the two definitions of non-uniformities for two stress states (b = 0.5, α = 0) and (b = 0, α = 45°). The specimens had an outer radius of 7.1cm and an inner radius of 5.1cm. It can be seen that both β_R and β_3 increase with R. If stress nonuniformities were assessed in terms of β_3, full range of R levels could be explored. However, in terms of β_R, unacceptable nonuniformities occur for R in excess of about 2.0 to 2.2 for the specimen geometry under consideration. The authors suggested that the stress non-uniformities were considered acceptable if the maximum difference between R_{max} and R_{av} was below 10%, which corresponds to a value $\beta_R \leq 20\%$. In order to keep the non-uniformities levels acceptable, they also recommended keeping the stress ratio R < 2.5. Shown in the Figure 2-50 is a schematic representation of a new 'no-go' regions in q, b, α space suggested by Sayao and Vaid.

The influence of specimen geometry has also been profoundly studied by Sayao and Vaid. Based on both practical and theoretical considerations of limiting stress nonuniformities to acceptable levels, they suggested the following criteria for the specimen geometry:

a) Wall thickness: $20\text{mm} \leq r_o - r_i \leq 60$ mm

b) Inner radius: $0.65 \leq r_i / r_o \leq 0.82$

c) Height: $1.8 \leq \text{H}/2\, r_o \leq 2.2$

The geometry of the hollow cylindrical specimens used in this study meets criteria a) and c), and is just outside the recommendation b). Thus, the dimensions of the specimens tested in this study were assumed to be acceptable.

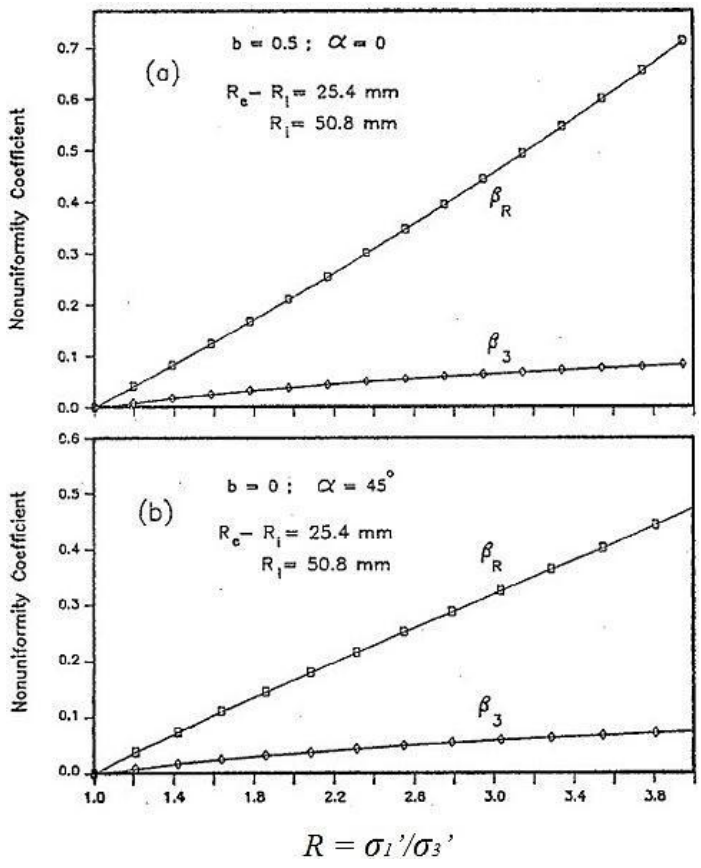

Figure 2-49: Effect of stress ratio level on non-uniformity coefficients (Sayao and vaid 1991).

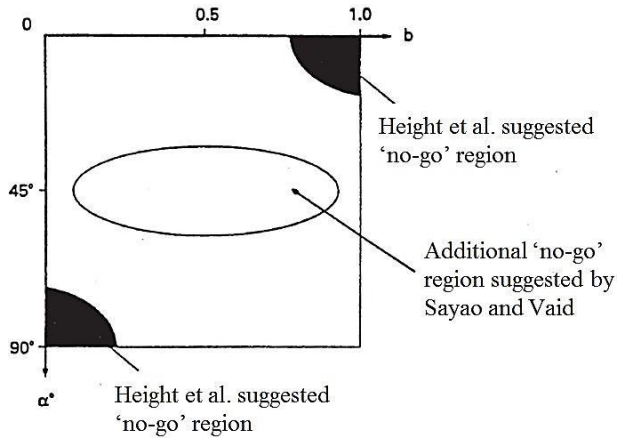

Figure 2-50: Additional "no-go" areas proposed by Sayao & Vaid (1991).

Using an isotropic linear elastic analysis and applying Sayao and Vaid's criteria, Naughton and O'Kelly (2007) studied the stress distribution in sand specimens with the dimension of 200 mm H, 100 mm OD and 71 mm ID. The level of stress non-

uniformity, quantified in terms of the stress non-uniformity coefficient β_R, was found to be acceptable for R < 1.5 throughout the stress space with β_R < 20%. Same as Height et al.'s results, the ratio of the confining pressures was limited within the range $0.9 < p_0 / p_i < 1.2$. Figure 2-51 shows the 'no-go' regions in R, b, α space suggested by Naughton and O'Kelly (2007). In the present study, this condition was well satisfied, and in this respect the non-uniformity is considered less significant.

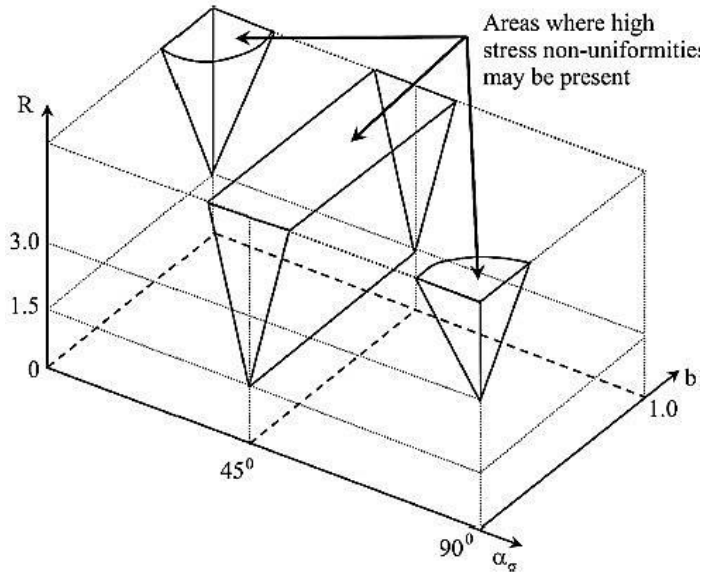

Figure 2-51: Areas where unacceptable stress non-uniformity may arise (Naughton and O'Kelly 2007).

By a thorough review of the previous studies on the stress non-uniformities in hollow cylinder specimens (e.g. Hight et al. 1983; Gens and Potts 1984; Sayao and Vaid 1991; Wijewickreme and Vaid 1991; Menkiti 1995; and Porovic 1995), Reinaldo (2003) summarized that the most severe cases of non-uniformities is confined to the space where the difference between p_0 and p_i is large. The assessment of the stress non-uniformities depends highly on the assumed soil model. The stress non-uniformity seems to be overestimated in all the linear elastic analyses and in the non-linear elastic analyses the level of stress non-uniformity increases with increasing stress ratio for

free-ends samples. But elastic-plastic analyses show that it decreases as yielding is approached. And with regard to the sample geometry, it concluded that for a given diameter, increasing the sample's wall thickness increases the level of non-uniformity. For a fixed wall thickness, increasing the inner and outer diameters decreases the level of non-uniformity. An aspect ratio of H/OD $\geq$ 1.8 was suggested to provide end restraint free conditions.

2.5.3.3 Membrane penetration (MP) errors

Hollow cylinder tests on granular soils are often carried out on specimens enclosed between outer and inner rubber membranes. Since thin rubber membranes have very low flexural stiffness, the membrane penetration (MP) is caused mainly by the intrusion of the membrane into the peripheral voids of a granular specimen. As shown schematically in Figure 2-52, under loading paths involving changes in effective confining stress, the penetration of the membrane into (or withdrawal out of) the interstices of the granular soil specimen causes a systematic error in the measured excess pore pressures in undrained tests (Figure 2-52 (b)) or volume changes in drained tests (Figure 2-52(c)). A systematic error in measured volume changes results in errors when the actual inner and outer dimensions of the hollow cylindrical specimen are calculated form measured volume changes of the specimen itself and the inner bore cavity (Naughton and O'Kelly 2003).

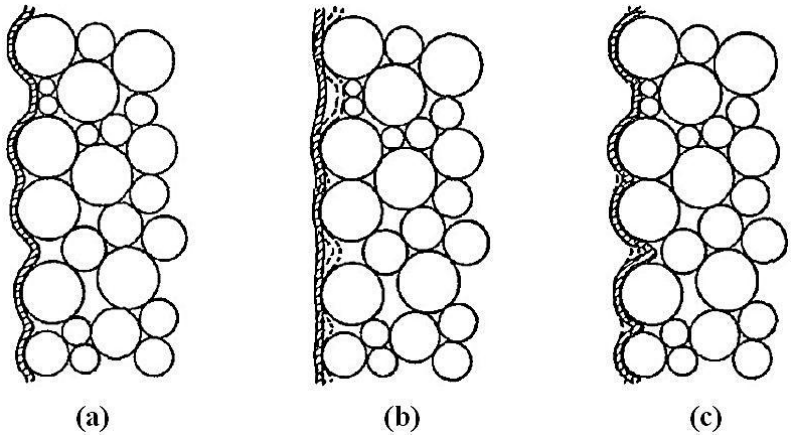

Figure 2-52: Deformed shape of membrane: (a) at end of consolidation; (b) during undrained test with increasing porewater pressure; (c) during drained test with increasing cell pressure (Kramer et al. 1990).

In order to make a confident assessment of actual stress-strain behaviour of saturated granular materials in a test, extensive experimental and theoretical investigations on the membrane penetration have been carried out throughout the years (Newland and Allely 1959; Duncan and Seed 1965; Tokimatsu and Nakamura 1986; Ohara and Yamamoto 1991; Molenkamp and Luger 1981; Baldi and Nova 1984; Kramer and Sivaneswaran 1990; Miura and Kawamura 1996; Sivathayalan and Vaid 1998; Kuwano 1999; Naughton and O'Kelly 2003). In general, the researchers found that the particle size is one of the most important factors in determining the membrane penetrability. For materials of medium sand size having mean particle size of $D_{50} \geq$ 0.1mm, correction for the MP is of great importance (Molenkamp and Luger 1981). On the other hand, membrane penetration depends strongly on the value of the effective lateral stress σ_3. The curve of MP versus the magnitude of σ_3 is concave downward (Baldi and Nova 1984). It has also been suggested that the effect of MP, however, is difficult to eliminate despite its great significance. It has to be evaluated, therefore, to be applied as a correction, or eliminated or reduced to a convenient level (Miura and Kawamura 1996).

For the MP correction, Kuwano (1999) suggested the following equation to calculate the apparent volumetric strains due to MP over the vertical sides of the samples ε_{MP}:

$$\varepsilon_{MP} = \frac{A_{MP} \cdot v_{MP}}{V_{soil}} \tag{2-30}$$

Where: ε_{MP} are volumetric strains due to MP over the vertical sides of the sample, A_{MP} is the surface area of membrane (in mm), v_{MP} is the unit membrane penetration (in mm) and V_{soil} is the volume of soil specimen (in mm^3).

Theoretical equations for the unit membrane penetration suggested by Baldi and Nova (1984) and Kramer and Sivaneswaran (1989) are as following:

$$A_{MP} \cdot v_{MP} = \frac{1}{2}\frac{d}{D} V_{soil} \left(\frac{\sigma_h' d}{E_m t_m} \right)^{\frac{1}{3}} \tag{2-31}$$

$$v_{MP} = 0.395 d (1-\alpha) \left(\frac{1-\alpha}{5 + 64\alpha^2 + 80\alpha^4} \right)^{\frac{1}{3}} \left(\frac{\sigma_h' d}{E_m t_m} \right)^{\frac{1}{3}} \tag{2-32}$$

$$\alpha = 0.15 \left(\frac{\sigma_h' d}{E_m t_m} \right)^{0.34} \tag{2-33}$$

where: d is the mean particle size D_{50} (in *mm*), D is the specimen diameter (in mm), E_m is the Young's modulus of membrane (in kN/m^2), t_m is the thickness of membrane (in mm) and σ'_h is the effective confining pressure (in kPa).

A new approach for the assessment of MP was obtained from the differences between measured volume strain of the specimen and the volume of the inner chamber using a

single hollow cylindrical specimen under hydrostatic loading by Sivathayalan and Vaid (1998). The proposed expression for the unit membrane penetration is:

$$\varepsilon_m = \frac{\Delta V_r - \Delta V_{ir}(\chi^2 - 1)}{\chi(A_{mi} + A_{me})} \tag{2-34}$$

Where, ε_m is the unit membrane penetration; ΔV_r and ΔV_{ir} are the measured volume changes of the inner chamber and the specimen, respectively, A_{mi} and A_{me} are the inner and outer surface areas of the test specimen covered by the inner and outer membranes, respectively, and χ is the ratio of the outer-to-inner radii of the test specimen.

It was found by Kuwano (1999) that Equation 2-34 matches the expressions suggested by Baldi and Nova (1984) and Kramer and Sivaneswaran (1989) very well. Thus, Equation 2-34 has been used in this study to provide a reasonable prediction of experimental MP errors in the hollow cylindrical specimens.

2.6 Summary

Previous studies clearly show that geomaterials are anisotropic: directional dependency of material behaviour. The anisotropy of soil physical properties is primarily developed as a result of depositional processes and grain characteristics (inherent anisotropy). Subsequent redistribution of particles and interparticle contacts during stress or strain processes results in further anisotropy (induced anisotropy). The engineering properties of the granular soils such as shear strength and deformational characteristics are greatly influenced by their anisotropic properties. As an important aspect of anisotropy of granular materials, non-coaxiality

between the axis of principal stress and that of principal strain increments during plastic deformation has been observed in a large number of laboratory experiments. The microscopic information obtained from numerical simulations suggested that soil fabric and its evolution is the main reason for its non-coaxial behaviour.

In reality, soil sediments are most likely to subject a three-dimensional anisotropic stress state ($\sigma_1 \neq \sigma_2 \neq \sigma_3$), together with rotation of the principal axis. Hence, understanding of stress-strain-strength behaviour of soils in such complex stress states is necessary and important. Although great efforts have recently been made in understanding the effects of principal stress direction α and intermediate principal stress parameter b on granular soils, most experimental tests with varying inclination angle α were mostly conducted either at $b = 0$ or $b \approx 0.5$. Thus combined effects of α and b on soil response is not fully understood. Also, due to the limitations of the testing device, previous studies on the effects of α and b on soil response were all limited to small strains and deformations (pre-peak). Furthermore, most studies on soils undergoing cyclic rotation of principal stress axes have mainly focused on the undrained behaviour of soils. The cyclic behaviour in drained conditions has not attracted as much interest despite its relevance to soil-structure interaction problems. Therefore, more experimental investigation is still needed to provide a better understanding of stress-strain behaviour, failure characteristics and non-coaxiality of granular soils under generalized stress conditions.

The study of soil mechanics relies fundamentally on the assessment of soil behaviour by means of laboratory testing. Several types of apparatuses have been developed that can study different features of the anisotropic soil behaviour. Each device is ideally suitable for investigations of only specific regions of the general stress space and

many of them also present limitations with regard to stress and strain non-uniformities or drainage conditions. For all the devices currently available, the HCA is the only one that offers the possibility of independent control of the three principal stresses and the inclination of the major-minor principal stress axes. Consequently, studies on fundamental behaviour of anisotropic soils under generalized stress conditions can only be performed with HCA. The non-uniformities of stress and strain, which are inherently associated in all testing devices, should be addressed carefully in the application of HCA. Quality assessment of actual stress-strain behaviour of soils in HCA could be achieved only by minimizing these nonuniformities to an acceptable level.

Chapter 3 Methodology

3.1 Introduction

This chapter introduces the testing device used in the research project, as well as the testing materials and procedures used. It begins with a detailed description of the GDS Small-Strain Hollow Cylinder Apparatus (SS-HCA), followed by a brief introduction of the physical properties and particle characteristics of testing materials. The testing procedures, including specimen preparation, saturation and consolidation, as well as the overall testing program designed in this study will then be presented. Finally the chapter demonstrates the preliminary tests carried out to evaluating the performance of the SS-HCA testing system.

3.1.1 General description

In this study, the Small Strain Hollow Cylinder Apparatus (SS-HCA), developed by GDS Instruments Ltd, has been used. It has specifically been designed to be capable of testing at very small axial strains (down to 0.00004%).The device is suitable for controlled stress path testing of reconstituted sand specimens under drained or undrained, monotonic or cyclic stress conditions. The application of axial load *W*, torque M_T, inner cell pressure p_i, outer cell pressure p_o on a hollow cylindrical specimen enables independent control of the magnitudes of the three principal stresses and the rotation of the major-minor principal stress axes. Therefore, a wide range of stress paths can be applied. For the chosen geometry, however, certain regions of

stress space cannot be investigated without significantly compromising stress uniformity, as already discussed in Chapter 2.

The experimental setup and schematic cross section of the SS-HCA used in this study is shown in Figure 3-1 and 3-2 respectively. The cell is used to contain the hollow cylindrical specimen with an inner radius of 30 mm, outer radius of 50 mm and height of 200 mm. The test specimen fixed at the top is laterally confined by internal and external fluid pressures acting on flexible rubber membranes with a thickness of 0.3 mm. Axial load and torque are applied at the bottom of a specimen through the base pedestal. Drainage from the specimen is provided by a drainage line connected to the base pedestal. The loading capacities for the SS-HCA are 12kN of axial load and 200Nm of torque.

A total of ten transducers are used to measure the stress and strain as well as pore pressure in general stress path tests with the SS-HCA device. Test is controlled by means of user friendly software (GDSLAB control and acquisition software) installed in a desktop computer. During the test data are collected stably and quickly without manual operation.

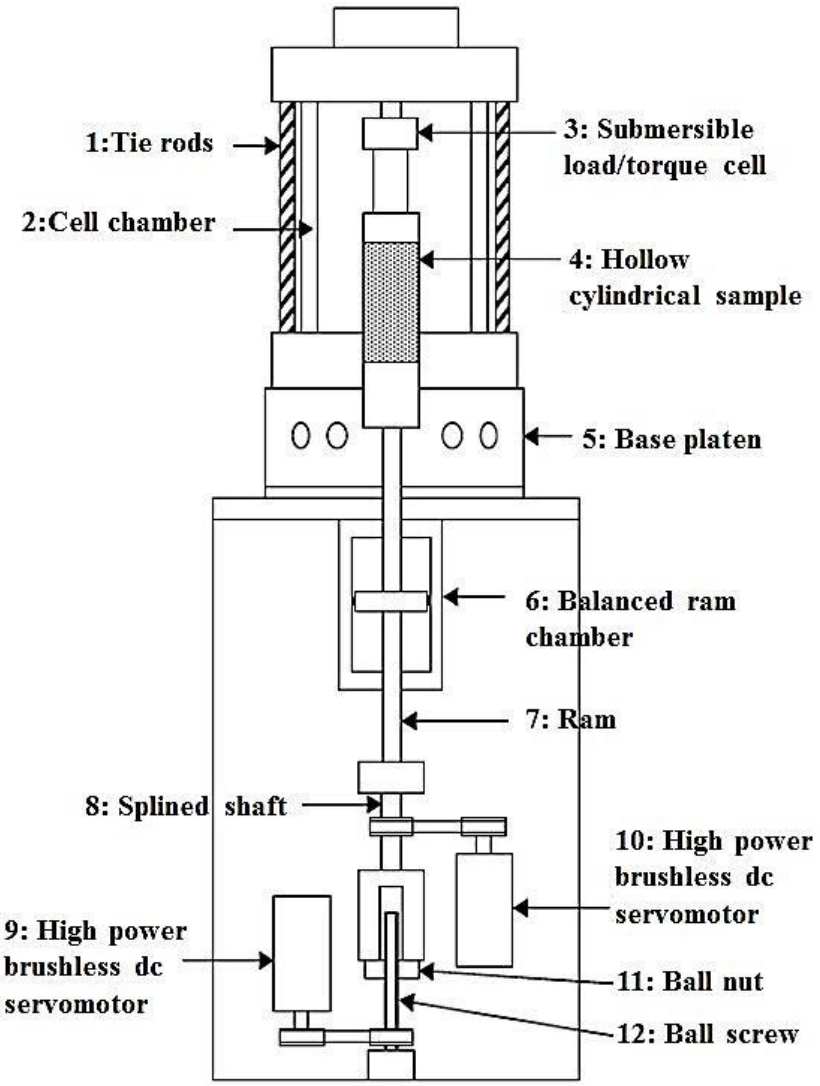

Figure 3-1: Schematic cross section of the SS-HCA (Serra and Hooker 2011).

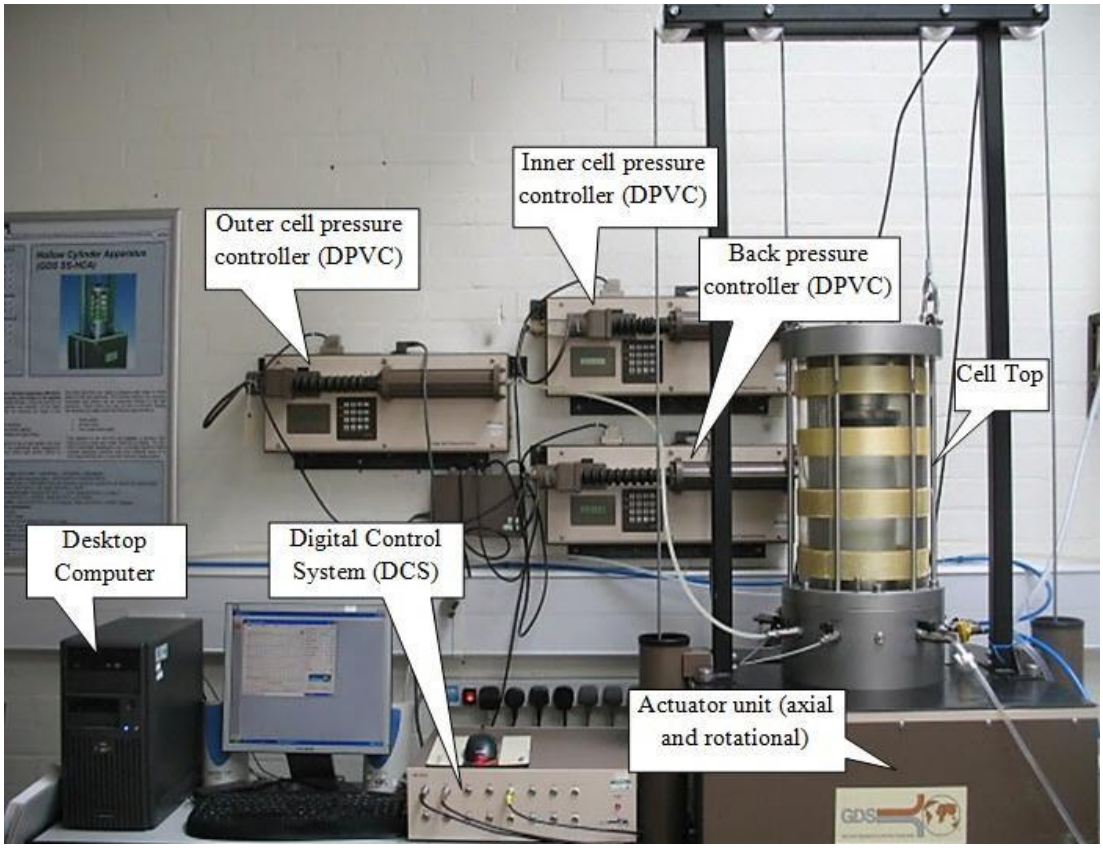

Figure 3-2: Experimental setup of the SS-HCA used in this study.

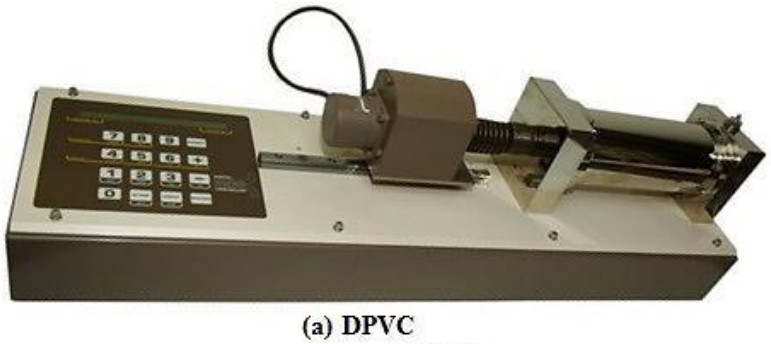

(a) DPVC

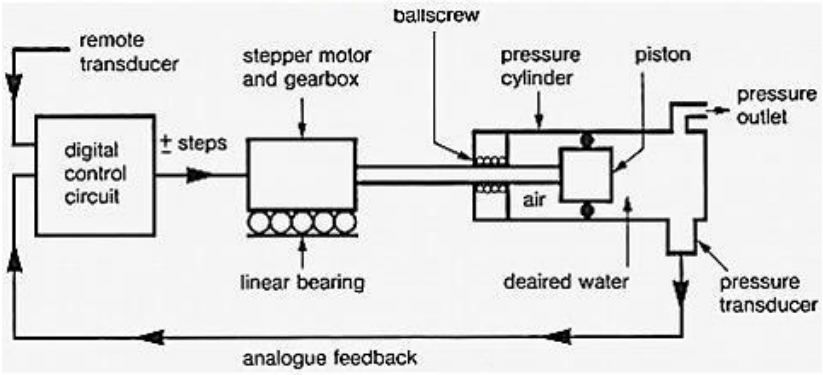

(b) Operational schematic of DPVC

Figure 3-3: The Digital Pressure/Volume Controller: (a) DPVC; (b) Operational schematic of DPVC (Cai, 2010).

3.1.2 Loading and measuring systems

As shown in Figure 3-1 the axial load and displacement is generated by a high power brush servomotor attached to the base of the ball screw. Rotational motion is added to the axial motion by means of the splined shaft. A second servomotor is attached to the splined shaft and is used to generate torque or displacement as required. The axial load and torque are monitored by a submersible load/torque cell attached rigidly to the cell top. Axial and rotational displacements are measured by high quality LVDTs on the load ram. Inner, outer and back pressures together with the volume changes of inner and outer cells and specimen are controlled and measured by three digital pressure/volume controllers (DPVC) of 2 MPa/200cc capacities (see Figure 3-3). Pore pressure is measured using an external pore pressure transducer connected to the base pedestal.

The 'heart' of the SS-HCA system is a 16 bit Digital Control System (DCS), shown in Figure 3-2, connected to the PC via a high speed USB connection, which is used to connect the DPVCs, pore pressure transducer and actuator units. The actuator unit (see Figure 3-2) is used for the control and measurement of torque, angular rotation, axial force and axial displacement of the specimen. The DCS gives a direct closed loop servo control of axial force and displacement as well as torque and angular rotation (Cai, 2010).

The transducer resolutions for axial and rotational measurement are: axial load $\leq$ 0.7N, axial displacement encoder $\leq$ 1μm, and torque $\leq$ 0.008Nm, rotational encoder: $\leq$ 0.00011 degrees. The resolution of pressure measurement is 1kPa on display and 0.1kPa via software, while the resolution of volume measurement is 1mm^3. The accuracy of measurement for the DPVC is shown as the follows: pressure $\leq$ 0.1% full

range, volume ≤ 0.1% measured value with ±20 mm^3 backlash. The key features of the HCA are summarized in Table 3-1.

Table 3-1: Summary of key features of the SS-HCA (Cai, 2010)

Transducer	Type of measurement	Capacity	Resolution	Maximum error* Accuracy
DPVC	Pore and cell pressures	2000kPa	0.1kPa	2kPa 0.1%
	Volume change	200cm^3	0.001cm^3	0.1% +0.02cm^3 back flash 0.1% of volume change
Pore Pressure	Pore pressure	2000kPa	0.1kPa	2kPa 0.1%
Axial	Axial load	12kN	0.0007kN	0.0012kN 0.1%
	Axial displacement	40mm	0.001mm	0.062mm 0.15%
Rotational	Torque	200Nm	0.008Nm	0.220Nm 0.11%
	Rotational displacement	360°	0.00011°	0.206° 0.057%

3.1.3 Test control and data acquisition

The test system is controlled by the user's PC running GDSLAB software. The operator chooses the type of test from a test menu (e.g. dynamic HCA, HCA stress path, advanced loading etc.) and enters the test parameters (e.g. p, q, b, α, and drainage conditions) as well as test termination conditions. The test will then be preceded automatically. It can be used to perform not only a hollow cylinder test but also triaxial and direct shear tests. The transducers can easily be set up with the software. Figure 3-4 shows the object display of the SS-HCA arrangement.

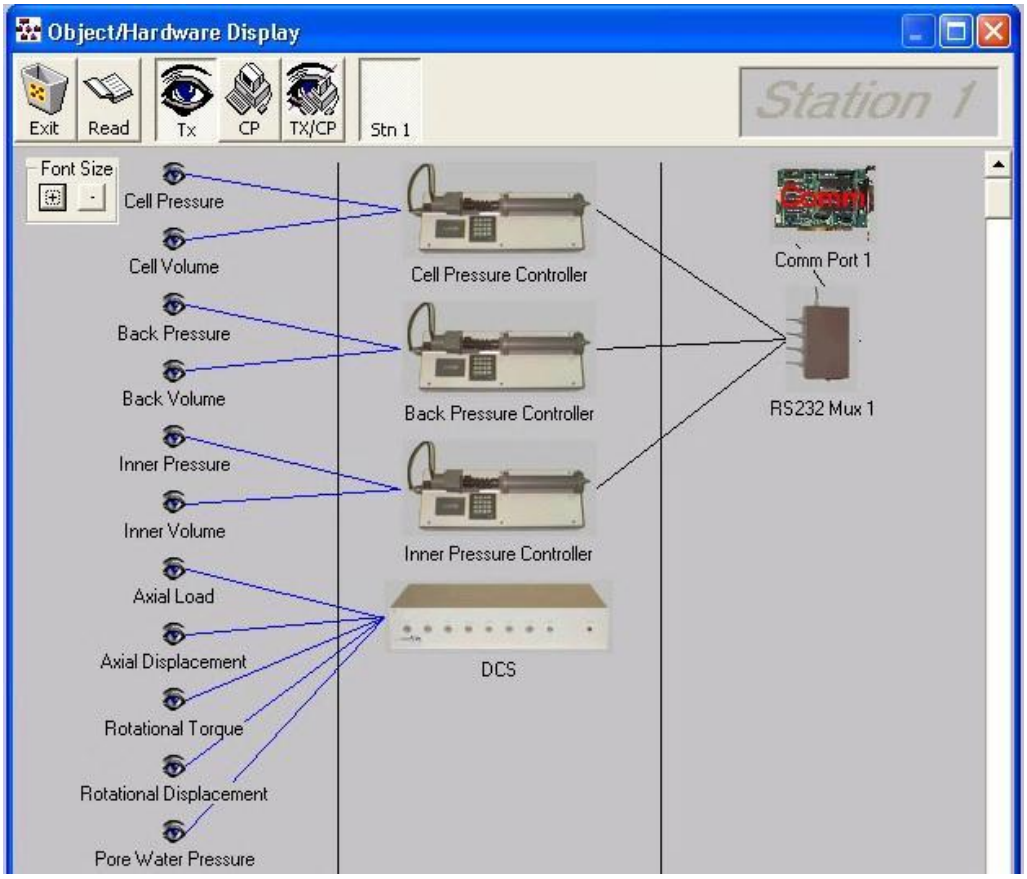

Figure 3-4: Object display showing a GDS SS-HCA arrangement.

There are three default modules for HCA tests used in this study:

a) Advanced Loading. This module independently controls the five principal parameters, i.e. axial control, rotational control, outer cell pressure, inner cell pressure and back pressure. The axial control can be achieved by: axial stress (kPa), axial displacement (mm) or axial load (kN). Rotational control can be achieved by: rotational stress (kPa), rotational load (Nm) or rotational displacement (degs). This loading mode can be used for the saturation and consolidation stages.

b) HCA Stress Path Loading. This module controls the test by four parameters, p, q, b and α and an option for a drained or undrained test is provided.

c) HCA Strain Path Loading. This module provides independent linear control of p, axial displacement, b and α, where q is a passive variable dependent on the applied axial displacement. An option for a drained or undrained test is also provided.

The software records the values measured by all transducers and controllers connected to the system and uses these values to calculate all relevant stresses, strains and displacements. All measured and calculated data can be displayed graphically in real-time on up to three graphs. The user can choose what data is to be displayed before and during a test and change the displaying options at any time. All the raw data and calculated data are saved to a data file in GDS format at any specified time interval.

3.2 Test Materials

3.2.1 Introduction

In this research, Leighton Buzzard (Fraction B) sand and Glass Ballotini were used in the HCA test program. Leighton Buzzard sand was chosen, since the sand has a natural geological origin, comparatively uniform particle size distribution and excellent drainage properties which make it suitable for laboratory investigation to study the mechanics of granular soils. The sand has also been used by many geotechnical researchers in the study of soil anisotropy (Arthur and Menzies 1972; Arthur et al 1977; Height et al. 1983; Naughton and O' Kelly 2003; Cai 2010) Ballotini solid glass balls were used as an analogue soil. Their relatively simple geometry and uniform particle size distribution allowed the influence of particle shape and inter-particle friction to be examined independently. On the other hand, the

application of glass spheres in laboratory test provides ideally comparable data for numerical as well as theoretical modelling of granular materials.

3.2.2 Index properties and particle shapes

Leighton Buzzard sand is quarried in and around Leighton Buzzard, Bedfordshire in the east of England. It is a widely used standard sand consisting of sub-rounded particles and containing mainly quartz with some carbonate materials. Ballotini solid glass balls are produced from high quality and pure soda-lime glass. The unique washing and polishing process does not involve the addition of hydrofluoric acid and thus gives the balls a pure shiny surface without contamination. The maximum and minimum void ratios of the two materials were determined in accordance with the British Standard 1377-4 (1990). The index properties of the two materials are summarized in Table 3-2. The particle size distribution is given in Figure 3-5 and the scanning electron micrograph of the two materials are shown in Figure 3-6.

Table 3-2: Physical properties of Leighton Buzzard sand and Glass Ballotini

Property	Leighton Buzzard Sand	Glass Ballotini
Mean grain size D_{50}: mm	0.62	1.35
Effective grain size D_{10}: mm	0.45	1.15
Uniformity coefficient Cu: D_{60}/ D_{10}	1.56	1.18
Specific gravity G_s	2.65	2.50
Minimum void ratio e_{min}	0.52	0.52
Maximum void ratio e_{max}	0.79	0.68

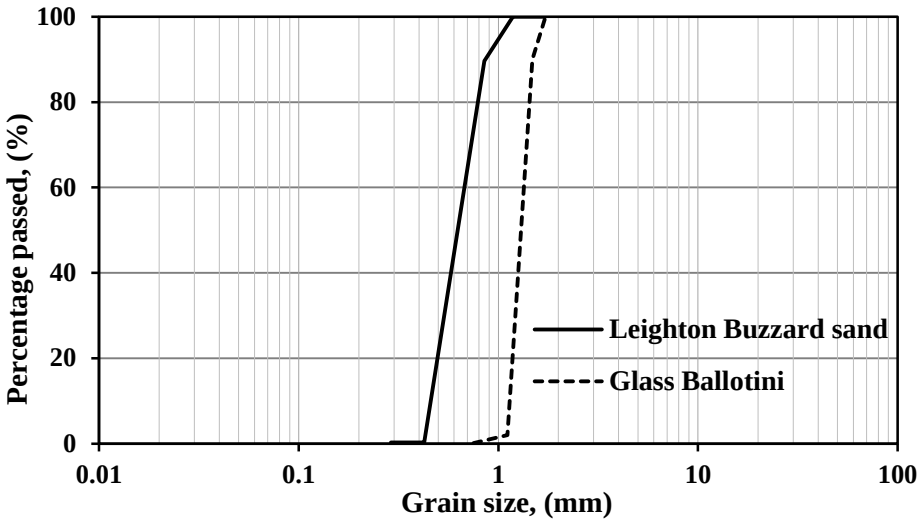

Figure 3-5: Particle size distribution of Leighton Buzzard sand and Glass Ballotini.

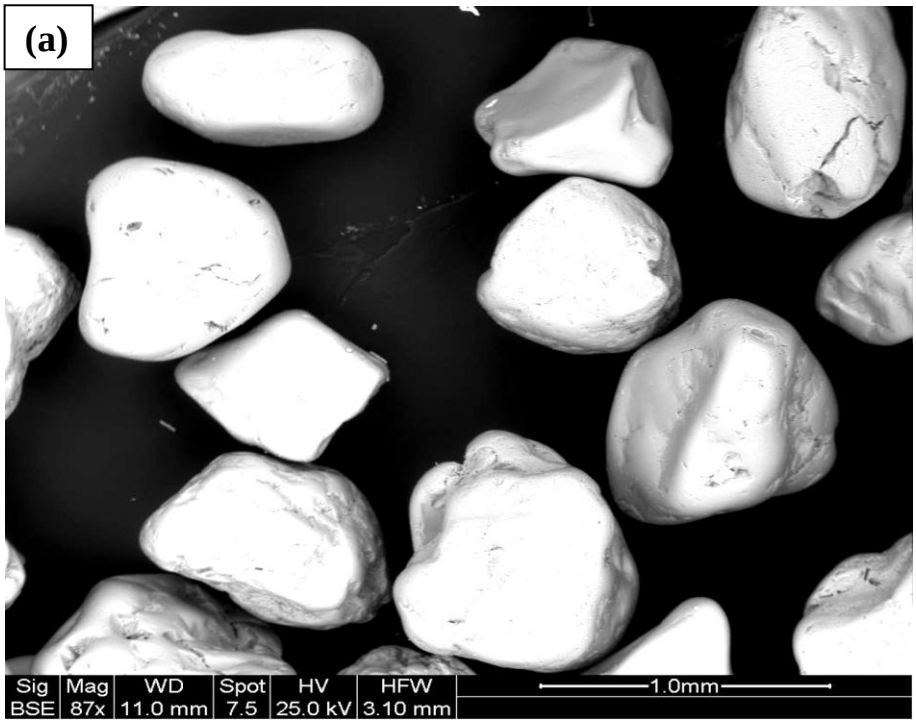

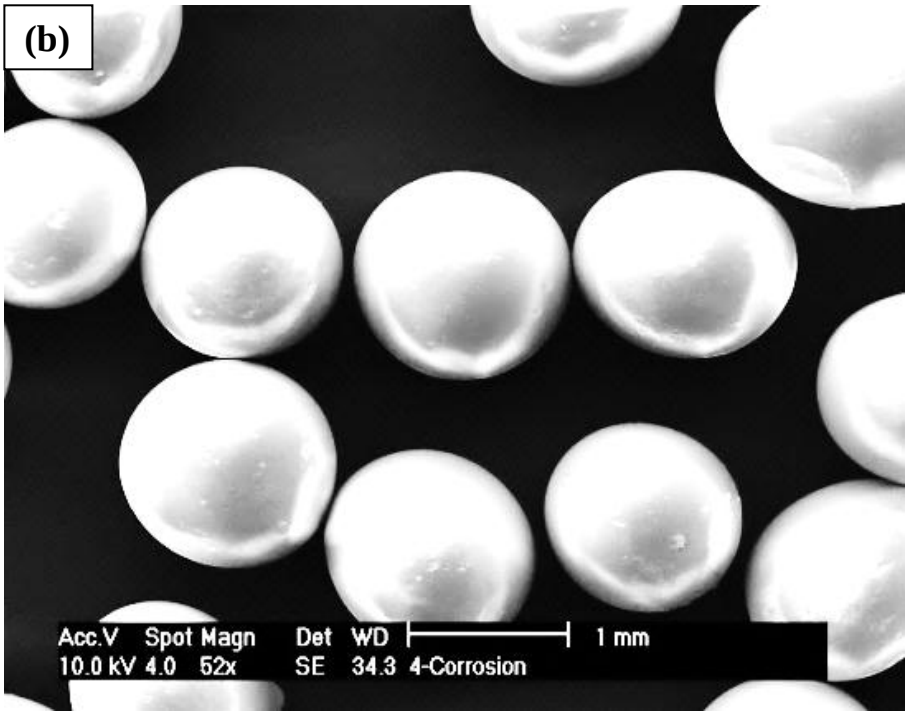

Figure 3-6: Scanning electron micrograph of (a) Leighton Buzzard B sand (Cai 2010) and (b) Glass Ballotini.

3.3 Testing Procedures

3.3.1 Sample preparation

Specific particle arrangements were associated with different depositional conditions and that these structures were closely linked to the subsequent mechanical properties of the soil mass. Numerous studies (Oda 1972a, 1972b; Miura and Toki 1982; Zlatovic and Ishihara 1997; Vaid et al. 1999, Yamamuro et al. 2004; Sadrekarimi and Olson 2012) have reported that the behaviour of sands can be greatly influenced by specimen reconstitution method. Thus, strict adherence to identical specimen preparation technique is central to achieve repeatable test results in the experimental study of soil mechanics.

In this study, the water sedimentation method was adopted to prepare all samples, since it simulates certain natural depositional environments satisfactorily and enables preparation of relatively homogeneous reconstituted sand samples with controlled density (Ishihara 1993).

All the components of the specimen preparation mould are shown in Figure 3-7. Three segments of the outer split mould fixed together with an adjustable steel ring (Figure 3-7(a)), four segments of the inner split mould (Figure 3-7(b)), together with the base pedestal (Figure 3-7(c)), top cap (Figure 3-7(d)) and top cover (Figure 3-7(e)) are used for hollow cylindrical specimen preparation. Flexible latex membranes with thickness of 0.3mm and diameters of 100mm and 60mm (Figure 3-7(f)) are used to enclose the specimen with O-rings.

Figure 3-7: Specimen assembly components: (a) outer split mould; (b) inner split mould; (c) base pedestal; (d) top cap; (e) top cover; (f) Outer and inner membranes.

All samples in this study were prepared according to the following procedures concluded by Cai (2010) (corresponding photos to each step are shown in Figure 3-8):

a) The inner membrane of 60mm in diameter and 300mm in length was put into the bottom of the base pedestal (Figure 3-7(c)) by the clamping ring. Four bolts were used for sealing the inner membrane.

b) The inner split mould (Figure 3-7(b)) was stood on the base supported by the steel bar which was scrolled into the base pedestal.

c) An outer membrane of 100mm in diameter and 300mm in length was put outside the base pedestal using two rubber O-rings.

d) Tubes from the base of the SS-HCA for applying water and drainage to the inner cell and the specimen were connected to the base pedestal (Figure 3.7(c)).

e) The outer mould (Figure 3-7(a)) fixed by the iron ring was assembled on the base pedestal. The outer membrane was then stretched against the mould.

f) A water sedimentation method was used to prepare all the specimens in this study. Water was applied to the cavity between outer and inner membranes to remove the air bubbles from the base pedestal and the specimen. The weighted sand for the required initial relative density was then poured into the cavity through a funnel and distributed uniformly. For denser specimens, the assembly was tapped to compact the sand to a uniform relative density. Water was supplied throughout this step to push out the air from the sand.

g) The top cap shown in Figure 3-7(d) was gently seated on the top of the specimen. And then outer and inner membranes were rolled up around the top cap and sealed with O-rings.

h) The upper drainage tube was connected to the top cap. A suction of 20kPa was imposed to prevent the specimen from collapsing. The inner mould was pulled out by the steel bar shown in Figure 3-7(b). The top cover (Figure 3-7(e)) was positioned on the top cap and tightened using four bolts. The upper drainage tube for the inner cell was connected to the top cover. Then, the whole specimen with the outer mould was seated on the base of the equipment and screwed with four bolts. After this, the outer mould was removed. By adjusting

the angle and axial displacement, the top cover was fixed to the submergible load cell with a very small axial load. After the specimen was set up, the final height and outer diameter of the specimen were measured.

i) The cell chamber was brought down and tightened. The outer and inner cells were filled with water. Then, cell pressures of 20kPa were applied and the suction was removed from the specimen.

j) To ensure a fully saturation of specimen, de-aired water was flushed throughout the specimen to get rid of air. The specimen was then left 12 hours with a back pressure of 400 kPa, outer and inner cell pressures of 420 kPa. The specimen was considered satisfactorily saturated when Skempton's *B*-value was checked to be greater than 0.96.

k) After saturation, outer and inner cell pressures were increased to 600 kPa with constant back pressure of 400 kPa, thus isotropically consolidating the specimen to effective confining pressure p' = 200 kPa.

Figure 3-8: Specimen preparation procedures (Cai, 2010).

3.3.2 Testing program

A testing program was developed with the main objective of studying the drained behaviour of anisotropic sand under generalized stress space. In particular, the anisotropic stress-strain characteristics, non-coaxiality and combined effects of α and b are intended to be studied. Accordingly, three testing programs composed of two main types of stress paths (e.g. monotonic loading with different inclinations of the major principal stress and cyclic rotation of principal stress axes) were planned.

Figure 3-9 illustrates the stress paths in the X-Y stress space for monotonic loading tests with different inclinations of the major principal stress (α = 0°,15°, 30°, 60°, 75°, 90°). During the test, monotonic loading was applied in HCA strain-controlled mode in terms of the axial displacement under drained condition. To ensure full discharge of water from the specimen, the axial strain was increased at a slow rate of 0.05%/min. For α < 45º, specimens were vertically compressed. For α > 45º specimens were vertically extended. However, with α = 45º, sample was neither compressed nor extended. Such a loading path is not included due to technical impossibility. All tests, were controlled so that the value of effective mean principal stress p' = 200 kPa and the value of the intermediate principal stress parameter was maintained. It needs to be noted that due to the limitations of the testing equipment, the value of α cannot be accurately controlled at low levels of deviatoric stress. Therefore, a deviator stress of 15kPa was applied using HCA stress-controlled mode before the rotation of the major principal stress direction was implemented.

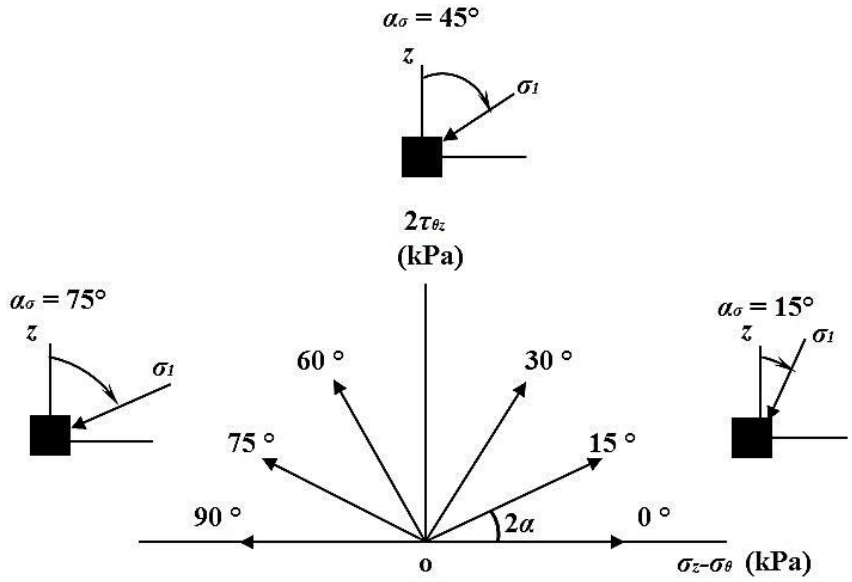

Figure 3-9: Stress paths in the X-Y stress space for monotonic loading tests.

The stress paths in *X-Y* stress space is shown in Figure 3-10. As illustrated in literature 2.2.2. During the tests, samples were first subjected to monotonic shearing in the vertical direction up to a specified stress ratio while keeping the effective mean stress *p'* constant. After that the principal stress axes were rotated counter clockwise (B→C→D→E→B) under drained condition, while keeping the deviatoric stress constant and maintaining the effective mean stress and the intermediate principal stress parameter constant. The loading was applied in HCA stress controlled mode in terms of the four parameters (*p*, *q*, *b* and α). To ensure full discharge of water from the specimen, the major principal stress direction α was rotated at a slow rate of 2°/min. Totally 50 cycles rotation have been conducted for each rotational shear test.

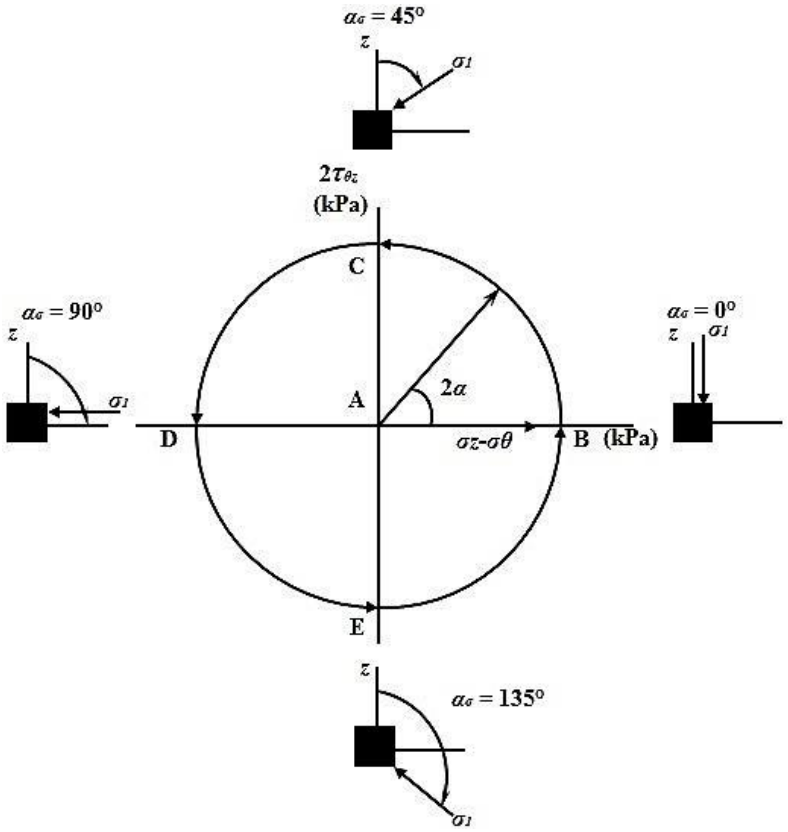

Figure 3-10: Stress paths in the X-Y stress space for rotational shear test.

Three testing programs planned in this study are summarized in Table 3-3 to Table 3-5. As shown in Table 3-3 four series of monotonic shear tests along different loading directions have been carried out using HCA strain path control. The first series of tests were performed on dense Leighton Buzzard sand. The result from this series of tests was used as a reference for comparison. The second series of tests were performed on Glass Ballotini in order to examine the influence of particle shape. The third series of tests performed on loose Leighton Buzzard sand had the purpose to investigate the effects of material density. The fourth series of tests was performed on preloaded specimen, prepared by loading and unloading the dense Leighton Buzzard sand in the deposition direction, with the purpose of investigating the effects of loading history.

Presented in Table 3-4 are the three series of rotational shear tests carried out to investigate the behaviour of sands during cyclic rotation of principal stress directions. The first series of tests has been performed on dense Leighton Buzzard sand. In the tests, samples were subjected to cyclic rotation of principal stress axes at different effective stress ratios. Investigations of the influence of particle shape (Series 2) and the effects of material density (Series 3) have also been conducted in this testing program.

Shown in Table 3-5 are the tests carried out on dense Leighton Buzzard sand. The emphasis of this testing program was placed on the effects of the intermediate principal stress, characterised by different *b* values, under the two stress paths as described above. Each serial covered two *b* values, b = 0.2 and 1.0. Combined with tests at b = 0.5 in testing program I and II. There are three *b* values, b = 0.2, b = 0.5 and b = 1.0 been investigated.

All the tests described above were performed under fully drained condition, with an effective confining pressure p' = 200 kPa. To reduce the non-uniformity, it has been suggested by previous researchers (Hight 1993; Naughton and O'Kelly 2007) the outer and inner cell pressures have been limited to a range of $0.9 < p_o / p_i < 1.2$. In the present study, this condition was well satisfied, and in this respect the non-uniformity is considered less significant.

Table 3-3: Summary of the Testing Program I

EFFECTS OF LOADING DIRECTION ON THE BEHAVIOUR OF GRANULAR SOIL IN MONOTONIC SHEARE			
Series 1 Dense Leighton Buzzard sand	Initial relative density, D_{ri}: %	Principal stress direction (º)	Principal stress parameter, b
	70	0	0.5
	70	15	0.5
	70	30	0.5
	70	60	0.5
	70	70	0.5
	70	90	0.5
Series 2 Glass Ballotini	Initial relative density, D_{ri}: %	Principal stress direction (º)	Principal stress parameter, b
	74	0	0.5
	74	15	0.5
	74	30	0.5
	74	60	0.5
	74	75	0.5
	74	90	0.5
Series 3 Medium dense Leighton Buzzard sand	Initial relative density, D_{ri}: %	Principal stress direction (º)	Principal stress parameter, b
	37	0	0.5
	37	15	0.5
	37	30	0.5
	37	60	0.5
	37	75	0.5
	37	90	0.5
Series 4 Pre-shearing	Initial relative density, D_{ri}: %	Principal stress direction (º)	Principal stress parameter, b
	70	0	0.5
	70	15	0.5
	70	30	0.5
	70	60	0.5
	70	70	0.5
	70	90	0.5

Table 3-4: Summary of the Testing Program II

BEHAVIOUR OF GRANULAR SOIL DURING ROTATIONAL SHEAR			
Series 1 Different stress level	Initial relative density, D_{ri}: %	Stress ratio, η	Principal stress parameter, b
	70	0.60	0.5
	70	0.70	0.5
	70	0.80	0.5
	70	0.90	0.5
	70	0.93	0.5
	70	0.95	0.5
	70	0.97	0.5
	70	1.02	0.5
	70	1.10	0.5
Series 2 Glass Ballotini	74	0.70	0.5
Series3 Medium dense Leighton Buzzard sand	Initial relative density, D_{ri}: %	Stress ratio, η	Principal stress parameter, b
	30	0.70	0.5

Table 3-5: Summary of the Testing Program III

EFFECTS OF INTERMEDIATE PRINCIPAL STRESS ON THE SOIL BEHAVIOUR			
Series 1 Monotonic loading	Initial relative density, D_{ri}: %	Principal stress direction (º)	Principal stress parameter, b
	70	0	0.2
	70	15	0.2
	70	30	0.2
	70	60	0.2
	70	75	0.2
	70	90	0.2
	70	0	1.0
	70	15	1.0
	70	30	1.0
	70	60	1.0
	70	75	1.0
	70	90	1.0
Series 2 Rotational Shear	Initial relative density, D_{ri}: %	Stress ratio, η	Principal stress parameter, b
	70	0.70	0.2
	70	0.70	1.0

3.4 Equipment Evaluation

3.4.1 Reliability of test result

The prerequisite for the use of SS-HCA was to prove its ability to duplicate results obtained with other testing devices. A series of preliminary experiments was then designed with the purpose to validate the reliability of the SS-HCA testing result. Four triaxial compression tests on dense Leighton Buzzard (Fraction B) sand were carried out in SS-HCA and Triaxial Device. A summary of the tests is given in Table 3-6. HCA-100 and HCA-300 denote conventional triaxial compression tests performed in SS-HCA with constant confining pressure σ_3 = 100kPa and 300kPa respectively. TC-200 was conducted at σ_3 = 200kPa using a conventional Triaxial Device with a cylinder specimen dimension of 50mm×100mm ($\Phi \times H$). HCA-SP represents the triaxial compression test performed in SS-HCA with constant effective confining pressure p' = 200kPa. The purpose of this series of tests was to verify the measurement of strength parameters in SS-HCA. Therefore, the comparison was focused on stress paths and friction angles. Comparative results using the two test devices are presented in Table 3-6 and Figure 3-11. It can be seen from the table that vary little difference in the values of stress ratio $(q/p')_f$ and friction angle φ_f was obtained from the four tests. From Figure 3-11 it can be observed that very consistent result in terms of failure line were obtained from the three HCA tests with different stress paths. Also, it can be seen that the failure point of TC-200 agreed well with the failure line obtained from HCA tests.

Table 3-6: Summary of the triaxial tests

Test No.	e_c	D_{rc} (%)	σ'_3 (kPa)	p'_f (kPa)	q_f (kPa)	$(q/p')_f$	φ_f (°)
HCA-100	0.584	76.3	100	228.6	332.7	1.46	33.5
HCA-300	0.582	77.1	300	612.7	881.1	1.44	35.4
HCA-SP	0.584	76.3	200	199.9	288.2	1.44	34.2
TC-200	0.583	76.7	200	406.1	589.6	1.45	35.8

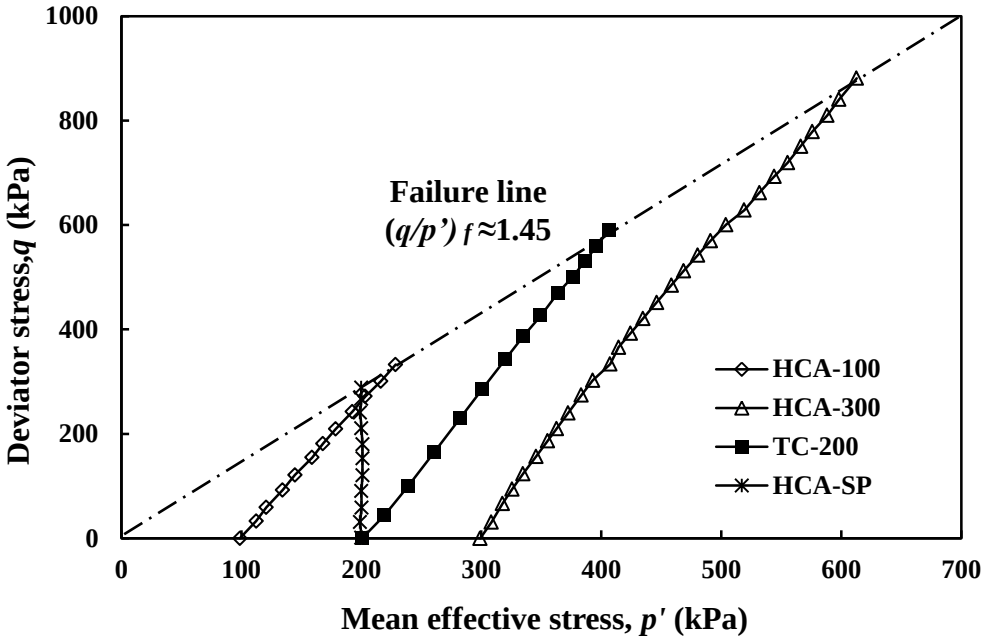

Figure 3-11: Stress paths of triaxial tests obtained from HCA and triaxial cell.

3.4.2 Stress path control

Simultaneous and independent control of four stress parameters (p, q, b and α) is required for general stress path tests with the SS-HCA. In order to follow the prescribed stress path precisely, smooth change in the controlling loads and pressures must be assured.

The performance of the control system is demonstrated in Figures 3-12 to 3-17 by a typical stress path test. In this test, an isotropically consolidated dense Leighton Buzzard sand (D_{rc} = 74.5%) specimen was loaded under cyclic rotation of principal stress axes with p' = 200kPa, q = 200kPa and b = 0 maintained constant. Figure 3-12

and Figure 3-13 show variation of the applied inner and outer cell pressures and the vertical load and torque against the number of cycles. The computed average values of stress components σ_z, σ_r, σ_θ, $\tau_{\theta z}$ are shown in Figure 3-14. In the test the four loads were independently controlled so that the magnitudes of the principal stresses were maintained constant but the direction of the major principal stress α was rotated continuously (Figure 3-15). In each cycle of rotation α was varied from 0° to 180° (Figure 3-16). The stress path plotted in the *X*-*Y* stress space is shown in Figure 3-17.

It is clear from the figures that all the stress parameters were smoothly varied during the test. The maximum excursion in any of the stress parameters *p*, *q* and *b*, from the prescribed constant values was noted to be less than 1%. Close agreement between the desired and the actual stress path shows the excellent capability of the automatic control system for carrying out generalized stress path tests.

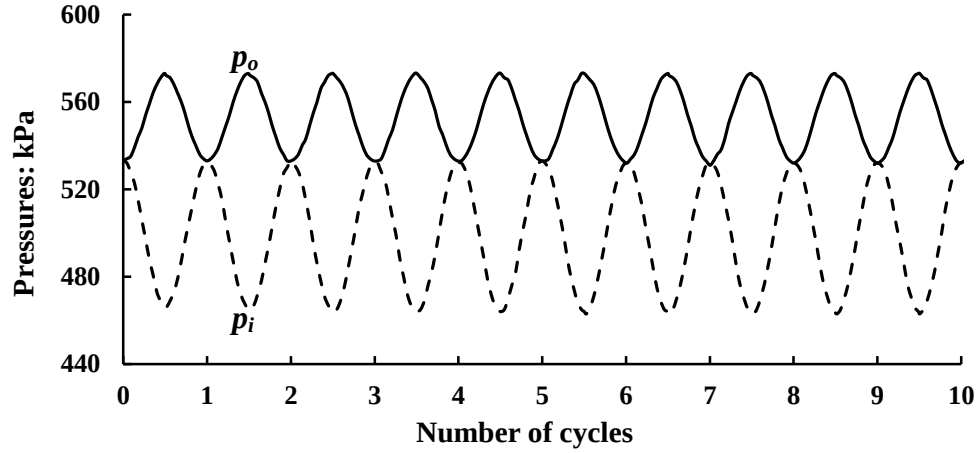

Figure 3-12: Variation of outer and inner cell pressures.

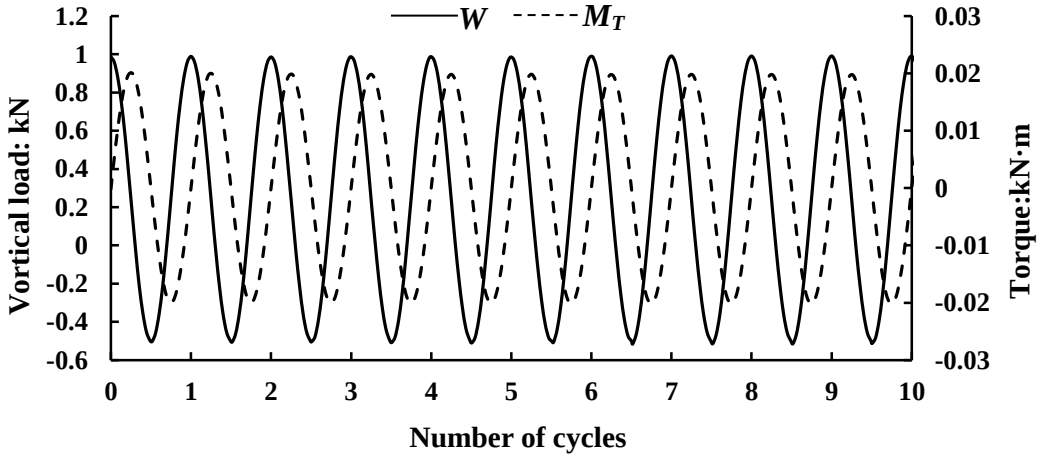

Figure 3-13: Variation of vertical load and torque.

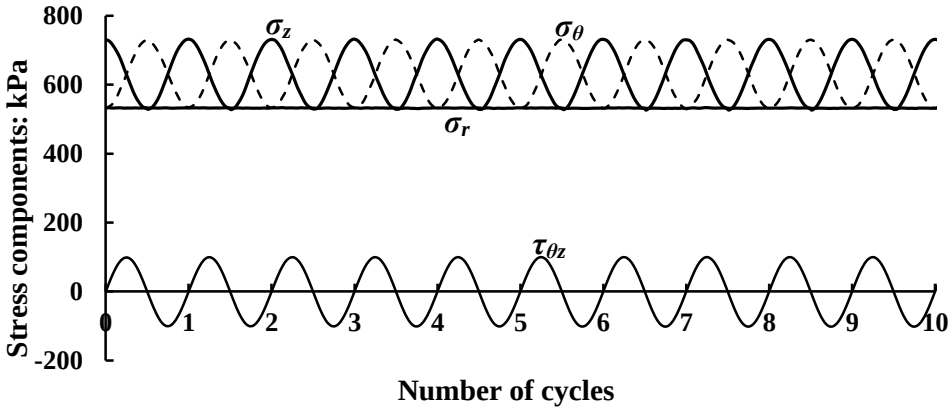

Figure 3-14: Variation of stress components.

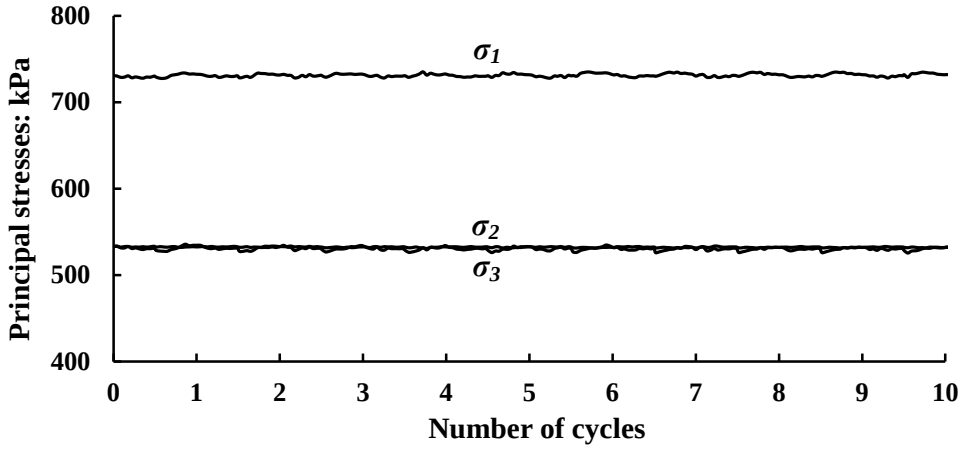

Figure 3-15: Magnitude of principal stresses.

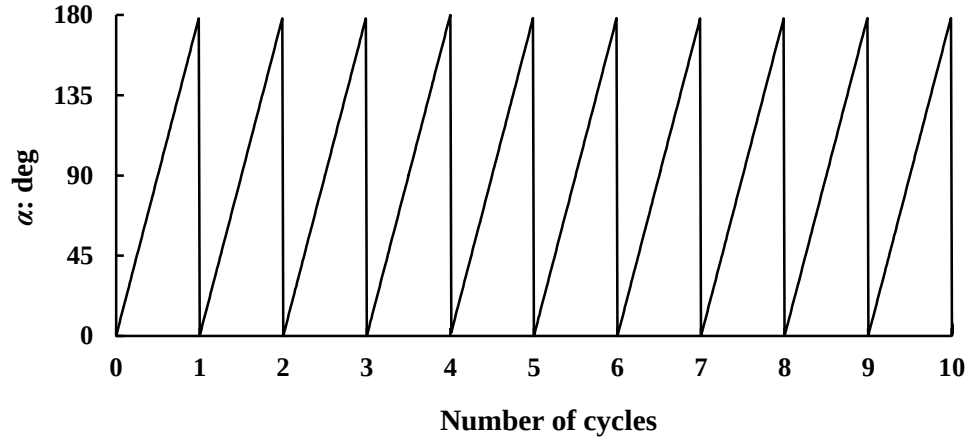

Figure 3-16: Direction of the major principal stress.

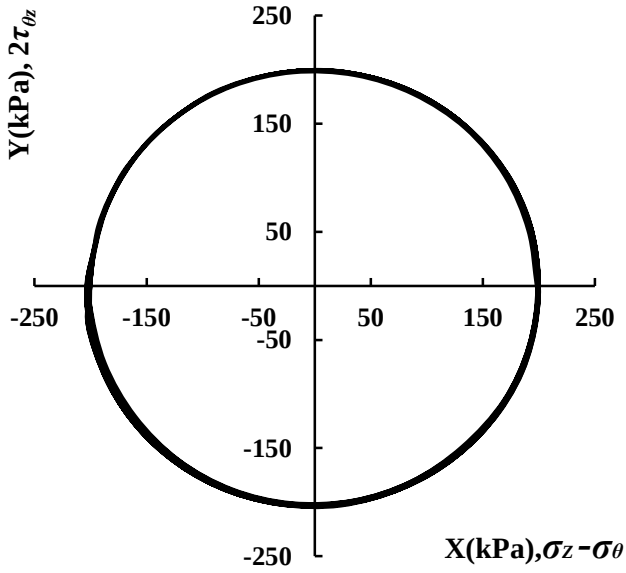

Figure 3-17: Stress trajectories plotted in the X-Y stress space.

As mentioned in section 3.2.4, in order to get complete stress-strain curve including post-peak response, all the monotonic shearing tests in this study have been carried out using HCA strain-controlled mode. Most of the previous monotonic shearing tests using HCA, however, were carried out using stress-controlled mode. Therefore a validation of the results of strain controlled test in SS-HCA is necessary.

Two dense Leighton Buzzard sand specimens at $D_{rc} \approx 75\%$ were first isotropically consolidated to an effective confining pressure of p' = 200kPa and then subjected to monotonic shearing in the vertical direction ($\alpha = 0$) with constant p' = 200 kPa and $b = 0$. The stress-controlled test was performed by increasing the deviator stress q (5kPa/min) monotonically until failure. The strain-controlled test was performed by increasing the axial displacement (0.05mm/min) monotonically to a large axial strain (40%).

Figure 3-18 presents the stress ratio versus deviatoric strain relationship obtained by the two tests. It can be seen that for stress controlled test, the stress-strain curve is ceased at the peak stress. For strain controlled test, the curve shows a peak followed by a strain softening and the specimen has been continuously sheared to a large deviatoric strain. For easy of comparison between the two curves, the maximum deviatoric strain is fixed at 2% in Figure 3-19. Slightly stiffer response can be observed from the curve of the strain-controlled test. However, the strain to reach a peak stress ratio for the two tests was almost the same and very little difference between the curves can observed before the peak was reached. The good agreement of the stress-strain curve obtained by the two loading mode indicates that the monotonic shearing test with fixed principal stress direction could be successfully performed

either by using the HCA strain-controlled loading mode or HCA stress-controlled loading mode in SS-HCA.

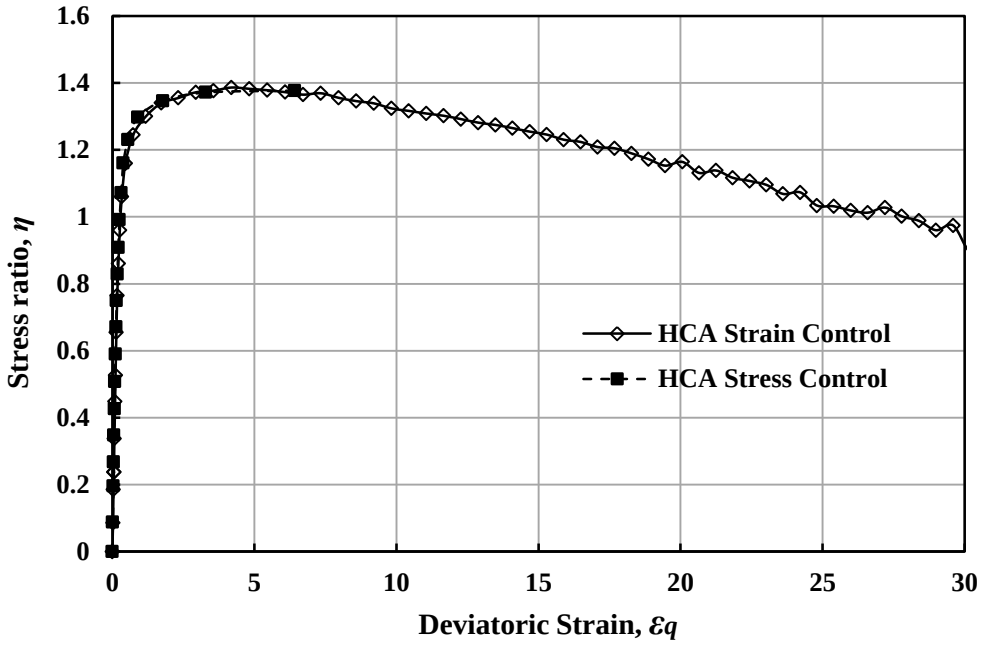

Figure 3-18: Stress ratio vs. deviatoric strain for strain and stress controlled monotonic shearing test.

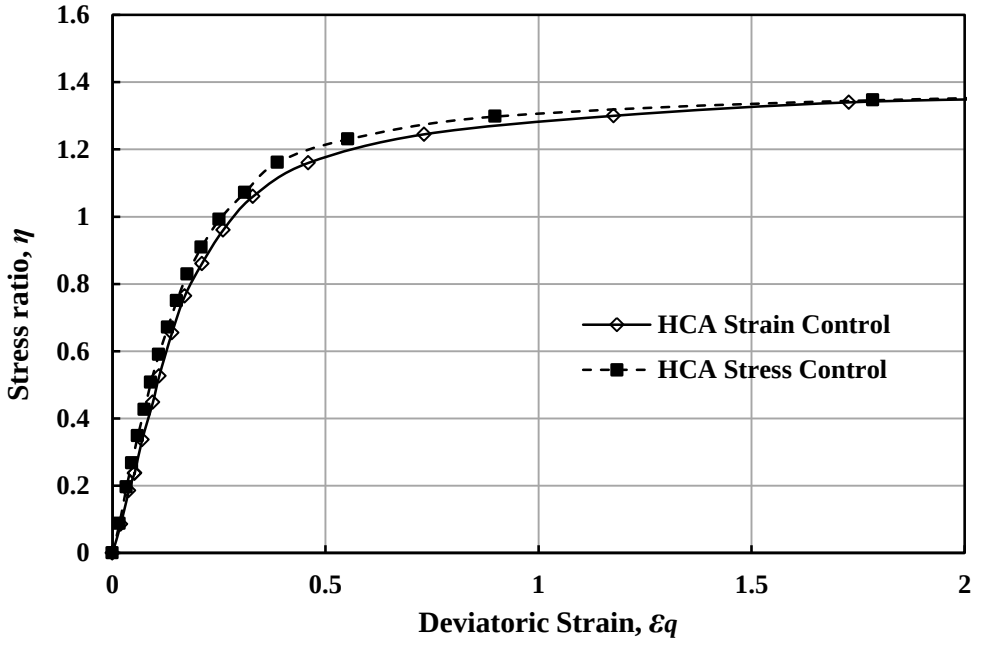

Figure 3-19: Stress ratio vs. deviatoric strain for strain and stress controlled monotonic shearing test ($\varepsilon_q \leq 2\%$).

3.4.3 Repeatability of test results

Repeatability of the tests and the accuracy of the results are the important requirements for the consistency of conclusions to be derived from HCA test. Good repeatability can be achieved only by following identical sample preparation techniques and test control routines. To evaluate the repeatability of test results generated by the SS-HCA, identical sand samples were loaded along identical stress paths.

Two Leighton Buzzard sand specimens were prepared to an initial relative density D_{ri} ≈ 70% by strictly following the sample preparation procedures mentioned in Section 3.4.1. After an isotropic consolidation, specimens were first sheared in the deposition direction up to the peak and unloaded to nearly isotropic stress state with deviatoric stress q = 20kPa. Monotonic loading with fixed principal stress directions α = 30° was then applied on the specimens. Effective mean stress p' = 200 kPa and the intermediate principal stress parameter b = 0.5 were maintained throughout the tests.

Comparative results from the two samples are presented in Figure 3-20 and Figure 3-21. Followed by the loading, unloading and reloading procedures, it can be seen from the two figures that the stress-strain curves obtained from the two samples coincides with each other very well when ε_q < 15% . When same deviatoric strain was induced, the maximum deviation of the deviatoric stress and volumetric strain was less than 2.4% and 2.8% respectively. However, at larger strains, the deviations are significant. This could be due to the increase of stress non-uniformities as the geometry of the HCA specimen changed significantly at large strains. Nevertheless, considering the small magnitude of induced strains, excellent repeatability of test results can be achieved by using the HCA.

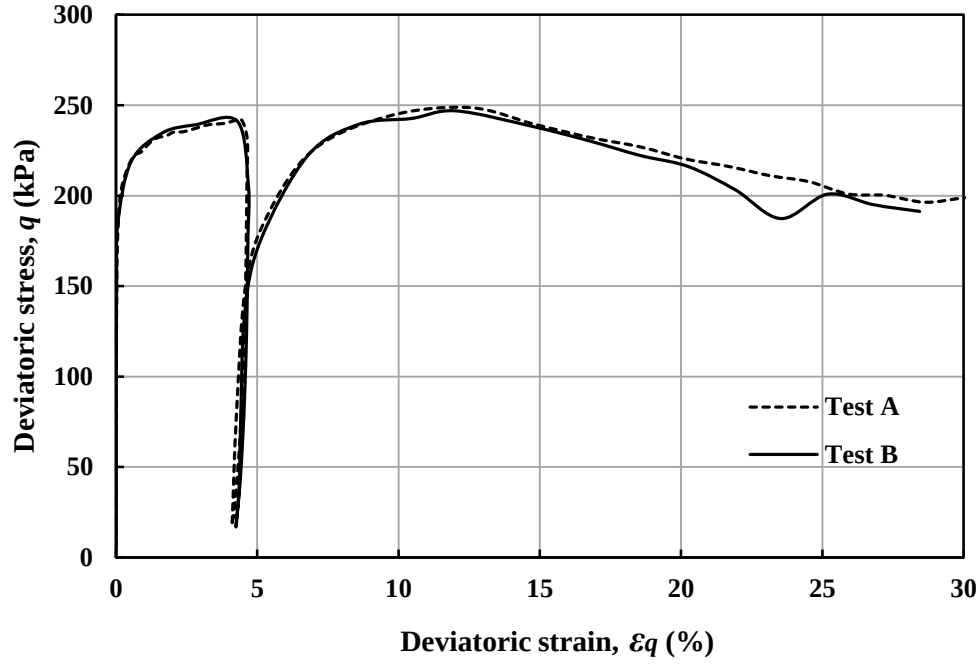

Figure 3-20 Deviatoric stress vs. deviatoric strain.

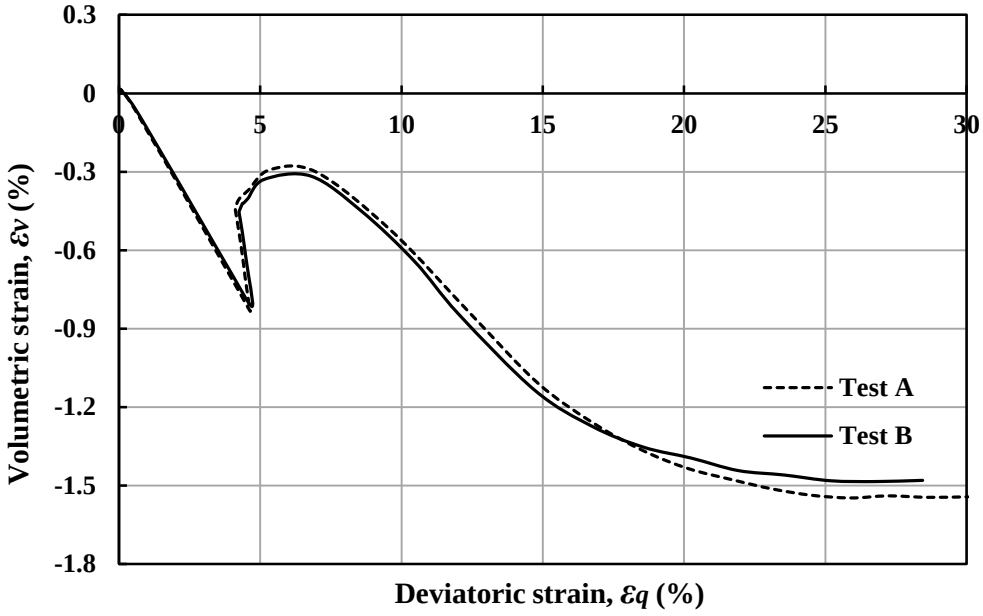

Figure 3-21 Volumetric strain vs. deviatoric strain.

3.4.4 Membrane penetration error correction

The membrane penetration (MP) correction was determined in accordance with the value of equations introduced by Sivathayalan and Vaid (1998) (see Equation 2-32 in

Chapter 2). Figure 3-22 shows the effect of MP on the change of the specimen volume. From the figures, the corrected volumes were slightly different from the values recorded in test. However, the MP did not affect the volume changes significantly, especially when the specimen was approaching failure.

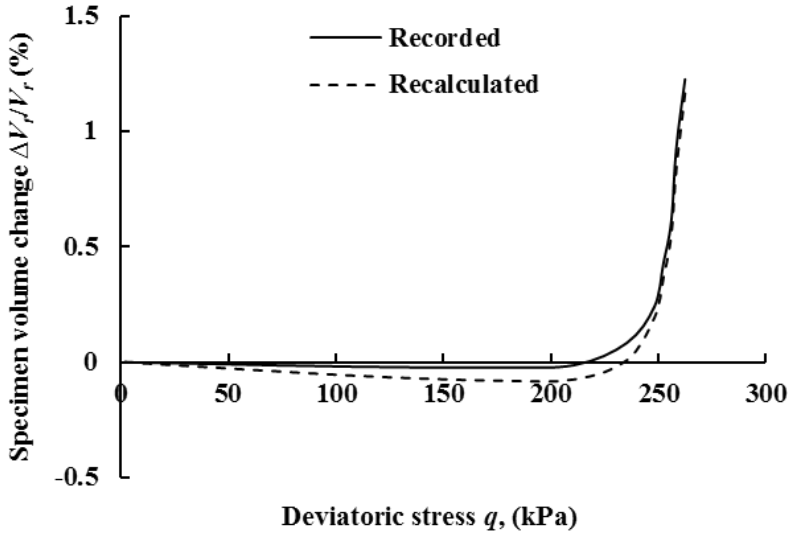

Figure 3-22 Effect of MP on specimen volume change.

The effects of MP on stress-strain curves are shown in Figure 3-23 when the radial strain, ε_r, circumferential strain, ε_θ, and volumetric strain, ε_v, are plotted against the deviator stress, q. As shown in Figures 3-23 (a) and (b), there were small differences between the recorded values and recalculated values of radial strain and volumetric strain. However, as shown in Figure 3-23 (c), the difference between the recorded values and recalculated values of circumferential strain was very small. As the research was focused on the stress-strain and volume change behaviour of sands, therefore, MP correction has been made using the method provided by Sivathayalan and Vaid (1998) in the subsequent analyses.

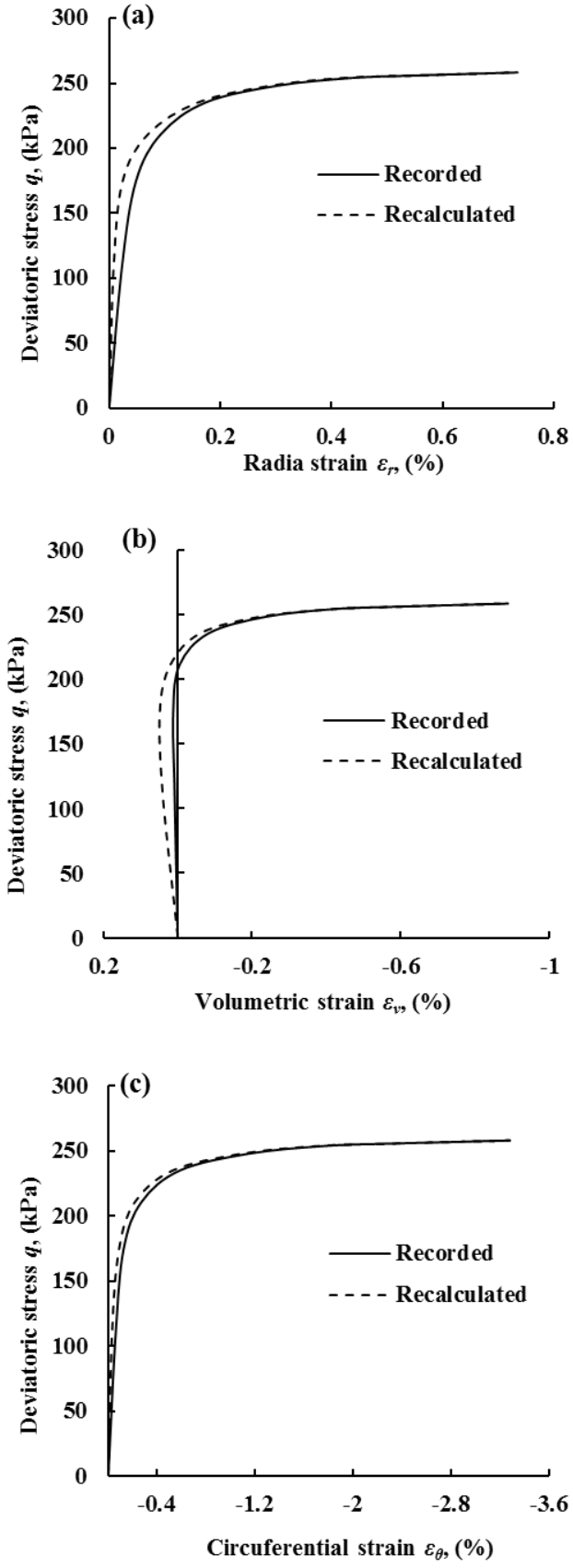

Figure 3-23 Effect of MP on stress-strain behaviours: (a) radial strain; (b) volumetric strain; (c) circumferential strain.

3.5 Summary

In this chapter, the GDS Small-Strain Hollow Cylinder Apparatus (SS-HCA) has been described in detail. The operation of SS-HCA system is based on the high speed digital control system (DCS), which was used for the control and measurement of torque, angular rotation, axial force and axial displacement of the specimen. Pressure/volume control for the outer and inner cell pressure/volume and the back pressure/volume are provided using digital pressure/volume controllers (DPVC). Pore water pressure was measured by an external water pressure transducer connected to the sample. GDSLAB software installed in the user's PC was used for test control and data acquisition.

Granular materials, namely Leighton Buzzard sand and Ballotini solid glass balls were used in this study. Physical properties of the two materials including their index properties, particle size distributions and particle shapes have been presented. Furthermore, the specimen preparation techniques and the overall testing program designed in this study have been described.

This chapter also deals with the verification of experimental tests and results. Triaxial compression tests using SS-HCA and conventional Triaxial Device were conducted and compared. Good agreement of the test results validated the reliability of the SS-HCA testing result. Another five tests, following different stress paths, were carried out to check the capability of the SS-HCA controlling systems and the repeatability of testing result. According to the results, the SS-HCA is capable to carry out generalized stress path tests, and excellent repeatability of the test results can be achieved by using the SS-HCA.

Chapter 4 Drained Behaviour of Granular Soil in Monotonic Shear

4.1 Introduction

This chapter presents a detailed examination of the results obtained from the testing program I outlined in Chapter 3. In this testing program four series of monotonic shear tests along different loading directions have been carried out in order to investigate the effects of particle shape, material density and preshearing on the behaviour of granular soils. All the tests followed monotonic loading stress paths, in which specimens were sheared with the major principal stress direction fixed in the prescribed direction. The experimental testing information will be introduced in Section 4.2. Then the results of the four series of tests will be presented with the focus on the stress-strain behaviour, failure characteristics and non-coaxiality. Finally the summary of this chapter will be given in Section 4.5.

4.2 Test Details

4.2.1 Initial conditions

Leighton Buzzard (Fraction B) sand and Glass Ballotini were used in this testing program. The procedures of sample preparation, saturation and consolidation strictly followed the sample preparation procedures mentioned in Section 3.4.1. All specimens were consolidated isotropically to an effective mean pressure p' of 200kPa,

using a back pressure of 400kPa to ensure 'full' saturation. A summary of the initial conditions of the tests is given in Table 4-1.

Table 4-1: Summary of the initial conditions of the tests in Testing Program I

	Relative density after consolidation *Drc*: %	Void ratio after consolidation e_c	Principal stress direction α (º)	Principal stress parameter, *b*
Series 1 Dense Leighton Buzzard sand	77	0.582	0	0.5
	76.6	0.583	15	0.5
	76.3	0.584	30	0.5
	75.9	0.585	60	0.5
	75.9	0.585	75	0.5
	76.3	0.584	90	0.5
	Relative density after consolidation *Drc*: %	Void ratio after consolidation e_c	Principal stress direction α (º)	Principal stress parameter, *b*
Series 2 Glass Ballotini	90	0.536	0	0.5
	91.8	0.533	15	0.5
	89.4	0.537	30	0.5
	90.6	0.535	60	0.5
	91.8	0.533	75	0.5
	90	0.536	90	0.5
	Relative density after consolidation *Drc*: %	Void ratio after consolidation e_c	Principal stress direction α (º)	Principal stress parameter, *b*
Series 3 Medium dense Leighton Buzzard sand	44.4	0.67	0	0.5
	44.8	0.669	15	0.5
	44.1	0.671	30	0.5
	43.3	0.673	60	0.5
	42.2	0.676	75	0.5
	41.9	0.677	90	0.5

	Relative density *Dr*: %		Void ratio after *e*		Principal stress direction α (º)	Principal stress parameter, *b*
	After consolidation	After preshearing	After consolidation	After Preshearing		
Series 4 Pre-shearing	75.6	73.3	0.586	0.592	0	0.5
	75.9	73.3	0.585	0.592	15	0.5
	75.9	72.8	0.585	0.594	30	0.5
	75.2	73.3	0.587	0.592	60	0.5
	75.9	72.9	0.585	0.593	75	0.5
	75.6	73.3	0.586	0.592	90	0.5

4.2.2 Stress paths

In this testing program, monotonic loading was applied in HCA strain-controlled mode with a rate of axial strain 0.05%/min under drained condition. The data was recorded in every 30 seconds. As mentioned in Chapter 3, for $\alpha < 45^{o}$, specimens were vertically compressed. For $\alpha > 45^{o}$ specimens were vertically extended. Due to technical impossibility, $\alpha = 45^{o}$ is not included in this testing program. The accurate control of principal stress direction α is vital to determine the accuracy of stress path. Figure 4-1 shows an example of actual stress paths obtained from the monotonic loading tests. It can be seen that in the whole procedure, α was controlled sufficiently well so as to be consistent with the prescribed directions.

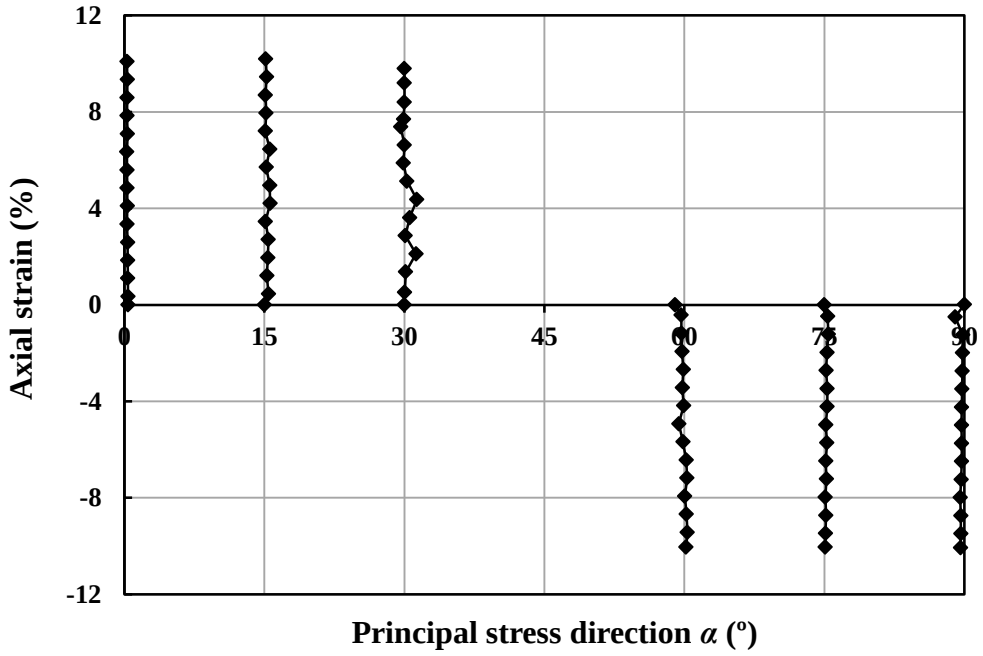

Figure 4-1: Actual stress paths followed in test series 3 on medium dense Leighton Buzzard sands.

In test series 4, a presheared specimen was obtained by shearing the isotropically consolidated specimen in the vertical direction ($\alpha = 0°$) up to the peak (corresponds to 2.1% axial strain, using strain-controlled mode) and unloading it to a stress state with

deviatoric stress q = 20kPa (using stress-controlled mode with a rate of deviatoric stress 5kPa/min) (see Figure 4-2). Monotonic loading with fixed principal stress directions was then applied on the specimens under drained condition (using strain-controlled mode).

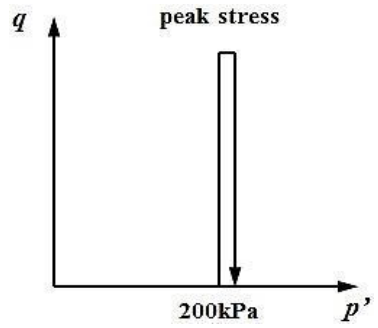

Figure 4-2: Designed stress paths in *q-p'* stress space for pre-loading tests.

During all tests, following two conditions were maintained, the value of effective mean principal stress p' = 200 kPa and the value of the intermediate principal stress parameter b = 0.5.

4.3 Results on Dense Leighton Buzzard Sand

4.3.1 Stress-strain and volume change behaviour

The first series of tests were performed on dense Leighton Buzzard sand in order to generate a basic understanding of the stress-strain and volume change behaviour, failure characteristics and non-coaxiality of granular soils under monotonic loading with different loading directions. Also, the result from this series of tests was used as a reference for comparison with the other three series of tests.

Figure 4-3 presents the dependence of stress-strain and volumetric change characteristics on the direction of principal stress axes under monotonic shearing with

different inclinations of major principal stress. To have a better view of the curves at small strains the maximum deviatoric strain was fixed at 5% in Figure 4-4. For volumetric strain on the two figures, a positive value along the vertical axis indicates contraction and the negative indicates dilation. It should be noted that significant strain localization was interpreted as clear visualization of shear banding, necking and bulging observed postpeak in all the tests. Once significant strain localization occurred, the specimen was distorted severely, the non-uniformities of stresses and strains in the nonhomogeneous and disturbed specimens can thus be exacerbated. There was no reasonable approach to interpret the stress-strain state within the specimen with satisfactory accuracy based on the geometry of the distorted specimen. Therefore, the true stress-strain state after the onset of strain localization cannot be obtained with the current experimental facilities and interpretation techniques. It was observed from the tests that visible strain localization was initiated corresponds to the peak in the stress-strain curve. Thus, the postpeak stress-strain measurement could not accurately predict the soil behaviour due to strain localizations. However, it is a common practice in the literature to report the postpeak stress-strain state in the stress-strain curves.

It can be seen from Figure 4-3 and Figure 4-4 that the effect of inherent anisotropy of dense Leighton Buzzard sand is apparent in both deviatoric strain and volumetric strain responses. The stiffest response is seen for loading in the deposition direction (i.e. $\alpha = 0°$). In general, the stiffness and shear strength of sands reduces and the volumetric compressibility increases with increasing values of α. The highest peak was obtained when the major principal stress direction was vertical and it was reduced dramatically as the direction of the major principal stress was rotated from $\alpha = 30°$ to $\alpha = 60°$. It can also be observed that the peak stress ratio was obtained at a

comparatively smaller deviatoric strains in the tests with α = 0°, 15°, 30° than in the tests with α = 60°, 75°, 90°. The results clearly demonstrate that the effects of initial anisotropy produced during deposition are quite pronounced on the subsequent mechanical response of granular soils.

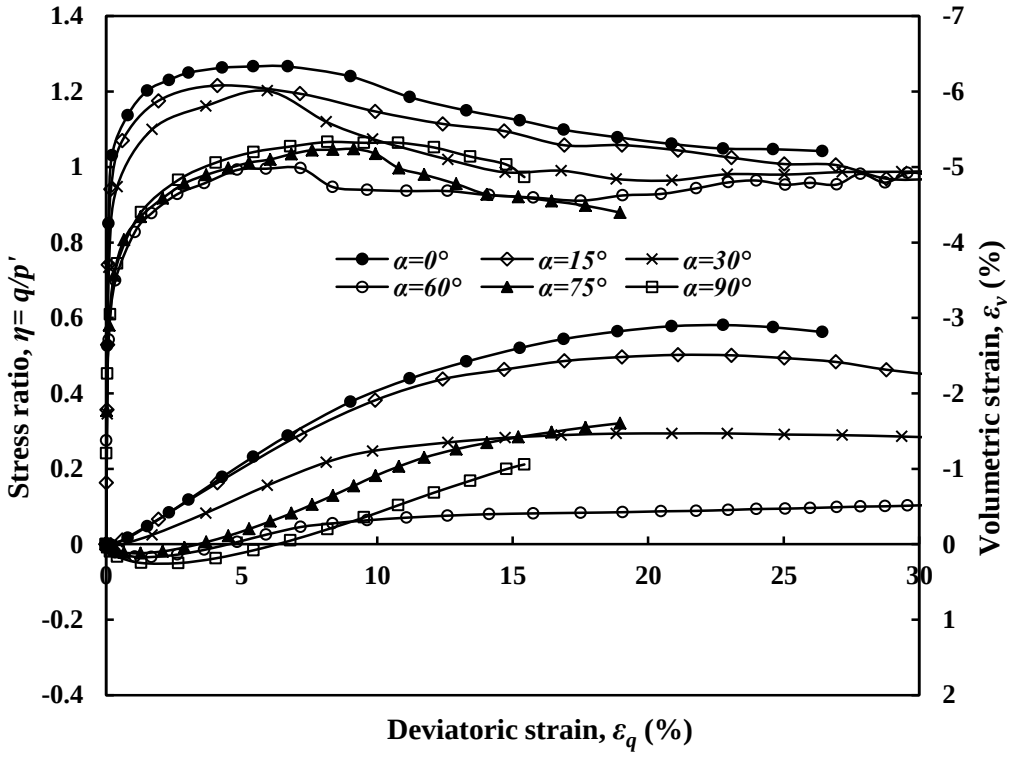

Figure 4-3: Stress ratio-deviatoric strain-volumetric strain relationship for dense Leighton Buzzard sand ($\varepsilon_q \leq 30\%$).

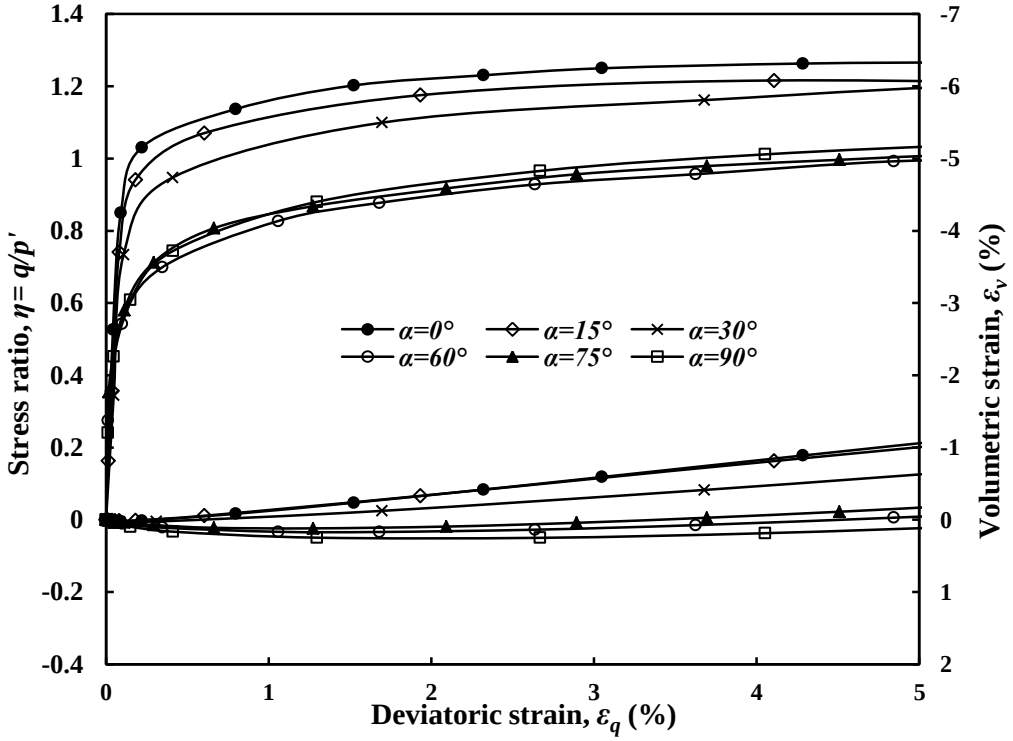

Figure 4-4: Stress ratio-deviatoric strain-volumetric strain relationship for dense Leighton Buzzard sand ($\varepsilon_q \leq 5\%$).

4.3.2 Failure characteristics

The variation of measured peak stress ratio η_p with major principal stress direction α is shown in Figure 4-5. It ranges from 1.02 to 1.26. The highest peak stress ratio was obtained when the major principal stress direction was parallel to the deposition direction (i.e. α = 0°) and the lowest value was obtained at α = 60°. Similar to observations reported by previous researchers (Oda et al. 1978; Symes et al. 1982; Cai et al. 2012), the specimen strength experienced a slight reduction as α goes from 0° to 30°, followed by a shape drop between α = 30° and 60°, then the specimen strength reverted slightly from α = 60° to 90°.

The actual stress paths together with failure point corresponding to the peak deviatoric stress obtained in each test is plotted in the *X*-*Y* stress space in Figure 4-6. By connecting the failure points with a smooth line, an unsymmetrical failure envelope was obtained. The stress paths show that major principal stress direction was precisely controlled during the tests. The effect of the loading direction on the strength of the sand is clearly manifested in this figure as the failure points are not equidistant from the origin of the *X*-*Y* stress space.

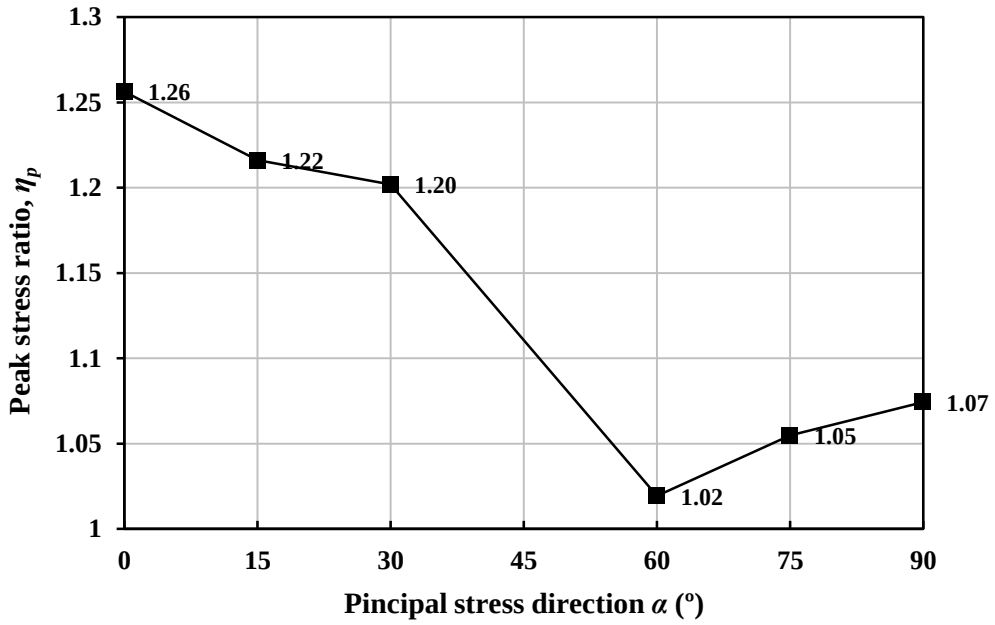

Figure 4-5: Peak stress ratio at different major principal stress directions for dense Leighton Buzzard sand.

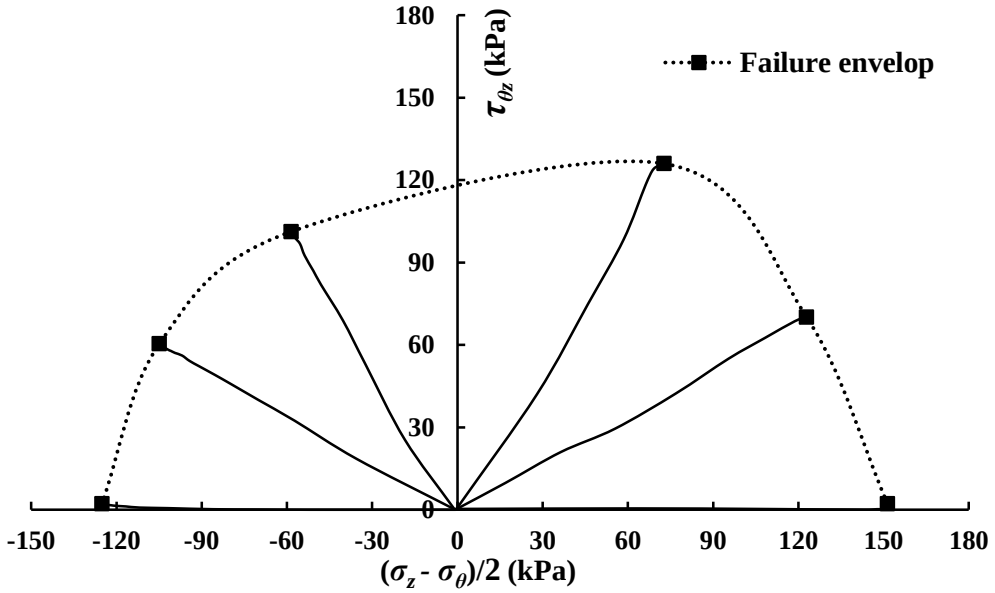

Figure 4-6: Stress path and failure envelop in *X-Y* stress space for dense Leighton Buzzard sand.

After the test, specimen was held under vacuum in order to record any shear bands that had developed. Figure 4-7 presents different shear band patterns and inclination angles obtained from the tests at different loading directions. As shown in the figure,

the angle of shear band inclination is measured from the vertical direction (centre line on the front surface of the specimen) to the direction of shear band plane on the front of the specimen. It was observed from the tests that the shear banding process was initiated near the peak stress state and developed through the residual stress states. Table 4-2 summarizes the angles of inclination and different patterns of the shear bands obtained from the tests. In general it can be seen from Figure 4-7 that bulging phenomenon was observed for specimens tested with α = 0°, 15° and 30°, and necking was observed for specimens tested with α = 60°, 75° and 90°.

For tests with different loading directions, different shear band patterns were developed in the hollow cylinder specimens. Crossed shear bands were produced at α = 0° and 90°, and the intersections of the shear bands were mainly concentrated in the middle part of the specimen. For α = 15°, several parallel spiral-like shear bands were wrapped around the entire body of the specimen with almost equal distance between each other. For α = 30 and 75° a single spiral-like shear band were developed. However, for α = 60°, specimen was twisted at the interface between the base pedestal and the specimen ends.

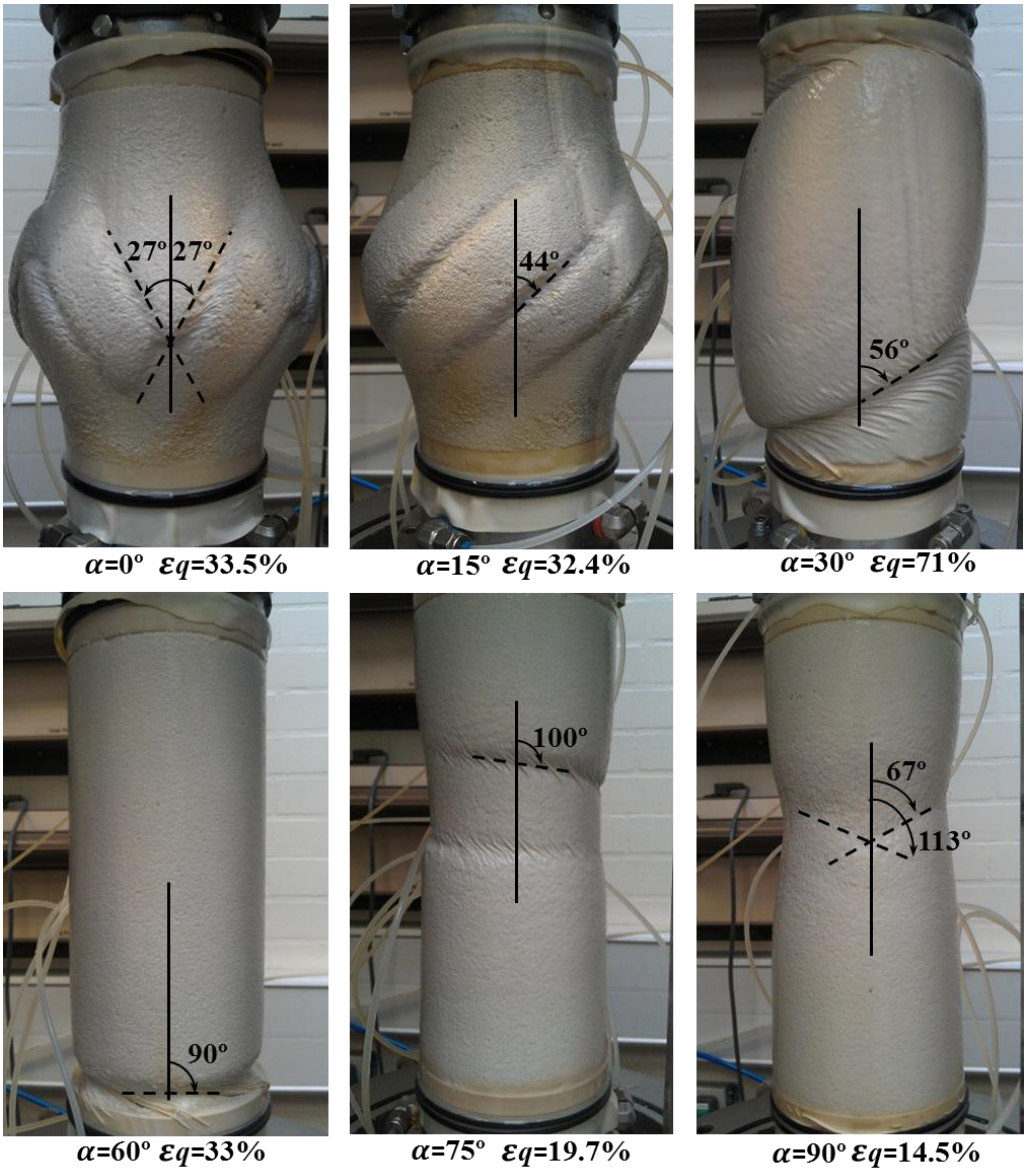

Figure 4-7: Shear bands developed in dense Leighton Buzzard sand specimens at different loading directions.

Table 4-2: Summary of shear band inclination angles and patterns

α (°)	0	15	30	60	75	90
α_{sb} (°)	27	44	56	90	100	67, 113
Patterns	Crossed	Parallel spirals	Single spiral	horizontal	Single spiral	Crossed

α_{sb}: shear band inclination angle

Based on force equilibrium, Coulomb's theory states that failure occurs at the point of maximum obliquity, and the inclination of shear bands therefore coincides with the inclination of planes on which the ratio of shear to normal stress reaches its maximum value (mobilized plane). Figure 4-8 presents the schematic definition of the mobilized plane.

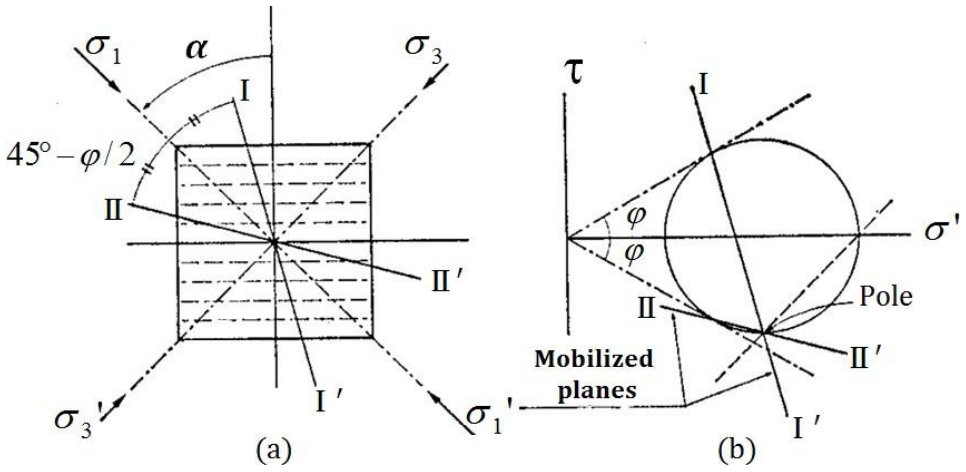

Figure 4-8: 'Mobilized Plane' after Matsuoka (1974); (a) direction in an element, (b) Mohr's stress circle representation.

The angle between the direction of mobilized plane and the major principal stress is then calculated by the following equation:

$$\theta_\sigma = 45° - \varphi/2 \tag{4-1}$$

where: θ_σ is the angle between the mobilized plane and σ_1, φ is the friction angle

The friction angle can be calculated as follows:

$$\varphi = \arcsin \frac{\sigma_1' - \sigma_3'}{\sigma_1' + \sigma_3'} \tag{4-2}$$

By taking the magnitude of effective major and minor principal stresses at the peak stress state, the value of φ at different loading directions was calculated and the value of the angle θ_σ can therefore be obtained by applying Equation 4-1 (table 4-3). The actual shear band inclinations obtained in the experiments are then compared with the theoretical predictions in table 4-4.

Table 4-3 Calculated values of φ and θ_σ at different loading directions

α (°)	0	15	30	60	75	90
φ (°)	48	44	43	36	38	38
θ_σ (°)	21	23	23	27	26	26

Table 4-4: Comparison of experimental shear band inclinations with theoretical predictions

α (°)	0	15	30	60	75	90
α_{sb} (°)	-27, 27 crossed	44 parallel	56 single	90 single	100 single	67,113 crossed
θ_v (°)	-21 (I) 21 (II)	-8 (I) 38 (II)	-7 (I) 53 (II)	33 (I) 87 (II)	49 (I) 101 (II)	64 (I) 116 (II)

θ_v: the angle between the shear band and the vertical; I and II : mobilized planes.

For easy of comparison, the experimental shear band inclinations (sb) and theoretical predictions (Mobilized plane I and II) are sketched in Figure 4-9. It can be seen that at α = 0° and 90° crossed shear bands were developed asymmetrically about the vertical direction, and they matched reasonably well with the two mobilized planes predicted by Coulomb's theory. However, inconsistent with theoretical predictions, spiral-like shear bands were developed in just one direction in the cases of α = 15°, 30°, 60° and 75°.

The spiral shapes of the shear bands can be attributed to the hollow cylindrical structure of the sample. On the other hand, from a microscopic point of view, Miura

(1986) pointed that the interlockings between elongated sand particles with their long axes laid horizontally have the weakest resistance to shear stress on the bedding plane. As shown in Figure 4-10, after deposition, the contact planes between particles are statistically parallel to the bedding plane, obliquity of contact forces relative to the contact normals are related most directly to the shear-normal stress ratio on the bedding plane. Consequently, the specimen deforms most easily when the mobilized plane coincides with the bedding plane. By taking this anisotropic behaviour into consideration, it can be seen from Figure 4-9 that for α = 15°, 30°, 60° and 75° mobilized plane II is closer to the bedding plane than Mobilized plane I. It means that the lowest shear resistance and largest sliding displacement will be more likely to occur on Mobilized plane II than on Mobilized plane I. The observed inclinations of shear bands from the experiments confirmed Miura's theory.

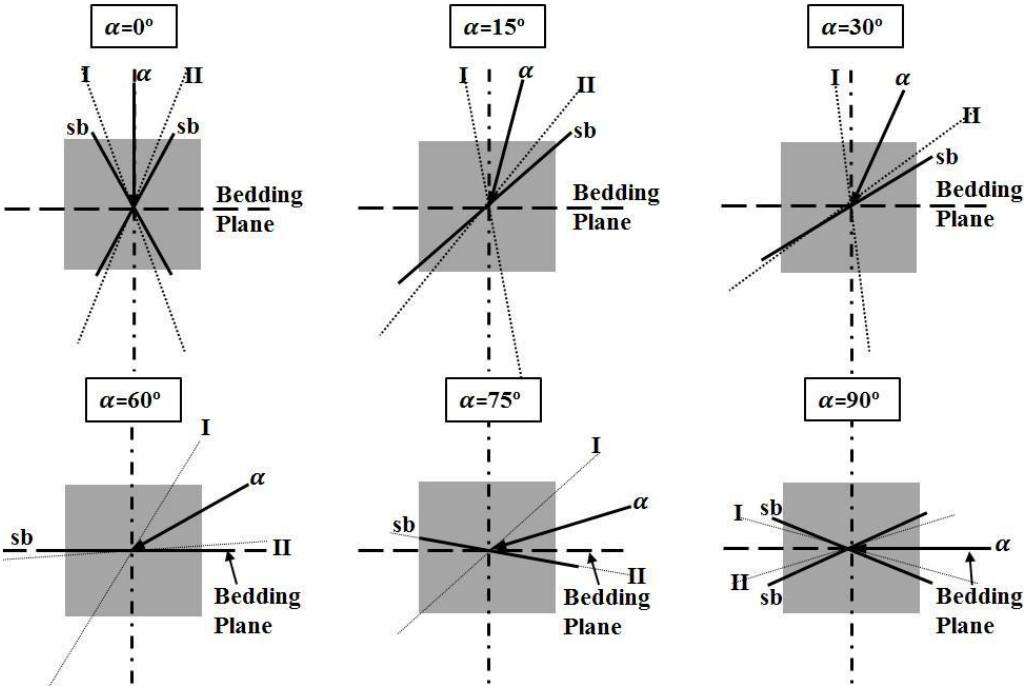

Figure 4-9: Comparison of experimental shear band inclinations with theoretical predictions.

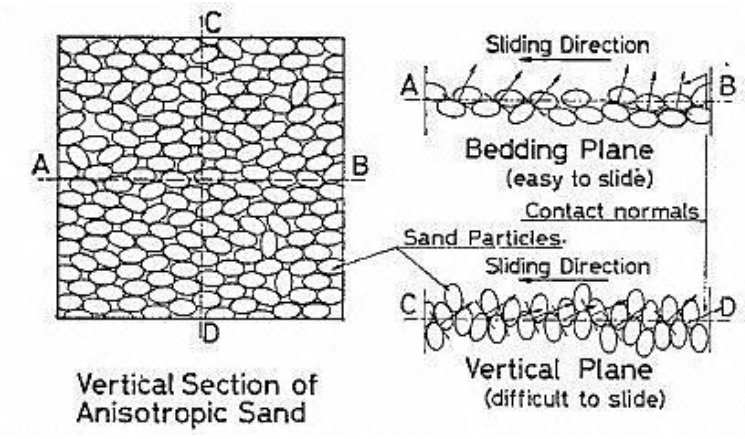

Figure 4-10: Schematic explanation for the lowest resistance against sliding on bedding plane (Miura et al. 1986).

4.3.3 Non-coaxiality

The major directions of stress and strain increment are plotted against the stress ratio in Figure 4-10. During shearing, the direction of major principal stress α was fixed and it is indicated by the vertical lines in the figure. As mentioned in Chapter 3, due to the limitations of the testing equipment, the value of α cannot be accurately controlled at low levels of deviatoric stress. Therefore, the data was recorded after q reaches 15 kPa. Moreover, as there are great stress and strain non-uniformities after failure, only stresses and strains below the peak are considered in the following analysis. The calculated strain incremental direction is indicated in Figure 4-11 as the circle symbols. It can be seen that discontinuous data points were displayed on the figure. This is because the HCA strain controlled mode in terms of axial displacement control was used in the tests and consequently the deviatoric stress q is a passive variable and it was not increasing linearly with axial displacement. Also, it needs to be noted that as elastic strain increment takes a much smaller proportion in the total strain increment compared to that of the plastic strain increment (Gutierrez et al. 1991), the

total strain increment instead of the plastic strain increment is used in the following analysis.

As presented in the figure, the sand behaves almost coaxial when the samples were loaded with the direction of major principal stress coincides with (α = 0°) or perpendicular to (α = 90°) the deposition direction. However, non-coaxiality can be observed for tests with α = 15°, 30°, 60° and 75°. The largest deviations between the major directions of stress and strain increment occurred in the tests with α = 30°, where it was about 11°. The data also shows that the degree of non-coaxiality gradually reduces with increasing stress ratios and specimens were nearly coaxial when close to failure. These results agree well with the laboratory test results reported by other researchers (e.g. Hight et al. 1983; Symes et al. 1984; Miura 1986; Gutierrez et al. 1991).

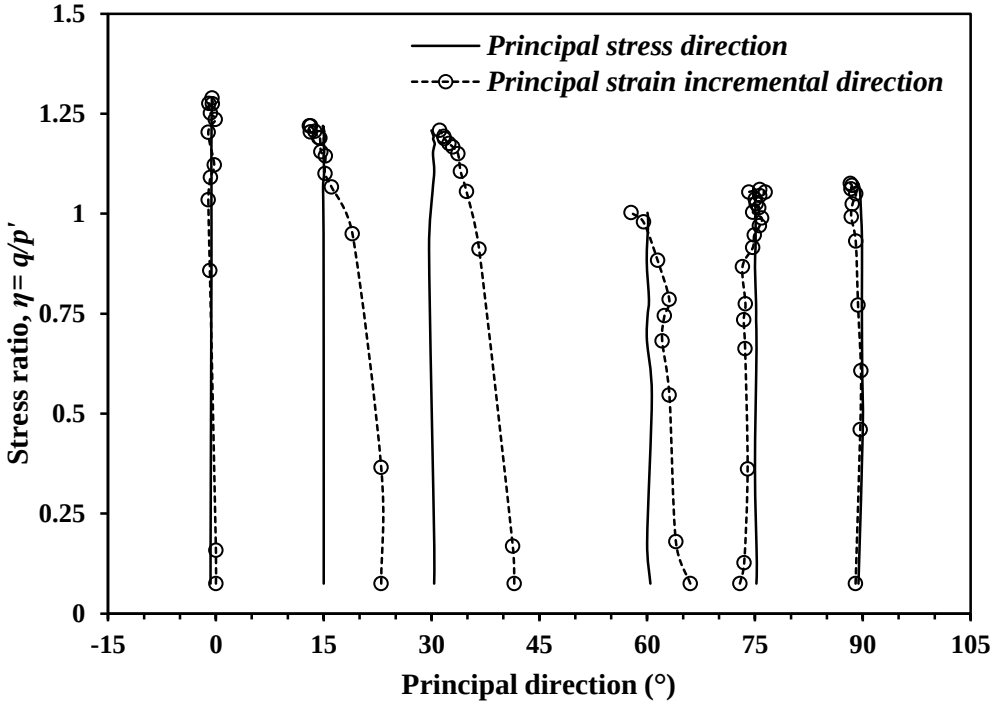

Figure 4-11: Stress and strain increment directions of the dense Leighton Buzzard sand.

4.4 Effects of Particle Shape

4.4.1 Stress-strain and volume change behaviour

In general, the mechanical behaviour of granular materials is dependent on their fabric, which includes particle arrangement, size and shape, and surface roughness. The monotonic loading tests were performed on Glass Ballotini samples in test series 2 in order to examine the effects of particle shape on the behaviour of granular materials. On the other hand, the application of glass spheres in laboratory test provides ideally comparable data for numerical as well as theoretical modelling of granular materials.

The results of the monotonic loading tests for Glass Ballotini is presented in Figure 4-12, and they are compared with the ones for Leighton Buzzard sand at three representative loading directions (α = 0°, 30° and 90°) in Figure 4-13. For a comparison purpose, the results of Leighton Buzzard sand are plotted with dash lines while the corresponding results of Glass Ballotini are shown with solid lines in Figure 4-13.

It can be seen from Figure 4-12, the response of Glass Ballotini also depended strongly on the loading direction in despite of their spherical particle shapes. With the loading direction deviates from the vertical deposition direction (α = 0°) the samples tend to contract more and the strain response becomes softer. This anisotropic response further supports the early findings from Kallstenius and Bergau (1961) and Oda (1981) that inherent anisotropy is not only presents in assembly of irregular shaped particles but also in spherical particles.

By comparing the tests results obtained from Leighton Buzzard sand and Glass Ballotini, it can be observed that Leighton Buzzard sand tends to have stiffer response in stress-strain relationship and larger shear strength than that of Glass Ballotini, even though the former has lower relative density than the latter. This difference may be due to different material characteristics of two materials. Similar observation has also been reported from 2D DEM simulations carried out by Matsushima and Konagai (2001), who performed a series of simple shear simulations with circular, elliptical, and regular polygonal particles for various initial packing densities. Their results revealed that an assembly of regular polygonal particles has a higher shear resistance than an assembly of circular particles even at the same packing density. The authors further pointed out that the fabric of a granular material determines the level of interlocking between the particles. The higher the angularity of the particles, the stronger the particle interlocking will be created, and hence the higher friction resistance between the particles can be produced.

The general trend of the volumetric strain with increasing deviatoric strain at different loading directions is similar for the two materials. However, the Glass Ballotini appeared to be more contractive than the Leighton Buzzard sand. In the test with α = 90°, the Glass Ballotini specimen was contracted completely throughout the test, while dilation followed by initial contraction was observed for Leighton Buzzard sand. The difference in the volumetric strain between the two materials is due to either or both the difference in their relative densities (90% for Glass Ballotini and 76% for Leighton Buzzard sand) and the difference in their particle shapes. However, their influence cannot be distinguished in this experiment.

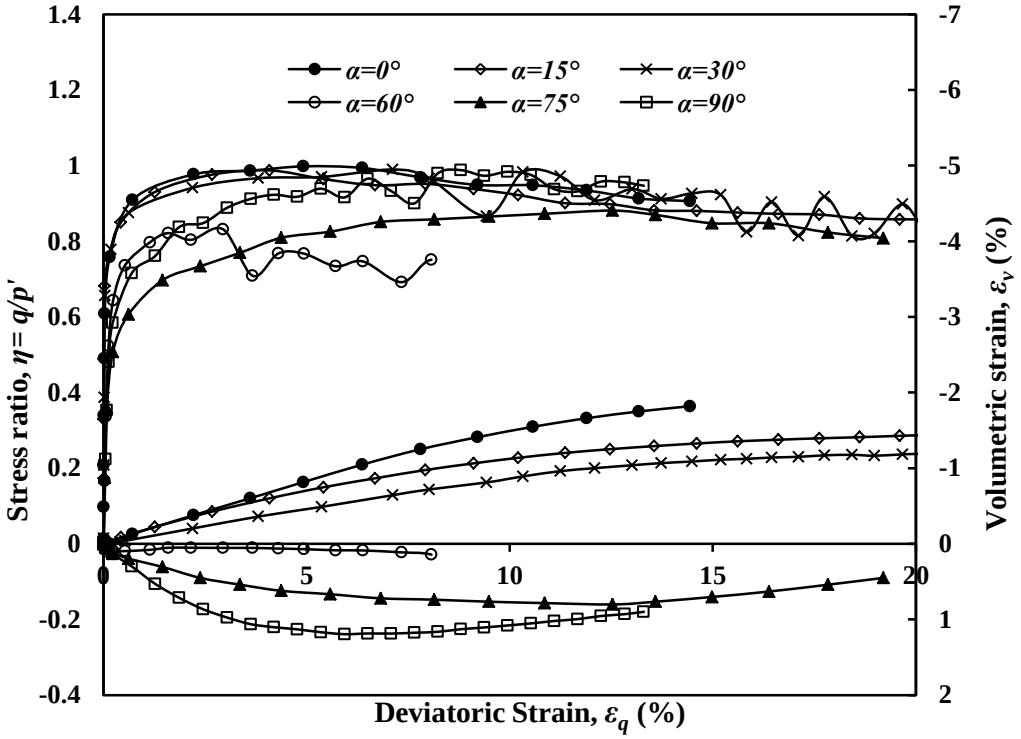

Figure 4-12: Stress ratio-deviatoric strain-volumetric strain relationship for Glass Ballotini.

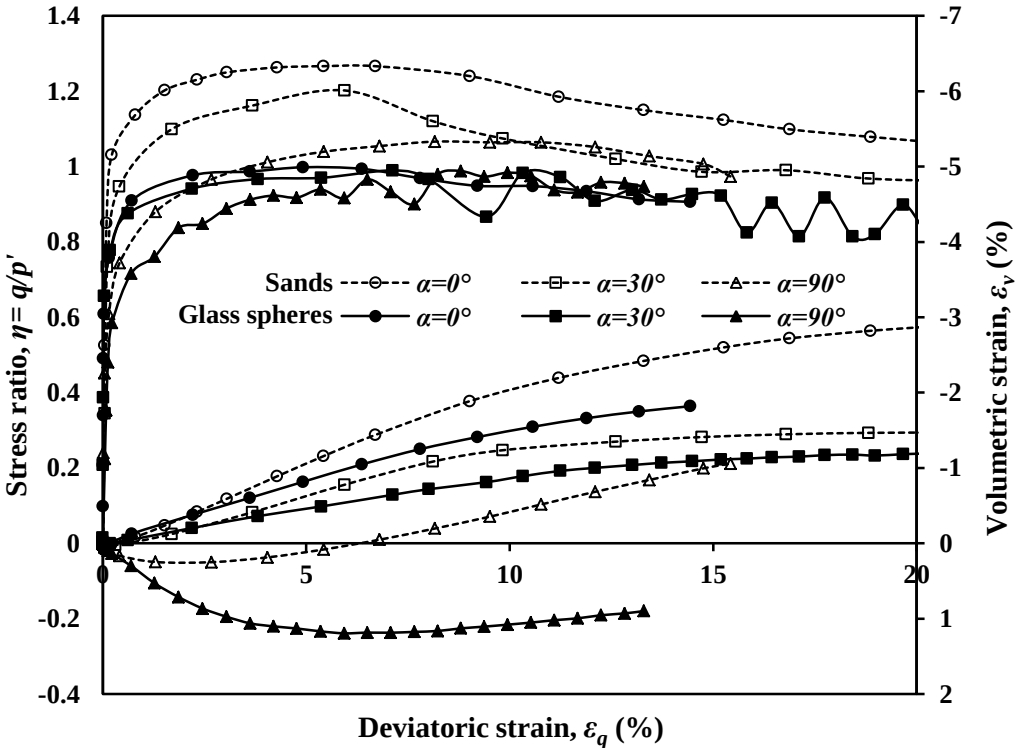

Figure 4-13: Comparison of the test results between Leighton Buzzard sand and Glass Ballotini.

4.4.2 Failure characteristics

Different peak stress ratios measured at different major principal stress directions for the two materials are presented in Figure 4-14. The strength of the Glass Ballotini seems to be more or less isotropic when α rotated from 0° to 30° as the peak stress ratio obtained at α = 0°, 15° and 30° are almost the same. However, a sharp decline was occurred between α = 30° and 60°, and the specimen strength reverted significantly from α = 60° to 90°. Compared with the result of Leighton Buzzard sand, although the relative density of the Glass Ballotini is 14% higher than the Leighton Buzzard sand, an average reduction of 17% in the material strength was occurred when the angular sand changed to the spherical Glass Ballotini. The significant difference of the peak stress ratio obtained from the two materials indicating that the particle shape has a strong effect on the strength of granular assemblies.

The failure envelop in the *X*-*Y* stress space of the two materials are plotted in Figure 4-15. It can be seen that the shape of the failure envelope of Glass Ballotini coincides with that of Leighton Buzzard sand very well. The unsymmetrical shape of the two failure envelopes clearly indicates the presence of strength anisotropy in both irregular and spherical granular materials.

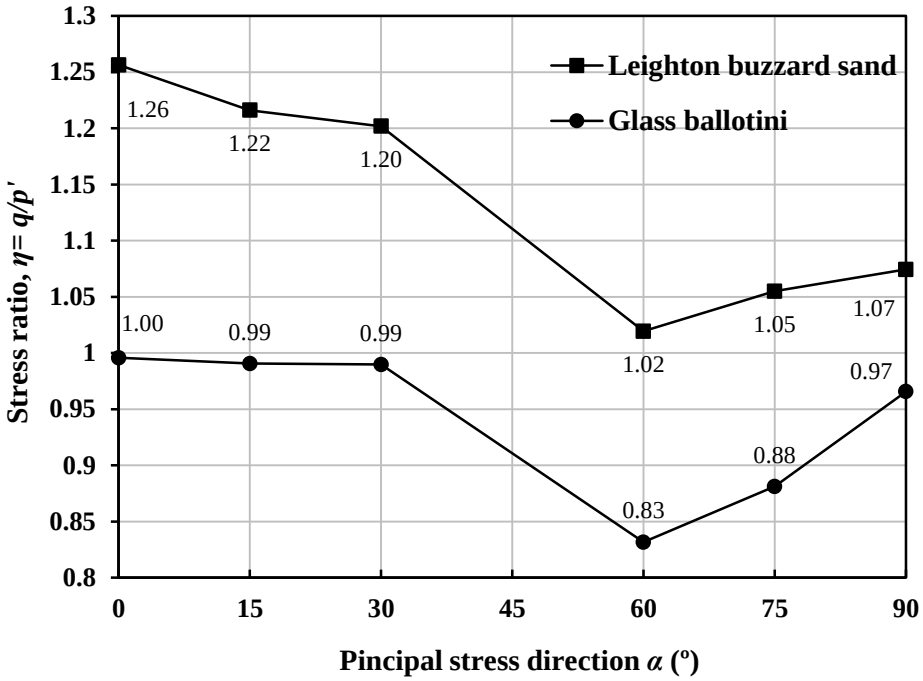

Figure 4-14: Comparison of peak stress ratio at different major principal stress directions for Leighton Buzzard sand sample and Glass Ballotini.

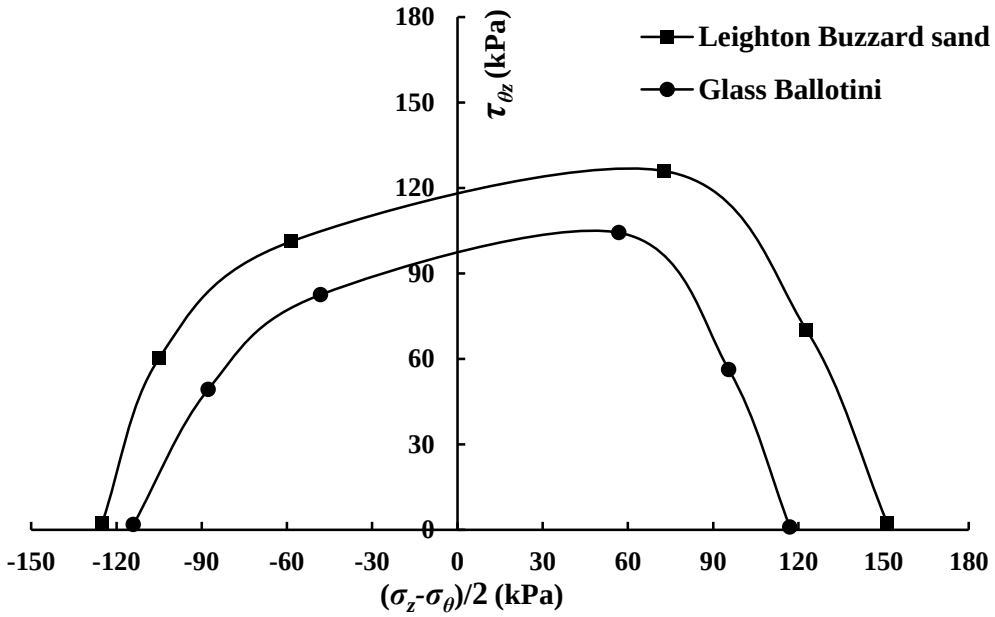

Figure 4-15: Comparison of the failure envelope in *X-Y* stress space for Leighton Buzzard sand sample and Glass Ballotini.

Figure 4-16 presents the photo of the Glass Ballotini samples recorded at the end of each tests. For test with α = 30° a single shear band with inclination angle of 58° was observed. For test with α = 60°, similar with the test on Leighton Buzzard sand, specimen was twisted at the interface between the top cap and the specimen ends. However, unlike the sand specimens, no clear shear bands was observed in the tests with α = 0°, 15°, 75° and 90°. This could be attributed to the spherical particle shape of the Glass Ballotini specimens. Shear band is a localized region where shear flows concentrate and large plastic shear taken place. From a microscopic point of view, due to the intensive shearing within the mobilized plane, around particles tend to move against neighbouring particles by sliding and/or rolling at contacts. The movement of the particles within the plane during shear finally lead to localized shear deformation into a narrow zone. As rounder particles can rotate and slide more freely than angular particles during shearing, the particle translations and rotations could occur in a comparatively larger zone around the mobilized plane in an assembly of rounder particles. Hence the deformation in an assembly of rounder particles could be more uniform than in an assembly of angular particles. In other words, the localized plastic deformation is more likely to develop in an assembly of angular particles.

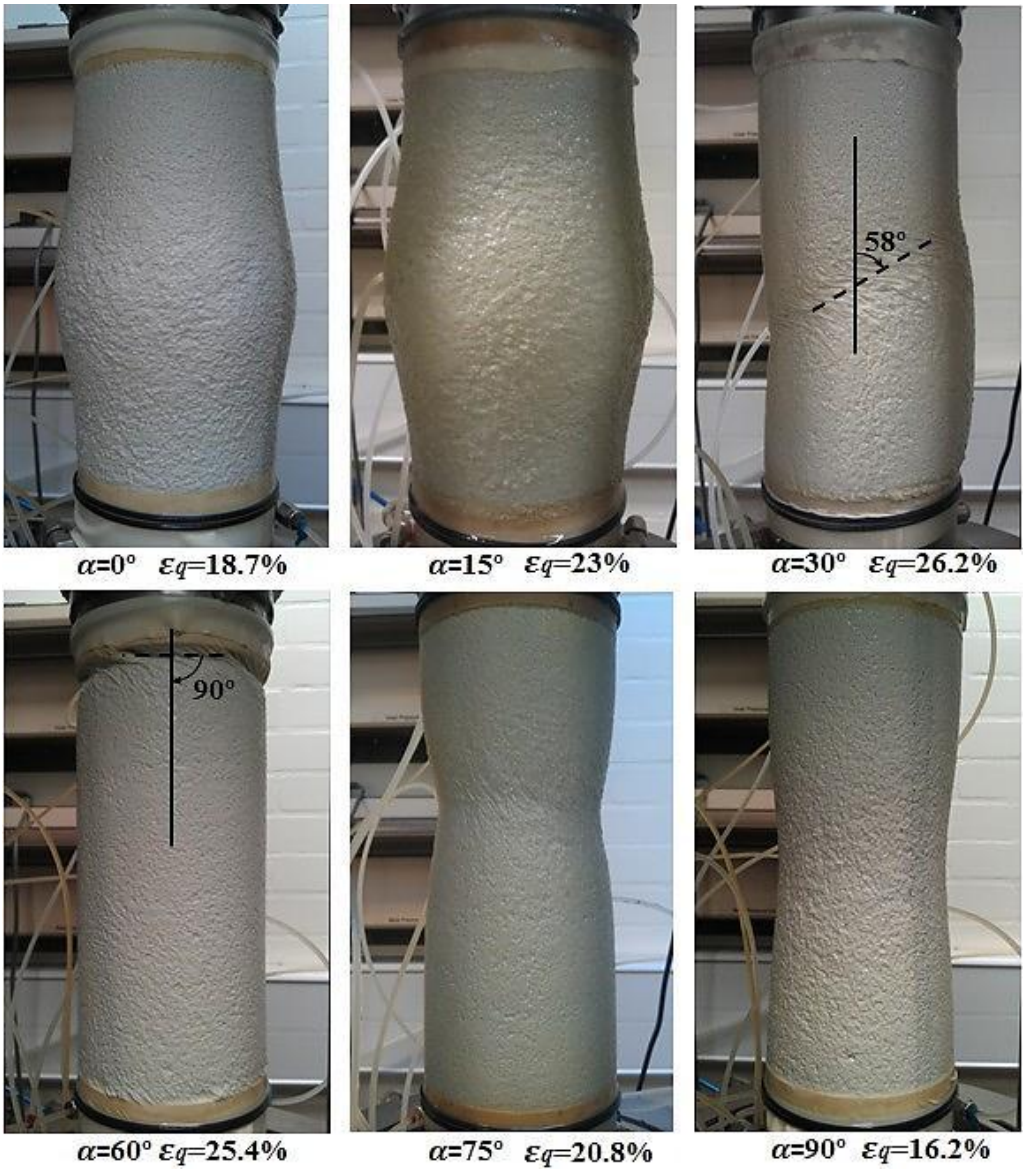

Figure 4-16: Shear bands developed in Glass Ballotini specimens at different loading directions.

4.4.3 Non-coaxiality

In order to compare the non-coaxial behaviour of Leighton Buzzard sand and Glass Ballotini, the stress and strain increment directions obtained at different loading directions for the two materials are presented in Figure 4-17. In general, it can be seen that the results of Glass Ballotini are similar to those of Leighton Buzzard sand. The Glass Ballotini behaves almost coaxial when α = 0° and 90°. And, an obvious non-coaxiality was observed when α =15° and 30°. Once again, the data shows that specimens were nearly coaxial when close to failure. Although the degree of non-coaxiality between the major principal stress and the corresponding principal strain increment directions was slightly smaller in the Glass Ballotini specimens, the margin by which the Leighton Buzzard sand non-coaxiality exceeded that of the Glass Ballotini was limited to 3°. Hence, the effect of the particle shape on the non-coaxial behaviour of granular materials under monotonic loading is not significant.

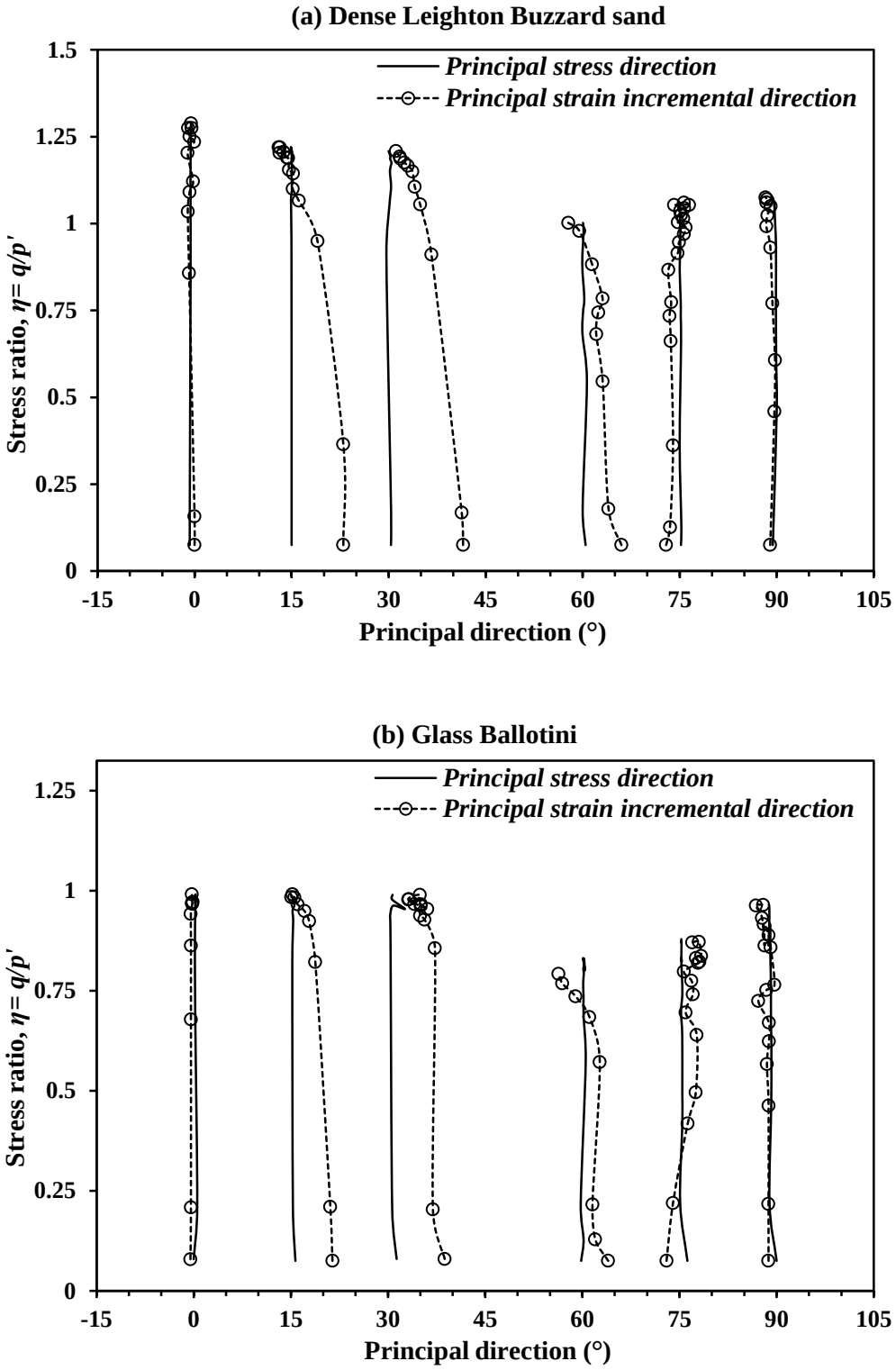

Figure 4-17: Stress and strain increment directions of: (a) Leighton Buzzard sand and (b) Glass Ballotini.

4.5 Effects of Material Density

4.5.1 Stress-strain and volume change behaviour

In order to investigate the effects of material density on the anisotropic behaviour of granular soils, monotonic loading test were also carried out on medium dense Leighton Buzzard sand with initial relative density D_{ri} = 36.5% in test series 3. The results of the monotonic loading tests for medium dense Leighton Buzzard sand is presented in Figure 4-18. Similarly, test at three representative loading directions (α = 0°, 30° and 90°) for both dense and medium dense Leighton Buzzard sand are plotted together in Figure 4-19.

It can be seen from Figure 4-18 that the medium dense Leighton Buzzard sand specimens also showing clear anisotropic stress-strain, volume change, and strength characteristics. Similar to the observations obtained from the dense sand, the stiffness and shear strength of the sands reduces and the volumetric compressibility increases with increasing values of α.

In Figure 4-19, solid lines illustrate the behaviour of dense Leighton Buzzard sand ($D_{rc} \approx 76\%$) and dash lines correspond to the behaviour of medium dense Leighton Buzzard sand ($D_{rc} \approx 42.5\%$). By comparing the results it can be seen that the effects of relative density on the behaviour of sand in monotonic loading is significant. As expected, no matter what the direction of the major principal stress is, the medium dense sand tend to exhibit softer response in stress-strain relationship, lower shear strength, and more contractive volumetric strain than the dense sand. Moreover, larger deviatoric strain was required for the medium dense sand to reach the peak in the stress-strain curves. An explanation to this behaviour is that due to the lower density

of the specimen, the interlocking between the particles is small, therefore, softer response, less shear resistance and more contractive behaviour is observed.

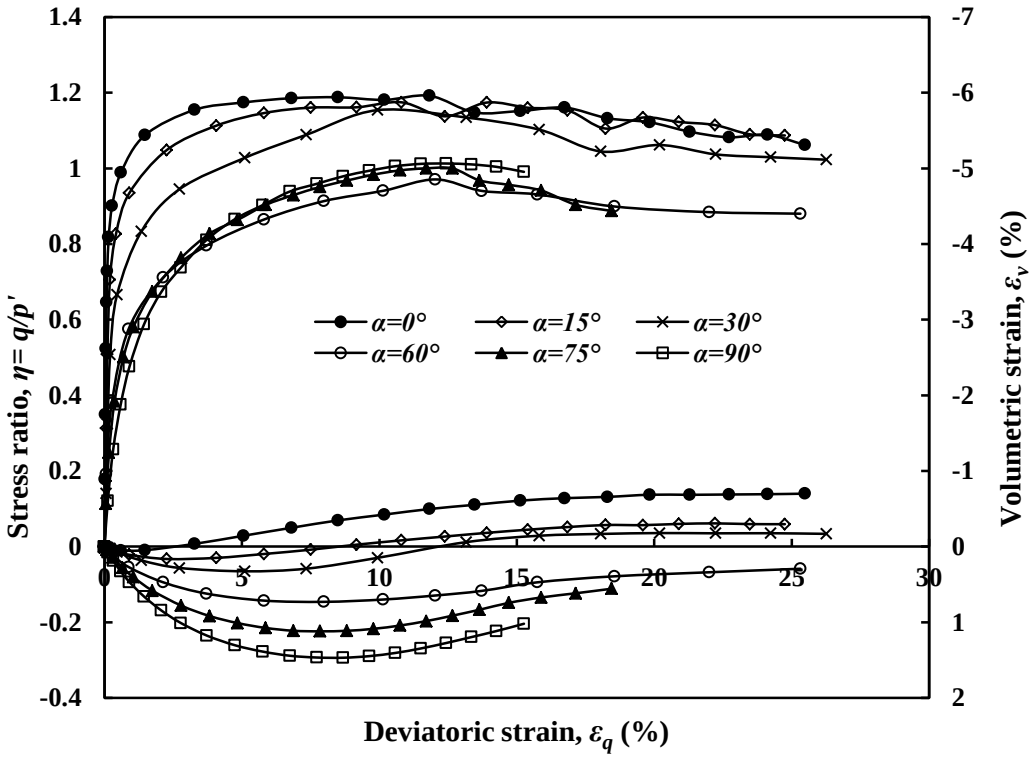

Figure 4-18: Stress ratio-deviatoric strain-volumetric strain relationship for medium dense Leighton Buzzard sand.

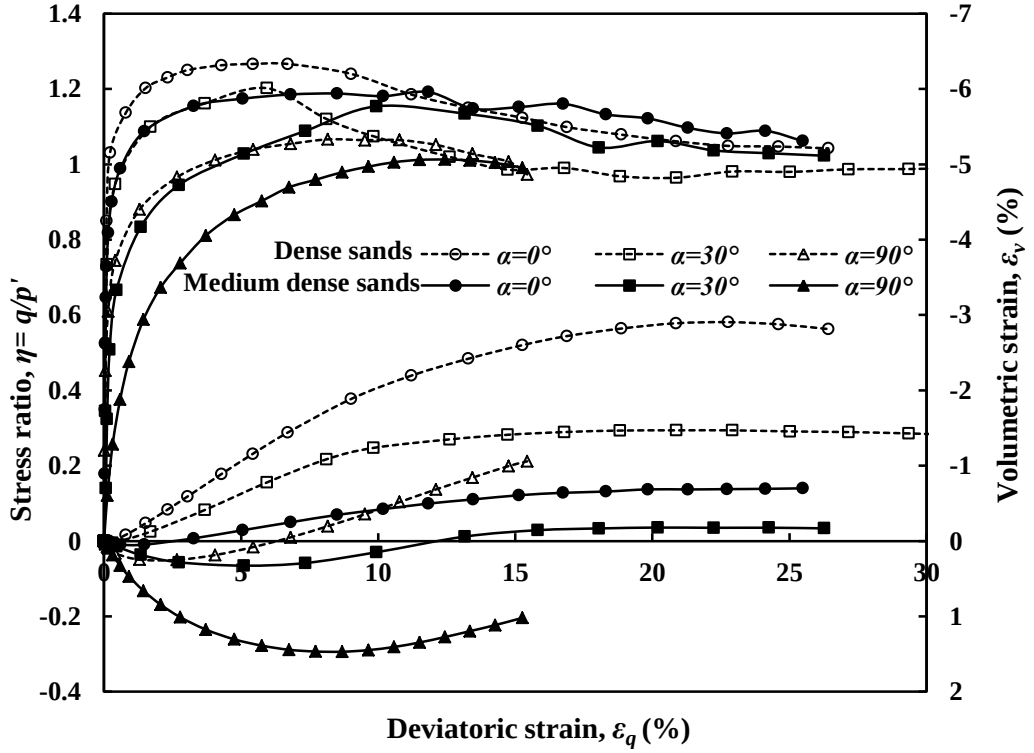

Figure 4-19: Comparison of the test results between dense Leighton Buzzard sand and medium dense Leighton Buzzard sand.

4.5.2 Failure characteristics

Figure 4-20 shows the peak stress ratios at different loading directions for the two materials. It can be observed that the general trend of the variation of peak stress ratios with increasing values of α is similar. Although the difference between the relative densities of the two samples is about 34%, the strength of the medium dense sample is just slightly lower than that of the dense sample as the maximum difference between the two peak stress ratios is 0.06 and it was obtained at α = 0°. Again, as shown in Figure 4-21 the shape of the two failure envelops in the *X*-*Y* stress space coincides with each other very well.

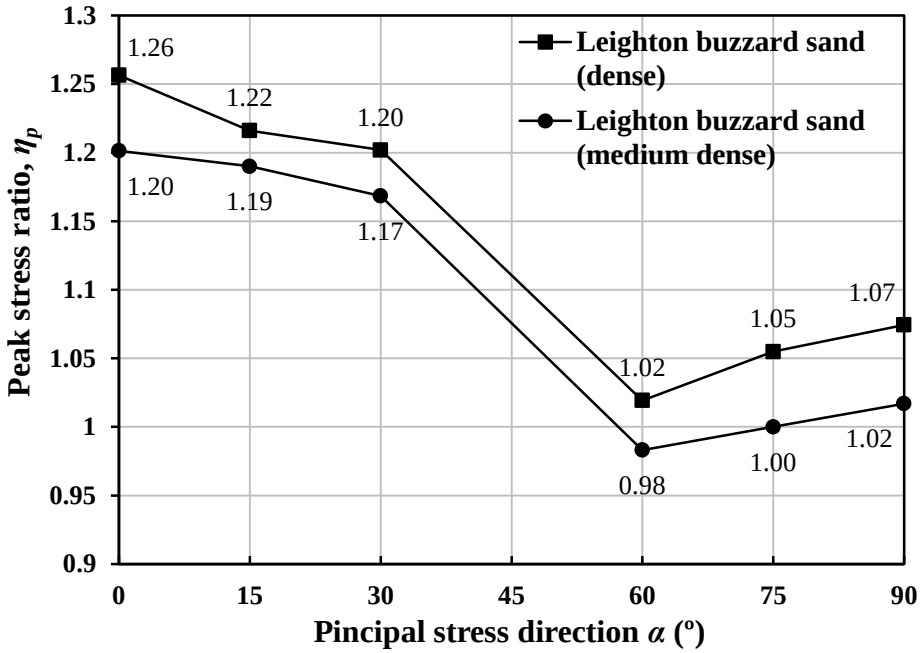

Figure 4-20: Comparison of peak stress ratio at different major principal stress directions for dense and medium dense Leighton Buzzard sand.

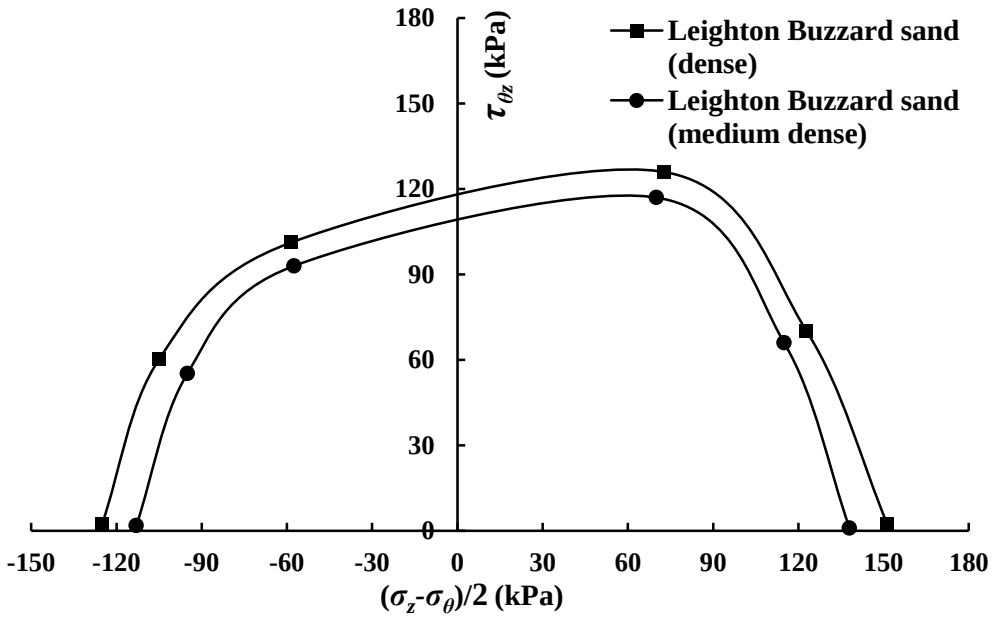

Figure 4-21: Comparison of the failure envelope in *X*-*Y* stress space for dense and medium dense Leighton Buzzard sand.

Figure 4-22 presents different shear band patterns and inclination angles obtained from the tests at different loading directions for medium dense Leighton Buzzard sand samples. It can be seen from the figure that similar to the shear bands observed in dense Leighton Buzzard sand samples, crossed shear bands were produced in the samples with α = 0° and 90° and parallel spiral-like shear bands were formed in the samples with α = 15°. For α = 30 and 75° a single spiral-like shear band were developed. However, for α = 60°, a circular shear band was observed in the upper part of the medium dense sand specimen, whereas the dense sand specimen was twisted at the ends. Table 4-5 present the comparison of the measured shear band inclinations obtained from the dense and medium dense specimens. It can be seen that the two results are closely consistent with each other as the difference is less than 4°.

Table 4-5: Comparison of the shear band inclinations obtained from the dense and medium dense Leighton Buzzard sand samples.

	α (°)	0	15	30	60	75	90
Dense	α_{sb} (°)	27 crossed	44 parallel	56 single	90 single	100 single	67,113 crossed
Medium dense	α_{sb} (°)	29 crossed	43 parallel	57 single	90 single	100 single	63,117 crossed

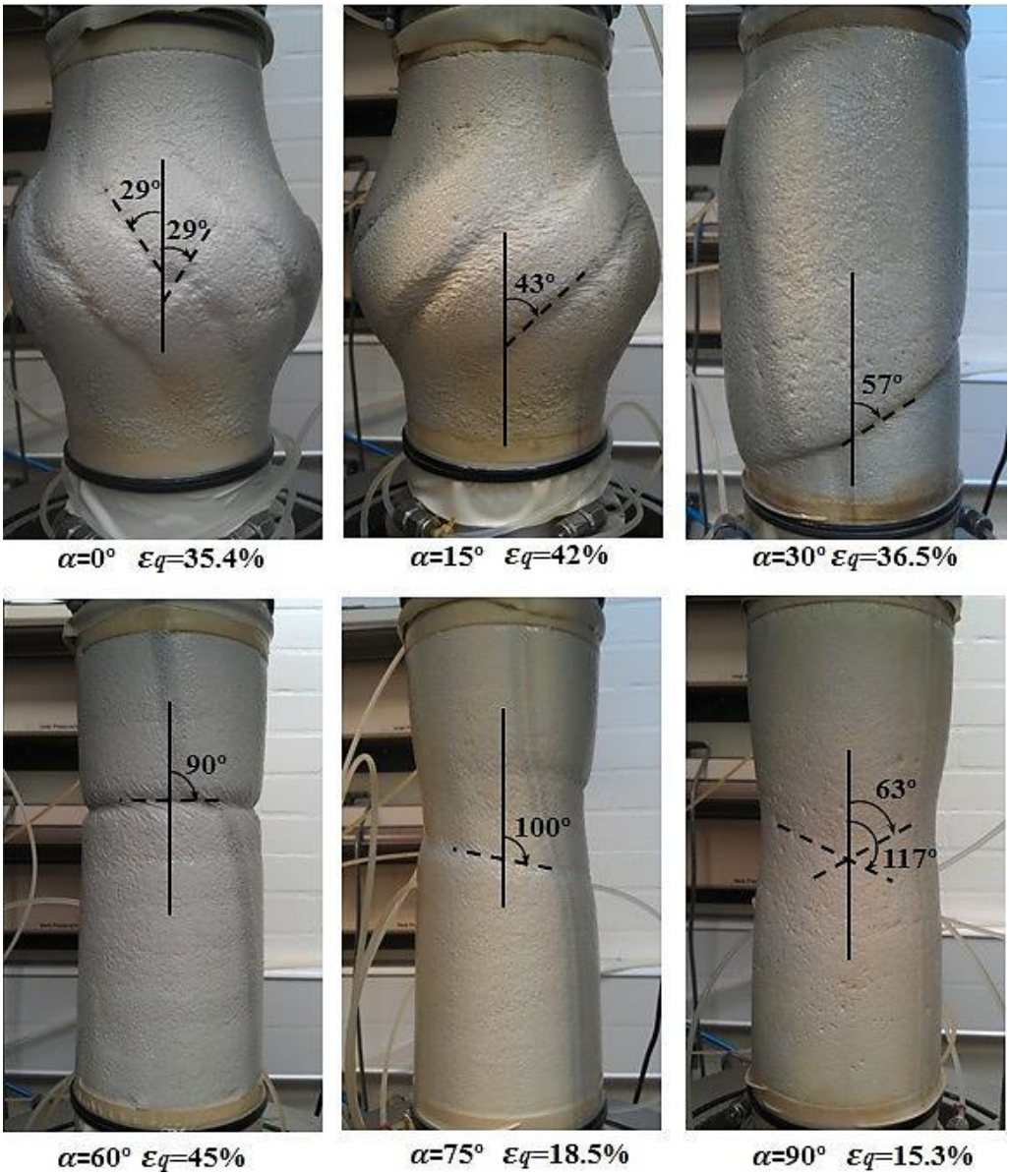

Figure 4-22: Shear bands developed in medium dense Leighton Buzzard sand specimens at different loading directions.

4.5.3 Non-coaxiality

The stress and strain increment directions obtained at different loading directions for the two materials are plotted in Figure 4-23. By comparing the results obtained from the dense sand and medium dense sand it can be seen that the deviations between the major directions of stress and strain increment are very similar at each loading direction. Therefore, the experimental results suggest that the effect of relative density on the non-coaxial behaviour of Leighton Buzzard sand in monotonic loading is not significant. A similar observation was reported by Cai (2012), who carried out a series of stress-controlled monotonic loading tests on Portaway sands using HCA.

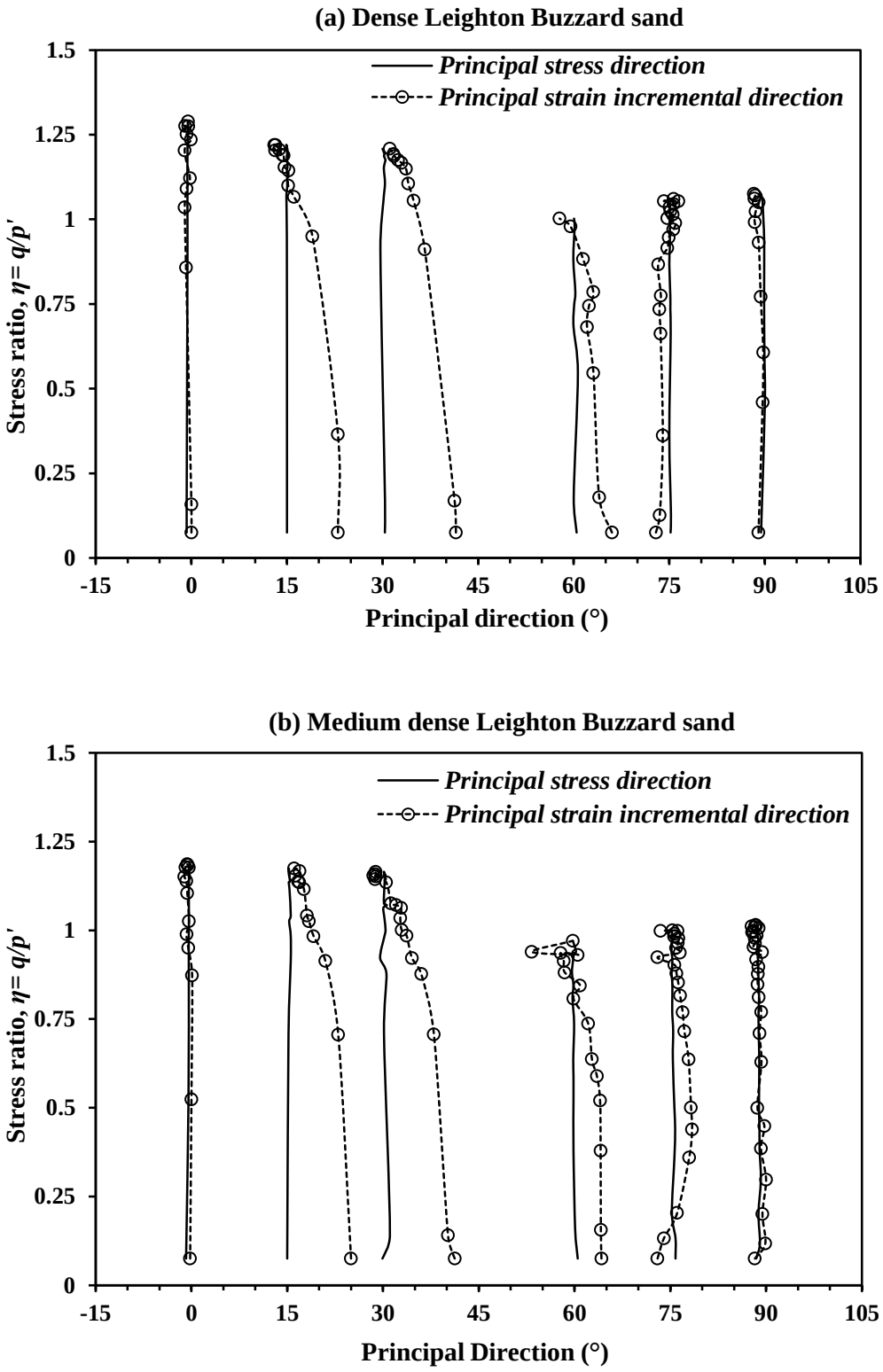

Figure 4-23: Stress and strain increment directions of: (a) dense Leighton Buzzard sand sample and (b) medium dense Leighton Buzzard sand.

4.6 Effects of Pre-loading History

4.6.1 Stress-strain and volume change behaviour

The fourth series of tests was carried out to examine the effects of the preloading history on the behaviour of granular soils. As mentioned in section 4.2.2 a preloaded specimen was obtained by shearing the isotropically consolidated specimen in the vertical direction and then unloading it to nearly isotropic stress state. The test results for presheared specimens are given in Figure 4-24. Again, test at three representative loading directions (α = 0°, 30° and 90°) for both non-presheared and presheared specimens are compared in Figure 4-24.

Similarly, it can be observed from Figure 4-24 with the reloading direction varied from vertical to horizontal, samples became less stiff and contracted more. For α = 60°, the test showing profound stress drop at relatively small deviatoric strains and the data was only collected before the stress drop has occurred.

In Figure 4-25 solid lines present the behaviour of presheared specimens and dash lines correspond to the behaviour of non-presheared specimens. Compared with the results from non-presheared samples, it can be seen from Figure 4-24 that the effects of preshearing to the peak stress on the subsequent stress-strain-volume change responses of the Leighton Buzzard sand is clear. A softer response in stress-strain relationship, severer initial contraction and larger strain to reach a peak stress ratio were observed at all three loading directions for the presheared samples. From Table 4-1 it can be seen that a slight increase of the void ratio was induced by preshearing. However the average increment of void ratio is about 1% and this is not enough to cause the significant difference in the mechanical behaviour between the non-

presheared and presheared specimens. Hence it can be deduced that the differences in stress-strain and volume change behaviours between the two samples depicted in Figure 4-25 are due to the fact that both the void ratios and soil fabrics are different at the same stress point.

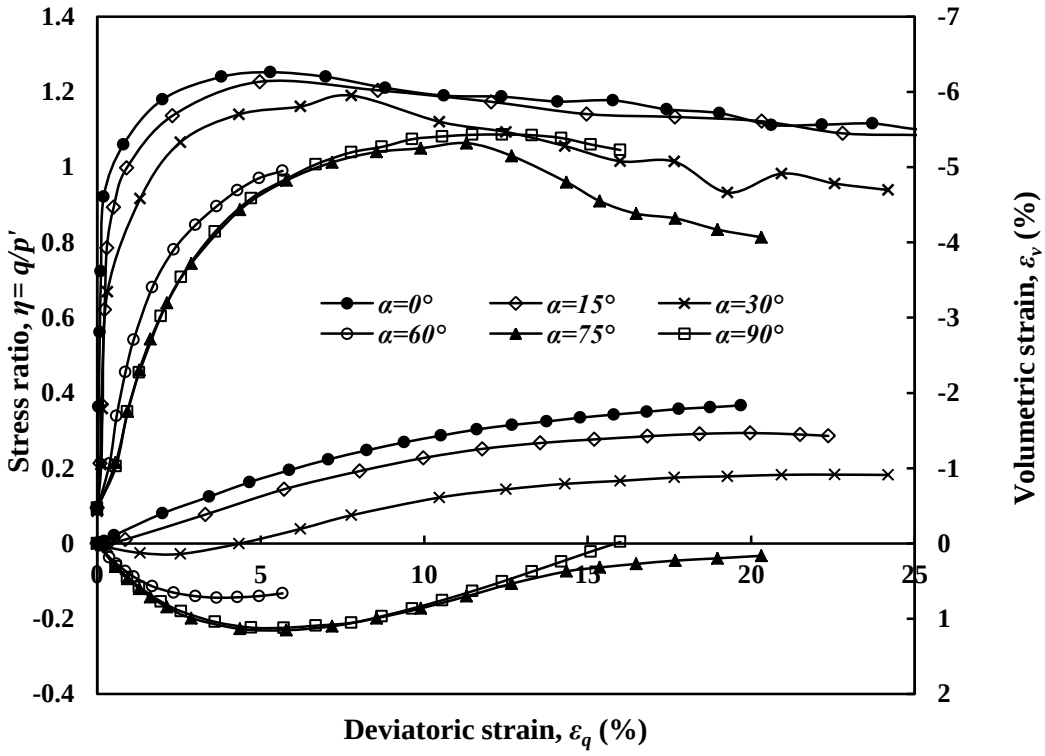

Figure 4-24: Stress ratio-deviatoric strain-volumetric strain relationship for presheared sample.

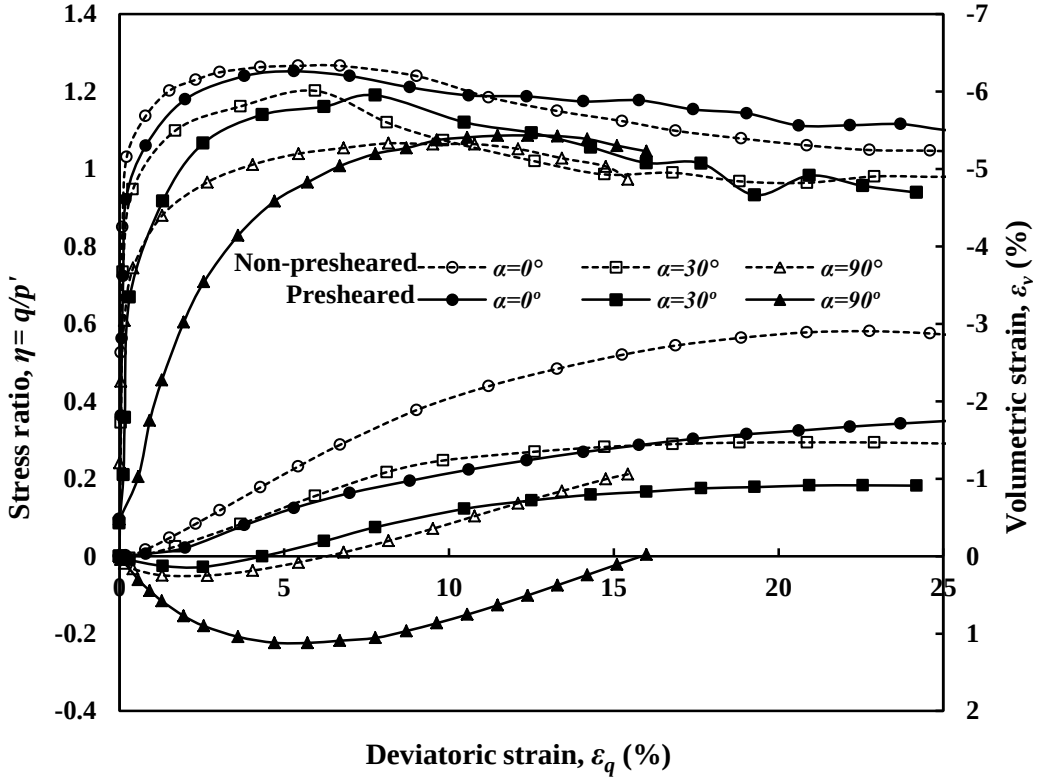

Figure 4-25: Comparison of the test results between presheared sample and non-presheared sample.

4.6.2 Failure characteristics

It is interesting to see from Figure 4-26 that the value of the peak stress ratio measured at different loading directions for the two samples are almost the same, in despite of the significant difference in their stress-strain-volume change responses. Microscopically, it has been pointed out by Oda (1972) that induced anisotropy is unlikely to have a significant effect on the internal friction angle of the soil as when the peak stress was achieved, the void and contact normal columns started breaking down and the soil fabric was altered. Therefore, the observations from this study providing confirmation of Oda's theory with respect to the peak stress ratio. Again, the failure envelops in the *X*-*Y* stress space for the non-presheared and presheared specimens are presented in Figure 4-27.

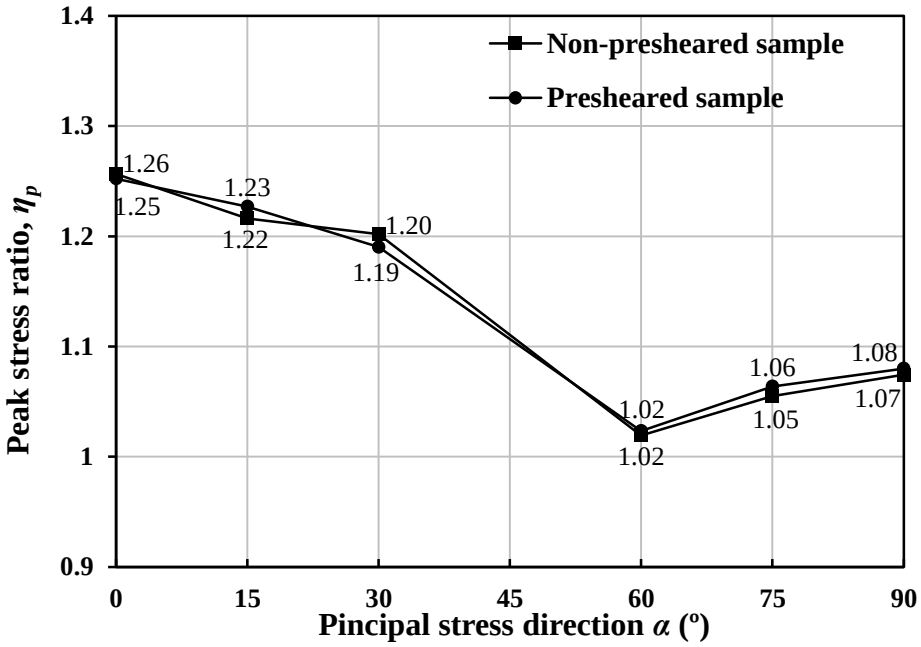

Figure 4-26: Comparison of peak stress ratio at different major principal stress directions for presheared sample and non-presheared sample.

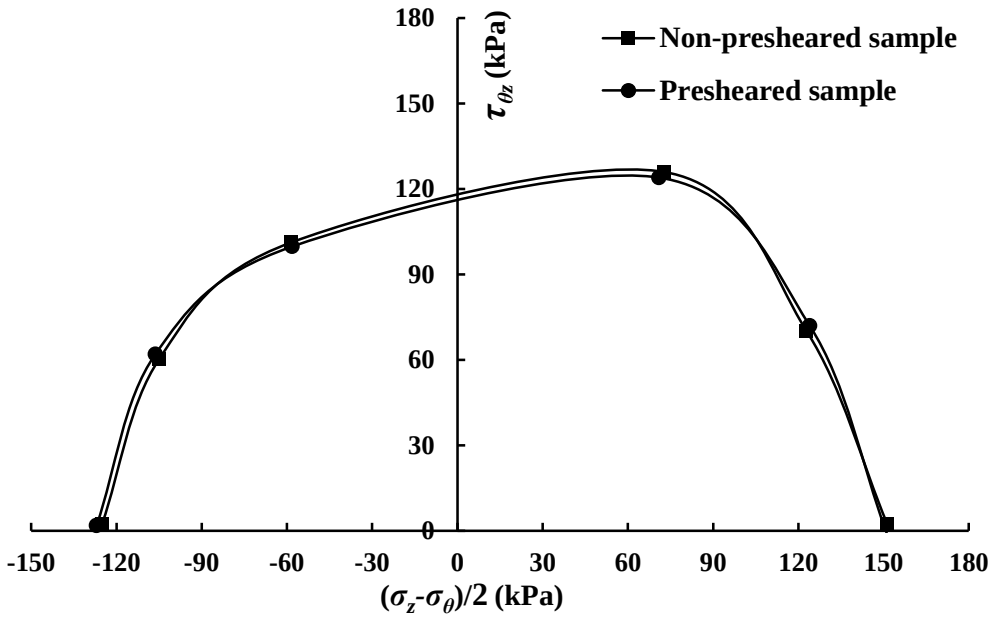

Figure 4-27: Comparison of the failure envelope in *X-Y* stress space for non-presheared sample and presheared sample.

Figure 4-28 presents different shear band patterns and inclination angles obtained from presheared samples. By comparing with the result obtained from the non-presheared samples, similar patterns and inclination angles can be observed in the samples with α = 0°, 15°, 30° and 90° (for α = 30° and 75° similar shear bands was presented on the back side of the sample). However, for α = 60°, no clear shear band can be observed from the sample and the test was stopped when a profound stress drop has occurred. Comparing to the non-presheared samples the thickness and the width of the shear bands developed in the presheared samples at same loading directions are less pronounced. This can be attributed to comparatively lower deviatoric strain of the presheared samples at the end of test. Table 4-6 presents the comparison of the measured shear band inclinations obtained from the two samples. It can be seen that the results obtained from the presheared samples are consistent with those obtained from the non-presheared samples except for test with α = 60°, in which no clear shear band are observed from the presheared sample.

Table 4-6: Comparison of the shear band inclinations obtained from the presheared and non-presheared samples.

	α (°)	0	15	30	60	75	90
Non-presheared	α_{sb} (°)	27 crossed	44 parallel	56 single	90 single	100 single	67, 113 crossed
presheared	α_{sb} (°)	29 crossed	42 parallel	58 single		99 single	64, 116 crossed

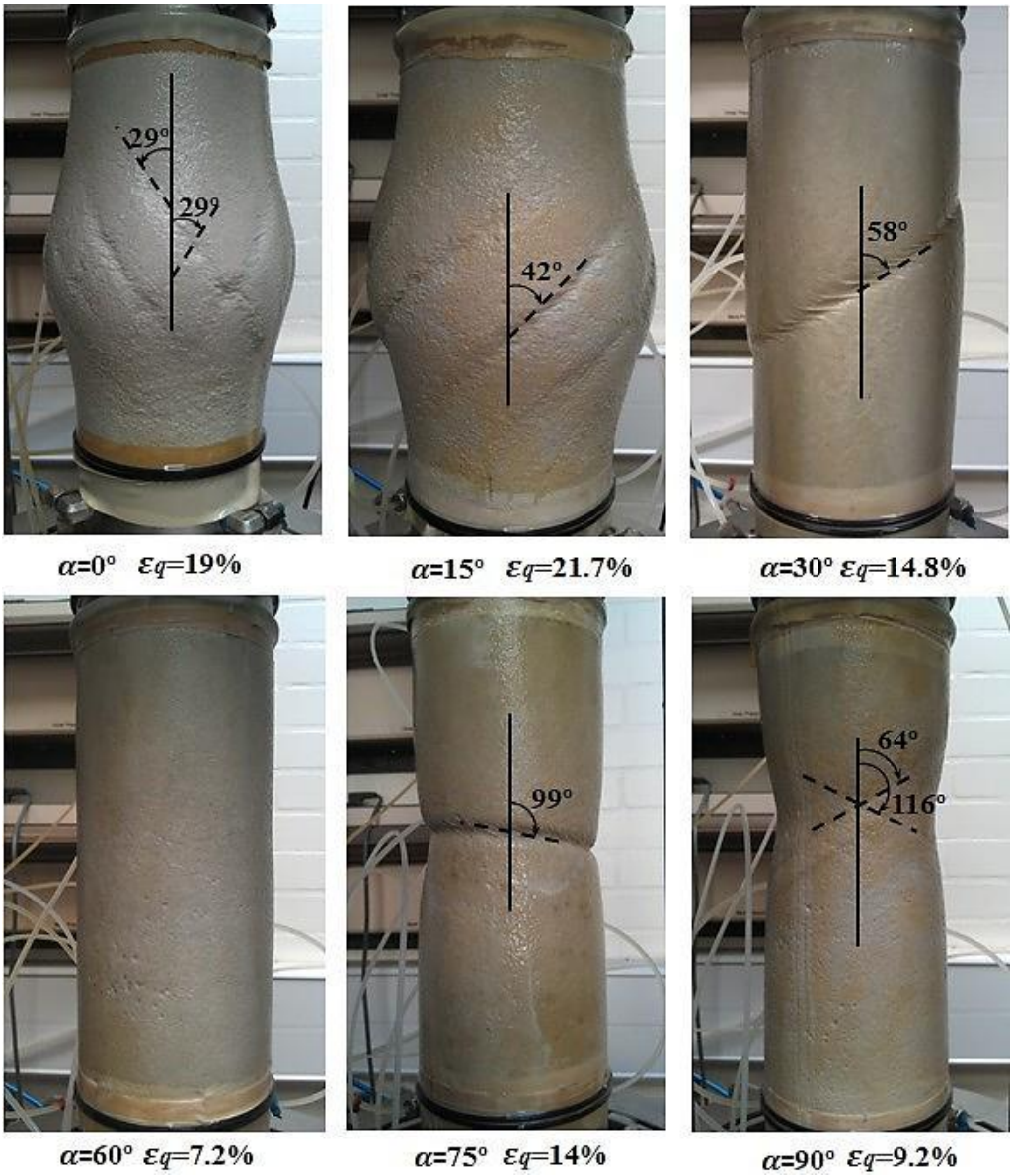

Figure 4-28: Shear bands developed in presheared specimens at different loading directions.

4.6.3 Non-coaxiality

The results of non-coaxiality of the non-presheared and presheared samples are given in Figure 4-29. It is interesting to see that the observed non-coaxiality of the presheared specimens is significantly different from that of the non-presheared specimens. Significant non-coincidence between the stress and strain increment directions was observed on presheared specimens tested with α = 15°, 30°, 60° and 75°. The deviations were especially significant when α = 30° and 60°, where the degree of non-coaxiality achieves 22 degrees in both cases. Similarly the deviation between the directions of the stress and strain increment diminished gradually as shearing progressed to larger stress ratio. A similar observation was reported from numerical simulations by Li and Yu (2009) using 2D DEM.

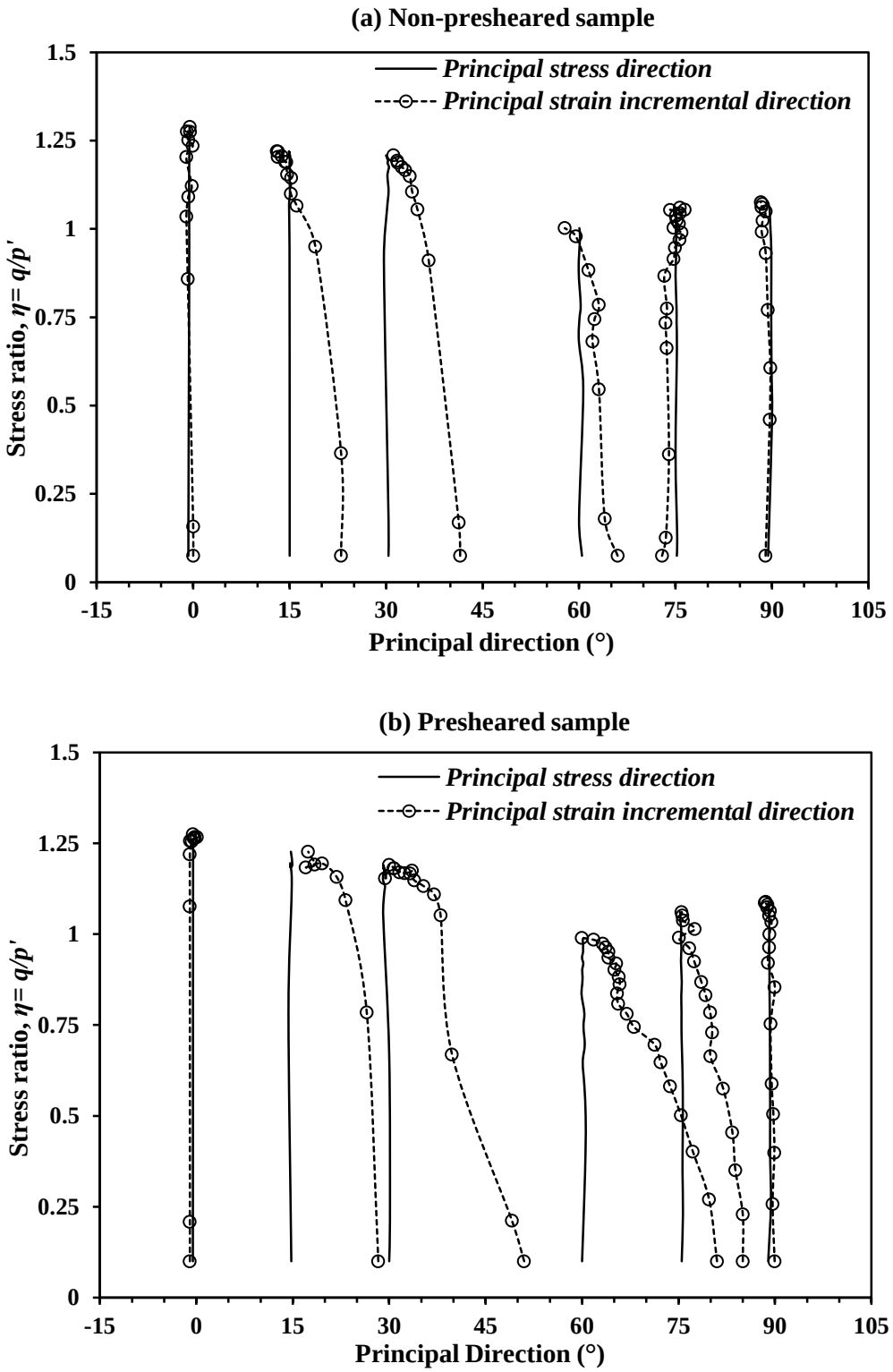

Figure 4-29: Stress and strain increment directions of (a) non-presheared sample and (b) pre-sheared sample.

4.7 Summary

This chapter presents a systematic investigation of the anisotropic behaviour of granular soil in monotonic shear with different fixed inclination of the major principal stress axis relative to the vertical. Four series of monotonic shear tests planned in Testing Program I have been carried out in SS-HCA using strain controlled mode (in terms of axial displacement control) to examine the effects of particle shape, material density and loading history on the stress-strain, failure characteristics and non-coaxiality of granular soils. All tests were performed on saturated specimens of Leighton Buzzard sand and Glass Ballotini under fully drained conditions.

Based on the experimental evidences presented in this chapter, it is concluded that the mechanical response of granular soils to monotonic shear is strongly dependent on the inclination of the major principal stress relative to the deposition direction. The observations suggest that the water deposited sand is inherently anisotropic, in spite of its particle shape and relative density. In general, as the loading direction deviates from the deposition direction, the stiffness and shear strength of sands reduces and the volumetric compressibility increases. Shear banding process is initiated near the peak and develops through the residual stress states. It has been found that the inclinations of the shear bands at different loading directions can be predicted reasonably well by taking account of the relative direction of the mobilized planes (Coulomb's theory) to the bedding plane. Non-coincidence of principal directions of stress and strain increment was observed in all the tests other than in the tests with the direction of major principal stress coincides with or perpendicular to the deposition direction. The result also indicates that the degree of non-coaxiality gradually reduces with increasing stress ratios and specimens were nearly coaxial when close to failure.

It is also suggested by the test results that for a given loading direction, rounder particle shape and lower relative density in an assembly of granular materials tend to produce softer response in stress-strain relationship, severer initial contraction and lower shear strength in monotonic shearing. The localized plastic deformation is more likely to develop in an assembly of angular particles than in an assembly of rounder particles. However, the effects of the particle shape and relative density on the non-coaxial behaviour of granular materials under monotonic shearing were found to be less significant. The sand samples experienced preshearing history to the peak were found to be less stiff and contracted more in the subsequent responses. For a given loading direction, the peak shear strength is relatively unaffected by preshearing to the peak stress. However, the preshearing history does have a significant effect on the noncoaxiality of sand specimens.

Chapter 5 Drained Behaviour of Granular Soil in Rotation Shear

5.1 Introduction

This chapter presents a detailed discussion of the experimental results obtained from the testing program II outlined in Chapter 3. In this testing program a series of drained rotational shear tests at different effective stress ratios have been carried out on dense Leighton Buzzard sands in order to examining the stress-strain behaviour, deformation characteristics and non-coaxiality of granular soils under rotational shear with drained conditions. The investigation of the effects of particle shape and material density on soil response in drained rotational shear has also been conducted in the testing program.

In this chapter, the testing details including the specimen initial conditions, actual stress path obtained and stress path control of the tests will be introduced first in Section 5.2. The results of the three series of rotational shear tests will then be presented and discussed in detail in Section 5.3. Finally, a brief summary of this chapter will be given in Section 5.4.

5.2 Test Details

5.2.1 Initial conditions

Same as Testing Program I, Leighton Buzzard sand and Glass Ballotini were used in the Testing Program II. The procedures of sample preparation, saturation and consolidation were strictly following the sample preparation procedures mentioned in Section 3.4.1. All specimens were consolidated isotropically to an effective mean pressure *p'* of 200kPa, using a back pressure of 400kPa to ensure 'full' saturation. A summary of the initial conditions of the tests is given in Table 5-1.

Table 5-1: Summary of the initial conditions of the tests in Testing Program II

	Relative density after consolidation *Drc*: %	Void ratio after consolidation e_c	Stress ratio η	Principal stress parameter, b
Series 1 Dense Leighton Buzzard sand	75.9	0.585	0.60	0.5
	76.3	0.584	0.70	0.5
	75.9	0.585	0.80	0.5
	75.9	0.585	0.90	0.5
	75.9	0.585	0.93	0.5
	76.3	0.584	0.95	0.5
	75.9	0.585	0.97	0.5
	76.6	0.583	1.02	0.5
	76.3	0.584	1.10	0.5
Series 2 Glass Ballotini	89.7	0.537	0.60	0.5
Series3 Medium dense Leighton Buzzard sand	43.5	0.671	0.60	0.5

5.2.2 Stress paths

The designed stress paths in *p'*- *q* and *X*-*Y* stress space are shown in Figure 5-1. During the tests, the samples were first subjected to monotonic shearing in the vertical direction up to a specified stress ratio while keeping the effective mean stress *p'* constant (A→B). After that the principal stress axes were rotated counter clockwise

(B→C→D→E→B) under drained condition, while keeping the deviatoric stress constant and maintaining the effective mean stress p' = 200 kPa and the intermediate principal stress parameter b = 0.5. To ensure full discharge of water from the specimen, the major principal stress direction α was rotated at a slow rate of 2°/min. Totally 50 cycles' rotation has been conducted for each rotational shear test.

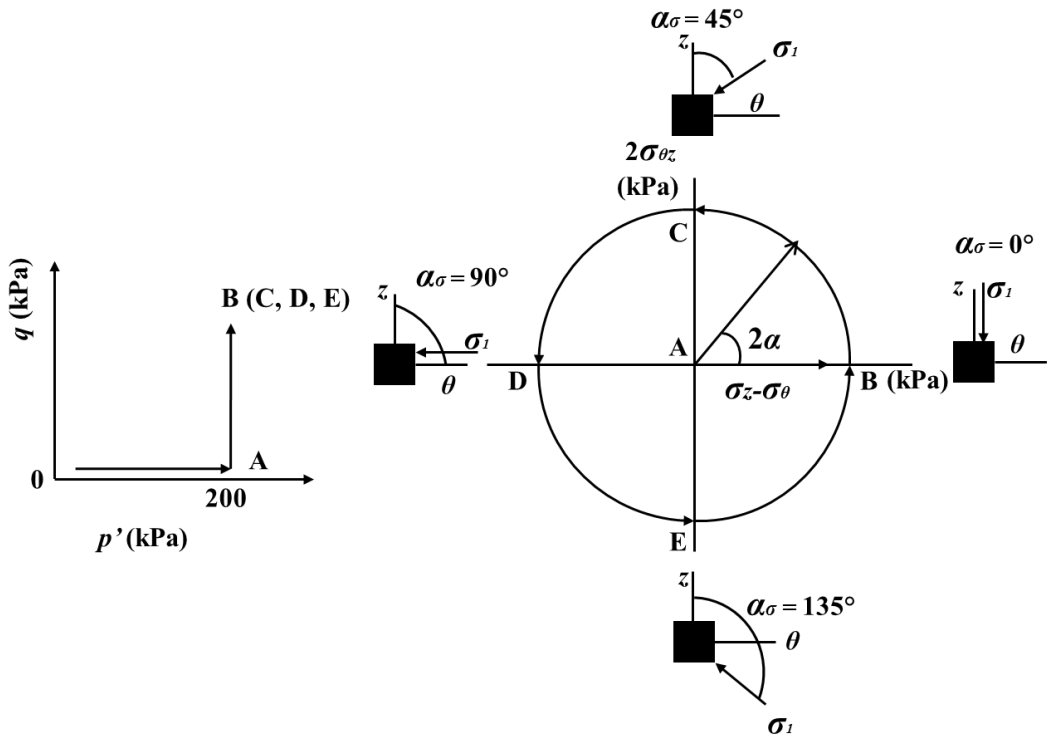

Figure 5-1: Stress paths in *q-p'* and *X-Y* stress space for rotational shear test.

5.2.3 Variation of applied loads and stress components

In order to follow the prescribed stress path precisely, smooth change in the controlling loads and pressures must be assured. Figure 5-2 shows the applied inner and outer cell pressures against the number of cycles for test with stress ratio η = 0.9, the variation of the vertical load and torque is shown in Figure 5-3. The computed average values of stress components σ_z, σ_r, σ_θ, $\tau_{\theta z}$ are shown in Figure 5-4. In each test the four loads were independently controlled so that the magnitude of the effective

principal stresses was maintained constant (Figure 5-5) but the direction of the major principal stress, characterised by the angle α was rotated continuously (Figure 5-6). In each cycle of rotation, α was varied from 0° to 180°. In test series 1 as stress ratio $\eta \leq$ 0.93 specimens did not reach failure and 50 cycles' rotation has been completed for these tests. For tests with η = 0.95 specimen was failed when α rotated to 56° in the second cycle. For test with η = 0.97 specimen was failed when α rotated to 104 ° in the first cycle. For tests with η = 1.02 and η = 1.1 specimens approached failure when α rotated to 48° in the first cycle. The stress trajectories plotted in the *X*-*Y* stress space for all the rotational shear tests in test series 1 are shown in Figure 5-7 and 5-8.

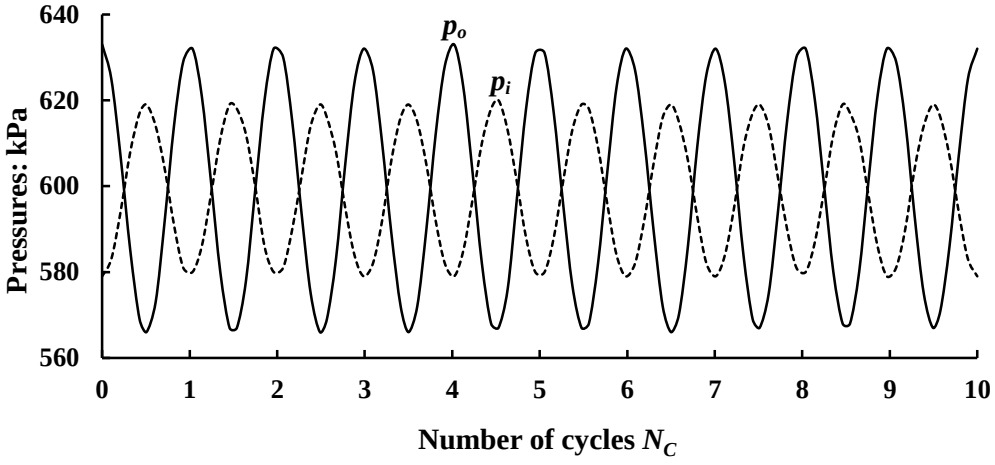

Figure 5-2: Variations of outer and inner cell pressures in rotational shear test (η = 0.9).

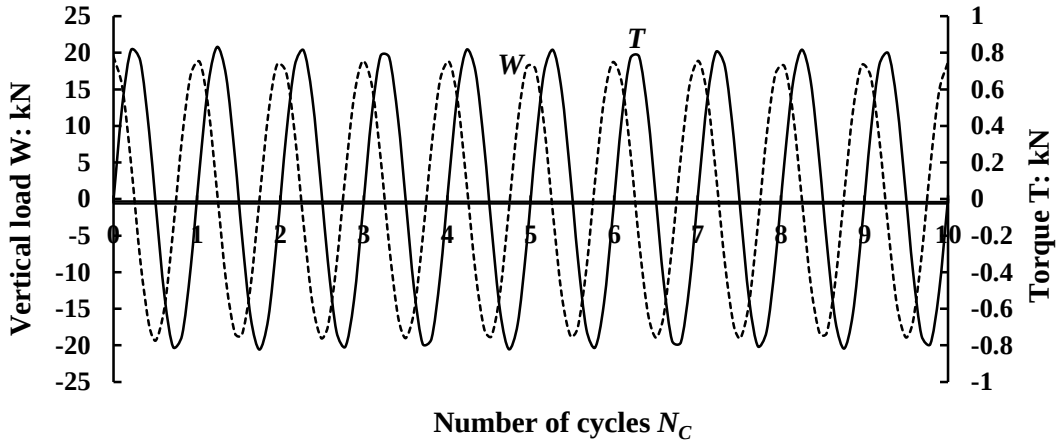

Figure 5-3: Variations of vertical load and torque in rotational shear test (η = 0.9).

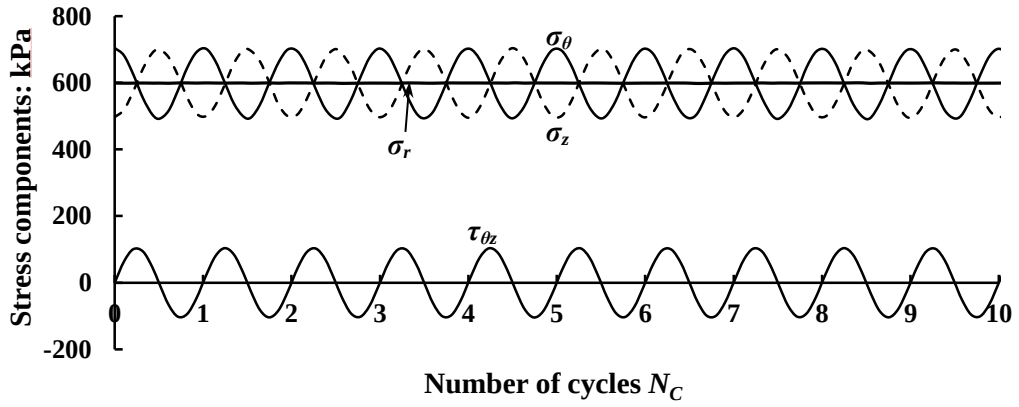

Figure 5-4: Variations of the stress components in rotational shear test (η = 0.9).

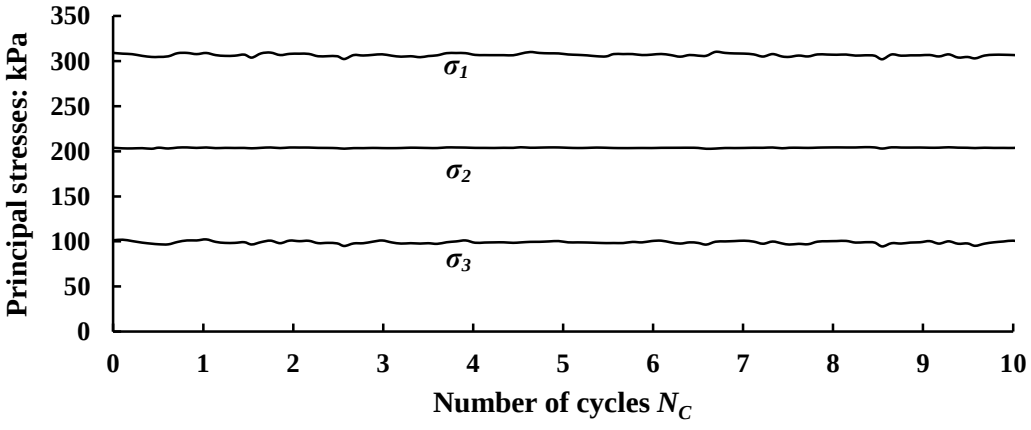

Figure 5-5: Magnitudes of effective principal stresses in rotational shear test (η = 0.9).

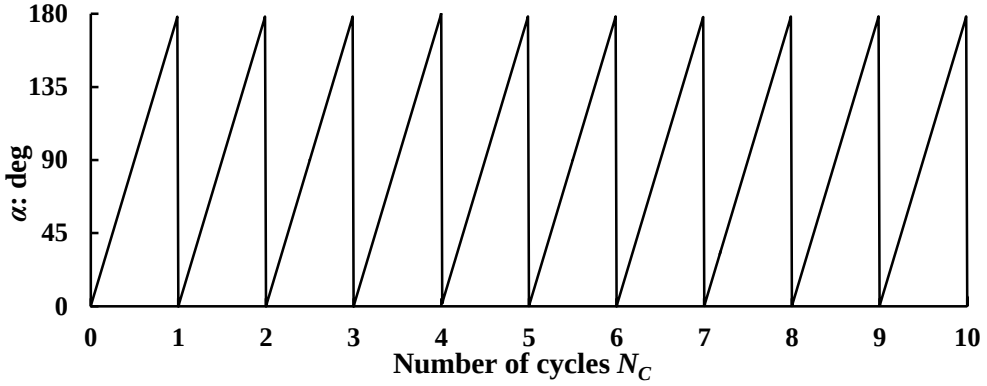

Figure 5-6: Variation of the principal stress direction in rotational shear test (η = 0.9).

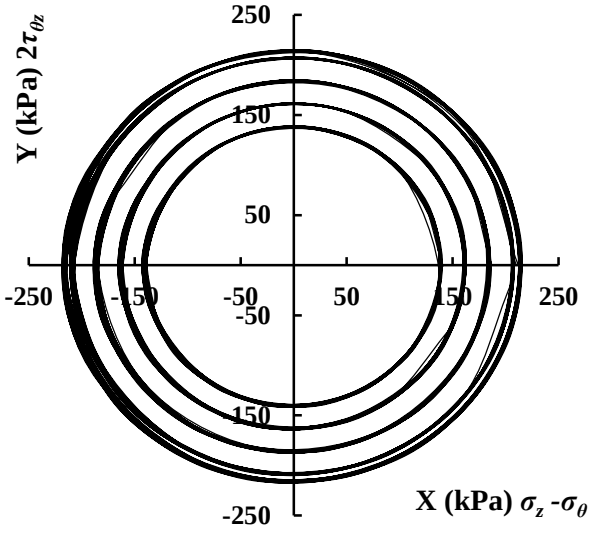

Figure 5-7: Actual stress paths followed in test series 1 for tests with: η = 0.6; η = 0.7; η = 0.8; η = 0.9; η = 0.93.

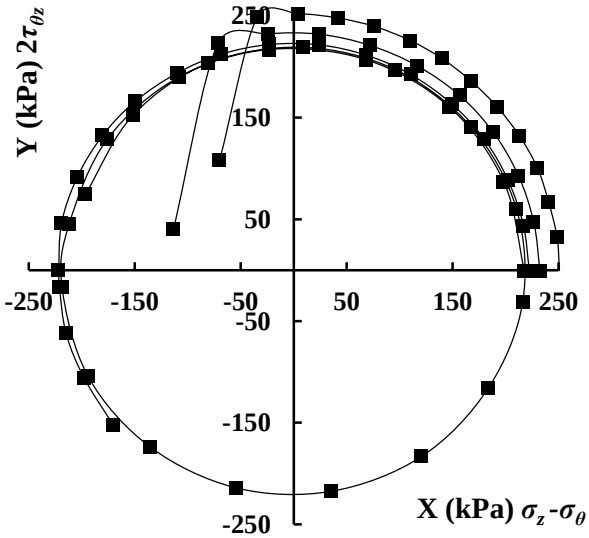

Figure 5-8: Actual stress paths followed in test series 1 for tests with: η = 0.95; η = 0.97; η = 1.02; η = 1.1.

5.3 Results of the Drained Rotational Shear Tests with Varying Stress Ratios

5.3.1 Variations in strain components

Figure 5-9 presents the development of the four strain components: ε_z, ε_r, ε_θ, $\gamma_{\theta z}$ with the number of cycles for tests at different stress ratios. In these figures, a positive value along the vertical axis indicates compression and negative indicates extension. It is observed that plastic strains are accumulated despite that the magnitudes of principal stresses are maintained constant. The strains are accumulated gradually with oscillation characteristics as the number of cycles increases and most of strains are generated during the first few cycles. Meanwhile, extensive axial and shear strains and compressive radial and circumferential strains are induced during the cyclic rotation of principal stress axes.

The stress components σ_z, σ_θ and $\tau_{\theta z}$ fluctuated sinusoidally with constant amplitude (see Figure 5-4). However, the amplitude of the consequent strain components ε_z, ε_θ and $\gamma_{\theta z}$ changed, showing a decrease in amplitude with increasing number of cycles. As shown in Figure 5-9, the amplitude of ε_z, ε_θ and $\gamma_{\theta z}$ was greatest in the first cycle and tended to converge to a constant level afterwards in succeeding cycles. This implied that the sand specimen stiffened and became stronger. The stiffening of the specimen may be due to the rearrangement of sand particles under cyclic rotation of principal stress axes. The sand specimen adjusts its particle arrangement in order to attain mechanical stability and when the stability is achieved the internal structure of the sand specimen reaches a relatively steady state (called as ‘ultimate state’ in this study).

Due to the gravity deposition during sample preparation and the applied initial major principal stress direction along the vertical deposition direction before principal stress axes' rotation, the sand specimen has lower compressibility along the vertical axis than that along the horizontal axis. Thus it can be seen from the figure that the high contractive radial strain ε_r is finally induced in all the tests due to easy compression tendency in the radial direction.

By comparing test with different values of stress ratio η, it can be seen that the magnitude of generated strains and the amplitude of their oscillations increases with the increase in the stress ratio η. The most dramatic change is that of the contractive radial strain ε_r, which increased about 3.5% as η increased from 0.6 to 0.93. For strain components ε_z, ε_θ and $\gamma_{\theta z}$, the fluctuations in the first few cycles were tended to be severer as η increases and the amplitude of these strain components in the ultimate state was increased.

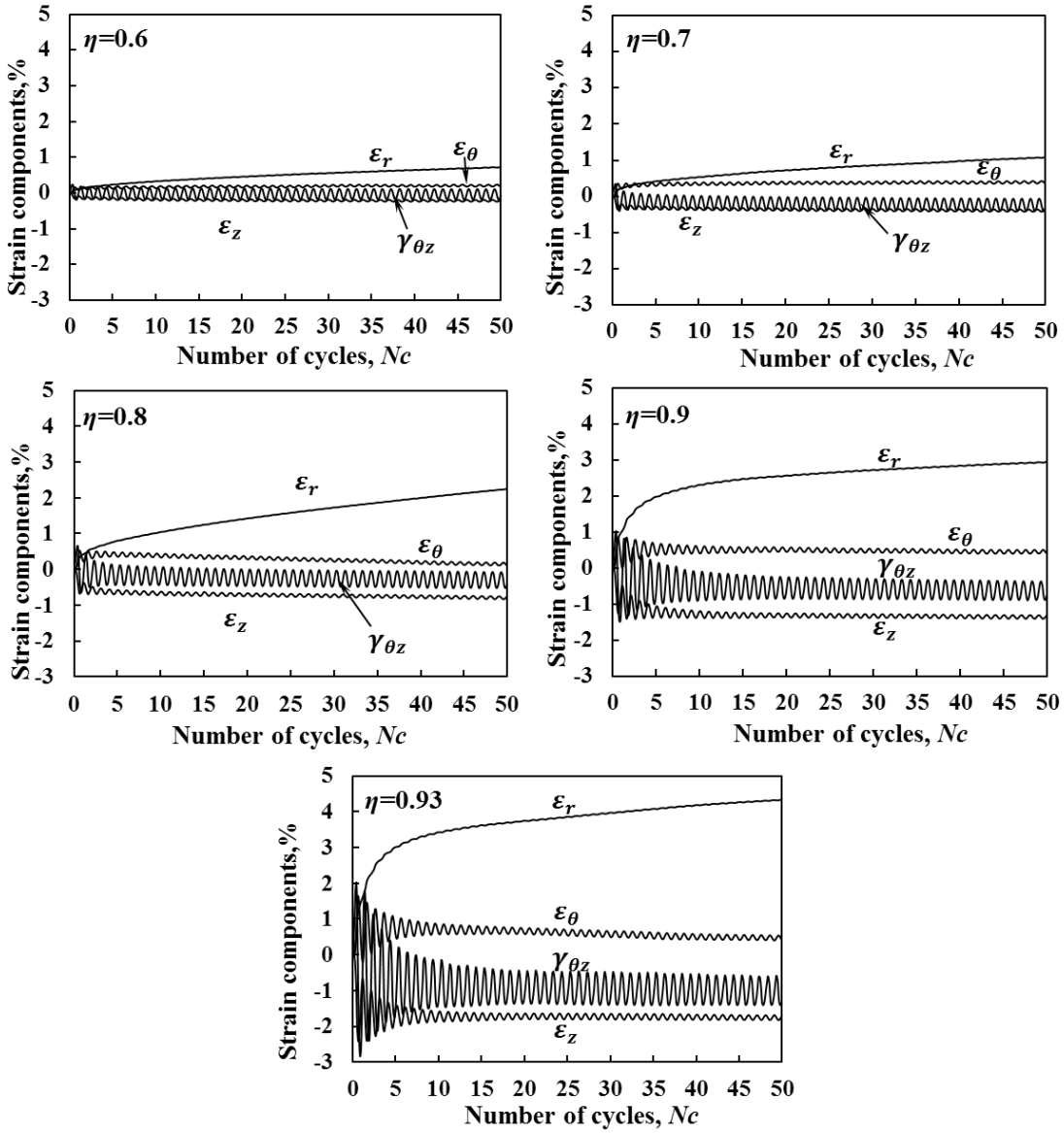

Figure 5-9: Development of strain components during rotational shear for test with: η = 0.6; η = 0.7; η = 0.8; η = 0.9; η = 0.93.

The results for tests with higher stress ratios are plotted in Figure 5-10. It is observed that although the magnitudes of effective principal stresses are maintained constant, all the samples approached failure during principal stress rotation. For test with η = 0.95 and 0.97, all of the four strain components fluctuated drastically with continuous rotation of principal stress axes. Unlike the tests with lower stress ratios, significant contractive shear strain $\gamma_{\theta z}$ was generated during the tests with η = 1.02 and 1.1, and both of the two specimens was failed in the first cycle when α close to 50 degrees.

As has been discussed in Chapter 3, particle deposition produces an initially anisotropic structure in granular soils. When subjected to shearing, such prepared specimen exhibits directional dependent shear strengths. Presented in Figure 5-11 is the peak stress ratio obtained from dense Leighton Buzzard sand with same relative density in monotonic loading tests with different fixed major principal stress directions. It can be seen that the lowest value of peak stress ratio (η_p = 1.02) was obtained at α = 60°. If pure rotation of the principal stress directions does not result in change of the material strength, specimen could not fail in rotational shear tests with η < 1.02. However, the experimental results showed that specimens approached failure in the tests with $\eta \geq 0.95$, indicating that the shear resistance of the sand specimen tends to be weakened by the continuous rotation of the principal stress axes.

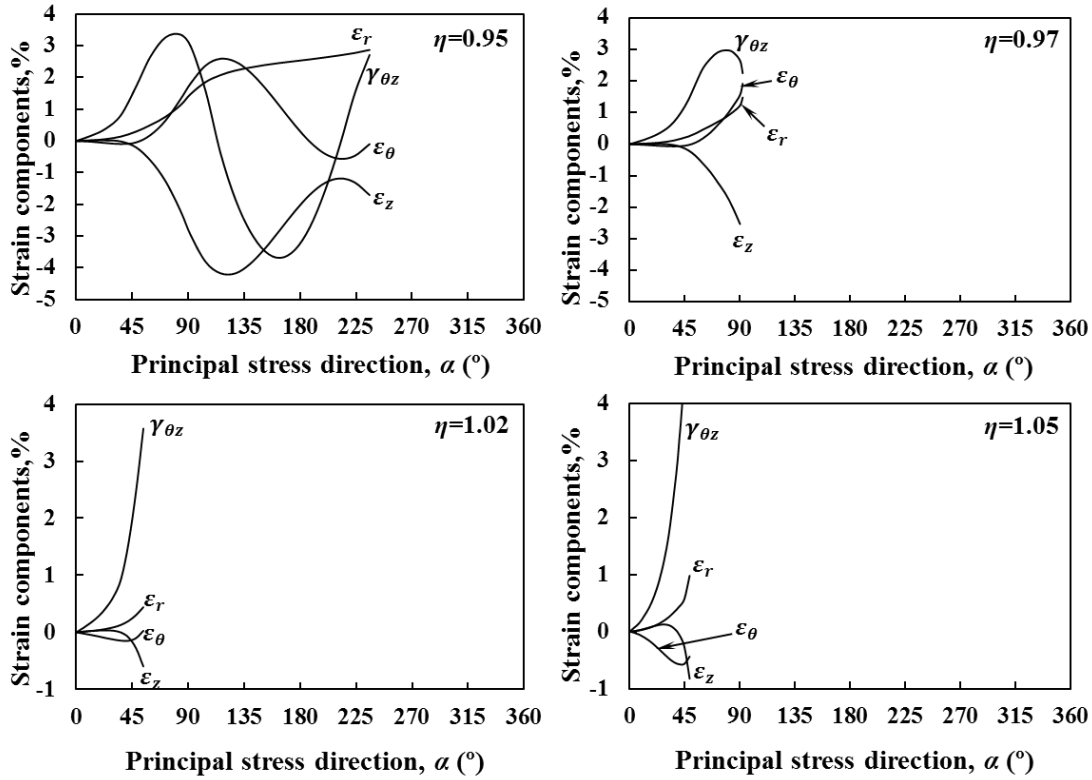

Figure 5-10: Development of strain components during rotational shear for test with: η = 0.95; η = 0.97; η = 1.02; η = 1.05.

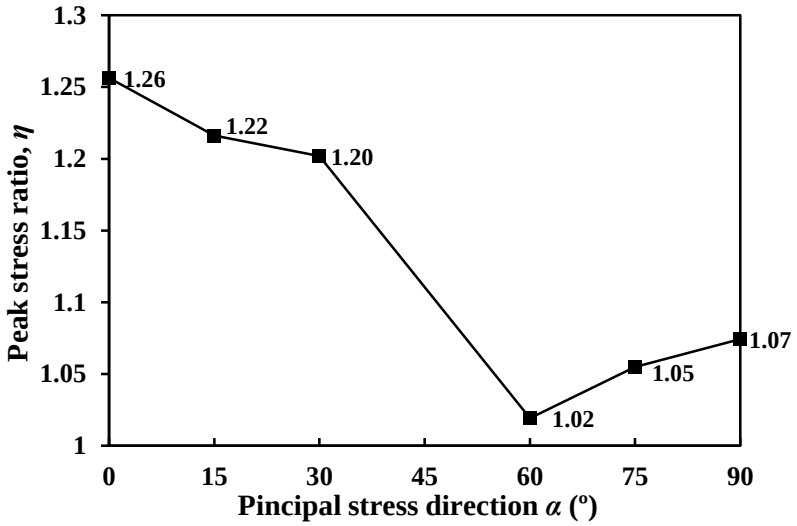

Figure 5-11: Peak stress ratio at different major principal stress directions for dense Leighton Buzzard sand.

5.3.2 Development of the volumetric strain

The evolution of the volumetric strain ε_v with the increasing number of cycles for test with lower stress ratios (e.g. η = 0.6, 0.7, 0.8, 0.9, 0.93) are shown in Figure 5-12. A positive value along the vertical axis indicates contraction and the negative indicates dilation. Although the magnitudes of principal stresses were maintained constant during each test, contractive volumetric strain was accumulated due to the rotation of principal stress directions. Most of the volumetric strain occurs during the first few cycles and its accumulation rate tends to decrease as the number of cycles increases. These observations showing consistency with experimental results reported by Tong et al. (2010) from the drained rotational shear tests and the numerical experiments carried out by Li and Yu (2010) using 2D DEM. In undrained rotational shear, the contractive volume change tendency is exhibited as the build-up of pore water pressure, as reported by Ishihara and Towhata (1983), Nakata et al. (1998) and Yang et al. (2007). Moreover, it is clear from the figure that the effect of stress ratio on the development of the volumetric strain is significant under otherwise identical

conditions. For all the five tests, the amount of the contractive volumetric strain at the same number of cycles increases with the increase in the stress ratio η.

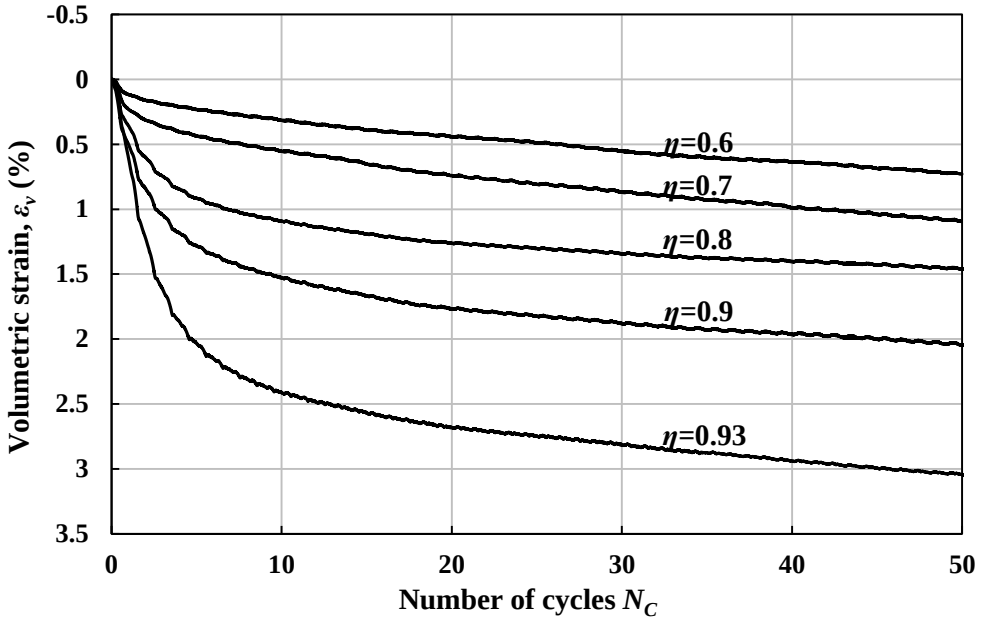

Figure 5-12: Development of the volumetric strain with number of cycles for test with: η = 0.6; η = 0.7; η = 0.8; η = 0.9; η = 0.93.

To have a better view of the development of volumetric strain in a single cycle, The volumetric strain ε_v against major principal stress direction α in the 1st , 25th and 45th cycle for test with η = 0.7 has been plotted in Figure 5-13. It can be seen that the contractive volumetric strain is induced when the major principal stress direction rotates from 0° to 180° in the first cycle and the accumulation rate is particularly significant when the major principal stress direction α rotates in the range of [45°, 135°]. The variation trend of the volumetric strain in a single cycle become similar as the number of cycles increases, such as N_C = 25 and 45 showing in the figure, the dilatant volumetric strain is induced first when α rotates from 0° to 90° and then the dilation changes to contraction as α rotates from 90° to 180°. However, in either case, the total contractive volumetric strain increases after a full rotation cycle.

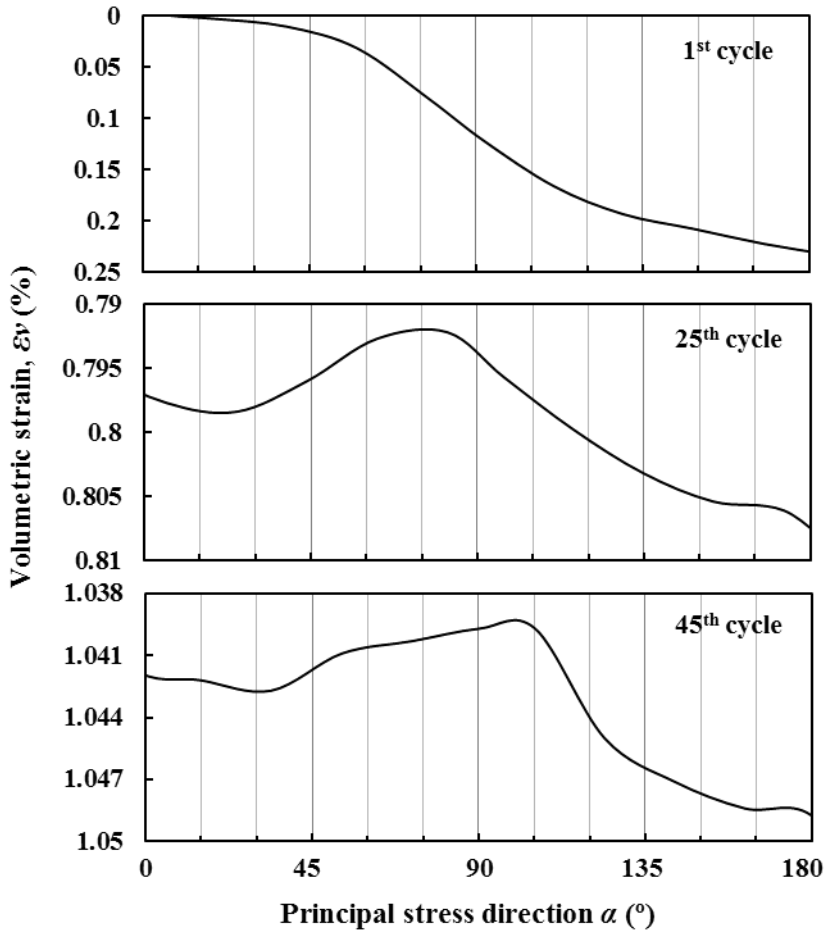

Figure 5-13: Volumetric strain vs. principal stress direction at different number of cycles for test with η = 0.7.

The results for tests with higher stress ratios (e.g. η = 0.95, 0.97, 1.02, 1.1) are plotted in Figure 5-14. It can be observed that for tests with η = 0.95 and 0.97 specimens were contracted until failure approached. However, for tests with η = 1.02 and 1.1, dilative volumetric strain was developed as the rotation started and both of the two specimens were failed in the first cycle when the major principal stress direction rotated to about 50 degrees.

The qualitative explanation for the different evolution tendency of the volumetric strains at different stress ratios could be given as follows. As mentioned early, the sand specimen tends to have lower compressibility along the vertical axis due to the

gravity deposition and initial vertical loading. For test with lower stress ratios, when principal stress axes begin to rotate clockwise from the vertical, soil particles are pressed together, reducing pore space between them thus developing load resisting columns with respect to the continuously changing principal stress direction. Therefore, contractive volumetric strain is induced. Meanwhile, recalling that the highest deformation rate of sands is induced in the first few cycles, the internal material structure produced in the initial stage is tend to be stabilized with increasing number of cycles. However for tests with higher stress ratios (e.g. η = 1.02 and 1.1), as frictional resistance and interlocking between particles failed to resist the large shear stress, soil particles are mobilized and transported along the direction of the applied shear stress leads to a dramatic expansion of the material volume.

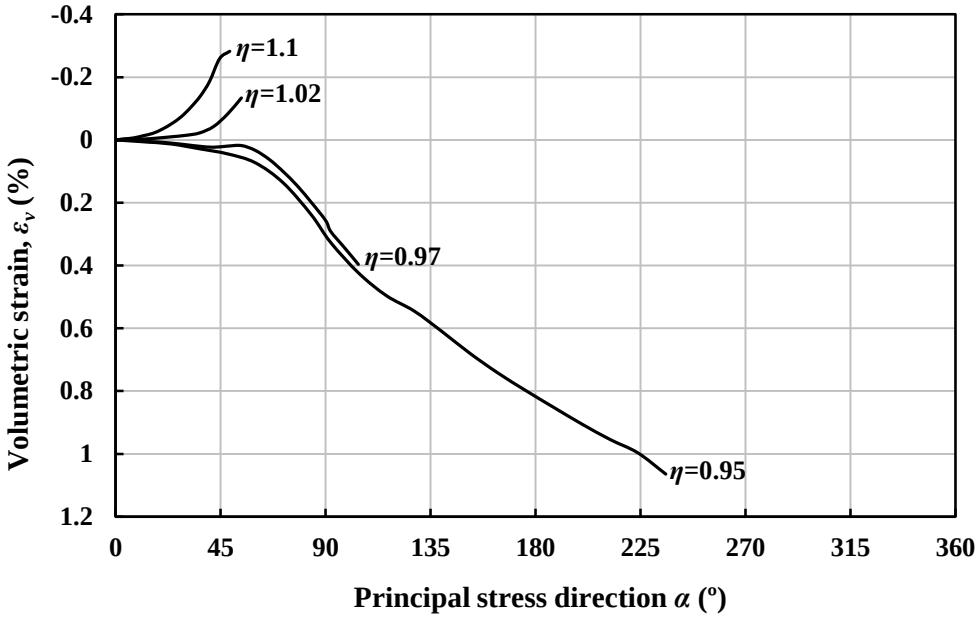

Figure 5-14: Development of the volumetric strain with principal stress direction for test with: η = 0.95; η = 0.97; η = 1.02; η = 1.10.

5.3.3 Shear stress-strain relationship

The shear stress-strain relationships for the rotational shear tests can be characterized as shown in Figure 5-15 and Figure 5-16. For test with lower stress ratios (e.g. η = 0.6,

0.7, 0.8, 0.9, 0.93), it can be seen from Figure 5-15 that the shear stress-strain curve for all the specimens showed hysteretic and plastic characteristics. The hysteretic loops appear open for the first cycle, indicating the occurrence of the plastic deformation due to principal stress rotation alone. As the number of cycles increases, the hysteretic loops tend to be closed and become more similar to each other, indicating that the internal structure of the specimens are gradually stabilized with the continuous rotation of principal stress axis. However, as shown in Figure 5-16 for tests with higher stress ratios (e.g. η = 0.95, 0.97, 1.02, 1.1) specimens were failed at large shear strains in the beginning stage except for test with η = 0.95, failure occurred after a full circle has been completed.

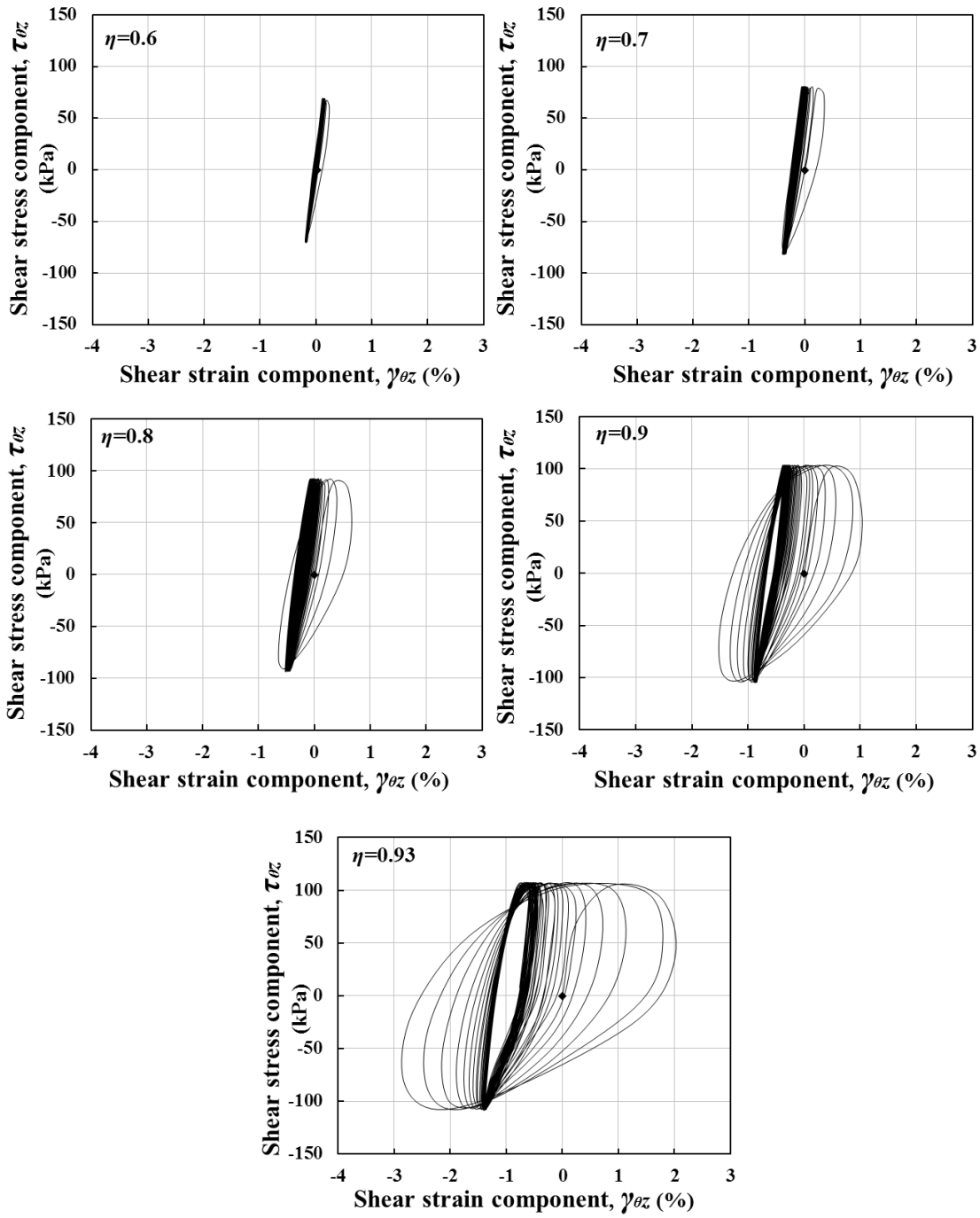

Figure 5-15: Shear stress-strain relationship for tests with: η = 0.6; η = 0.7; η = 0.8; η = 0.9; η = 0.93.

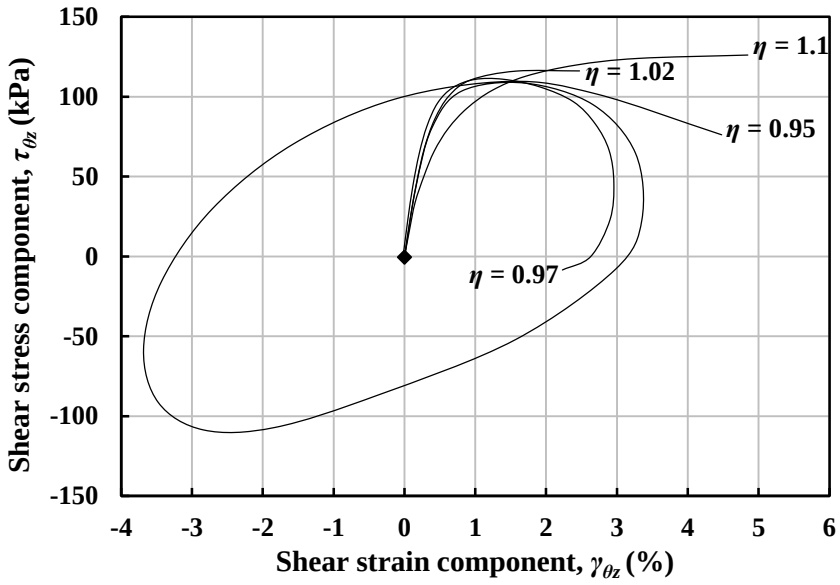

Figure 5-16: Shear stress-strain relationship for tests with: η = 0.95; η = 0.97; η = 1.02; η = 1.1.

5.3.4 Evolution of strain paths in deviatoric strain space

The strain trajectories in the deviatoric strain space for rotational shear tests with lower stress ratios (e.g. η = 0.6, 0.7, 0.8, 0.9, 0.93) are shown in Figure 5-17. It can be observed that the trajectories in the deviatoric strain space appear to be opened in the first cycle. However, when sand specimen is continuously sheared, the evolution of the trajectories appears as spirals and their shapes seemed to become more accordant as the number of cycles increases. Similar strain trajectories in undrained rotational shear tests were reported by Yang et al. (2007). For tests with different stress ratios, it can be seen clearly from the figure that the size of the trajectories increases significantly with the increase in the stress ratio. The shapes and positions of the strain trajectories of the five tests in the deviatoric strain space at the last cycle (N_C = 50) are plotted together in Figure 5-18. It can be seen that all the trajectories at the final cycle are elliptical with the major axis close to the vertical. With the increase in

the value of stress ratio, the position of the strain trajectories is gradually shifted away from the origin of the deviatoric strain plane.

To have a better view, the five ellipses are replotted together with the same centre in Figure 5-19. It is interesting to note that the long axes of the ellipses coincide with each other very well. They are all inclined to the horizontal line at an angle of about 86°. However due to the limitation of the laboratory investigation, the micro mechanisms responsible for these phenomenon have not been identified. Numerical experiments using 3D DEM would be highly appreciated in order to get a better understanding of the underlying mechanisms responsible for the observed behaviour.

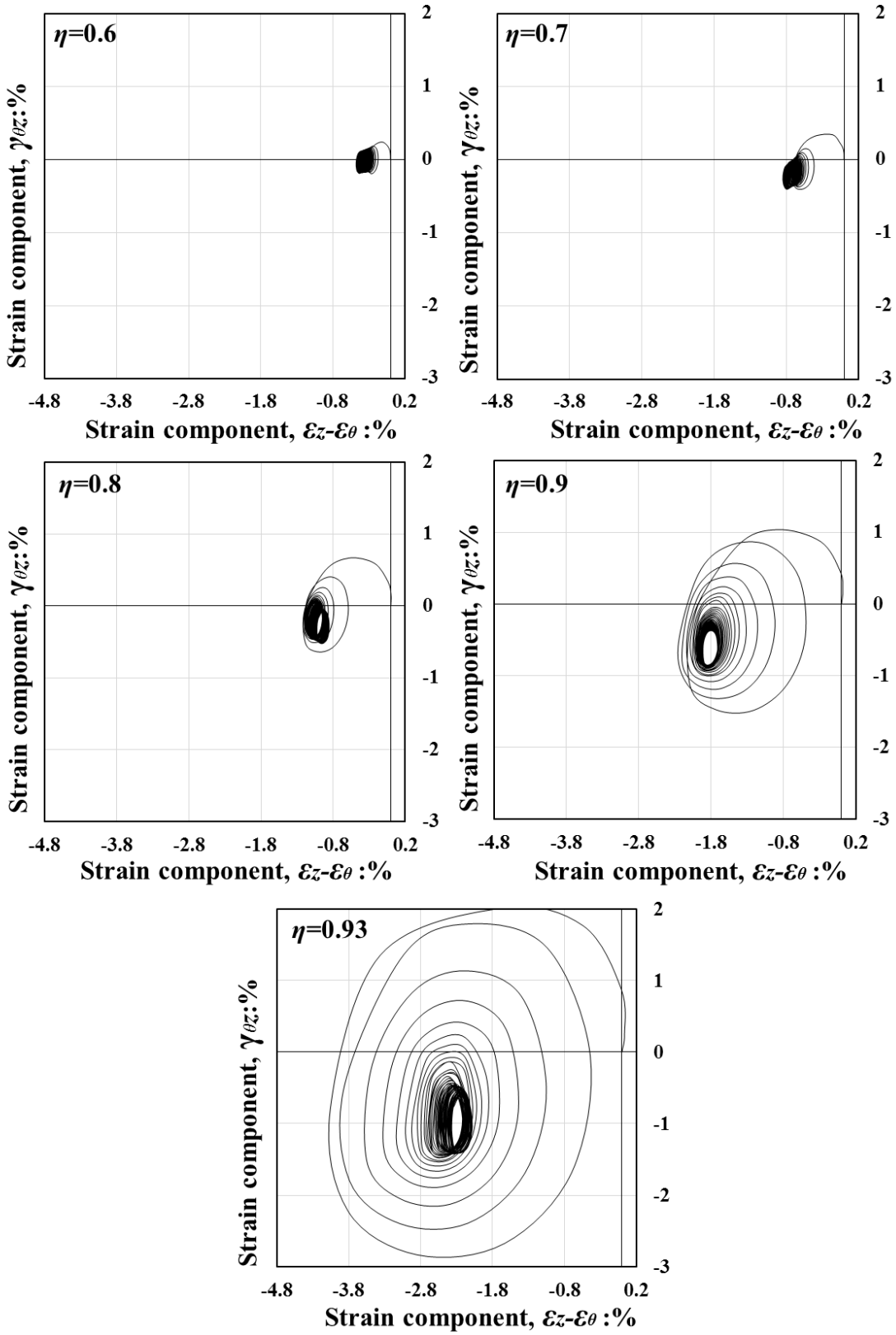

Figure 5-17: Evolution of the strain paths in the deviatoric strain space for tests with: η = 0.6; η = 0.7; η = 0.8; η = 0.9; η = 0.93.

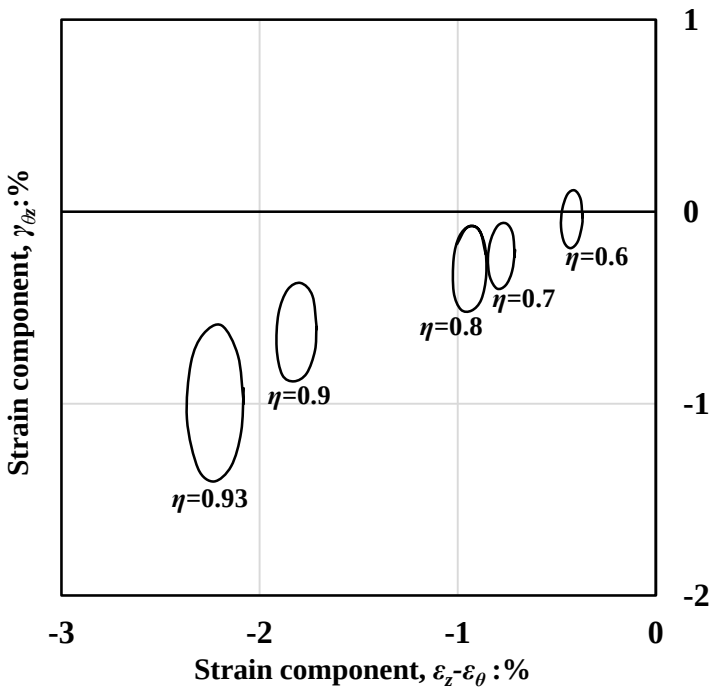

Figure 5-18: Final shape and position of strain paths in deviatoric strain space for tests with: η = 0.6; η = 0.7; η = 0.8; η = 0.9; η = 0.93.

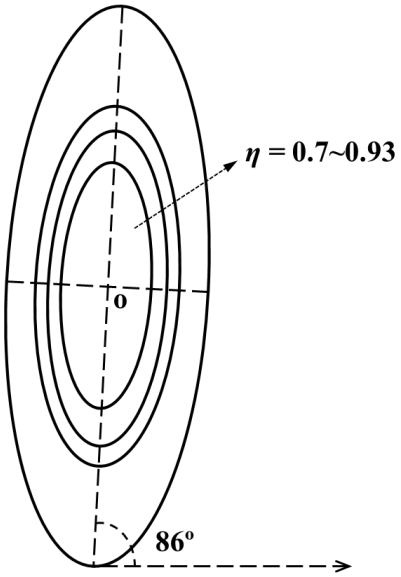

Figure 5-19: Superposition of the shape of strain path in the final cycle for test with: η = 0.6; η = 0.7; η = 0.8; η = 0.9; η = 0.93.

The strain trajectories in the deviatoric strain space for tests with higher stress ratios (e.g. η = 0.95, 0.97, 1.02, 1.1) are plotted in Figure 5-20. For tests with η = 0.95, it can be seen that a large deformation was developed in the first cycle and specimen approached failure in the second cycle. For tests with η = 0.97, 1.02 and 1.1, a drastic development of deformation was observed and specimens were failed in the first cycle.

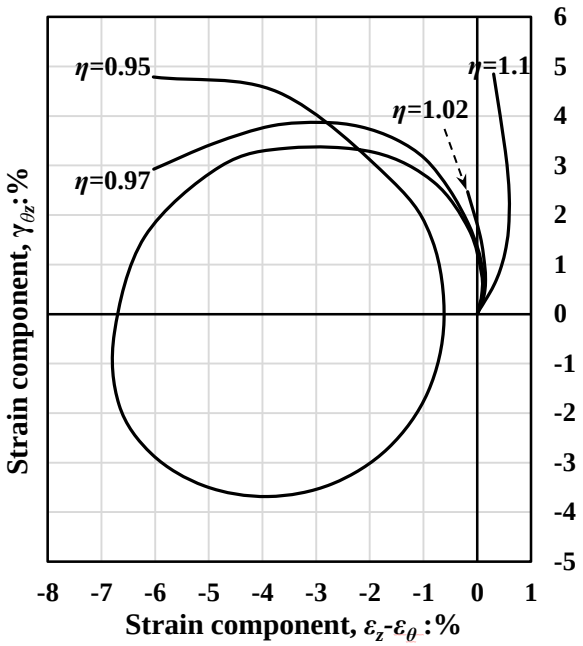

Figure 5-20: Strain paths in the deviatoric strain space for test with: η = 0.95; η = 0.97; η = 1.02; η = 1.1.

5.3.5 Non-coaxiality

The degree of non-coaxiality β as measured by the deviation between the major principal stress direction and the principal strain increment direction for tests with lower stress ratios (e.g. η = 0.6, 0.7, 0.8, 0.9, 0.93) are plotted in Figure 5-21. It needs to be noted that for tests with higher stress ratios (e.g. η = 0.95, 0.97, 1.02, 1.1) the strain components obtained from the tests could not accurately reflect the soil behaviour as large deformation occurred during the tests. Therefore, the non-coaxial behaviour of the sand specimen under rotational shear with higher stress ratios has not

been investigated in this study. Moreover, it is important to state that the total strain increment instead of the plastic strain increment is used in the following analysis.

From Figure 5-21 it can be seen that the variation trend of the non-coaxiality degree shows an obvious periodicity during the tests and as marked on the figure they are all started with $\beta \approx 40°$. Lower degrees of non-coaxiality are observed in the first few cycles. When the rotational shear continues, the strain increment direction becomes closer to the stress increment direction (e.g. $\beta = 45°$) and higher degrees of non-coaxiality are observed. After about 20 rotation cycles, the variation of the non-coaxiality degree appeared to be stabilized. It is clear that the increasing trend of the non-coaxiality degree at the initial stage is more obvious for tests with higher stress ratios.

The black solid lines in Figure 5-21 are the trend lines of the non-coaxiality degree. With a lower stress ratio (e.g. $\eta = 0.8$), β is closer to 45°, indicating the strain increment direction is closer to the stress increment direction. At the same number of cycles, the degree of non-coaxiality decreased with the increase of the stress ratio. This observation agrees well with the laboratory results presented by Gutierrez et al. (1991) and numerical results obtained by Li and Yu (2010) based on 2D DEM simulations.

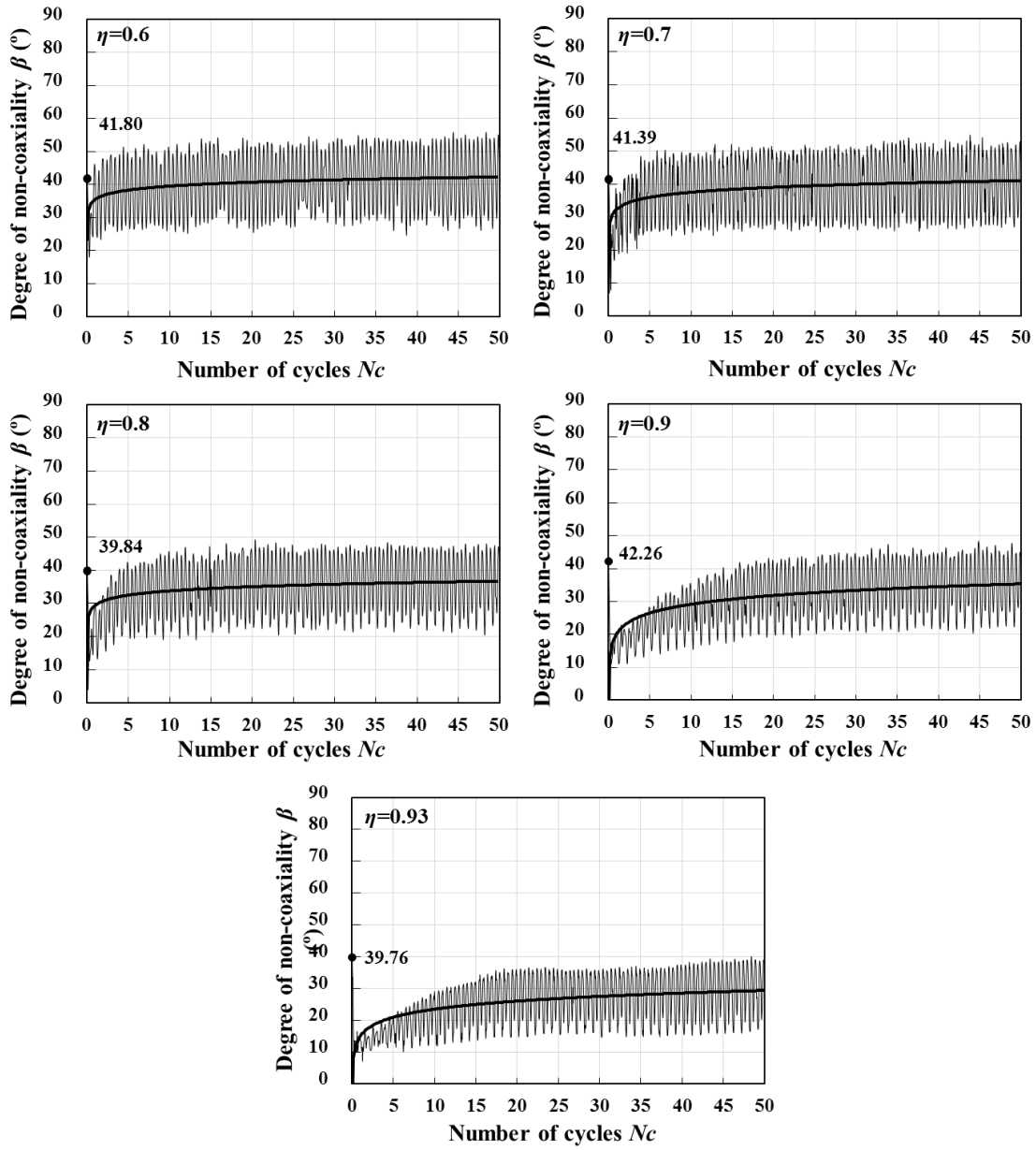

Figure 5-21: Degree of non-coaxiality against number of cycles for test with: η = 0.6; η = 0.7; η = 0.8; η = 0.9; η = 0.93.

As described above, the variation trend of the non-coaxiality degree shows an obvious periodicity during the tests. To have a better view, the relationship of the non-coaxiality degree with the major principal stress direction α at N_C = 1, 20 and 45 for tests with different stress ratios are presented in Figure 5-22 (a)-(c). It is clear that the variation of the non-coaxiality degree differs significantly at the initial stage and the ultimate state. At the initial stage when N_C = 1 the degree of non-coaxiality lies

approximately in the range of 10° to 40°, as shown in Figure 5-22 (a). It tends to decrease when α rotates from 0° to 90° and then increase during the latter half cycle's rotation. However, at N_C = 23 and 45, which represent the ultimate state of the sand specimen, it can be observed from Figure 5-22 (b) and (c) that the degree of non-coaxiality varies in a common manner for all the tests. That is, the fluctuation of the non-coaxial degree exhibits two periods of a sine wave displaced at 180 degrees intervals. It has two peaks larger at the direction of α = 67.5° and 157.5° and smaller at α = 22.5° and 117.5° respectively. This tendency is independent of the stress ratio and previous rotation cycles of principal stress axes. However, the stress ratio does have a significant effect on the magnitude of non-coaxiality degree. The larger the stress ratio, the lower non-coaxial degree between the directions of the strain increment and stress is induced.

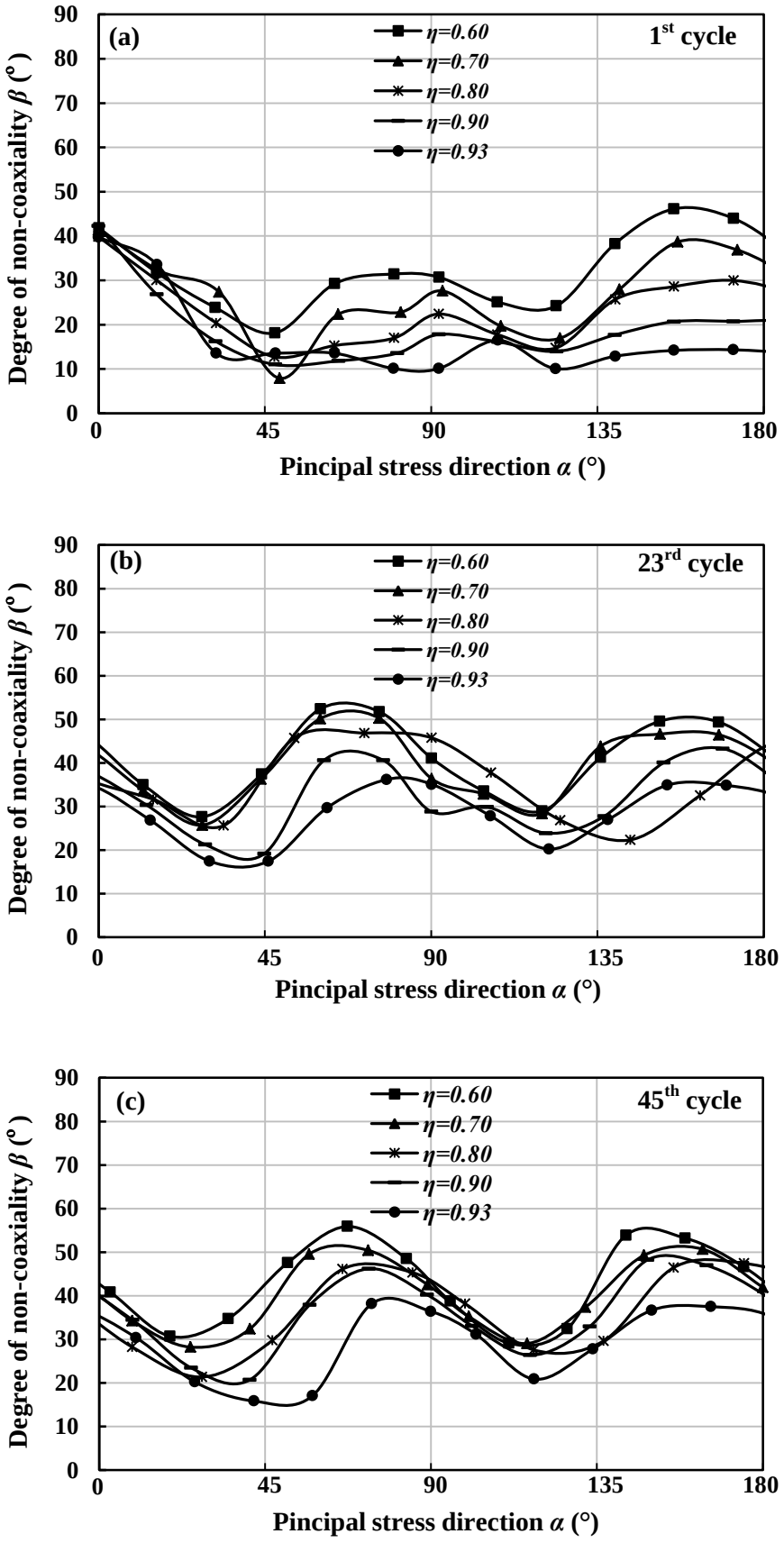

Figure 5-22: Degree of non-coaxiality for rotational shear tests at: (a) N_C = 1; (b) N_C = 23; and (c) N_C = 45.

Figure 5-23 compares the measured strain increments superimposed on the stress path on the *X*-*Y* stress space in the 1st and 45th cycle for the test with stress ratio η = 0.7, 0.8, 0.9. In general, it may be seen in the figure that the direction of the strain increment is neither parallel to the vector of stress increment nor current stress and it lies always between both of them. Consequently, it may be mentioned that the deformation of sand under rotational shear is neither purely elastic nor plastic and it contains both of the two components.

At both N_C = 1 and 45, the magnitude and direction of the strain increments are gradually enlarged with the increase of the stress ratio. It is interesting to see that for N_C = 45 the strain increment differs significantly in different sections. When the principal stress axis rotate along the stress paths of DA and BC, which correspond to the major principal stress direction α in ranges of [45°, 90°] and [135°, 180°], the amount of shear strain increment is small and the strain increment direction is very close to the stress increment direction, material behaves elastically. The phenomenon is particularly evident in the tests with lower stress ratios (e.g. η = 0.6, 0.7). However, when the principal stress axis rotate along the stress paths of AB and CD, corresponds to α in ranges of [0°, 45°] and [90°, 135°], the amount of shear strain increment is large and the directions of the strain increments are larger and a significant non-coaxiality between the directions of the strain increment and stress are induced. The above observations are consistent with the results reported by Tong et al. (2010) from the drained rotational shear tests performed on Toyoura sands in HCA.

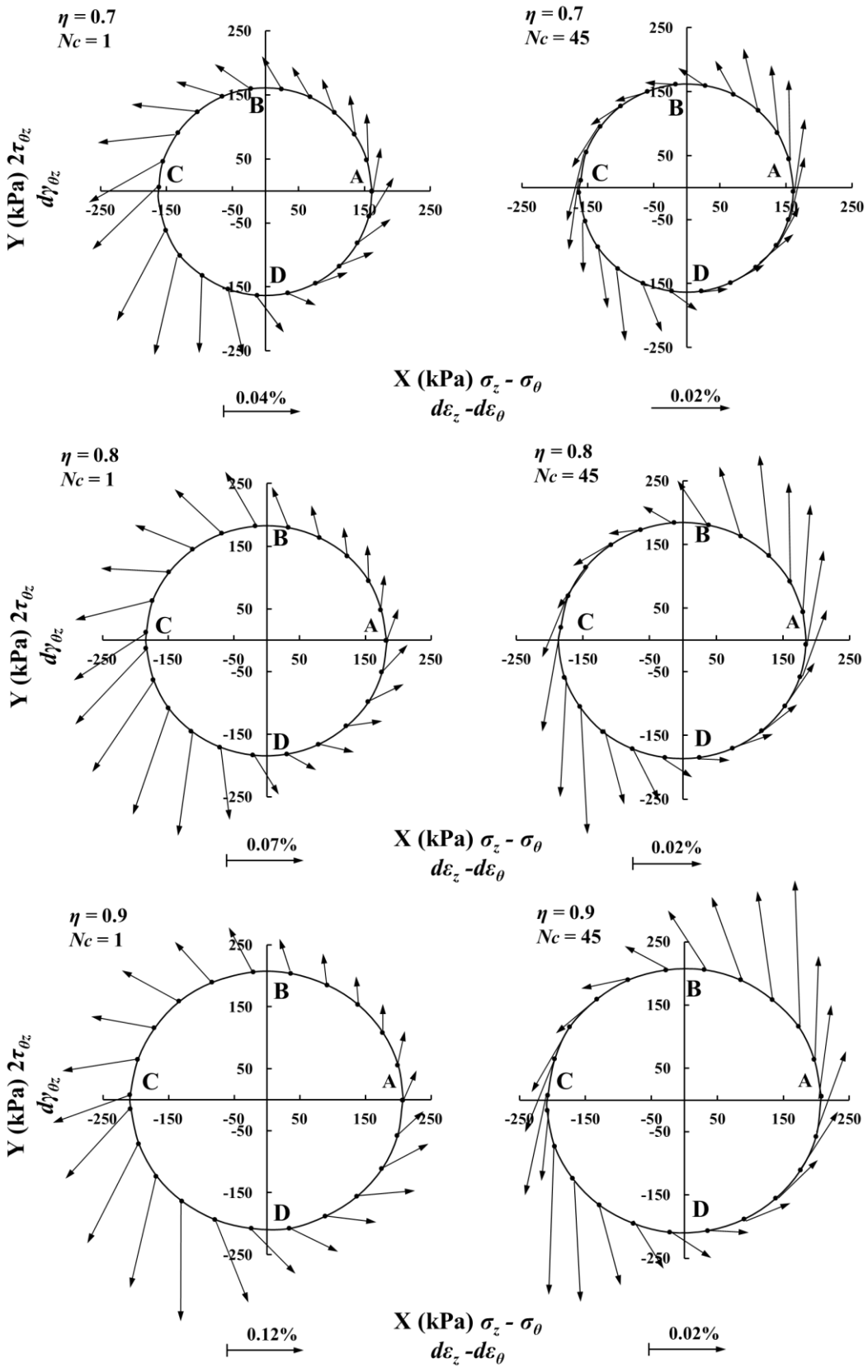

Figure 5-23: Stress paths and strain increments in rotational shear tests at N_C = 1 and N_C = 45.

5.4 Effects of Particle Shape and Material Density

5.4.1 Variations in strain components

As listed in Table 5-1 rotational shear test has also been carried out on Glass Ballotini (D_{rc} = 90%) and medium dense Leighton Buzzard sand (D_{rc} = 43%). The results are compared with those from dense Leighton Buzzard sand (D_{rc} = 76%) in order to investigate the effects of particle shape and material density on soil response in drained rotational shear. Figure 5-24 (a)-(c) presents the variations of the four strain components against the number of cycles for test performed on the three materials.

By comparing the results obtained from dense Leighton Buzzard sand and Glass Ballotini as shown in Figure 5-24 (a) and (b), it can be seen that the variation trend and the amplitude of the oscillations of strain components: ε_z, ε_θ and $\gamma_{\theta z}$ for the two materials is similar and the generated radial strain ε_r of Glass Ballotini is slightly lower than that of Leighton Buzzard sand. However, for test with lower relative density as shown in Figure 5-24 (c), the amplitude of the oscillations of all the four strain components in the first few cycles and the amount of generated strains at the end of test are much larger than those of dense Leighton Buzzard sand.

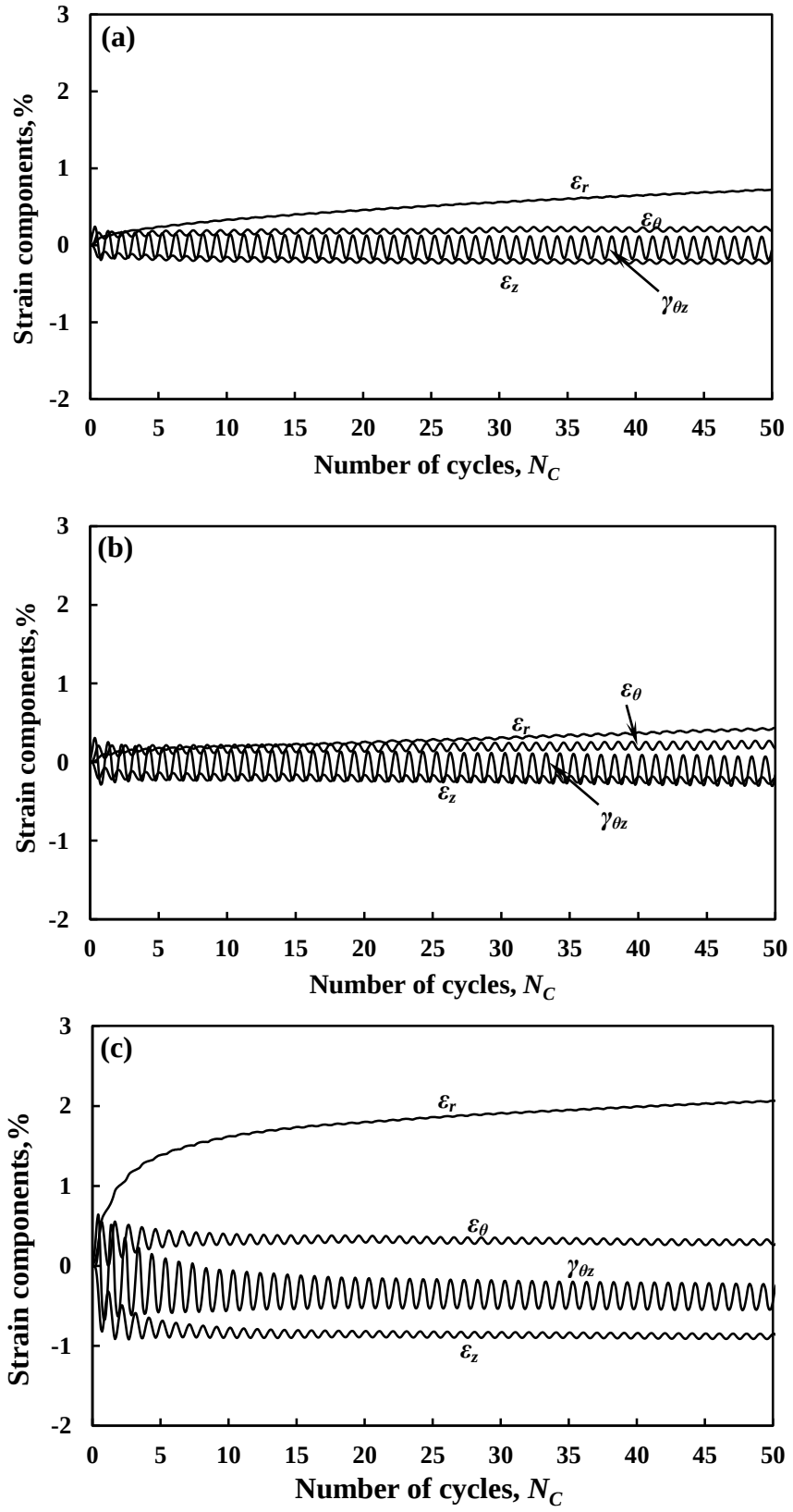

Figure 5-24: Development of strain components during rotational shear for test performed on: (a) Dense Leighton Buzzard sand; (b) Glass Ballotini; (c) Medium dense Leighton Buzzard sand.

5.4.2 Development of the volumetric strain

The developments of the volumetric strain with the increasing number of cycles for rotational shear test performed on the three materials are presented in Figure 5-25. Even though the Glass Ballotini has higher relative density than dense Leighton buzzard sand, the former is more contractive than the latter. The explanation for this phenomenon may be that due to particle shape effects, the shear resistance of the Glass Ballotini is lower than that of Leighton Buzzard sand. Therefore, as cyclic rotational shear stress was applied, Glass Ballotini specimen needs to contract more and become denser in order to attain mechanical stability. For test performed on medium dense Leighton Buzzard sand, as might be expected, the specimen exhibits much more volumetrically contractive behaviour than the other two.

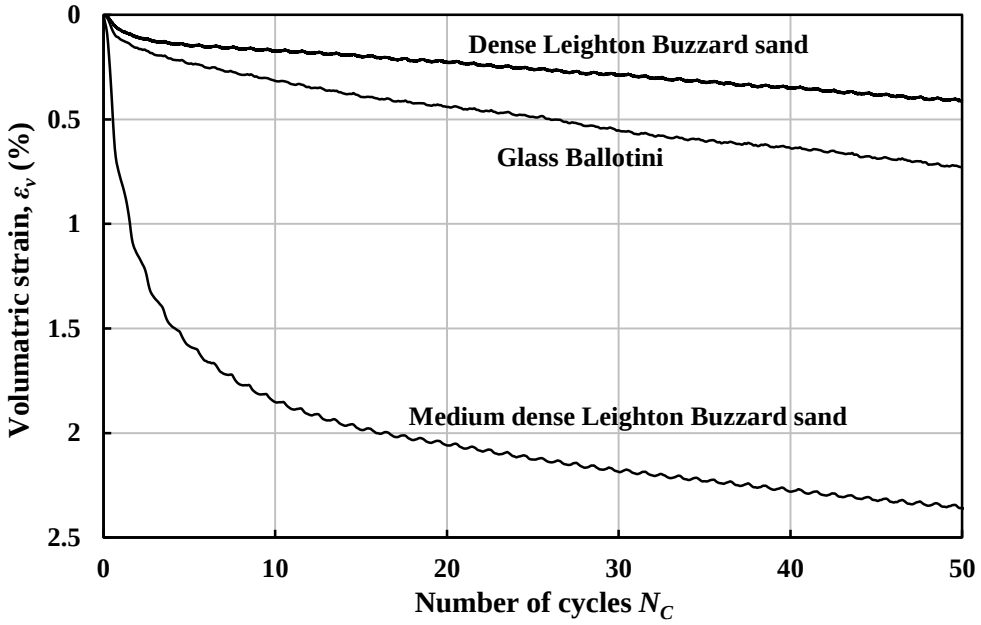

Figure 5-25: Development of the volumetric strain with number of cycles for rotational shear test performed on: Dense Leighton Buzzard sand; Glass Ballotini; Medium dense Leighton Buzzard sand.

5.4.3 Shear stress-strain relationship

The shear stress-strain relationships for the rotational shear test performed on the three materials are given in Figure 5-26 (a)-(c). In general, the shear stress-strain curve for all the three specimens showed similar characteristics. The hysteretic loop at the first several cycles for the Glass Ballotini appeared to be slightly larger than that of the dense Leighton Buzzard sand. For medium dense Leighton buzzard sand, the hysteresis loop was greater in the beginning stage, and then gradually stabilized as the mechanical stability of the specimen was achieved.

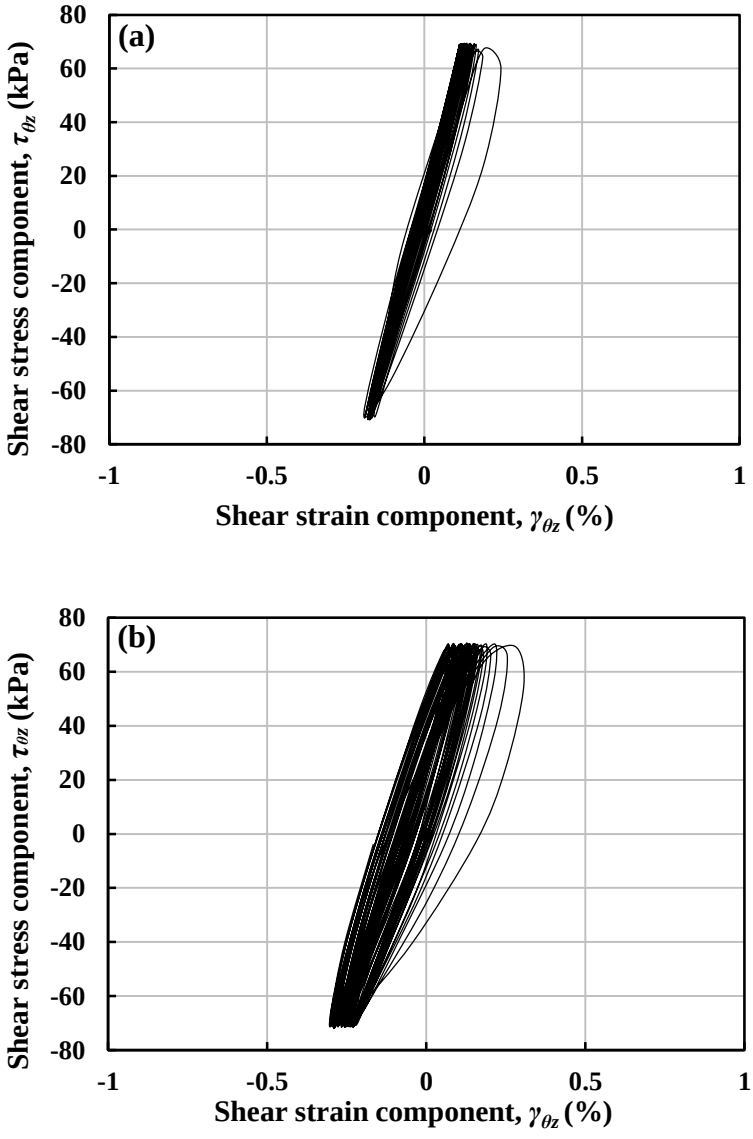

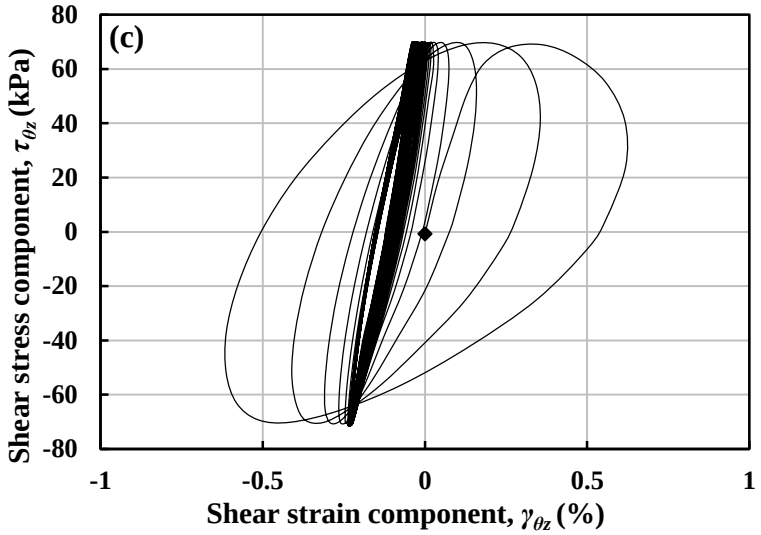

Figure 5-26: Shear stress-strain relationship for rotational shear test performed on: (a) Dense Leighton Buzzard sand; (b) Glass Ballotini; (c) Medium dense Leighton Buzzard sand.

5.4.4 Evolution of strain paths in deviatoric strain space

The evolutions of the strain trajectories in the deviatoric strain space for the rotational shear test performed on the three materials is shown in Figure 5-27 (a)-(c). It can be observed that for dense Leighton Buzzard sand (Figure 5-27 (a)) and Glass Ballotini (Figure 5-27 (b)) the shape of the trajectory in the deviatoric strain space is quite similar but with the size of the trajectory of Glass Ballotini is slightly larger than that of the dense Leighton Buzzard sand. For medium dense Leighton Buzzard sand it can be seen from Figure 5-27 (c), the trajectories appear to be large in the first few cycles and when the specimen is continuously sheared, they are gradually narrowed from the outside inward and tapered off to an ellipse after a large number of cycles rotation.

Once again, the final shapes of the strain trajectories in the deviatoric strain space for the three materials are replotted together with the same centre in Figure 5-28. The aspect ratio of the short axis *a* to the long axis *b* for the ellipses are labelled in the figure. It can be seen that the long axis of the ellipses from dense and medium dense

Leighton buzzard sands coincide with each other very well. They are all inclined to the horizontal line at an angle of 86°, and the aspect ratio of the two ellipses is almost equal. For Glass Ballotini, it demonstrates that the inclined angle to the horizontal is 2 degrees less than that of the Leighton Buzzard sand. And, the aspect ratio of the ellipse for Glass Ballotini is 0.45 which is smaller than that of the Leighton Buzzard sand, indicating the shape of the elliptical strain trajectory in the plane tends to be more circular for specimen with rounder particles.

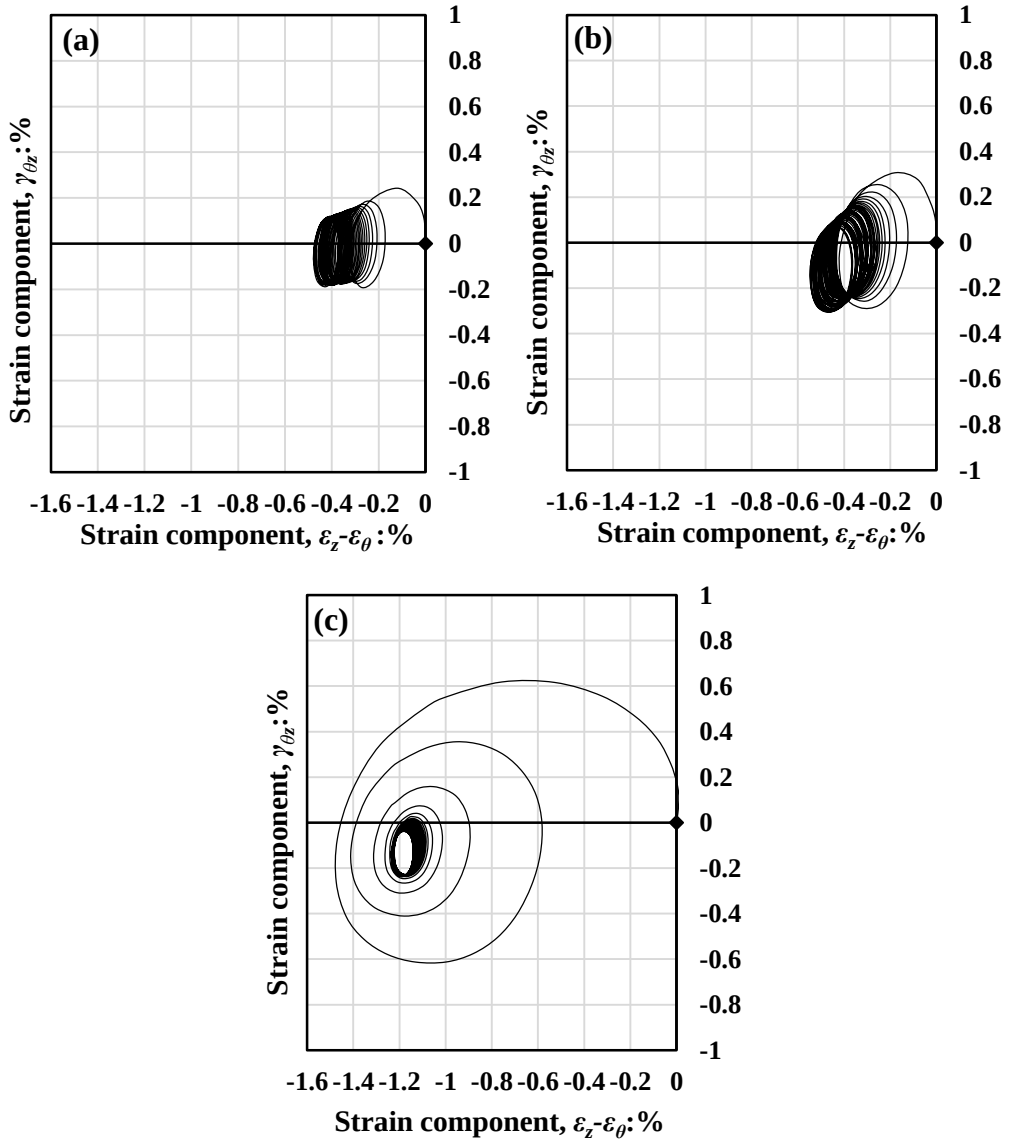

Figure 5-27: Evolution of the strain paths in the deviatoric strain space for rotational shear test performed on: (a) Dense Leighton Buzzard sand; (b) Glass Ballotini; (c) Medium dense Leighton Buzzard sand.

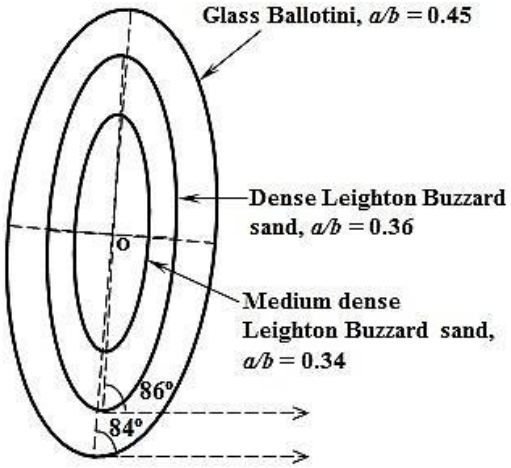

Figure 5-28: Superposition of the shape of strain path in the final cycle for test performed on dense Leighton Buzzard sand; Glass Ballotini and medium dense Leighton Buzzard sand.

5.4.5 Non-coaxiality

The degrees of non-coaxiality β for the rotational shear test performed on the three materials are plotted in Figure 5-29 (a)-(c) respectively. In general, they are all started with $\beta \approx 40°$ and the variation of the non-coaxiality degree shows an obvious periodicity characteristic during the tests. For different material density, it can be seen from Figure 5-29 (a) and (c), the results obtained from dense and medium dense Leighton Buzzard sand is generally very similar. By comparing the results obtained from Glass Ballotini (Figure 5-29 (b)) and dense Leighton Buzzard sand, the Glass Ballotini are found to display a slightly narrower fluctuation range than the dense Leighton Buzzard sand.

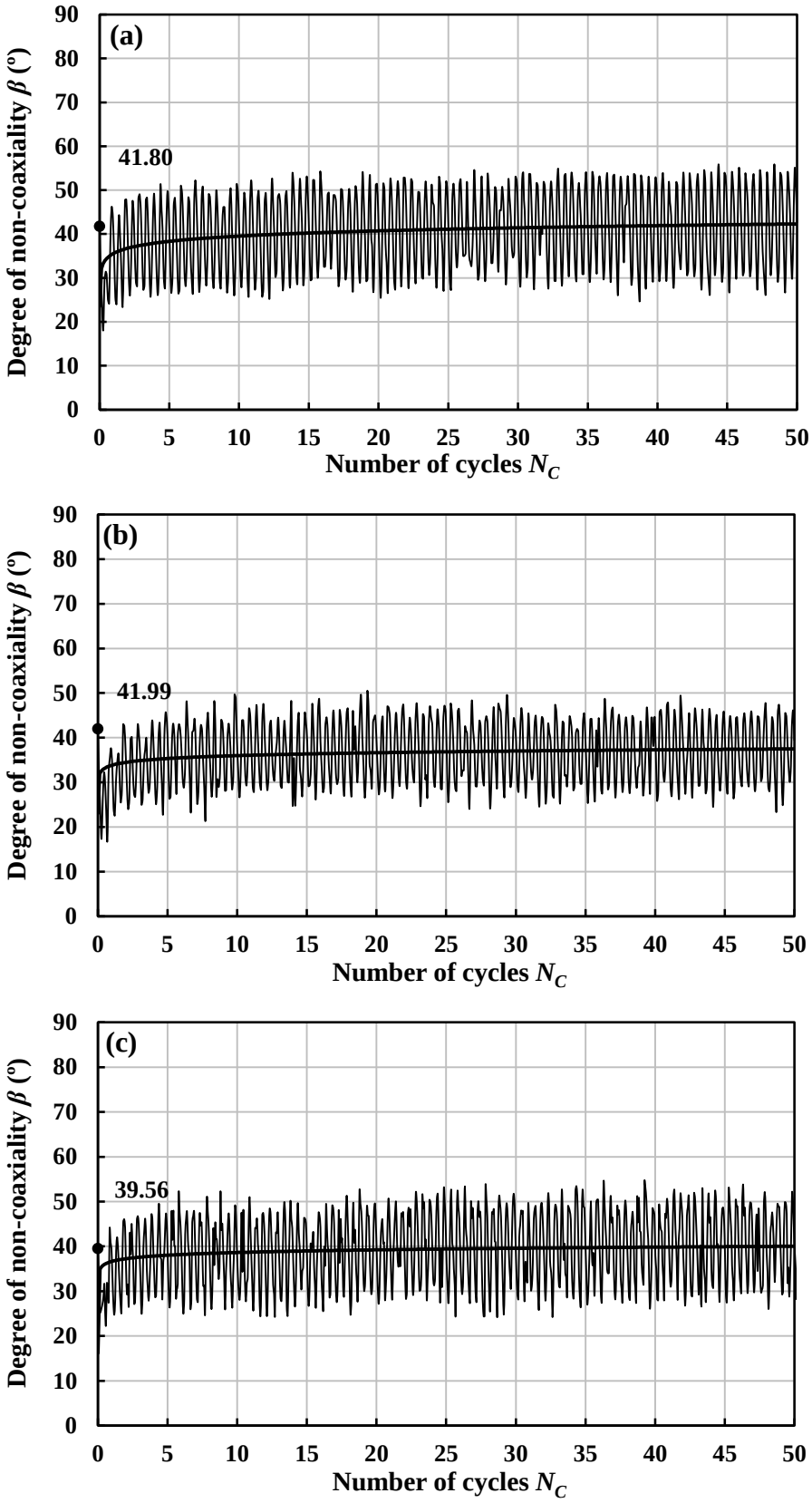

Figure 5-29: Degree of non-coaxiality against number of cycles for rotational shear test performed on: (a) Dense Leighton Buzzard sand; (b) Glass Ballotini; (c) Medium dense Leighton Buzzard sand.

To have a better view, the relationships of the non-coaxiality degree with the major principal stress direction α at the 25th cycle for test performed on the three materials are plotted together in Figure 5-30. It can be seen that the two curves represent the degree of non-coaxiality obtained from the dense and medium dense Leighton Buzzard sand almost coincide with each other, indicating the effect of relative density on the non-coaxial behaviour of Leighton Buzzard sand in rotational shear is not significant. Although the degree of non-coaxiality was slightly smaller in the Glass Ballotini specimen, the maximum difference appeared at the two peaks ($\alpha \approx 67.5°$ and 157.5°) of the curve was limited to 5°. Hence, the effect of the particle shape on the non-coaxial behaviour of granular materials under rotational is not significant.

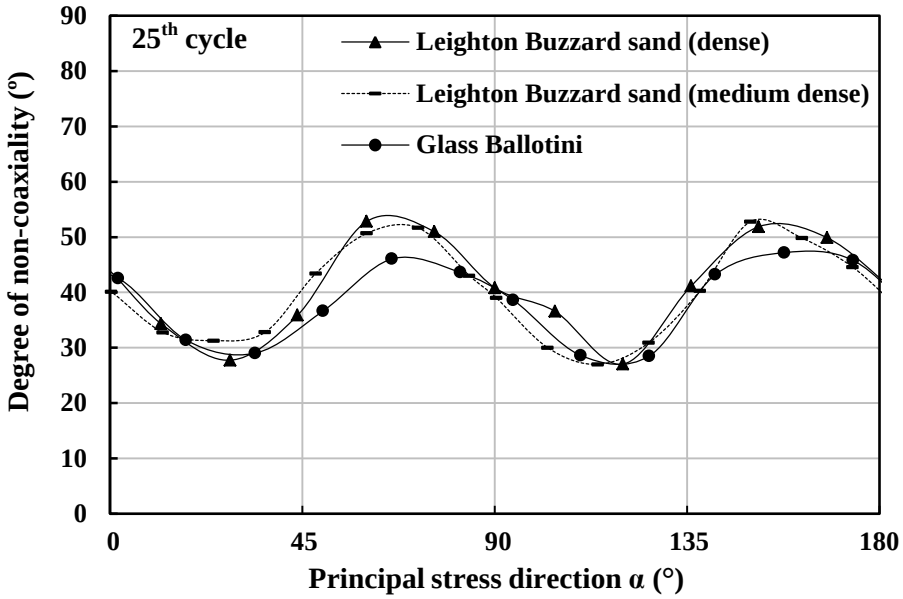

Figure 5-30: Degree of non-coaxiality at N_C = 25 for rotational shear test performed on: Dense Leighton Buzzard sand; Glass Ballotini; Medium dense Leighton Buzzard sand.

5.5 Summary

This chapter presents an experimental investigation of drained anisotropic behaviour of granular soil in rotational shear. In the tests samples were subjected to cyclic rotation of principal stress axes while the magnitudes of principal stresses were maintained constant. Three series of tests planned in Testing Program II have been carried out in SS-HCA in order to examine the effects of stress level, particle shape and material density on the stress-strain behaviour, deformation characteristics and noncoaxiality of granular soil subjected to the continuous rotation of principal stress axes. The conclusions drawn are as follows:

- A significant plastic deformation was induced during rotational shear despite the magnitudes of principal stresses remained constant. Most of strains were generated during the first 20 cycles and specimens were gradually stabilized afterwards in succeeding cycles. The magnitude of generated strains increased significantly with the increase in the stress ratio and decrease in the material density. The shear resistance of the sand specimen seemed to be weakened by the continuous rotation of the principal stress axis as failure was observed for specimens tested with the stress ratio below the peak.

- The volumetric strain induced by cyclic rotation of principal stress axes was mainly contractive. Most of the contractive volumetric strain occurred during the first 20 cycles and its accumulation rate tended to decrease as the number of cycles increases. The accumulated volumetric strain showed an increasing trend with the increase in the stress ratio. Samples with lower relative density and rounder particle shape were found to contract more during rotational shear.

- Irrespective of the stress level, material density and particle shape, the shear stress–strain relationship of all the specimens showed hysteretic and plastic characteristics. The hysteretic loop was open in the first cycle and then tended to be closed and became more accordant with the increasing number of cycles.

- The evolutions of the strain trajectory on the deviatoric strain space appeared as spirals, changing into ellipses after a large number of cycles. At the last cycle, with the increase in the stress ratio, the elliptical strain trajectories were gradually enlarged. The long axis of these ellipses made an angle of about 86° with horizontal direction. The shape of the elliptical strain trajectory in the deviatoric strain space for Glass Ballotini was more circular than that of the Leighton Buzzard sand.

- The mechanical behaviour of sand under rotational shear was generally non-coaxial, and the variation trend of the non-coaxiality degree showed an obvious periodicity during the tests. Lower degrees of non-coaxiality were observed in the first few cycles. When the rotational shear continues, the strain increment direction became closer to the stress increment direction and higher degrees of non-coaxiality were observed. The variation of the non-coaxial degree appeared to be stabilized after approximately 20 cycles of shearing. It was also observed that the stress ratio had a significant effect on the non-coaxiality. The larger the stress ratio, the lower degree of non-coaxiality between the directions of the strain increment and stress was induced. However, the effects of the particle shape and material density on the non-coaxial behaviour of granular materials under rotational shear were found to be less significant.

Chapter 6 Influence of Intermediate Principal Stress on Soil Response

6.1 Introduction

In this chapter, the investigation of the influence of the relative magnitude of the intermediate principal stress, characterized by the different *b*-values, on soil response will be investigated. The discussions are based on the results from testing program III, in which a series of monotonic and rotational shear tests have been performed on dense Leighton Buzzard sand with three cases of *b* values (b = 0.2, 0.5 and 1.0). Special attention in the investigation is focused on the significant role of the intermediate principal stress parameter *b* on the stress-strain and volume change behaviour, deformation characteristics and non-coaxiality of granular soils in generalized stress conditions. The experimental testing information will be introduced in Section 6.2. The results from the monotonic shear tests and rotational shear tests at different *b* values will then be presented and discussed in a systematic manner in Section 6.3 and 6.4. Finally a summary of this chapter will be given in Section 6.5.

6.2 Test Details

6.2.1 Initial conditions

Shown in Table 6-1 is a summary of the initial conditions and testing parameters of the tests in testing program III. Monotonic shear tests and rotational shear tests performed on dense Leighton Buzzard sand specimens has been identified as series 1 and 2 in the testing program. Each serial covered three *b*-values, namely, b = 0.2, 0.5 and 1.0 have been investigated. All specimens were prepared using water sedimentation method and were then consolidated isotropically to an effective mean pressure p' of 200kPa with a back pressure of 400kPa. The procedures of sample preparation, saturation and consolidation were strictly following the sample preparation procedures mentioned in Section 3.4.1.

Table 6-1 Summary of the initial conditions of the tests in Testing Program III

	Relative density after consolidation *Drc*: %	Void ratio after consolidation e_c	Principal stress direction α (°)	Principal stress parameter, *b*
Series 1 Monotonic shear tests	75.9	0.585	0	0.2
	76.6	0.583	15	
	77	0.582	30	
	76.6	0.583	60	
	77.1	0.582	75	
	76.3	0.584	90	
	77	0.582	0	0.5
	76.6	0.583	15	
	76.3	0.584	30	
	75.9	0.585	60	
	75.9	0.585	75	
	76.3	0.584	90	
	77	0.582	0	1.0
	76.6	0.583	15	
	76.6	0.583	30	
	75.9	0.585	60	
	76.3	0.584	75	
	76.6	0.583	90	
Series 2 Rotational shear tests	Relative density after consolidation *Drc*: %	Void ratio after consolidation e_c	Stress ratio η	Principal stress parameter, *b*
	76.3	0.584	0.7	0.2
	76.3	0.584	0.7	0.5
	76.6	0.583	0.7	1.0

6.2.2 Stress paths

After an isotropic consolidation as described above, all specimens were first subjected to a stage where *b* was changed to prescribed values (e.g. *b* = 0.2, 0.5 and 1.0) with a deviatoric stress *q* of 15kPa. In the monotonic shear test series, monotonic loading with fixed directions of principal stress was applied on the specimen in HCA strain-controlled mode with a rate of axial strain 0.05%/min. While in the rotational shear test series, the stress changes were performed so that deviatoric stress *q*, effective mean stress *p'* and *b*-value remained unchanged, so as to rotate the direction of the major principal stress axis cyclically with a rate of 2°/min. The same as the tests

conducted in testing program I and II, all the tests in this testing program was performed under drained conditions.

6.3 Results of the Monotonic Shear Tests with Different *b* Values

6.3.1 Stress-strain and volume change behaviour

The anisotropic behaviour of granular soils under monotonic shearing with different inclinations of major principal stress axes has been discussed in detail in Chapter 4, the results from the monotonic shear tests in testing programme III are therefore presented in this chapter with the emphasis on the comparison of the tests with different values of intermediate principal stress parameter *b*. Presented in Figure 6-1 (a)-(f) are the stress-strain and volume change behaviour at different loading directions for three cases of *b*-values.

It can be seen from Figure 6-1 (a)-(f) that the influence of intermediate principal stress parameter *b* is apparent in both stress-strain and volumetric strain responses of the dense Leighton Buzzard sand. In general, irrespective of loading directions, the stiffest response is seen for test with $b = 0.2$ and the material become increasingly soft as *b*-value increased. The highest peak was obtained when $b = 0.2$ and a significant decrease in material strength was observed with increasing values of *b*. The volumetric response also shows a consistent pattern, as *b*-value is increased, the volumetric compressibility of the specimen increases.

For tests with the major principal stress direction $\alpha = 0^o$, 15^o and 30^o, as is seen in the stress-strain curves presented in Figure 6-1 (a)-(c), the stress-strain curves become

increasingly steeper as *b*-value increases. For tests with b = 1.0, specimens failed quickly with a sharp drop in the stress-strain curve after peak was reached. Very consistently, at different loading directions the curves also show a clear decreasing strength from b = 0 to b = 1.0. When looking at the volume change, all the samples tested at α = 0º, 15º and 30º show a predominately dilatant response. For test with b = 0.2 and 0.5, there is no tendency for contraction, specimens were dilated throughout the tests. However, for tests with b = 1.0, volumetric strain became negative after the initial contraction and with the proceeding of shearing, associated with strain softening in the stress-strain curves, specimens were contracted dramatically until failure occurred.

As it can be seen from Figure 6-1 (d)-(f), the typical trend indicated in the tests with α = 0º, 15º and 30º can also be observed for tests with α = 60º, 75º and 90º, that is, the stiffness and shear strength of sands reduces and the volumetric compressibility increases with increasing values of b. Also, it is apparent that the stress-strain curves obtained from b = 1.0 tests tend to be steeper than the other two and it has a comparatively shorter strain to reach peak stress. However, unlike there exist an obvious gradient in the stress-strain and volume change curves in the α = 0º, 15º and 30º tests with different *b*-values. The pre-peak stress-strain curves of the tests with b = 0.5 and 1.0 are very close to each other at α = 60º and 90º. When looking at the volume change, it is interesting to note that the difference between the volumetric strains developed in the tests with different *b*-values tend to diminished as α increased from 60º to 90º.

Similar stress-strain and volume change behaviour has also been observed from monotonic loading tests in 3D DEM simulation carried out by Yang (2013) on

initially anisotropic specimen with non-spherical particles. The different deformation response of sands observed above may be attributed to the combined effects of the two factors: the inherent cross anisotropy of the sand sample and the relative magnitude of the intermediate principal stress.

The qualitative explanation of the different volume change behaviour observed in the tests could be given as follows. Due to the gravity deposition during sample preparation, sand particles tend to be more closely packed together in the vertical direction than in the horizontal direction. In a way, particle contact normals as well as the voids between the grains formed a stronger load resisting columns in the vertical direction. The sand sample thus tends to have lower compressibility and higher dilatancy along the vertical axis than that along the horizontal axis. Moreover, as it has been experimentally proved by Wong and Arthur (1985) that there is no directional dependence of mechanical properties on the horizontal plane. As a result, the horizontal plane was characterized as an 'isotropic plane'.

As the intermediate principal stress σ_2 in the HCA always equal to the radial stress σ_r. Therefore, the value of b reflects the constraint in the radial direction of the specimen. As the value of b increased from 0 to 1, the stress state of the specimen in the radial direction was changed from $\sigma_r = \sigma_2 = \sigma_3$ to $\sigma_r = \sigma_2 = \sigma_1$. In the tests with fixed values of α, the low constraint in the radial direction under $b = 0.2$ leads to the occurrence of the low volumetric compressibility of the sand specimen. However, under $b = 1.0$, the σ_r becomes to be the major principal stress. The high contractive volumetric strain is induced due to easy compression tendency in the radial direction. As α deviates from the vertical deposition direction to the horizontal isotropic plane, the effects of inherent anisotropy are gradually diminished and the influence of b-value become

increasingly dominant. Consequently, with the increase of the value of α, the difference between the volumetric strains developed in the tests with different *b*-values is decreased. When α = 90º, both the two major principal stresses σ_1 and σ_2 are acting on the horizontal isotropic plane, hence, *b*-value becomes the only factor that influences the material response.

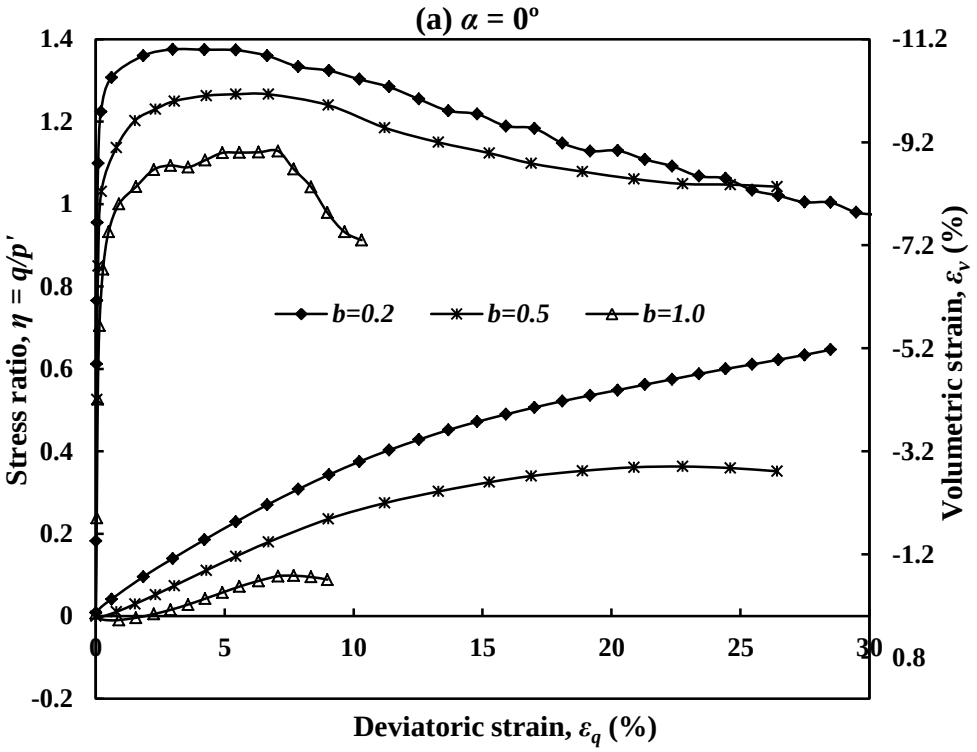

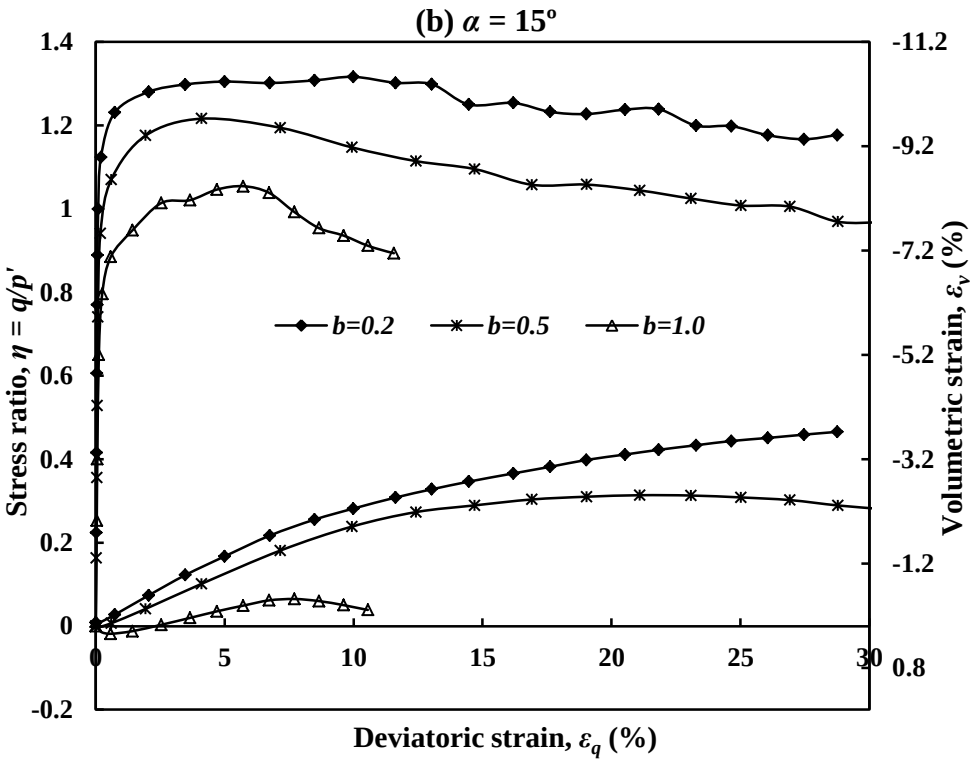
(b) α = 15°
Stress ratio, η = q/p'
Volumetric strain, εv (%)
Deviatoric strain, εq (%)
b=0.2
b=0.5
b=1.0
1.4
1.2
1
0.8
0.6
0.4
0.2
0
-0.2
-11.2
-9.2
-7.2
-5.2
-3.2
-1.2
0.8
0
5
10
15
20
25
30

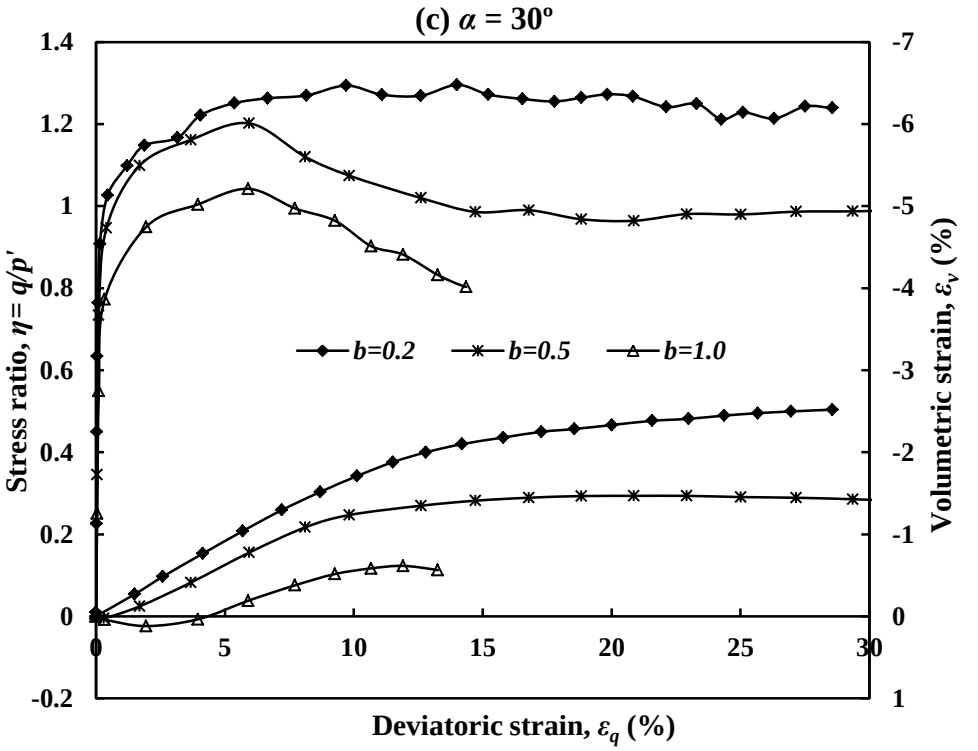
(c) α = 30°
Stress ratio, η= q/p'
Volumetric strain, εv (%)
Deviatoric strain, εq (%)
b=0.2
b=0.5
b=1.0
1.4
1.2
1
0.8
0.6
0.4
0.2
0
-0.2
-7
-6
-5
-4
-3
-2
-1
0
1
0
5
10
15
20
25
30

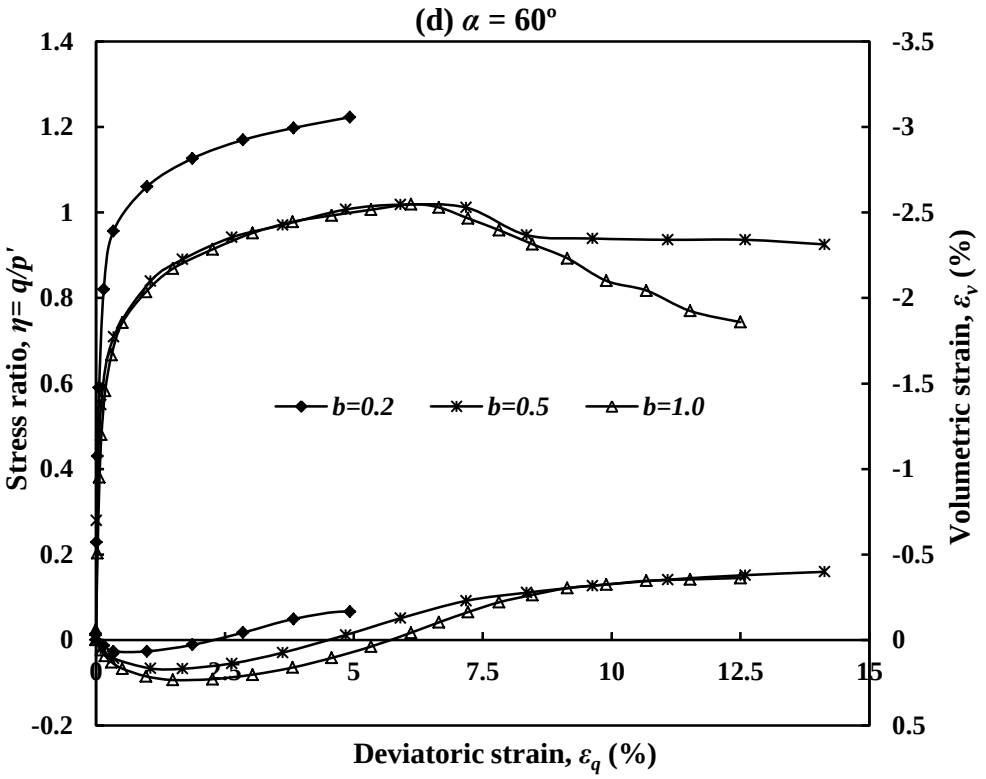
(d) α = 60º
Stress ratio, η= q/p'
Volumetric strain, εv (%)
Deviatoric strain, εq (%)
b=0.2
b=0.5
b=1.0
1.4
1.2
1
0.8
0.6
0.4
0.2
0
-0.2
-3.5
-3
-2.5
-2
-1.5
-1
-0.5
0
0.5
0
2.5
5
7.5
10
12.5
15

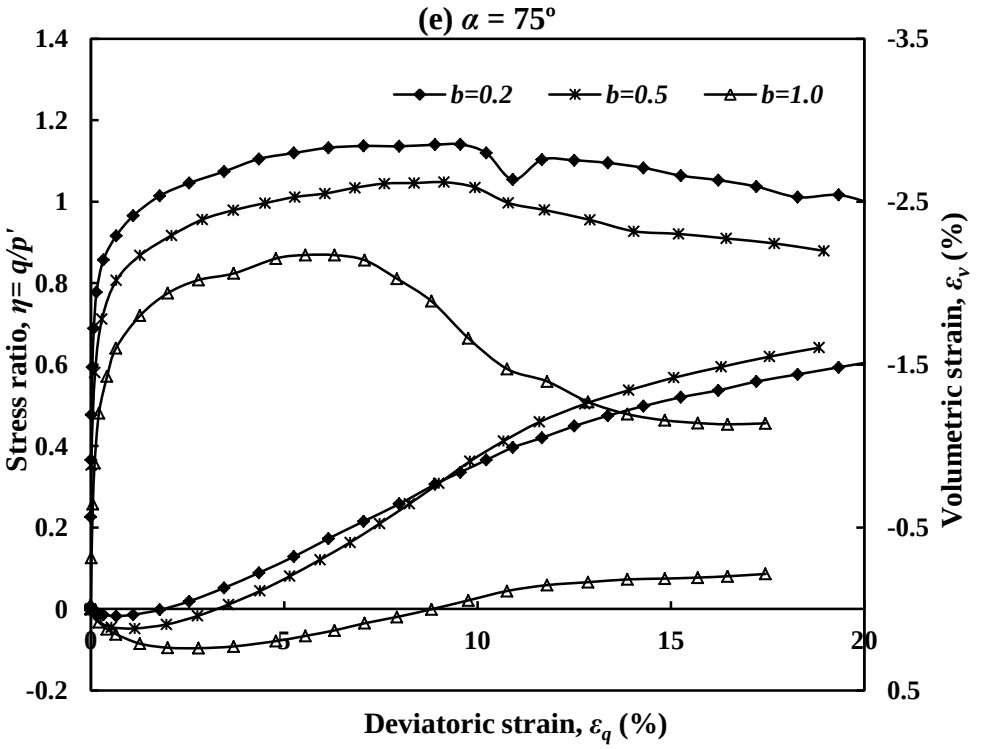
(e) α = 75º
Stress ratio, η= q/p'
Volumetric strain, εv (%)
Deviatoric strain, εq (%)
b=0.2
b=0.5
b=1.0
1.4
1.2
1
0.8
0.6
0.4
0.2
0
-0.2
-3.5
-2.5
-1.5
-0.5
0.5
0
5
10
15
20

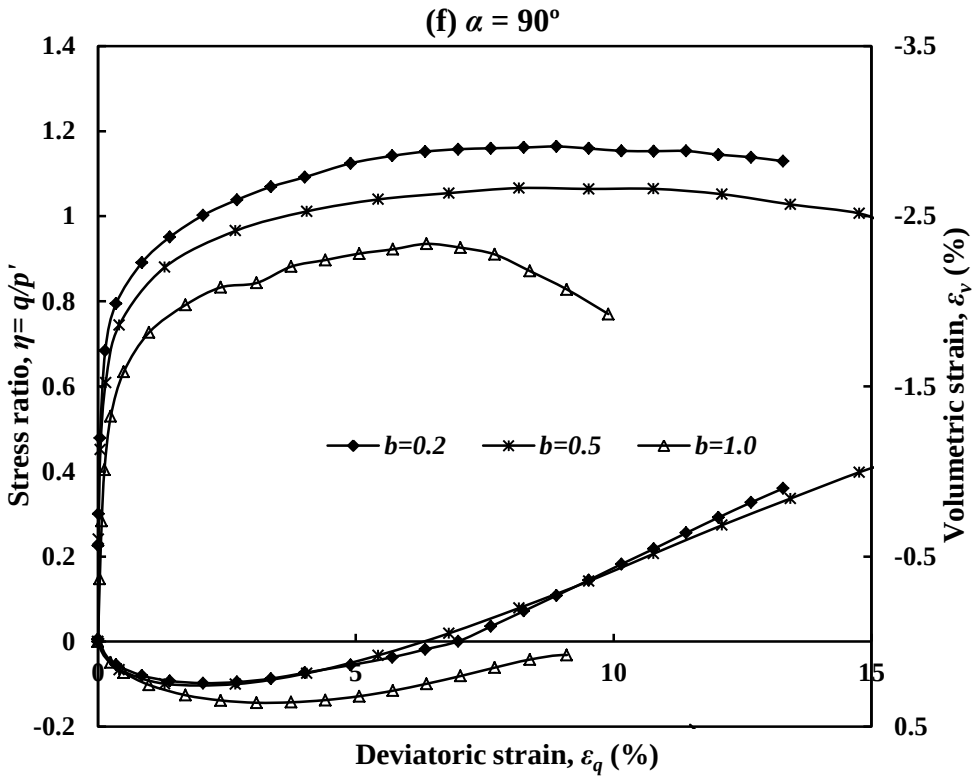

Figure 6-1: Stress-strain and volume change behaviour at: (a) α = 0º; (b) α = 15º; (c) α =30º; (d) α = 60º; (e) α = 75º; (f) α = 90º for tests with b = 0.2, 0.5 and 1.0.

6.3.2 Failure characteristics

Different peak stress ratios measured at different major principal stress directions for three cases of b-values are presented in Figure 6-2. It can be seen as the major principal stress direction deviates from the vertical, the peak stress ratios obtained at different b-values followed similar trend. That is, the stress ratio continued decreasing when the loading direction rotated further towards the vertical direction and a slightly recovery of the specimen strength is observed at α = 90º. However, for tests with b = 0.2 and 1.0 the minimum value of the peak stress ratio was achieved at α = 75º, whereas for b = 0.5 it was achieved at α = 60º.

As the friction angle φ has always been used to describe the influence of the b-value on the friction shear resistance of soils in previous studies, the relationship between

peak friction angle φ_p and *b*-values at different loading directions has been plotted in Figure 6-3. The data indicates that for a given value of *b*, the peak friction angle reduces with increasing value of α and it has a slight rebound at α = 90º. The above observation agreed well with the results reported by Van Dyck (2012) who carried out a series of drained monotonic shear tests on Fine Nevada Sand with various fixed α and *b* values in a HCA.

The variation of the peak friction angle measured at different loading directions for three cases of *b*-values is similar. As *b*-value changed from 0.2 to 0.5, the strength increases and there is a drop in strength as *b* further increased from 0.5 to 1.0. However, as indicated in the figure, the peak friction angles obtained at *b* = 1.0 gradually shifted down with the increasing value of α. For α = 0º, 15º and 30º, the lowest strength is reached at *b* = 1.0, whereas for α = 60º, 75º and 90º, it is obtained at *b* = 0.2. The above observations clearly show that both the inherent anisotropy and the intermediate principal stress may have a profound influence on the behaviour of sand with anisotropic fabric. Neglecting the effects of the soil anisotropy in the investigation of intermediate principal stress may results in improper plotting and interpretation of test results. Certainly, this missing factor could be one of the possible factors that can explain the confliction observations reported by many researchers as mentioned in the literature review.

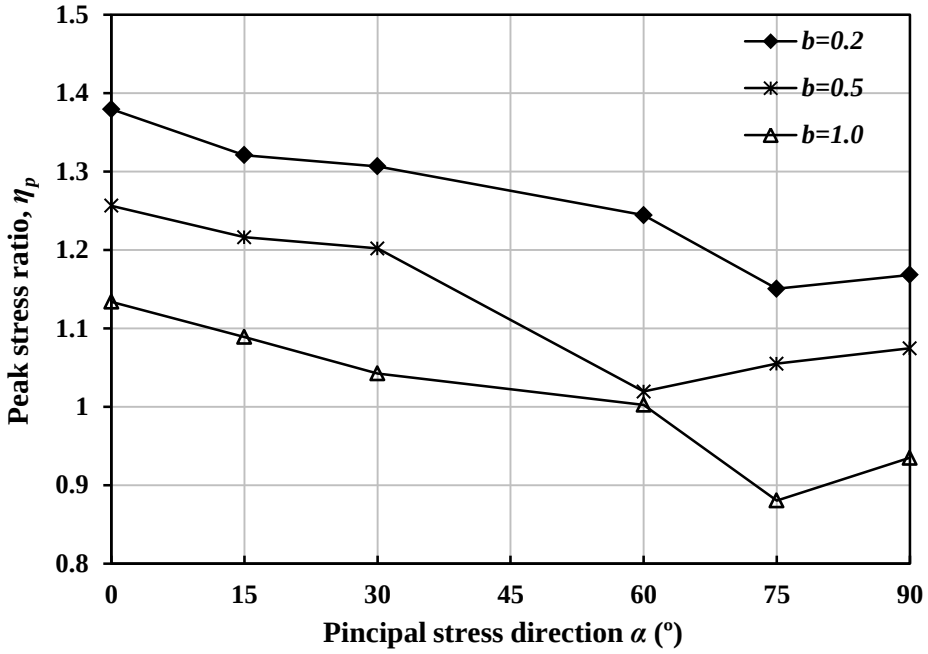

Figure 6-2: Peak stress ratio at different major principal stress directions for tests with *b* = 0.2, 0.5 and 1.0.

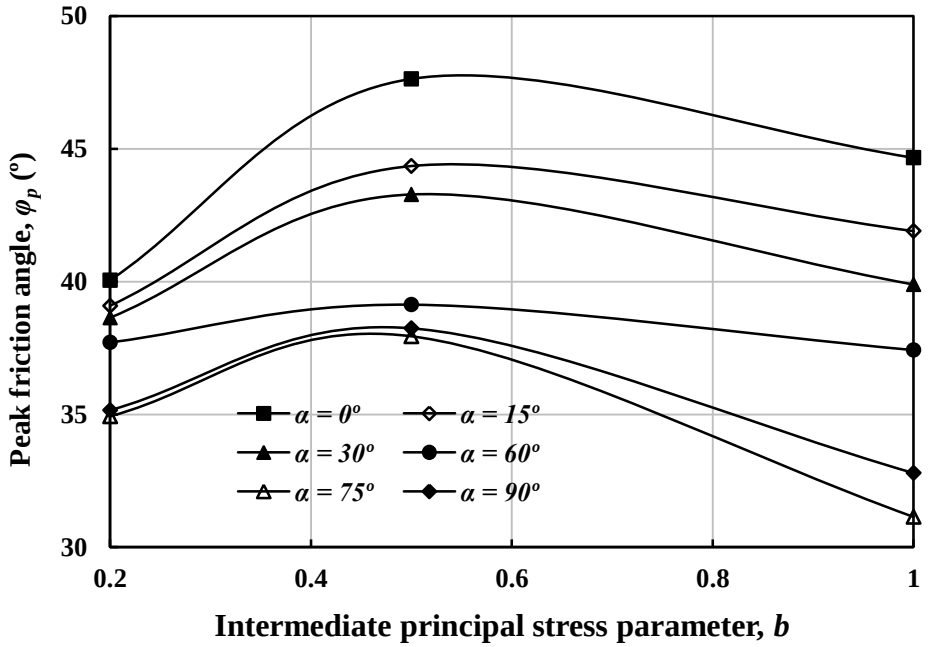

Figure 6-3: Relationship between friction angle and *b* values at different loading directions.

Figure 6-4 presents different shear band patterns and inclination angles obtained in sand specimens at different loading directions for tests with b = 0.2. Very similar to the shear bands observed in the b = 0.5 tests (see Figure 4-7), crossed shear bands

were generated at α = 0º and 90º, and for α = 15º parallel spiral-like shear bands were developed through the entire body of the sample. For α = 30º and 75º a single spiral-like shear band were developed around the middle part of the sample. However, for α = 60º, specimen was twisted at the ends. The comparison of experimental shear band inclinations with theoretical predictions for tests with b = 0.2 are summarized in Table 6-2. By taking account of the relative direction of the mobilized planes to the bedding plane, it can be found that the spans of shear band angles are slightly higher than the Coulomb prediction at α = 0º and 15º but then get closer to the prediction at α = 30º, 60º, 75º and 90º. It can also be observed that at the same loading direction the shear bands tend to be more pronounced in the tests with b = 0.5. For example, in the α = 15º tests, although the deviatoric strain ε_q in the test with b = 0.2 is 7% larger than that in the test with b = 0.5, apparently, the shear bands in the b = 0.2 sample are generally less pronounced.

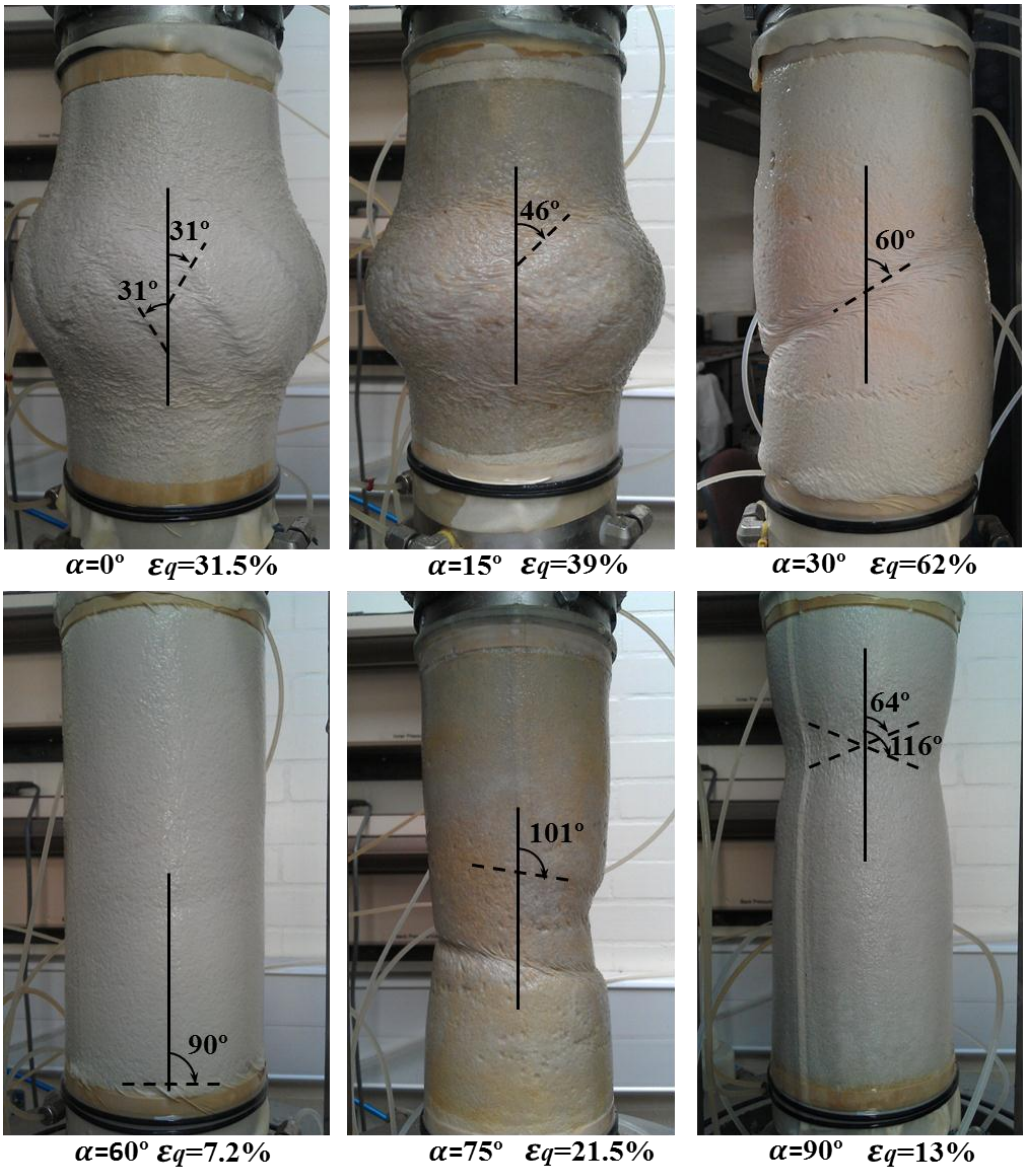

Figure 6-4: Shear bands developed in sand specimens at different loading directions for tests with b = 0.2.

Table 6-2: Comparison of experimental shear band inclinations with theoretical predictions for tests with b = 0.2.

α (°)	0	15	30	60	75	90
α_{sb} (°)	-31, 31 crossed	46 parallel	60 single	90 single	101 single	64, 116 crossed
θ_v (°)	-25 (I) 25 (II)	-10 (I) 40 (II)	-4 (I) 56 (II)	42 (I) 88 (II)	47 (I) 103 (II)	64 (I) 116 (II)

θ_v: the angle between the shear band and the vertical; I and II : mobilized planes.

Unlike similar shear bands were observed for tests with b = 0.2 and 0.5, for tests with b = 1.0, the shear bands were appeared on the sand specimen with completely different patterns. As shown in Figure 6-5, a large and pronounced lance-shaped shear band was appeared on the surface of the sample tested with α = 0° and for test with α = 15º a club-shaped indentation can be observed on the surface of the sample. For test with α = 30º two irregularly distributed shear bands were developed, while for test with α = 60º, 75º and 90º, a single shear band was looped around the middle part of the sample with a great width. Since the shear band inclinations are within the specimen wall and are not visible on the outside surface of the specimen, a direct comparison to the prediction angles is not possible for these situations.

Similar shear bands observed in the monotonic shear test with higher b-values ($0.75 \leq b \leq 1$) performed in HCA has been reported by Van Dyck (2012) and Rodriguez (2012). A possible explanation for the observation is that due to the cross-anisotropic behaviour of the sand specimen with the horizontal direction being weaker than the vertical direction, under conditions where b-values are close to unity, the magnitude of the radial stress σ_r becomes close to the major principal stress σ_1 (since at b = 1, $\sigma_r = \sigma_2 = \sigma_1$). In the tests when specimen is compressed (i.e. tests with $\alpha \leq 45^o$), as radial stress σ_r is sufficiently large, largest sliding displacement will be more likely to occur in the radial direction. Shear band inclinations were therefore seen to develop in the r-θ plane rather than the z-θ plane. However, in extension tests (tests with $\alpha \geq 45^o$), as necking develops in the middle part of the specimen, the soil grains within the area begin to pull away from each other rather than sliding against each other, resulting in a reduction of the shear strength in the z-direction. Hence it can be deduced that the shear band for this specimen appears to be a combination of the r-θ and r-z planes. A

schematic explanation of the typical shear band in different planes of the hollow cylinder specimen is shown in Figure 6-6.

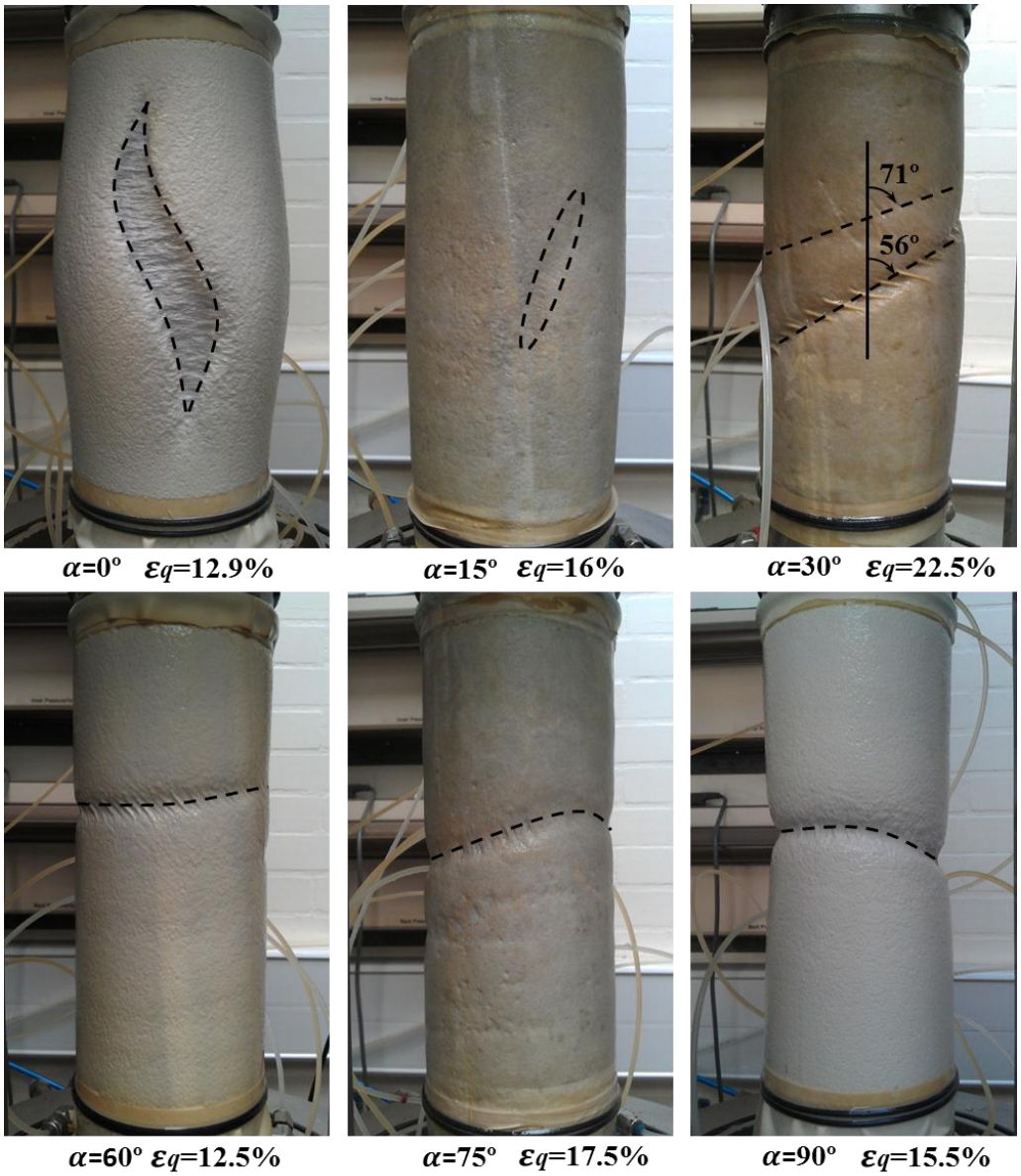

Figure 6-5: Shear bands developed in sand specimens at different loading directions for tests with *b* = 1.0.

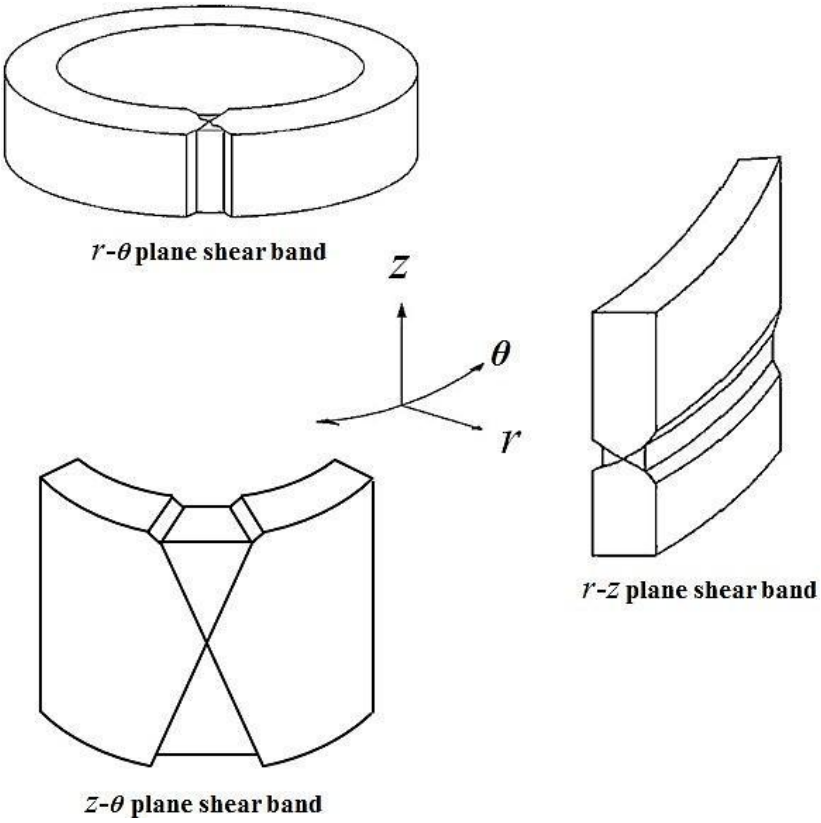

Figure 6-6: Schematic of typical shear band develops in the *r*-*θ*, *z*-*θ*, and *r*-*z* plane.

6.3.3 Non-coaxiality

The major directions of stress and strain increment against the stress ratio for tests under different loading directions with three cases of *b*-values are plotted in Figure 6-7 (a)-(c). In general, the trend of the deviations between the major directions of stress and strain increment for test with different *b*-values is similar. As indicated in the figures, the strain increment direction coincides with the major stress direction when samples were loaded with the direction of major principal stress α = 0º and 90º. Apparent non-coaxiality is observed for tests with α = 15º, 30º, 60º and 75º, and the direction of the strain increments gradually approaches that of the stress with the increase of stress ratio.

In a similar pattern, all α = 15º, 30º and 60º tests show higher strain increment directions (except for test with b = 1 at α = 60º) and α = 75º show slightly lower. For easy comparison, principal strain increments for all b-values at α = 15º, 30º and 60º are plotted together in Figure 6-8. It can be seen that the influence of the b-value on the non-coaxiality of sand is clear. In general, the lower the b-value is, the higher the degree of non-coaxiality is induced. Tests with b = 0.2 show a comparatively larger deviations between the major directions of stress and strain increment at α = 15º and α = 30º. The largest deviations between the two directions occurred in the tests with b = 0.2 at α = 15º, where it was about 15º. The variation of the strain increment direction show the most anomaly trend in the test with b = 1 at α = 60º, where the direction of strain increment is significantly lower (about 14º) than that of stress toward the beginning of the tests.

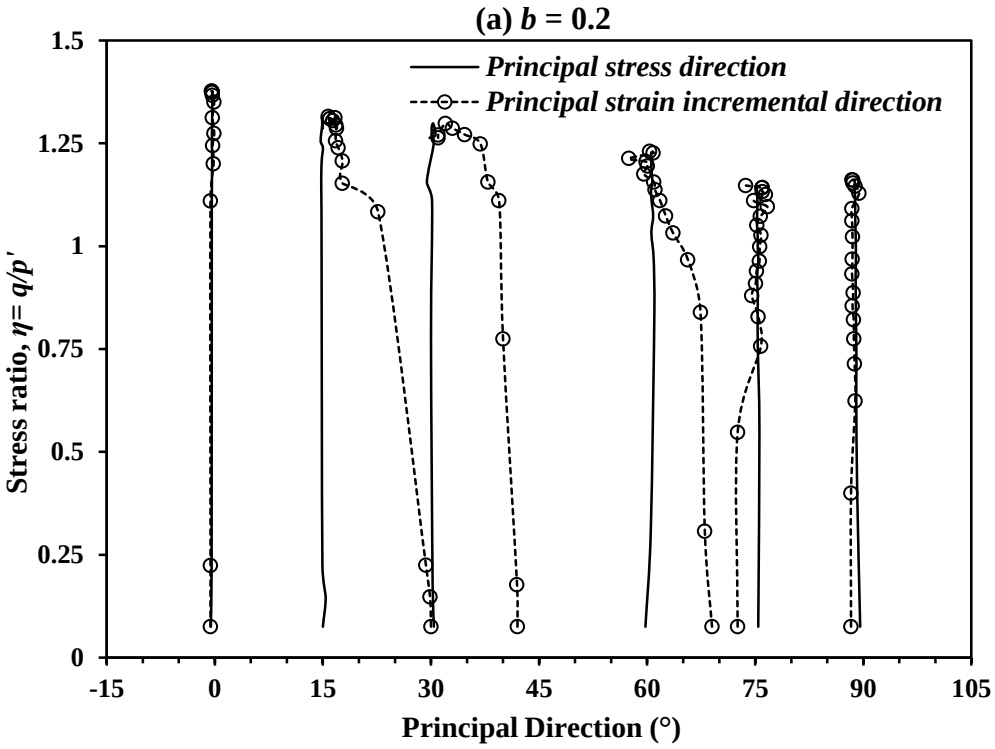
(a) b = 0.2
Principal stress direction
Principal strain incremental direction
Stress ratio, η= q/p'
Principal Direction (°)
1.5
1.25
1
0.75
0.5
0.25
0
-15
0
15
30
45
60
75
90
105

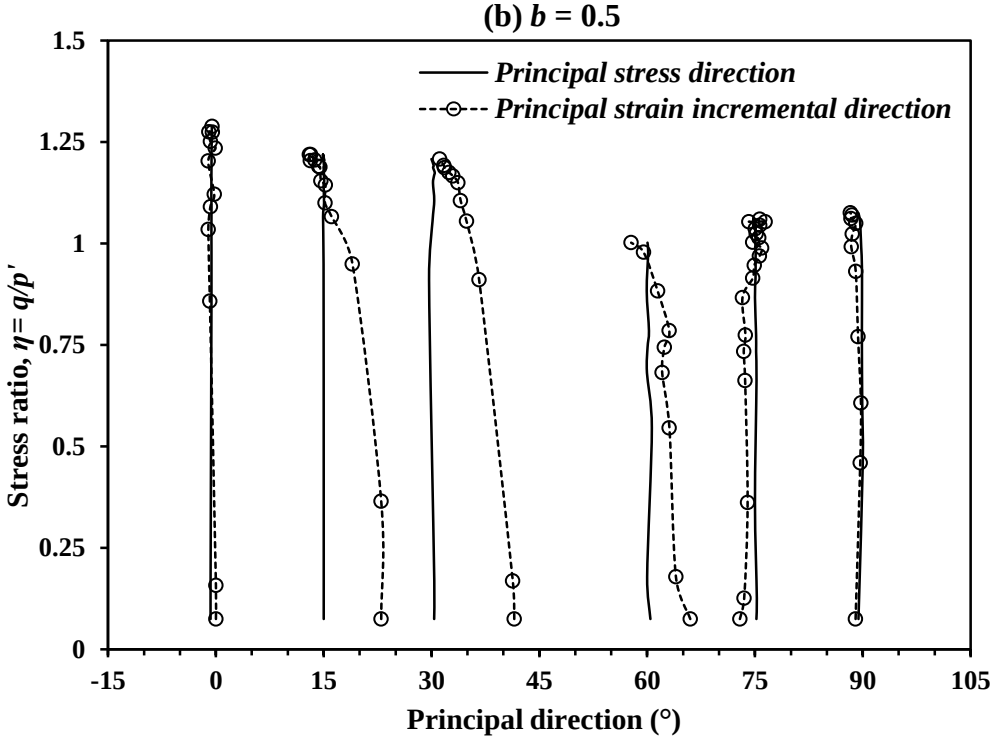
(b) b = 0.5
Principal stress direction
Principal strain incremental direction
Stress ratio, η= q/p'
Principal direction (°)
1.5
1.25
1
0.75
0.5
0.25
0
-15
0
15
30
45
60
75
90
105

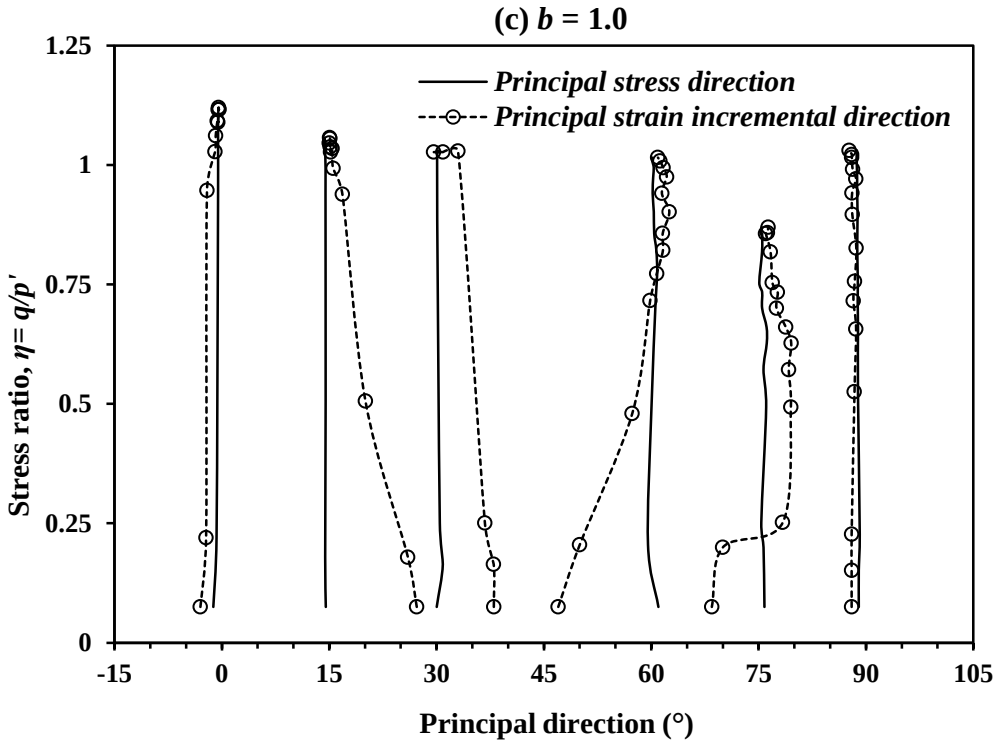

Figure 6-7 Stress and strain increment directions of the sand specimen tested at different loading directions with: (a) *b* = 0.2; (b) *b* = 0.5 and (c) *b* = 1.0.

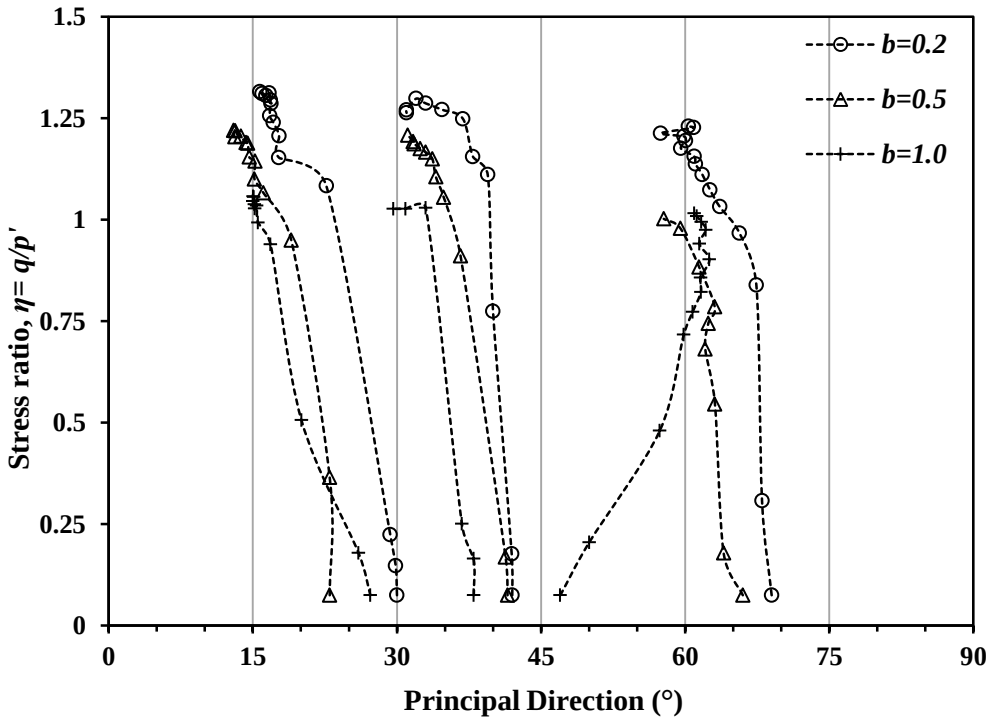

Figure 6-8 Strain increment directions of the sand specimen tested at α = 15º, 30º and 60º with three cases of *b*-values.

6.4 Results of the Rotational Shear Tests with Different *b* Values

6.4.1 Variations in stress and strain components

Figure 6-9 (a)-(c) shows the four stress components: σ_z, σ_r, σ_θ and $\tau_{\theta z}$ against the number of cycles for rotational shear test, in which the three plots represent three cases of *b*-values, that is, b = 0.2, 0.5 and 1.0 respectively. It can be observed that, all the stress components fluctuated sinusoidally with constant amplitude except radial stress σ_r which is maintained throughout the process. While the variation of the four stress components had a similar pattern for all three values of *b*, the amplitude σ_z, σ_r and σ_θ and the relative position of σ_r showed different patterns for different *b*-values.

The variation of the consequent strain components: ε_z, ε_r, ε_θ and $\gamma_{\theta z}$ against the number of cycles for the tests are presented in Figure 6-10 (a)-(c). In these figures, a positive value along the vertical axis indicates compression and negative indicates extension. It is observed that as the number of cycles increases the four strain components accumulated gradually with oscillation characteristics and most of strains are induced within the first few cycles. Meanwhile, by comparing Figures 6-10 (a)-(c) for tests with different values of *b*, it can be found that the intermediate principal stress plays a significant role in the development of the strain.

In general, the amount of generated strains increases with the increase in the *b*-value. Extensive vertical strain ε_z is induced under three cases of *b*. Great amount of ε_z was generated in the first cycle under b = 1.0, and its amplitude reduced significantly afterwards in succeeding cycles. The circumferential strain ε_θ induced is contractive and the amount of accumulation is greatest in the test with b = 0.5. The shear stain $\gamma_{\theta z}$

varied in a manner that it changes from expansion to contraction in each cycle and its amplitude tend to be the largest under b = 0.5. The contractive radial strain ε_r increased dramatically throughout the test under b = 0.5 and 1.0. However, the development of ε_r seems to be more stable under b = 0.2.

Possible explanations for these observations might be that with a cross-anisotropic material, the material has lower compressibility and higher dilatancy along the z-axis than that along the r-axis and the θ-axis. When principal stress axes begin to rotate from z-axis to θ-axis and back to z-axis, specimen tend to contract more in the θ-direction than in the z-direction. As a result, a large expansive vertical strain and contractive circumferential strain is induced.

Moreover, in tests with b-values approaching unity, the radial stress σ_r becomes closer to the major principal stress. Therefore, if the grains are aligned in a manner where the radial stress causes the most strain, as compared to the vertical stress, the specimen will be compressed in radial direction and extended in the vertical direction. Consequently, a larger extensive vertical strain and compressive circumferential strain are induced in the tests with higher b-values.

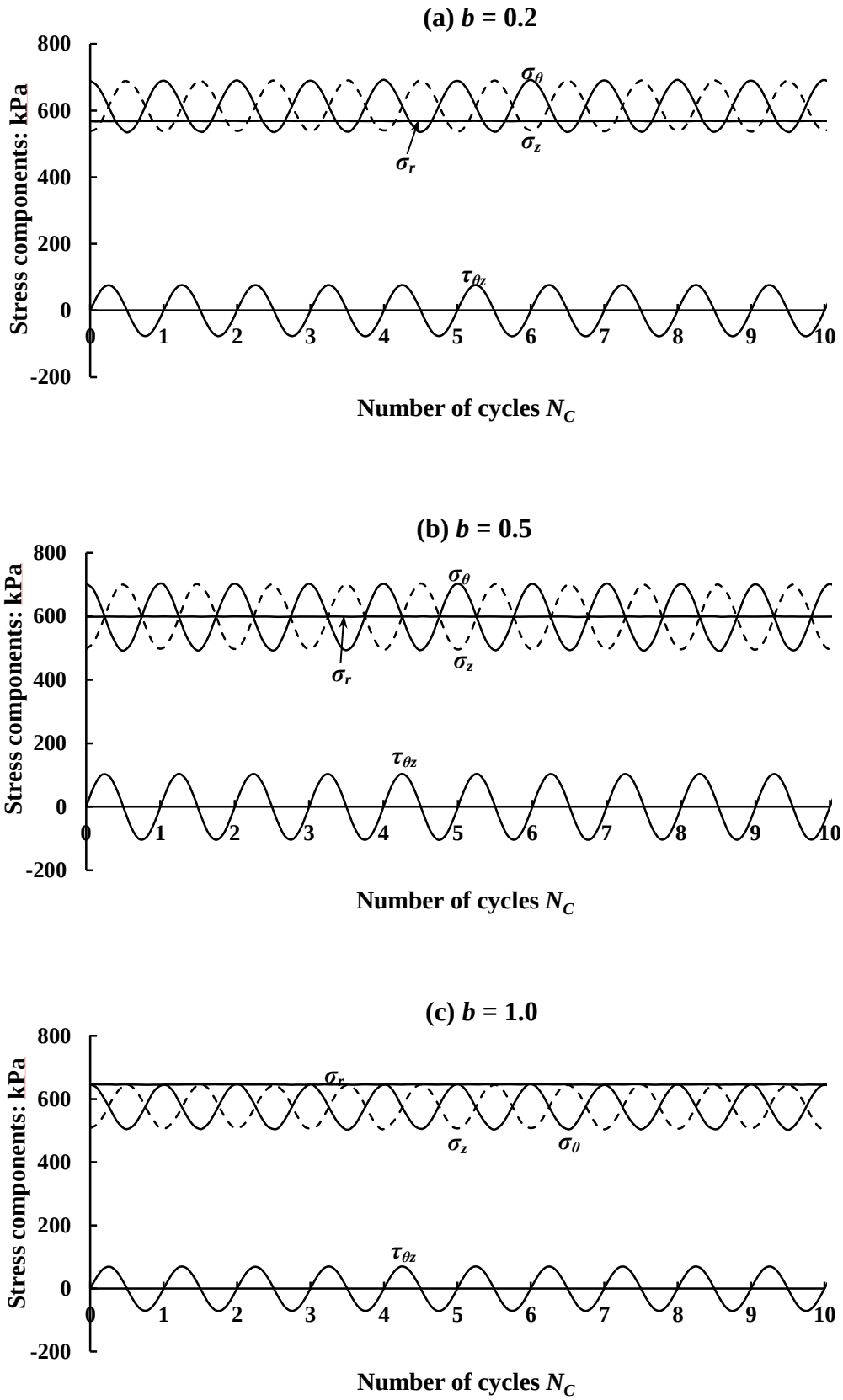

Figure 6-9: Variations of the stress components in rotational shear test with: (a) b = 0.2; (b) b = 0.5 and (c) b = 1.0.

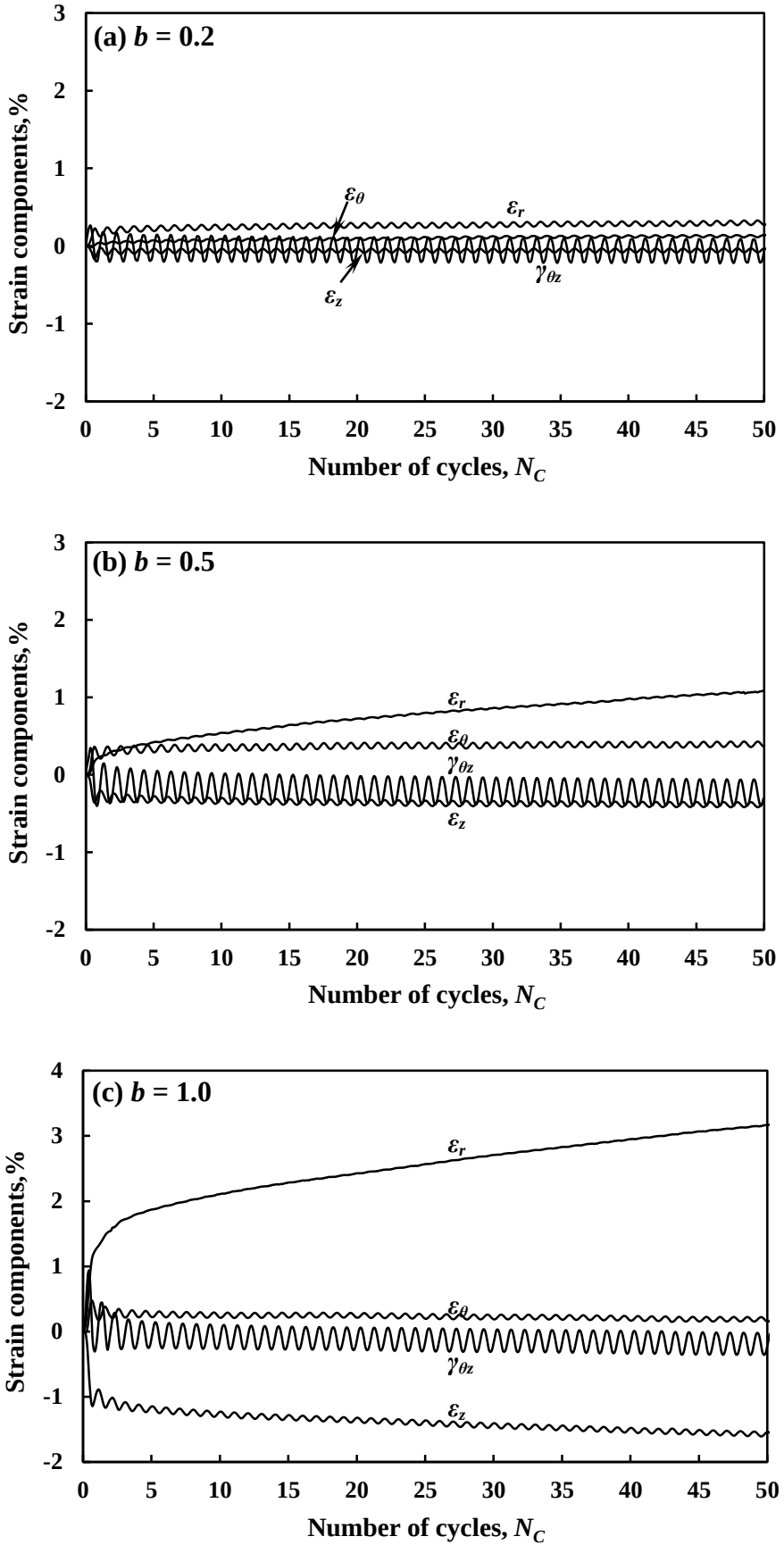

Figure 6-10: Development of strain components during rotational shear for test with: (a) b = 0.2; (b) b = 0.5 and (c) b = 1.0.

6.4.2 Development of the volumetric strain

The evolutions of the volumetric strain ε_v with the increasing number of cycles for rotational shear tests with three cases of *b*-values are shown in Figure 6-11. Once again, a positive value along the vertical axis indicates contraction and the negative indicates dilation. Although the magnitudes of principal stresses were maintained constant during each test, contractive volumetric strain was accumulated with oscillation characteristics. As shown in Figure 6-11, the effects of *b* on the development of the volumetric strain are significant under otherwise identical conditions. The amount of the volumetric strain at the same number of cycles increases with the increase in *b* and the accumulated volumetric strain under *b*=1.0 is much higher than that under *b*=0.2 and 0.5. In addition, after the first several cycles rotation, the development of the volumetric strain seems to be more stable under *b* = 0.2 than that under *b*=0.5 and 1.0.

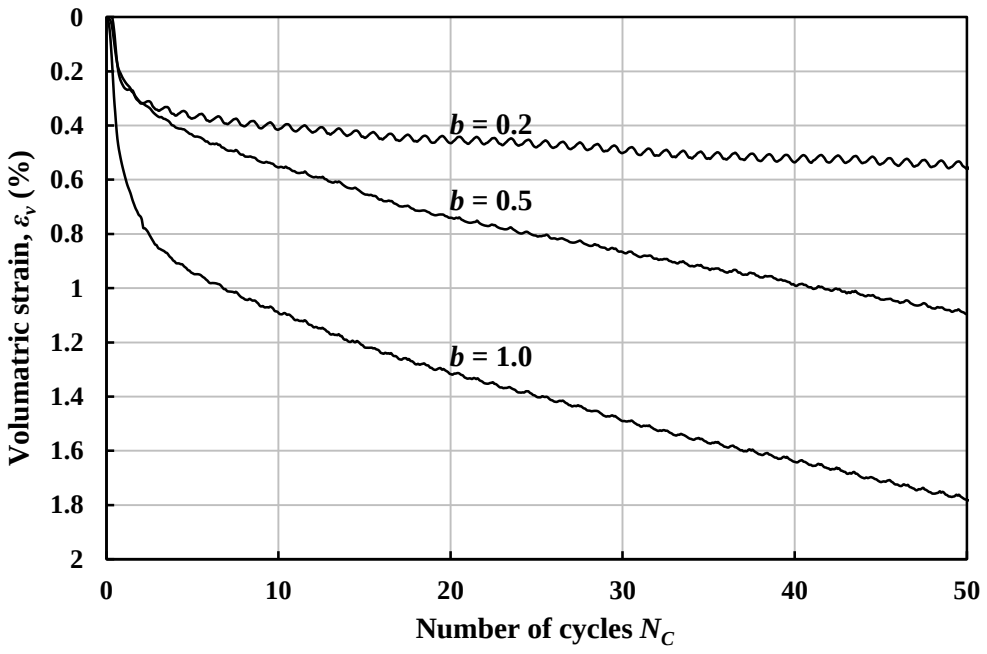

Figure 6-11: Development of volumetric strain during rotational shear for test with *b* = 0.2, 0.5 and 1.0.

6.4.3 Shear stress-strain relationship

The relationships between the shear stress-shear strain components for test under three cases of *b*-values are given in Figure 6-12 (a)-(c). The hysteresis loops of the shear stress-strain curves are obtained for three cases of *b*-values during cyclic rotation of principal stress axes. It can be found that the size of the loops in the first few cycles increased significantly with the increase in the *b*-value. However, as the number of cycles increases, all the three hysteresis loops tend to be closed and remained stable after a large number of cycles rotation.

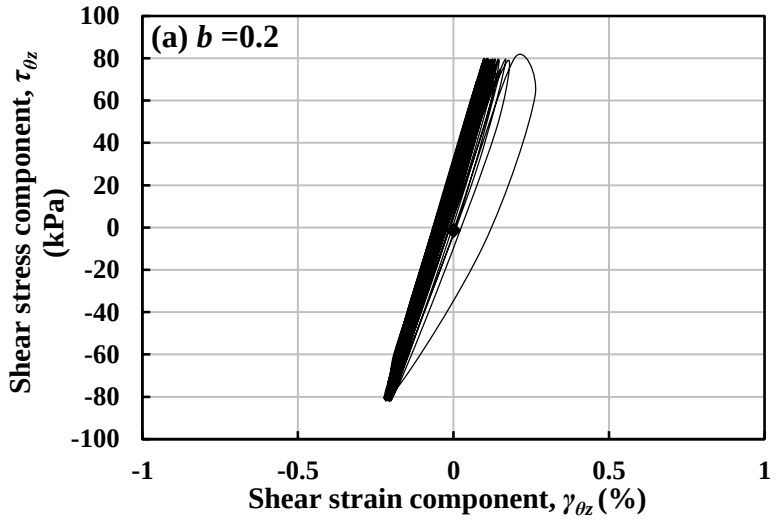

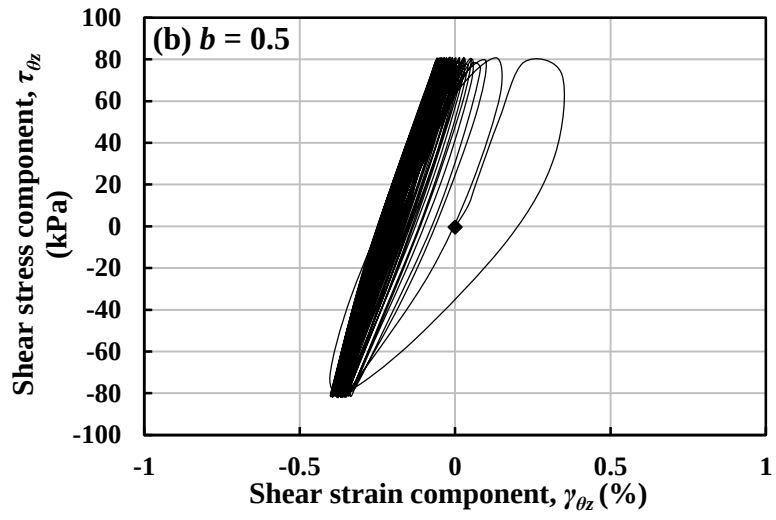

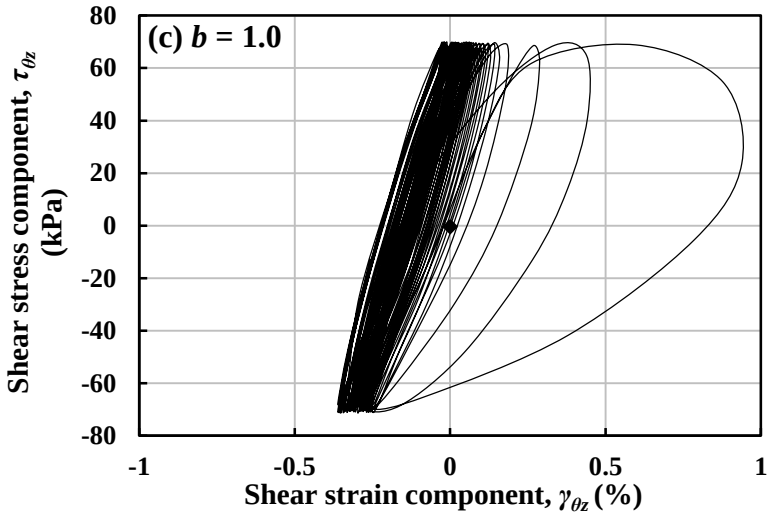

Figure 6-12: Shear stress-strain relationship for tests with: (a) *b* = 0.2; (b) *b* = 0.5 and (c) *b* = 1.0.

6.4.4 Evolution of strain paths in deviatoric strain space

Figure 6-13 shows the strain paths in the deviatoric strain space for test under three cases of *b*-values. Clearly, the magnitude of strains accumulated gradually with the cyclic rotation of principal stress axes. The higher the *b*-value the larger size of the strain trajectories is obtained in the first several cycles. It can be seen that for the test in the condition with b = 0.2, the strain paths were concentrated in a zone of very small deformation. However, a drastic development of deformation was observed in the test with b = 1.0 in the first 3 cycles. The final shapes of the strain trajectory in the deviatoric strain space for the three tests are replotted together with the same centre in Figure 6-14. It is interesting to see that irrespective of the *b*-values, the three elliptical-shaped trajectories are almost the same size and their long axis almost coincides with each other.

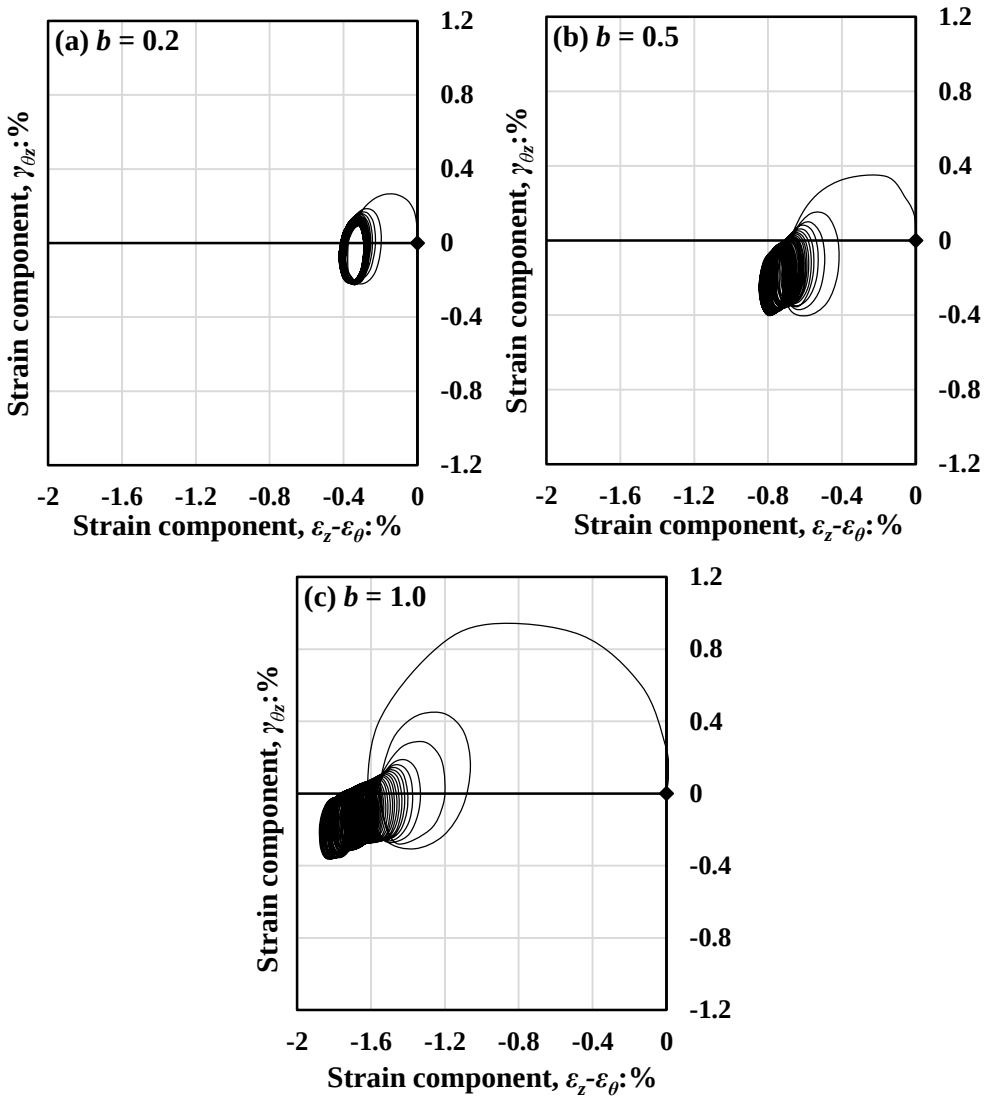

Figure 6-13: Evolution of strain paths in deviatoric strain space for tests with: (a) b = 0.2; (b) b = 0.5 and (c) b = 1.0.

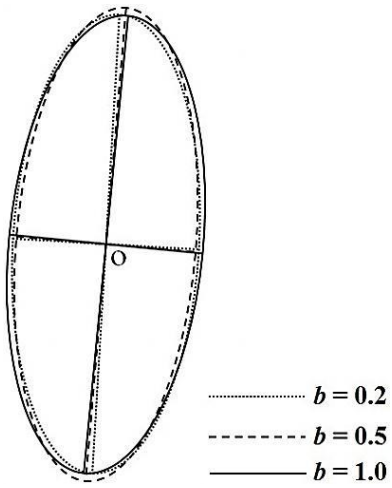

Figure 6-14: Superposition of the shape of strain path in the final cycle for test with b = 0.2, 0.5 and 1.0.

6.4.5 Non-coaxiality

The degree of non-coaxiality β for test under three cases of b-values is plotted against the number of cycles in Figure 6-15 (a)-(c). In general, the variations of the non-coaxiality degree under different b-values show similar characteristics. Lower degrees of non-coaxiality are observed in the first few cycles and the variation of the non-coaxiality degree appeared to be stabilized after about 20 rotation cycles. However it can be observed that the degree of non-coaxiality is slightly lower under b=1.0 than that under b=0.2 and 0.5.

In order to better compare of the results, the relationship of the non-coaxiality degree with the major principal stress direction α at the 1^{st} and 25^{th} cycle are presented in Figure 6-16 (a) and (b) respectively. It can be seen from Figure 6-16 (a) that the b-value seems to have some effects on the degree of non-coaxiality in the first cycle. Although the difference between the curves is not significant, the value of β tends to decrease with the increase in b-value. However, with the increasing number of cycles, in the 25^{th} cycle as shown in Figure 6-16 (b) the effects of b on the non-coaxiality degree are not so apparent and the relationship of β with α seems almost similar for the test with different values of b.

Figure 6-17 compares the measured strain increments superimposed on the stress path on the X-Y stress space at number of cycles N_C = 1 and 25 under three values of b. At both N_C = 1 and 25, the amount of the strain increments is increased with the increase in b-value. However, at both N_C = 1 and 25, the variation trend of strain increment direction in different sections of the circular stress path is similar for tests under different b-values.

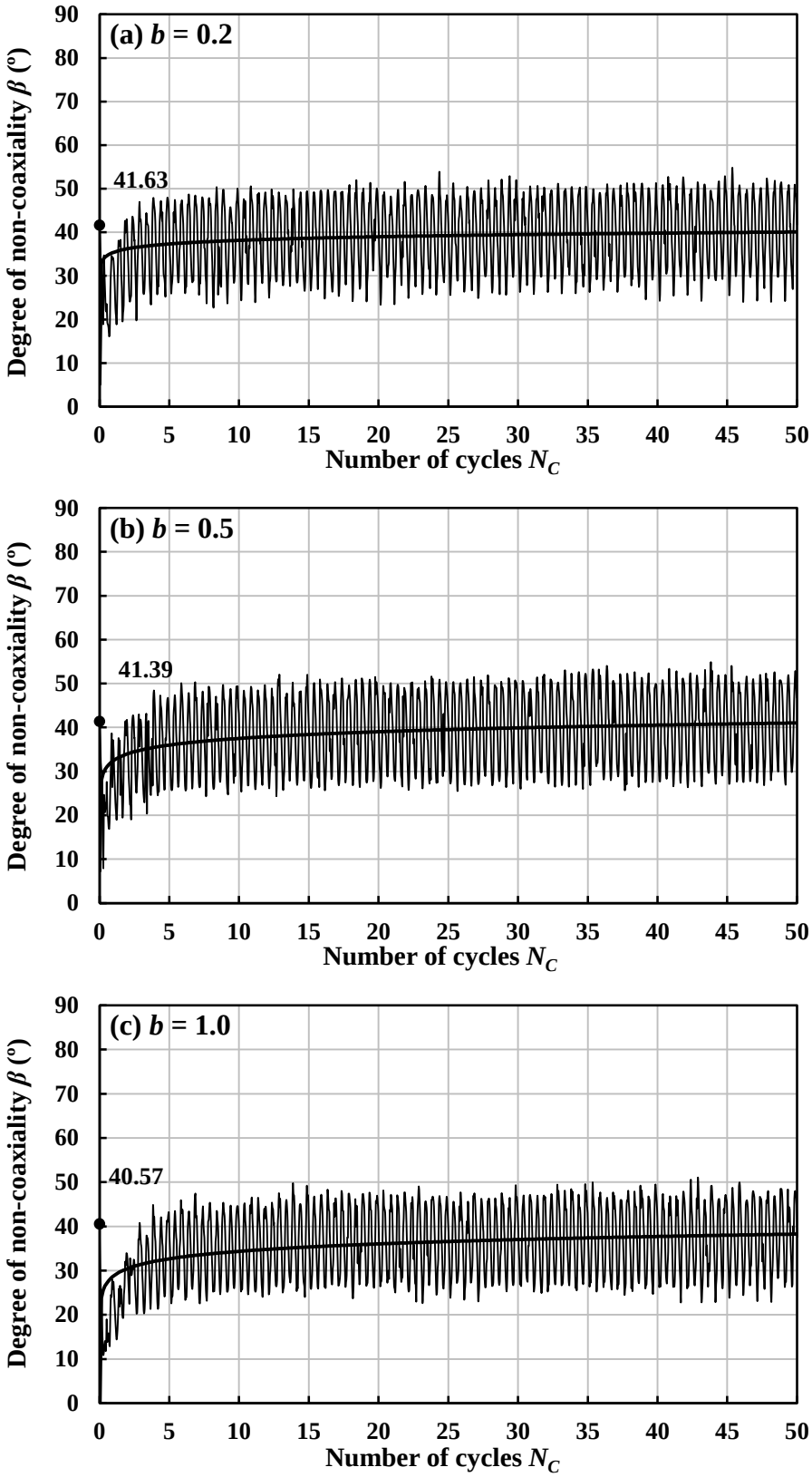

Figure 6-15: Degree of non-coaxiality against number of cycles for rotational shear test with: (a) b = 0.2; (b) b = 0.5 and (c) b = 1.0.

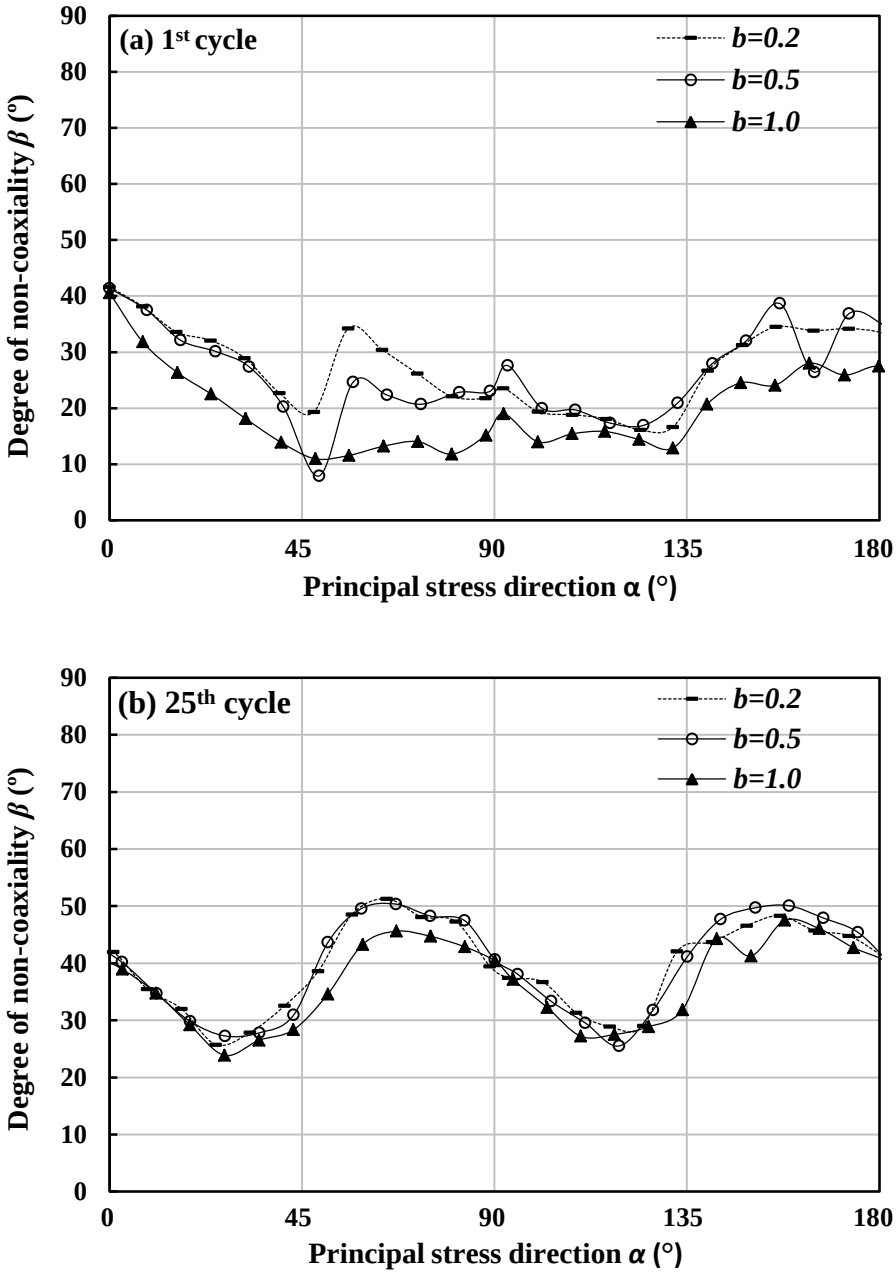

Figure 6-16: Degree of non-coaxiality at N_C = 1 and N_C = 25 for rotational shear test in: (a) 1st cycle; (b) 25th cycle.

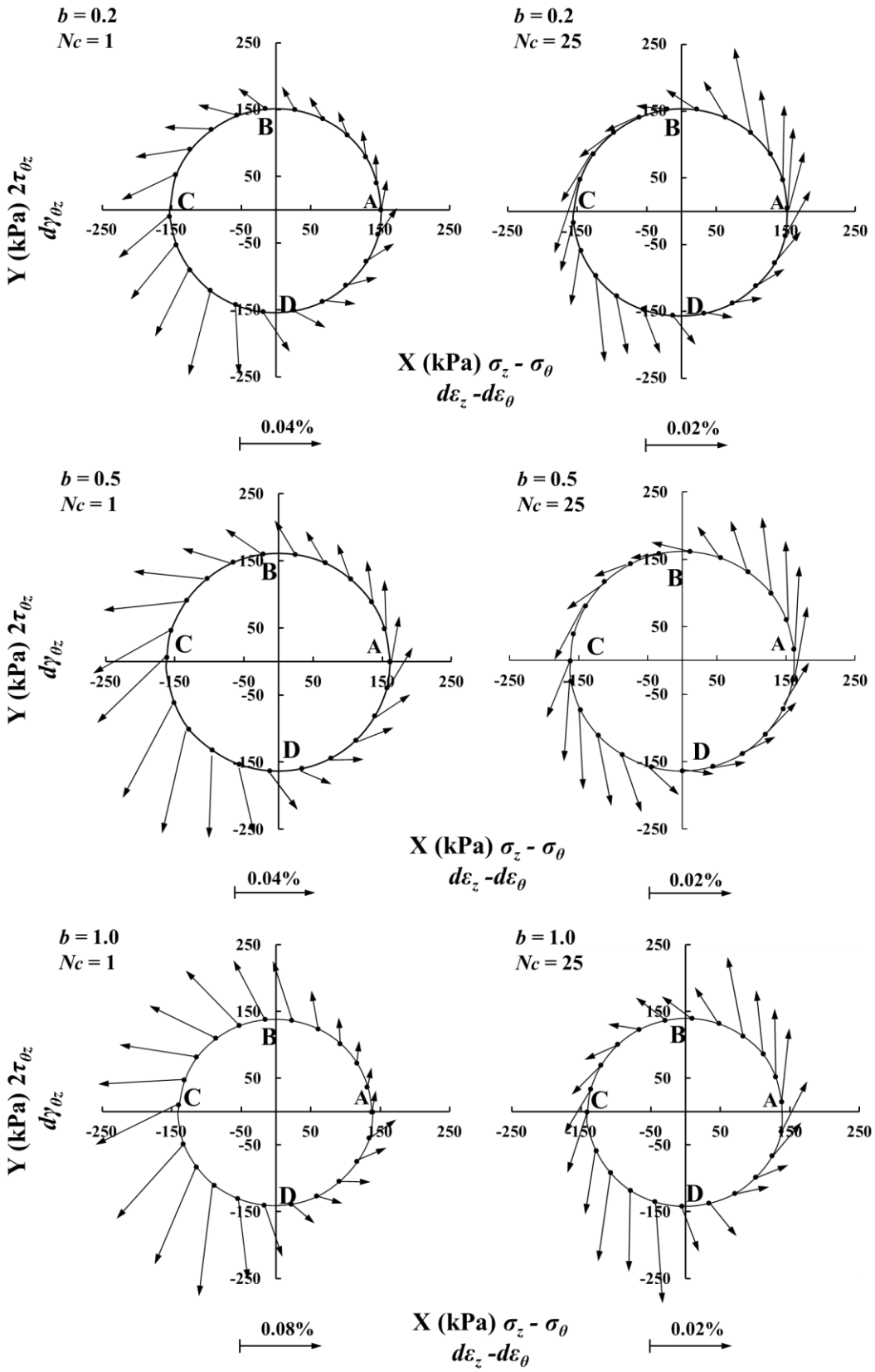

Figure 6-17: Stress paths and strain increments in rotational shear tests at N_C = 1 and N_C = 25 for rotational shear test with: (a) b = 0.2; (b) b = 0.5 and (c) b = 1.0.

6.5 Summary

This chapter consists of the presentation and analysis of the influence of intermediate principal stress on the behaviour of dense Leighton Buzzard sands with cross-anisotropic fabric. The investigation was based on the experimental results attained from testing program III, in which a series of monotonic and rotational shear tests have been performed on dense Leighton Buzzard sand with three cases of *b*-values (*b* = 0.2, 0.5 and 1.0).

As has been presented, the results obtained from the monotonic shear tests clearly show that not only the major principal stress direction α but also the intermediate principal stress parameter *b*, has significant effects on the stress-strain and volume change behaviour of cross-anisotropic sands. In general, at constant α-values, the stiffness and shear strength of sands reduces and the volumetric compressibility increases with increasing values of *b*. The soil exhibits its highest strength at $b = 0.2$ and $\alpha = 0^o$ and the lowest at $b = 1.0$ and $\alpha = 75^o$. The strength parameter in the form of the peak friction angle was also depended strongly on principal stress direction and the value of *b*. The peak friction angle was the highest ($\varphi_p = 48^o$) for $b = 0.5$ and $\alpha = 0^o$, whereas the lowest friction angle ($\varphi_p = 31^o$) was noted under the condition with $b = 1.0$ and $\alpha = 75^o$. The influence of the *b*-value on the non-coaxial behaviour of dense Leighton Buzzard sands under monotonic shearing was clearly manifested in the test result. In general, the lower the *b*-value is the higher the degree of non-coaxiality is induced.

Apparent shear band was developed in the tests with different *b*-values. As the *b*-value increased, shear bands developed quicker and were more pronounced. Under *b*

= 0.2 and 0.5 it was found that the inclinations of the shear bands at different loading directions followed well with theoretical predictions. However, in the case with b = 1.0, shear band inclinations were developed in the non-typical r-θ plane in the compression test when $\alpha \leq 45^{o}$ or the combination of r-z and r-θ planes in the extension test when $\alpha \geq 45^{o}$.

It was suggested by the results of the rotational shear test that the parameter b was also not a negligible factor for the sand deformation during rotational shear, but had significant impact. The amount of the accumulated volumetric strain increases at the same number of cycles with the increase in b under otherwise identical conditions. Meanwhile, although the size of the strain trajectories in the deviatoric strain space in the first few cycles tended to be larger for test under higher b-values, the final shape of the trajectories are almost the same size and their long axis are almost coincide with each other. Furthermore, the effects of b on the non-coaxiality appeared to be less pronounced in rotational shear with the increase in rotation cycles.

Chapter 7 Conclusions and Recommendations

7.1 Summary

Soils are described as continua at scales which are large in comparison with the particle size. It is desirable to model the soil as a continuum at the scale of typical geotechnical applications because the vehicle for their use is almost invariably a continuum numerical analysis program. However, this continuum response is a consequence of the particulate nature of the material: the overall or averaged behaviour is fundamentally determined by how discrete particles are arranged in space, the fabric, and by the nature of interactions between individual particles. A soil can be inherently anisotropic in its fabric, but such anisotropy can also evolve when the soil is subjected to external loading perturbation. Therefore, in order to understand the mechanical behaviour of real-life soils and geotechnical systems it is central to understand the effects of their fabric (inherent or induced).

Rotation of principal axes of stress or strain occurs in most ground engineering problems under a large type of loading. If soils were isotropic, rotation of principal axes of stress or strain would not affect their response. However, knowing the anisotropic nature of strength and deformation characteristics of soils, the multiaxial loading effects cannot be ignored. Available test apparatus for investigating the stress-strain behaviour of soils are limited in the number of degree of freedom that they can explore while maintaining homogeneity of the sample that is being tested. The hollow cylinder apparatus (HCA) allows not only independent control of the magnitude of the three principal stresses but also the rotation of the major-minor principal stress axes.

As a result, the HCA offers an opportunity conducting fundamental research into the effect of principal stress rotation under a reasonably generalized stress state.

Based on this context, this thesis presents a comprehensive experimental investigation of soil anisotropy using hollow cylinder apparatus. It offers a wide range of experimental data and evidence of some peculiar aspects of soil behaviour under multiaxial/complex loading conditions taking into account the effects of the inherent and induced anisotropy, density and particle shape, combined influence of the rotation of principal axes as well as the intermediate principal stress. The experimental data on natural sand is particularly important for the development and refinement of advanced constitutive models, while the tests on glass ballotini will have an impact on specific numerical simulations at the particle-scale level based on discrete element modelling (DEM). According to the experimental evidences presented in this thesis, the main findings and conclusions of this study are summarized and listed in bullet-point form in the following three subsections.

7.1.1 Drained behaviour of granular soil in monotonic shear

- The mechanical response of granular soils to monotonic shear is strongly dependent on the inclination of the major principal stress relative to the deposition direction. As the loading direction deviates from the deposition direction, the volumetric compressibility increases. A decrease in stiffness and strength of sands was observed from $\alpha = 0^{o}$ to $\alpha = 60^{o}$ followed by a moderate increase from $\alpha = 60^{o}$ to $\alpha = 90^{o}$.

- Non-coincidence of principal directions of stress and strain increment was observed in all the tests other than in the tests with the direction of major

principal stress coincides with or perpendicular to the deposition direction. The largest deviations between the major directions of stress and strain increment was presented in the tests with α = 30º. The degree of non-coaxiality gradually reduces with increasing stress ratios and specimens were nearly coaxial when close to failure.

- Shear banding process was initiated near the peak stress and was developed through the residual stress states. The inclinations of the shear bands at different loading directions can be predicted reasonably well by taking account of the relative direction of the mobilized planes (Coulomb's theory) to the bedding plane.

- For a given loading direction, rounder particle shape and lower relative density in an assembly of granular materials tend to produce softer response, severer initial contraction and lower shear strength in monotonic shear. Shear band is more likely to develop in an assembly of angular particles than in an assembly of rounder particles. However, the effects of the particle shape and relative density on the non-coaxial behaviour of granular materials under monotonic shear were found to be less significant.

- The sand samples experienced preshearing history to the peak were found to be less stiff and contracted more in the subsequent responses. For a given loading direction, the peak shear strength is relatively unaffected by preshearing to the peak stress. However, the preshearing history does have a significant effect on the non-coaxiality of sand specimens. The deviation between the major directions of stress and strain increment at α = 15º, 30º, 60º and 75º was greatly enlarged by pre-shearing.

7.1.2 Drained behaviour of granular soil in rotational shear

- A significant plastic deformation was induced during rotational shear despite the magnitudes of principal stresses remained constant. Most of strains were generated during the first 20 cycles and specimens were gradually stabilized afterwards in succeeding cycles. The magnitude of generated strains increased significantly with the increase in the stress ratio and decrease in the material density. The shear resistance of the sand specimen seemed to be weakened by the continuous rotation of the principal stress axes.

- The volumetric strain induced by cyclic rotation of principal stress axes was mainly contractive. Most of the contractive volumetric strain occurred during the first 20 cycles and its accumulation rate tended to decrease as the number of cycles increases. The accumulated volumetric strain showed an increasing trend with the increase in the stress ratio. Samples with lower relative density and rounder particle shape were found to contract more during rotational shear.

- Irrespective of the stress level, material density and particle shape, the shear stress–strain relationship of all the samples showed hysteretic and plastic characteristics. The hysteretic loop was open in the first cycle and then tended to be closed and became more accordant with the increasing number of cycles.

- The evolutions of the strain trajectory on the deviatoric strain space appeared as spirals, changing into ellipses after a large number of cycles. At the last cycle, with the increase in the stress ratio, the elliptical strain trajectories were gradually enlarged. The long axis of these ellipses made an angle of about 86^{o} with horizontal direction. The shape of the elliptical strain trajectory in the

deviatoric strain space for Glass Ballotini was more circular than that of the Leighton Buzzard sand.

- The mechanical behaviour of sand under rotational shear was generally non-coaxial, the variation trend of the non-coaxiality degree showed an obvious periodicity during the tests. Lower degrees of non-coaxiality were observed in the first few cycles. When the rotational shear continues, the strain increment direction became closer to the stress increment direction and higher degrees of non-coaxiality were observed. The variation of the non-coaxiality degree appeared to be stabilized after approximately 20 cycles of rotational shear.

- The stress ratio has a significant effect on the non-coaxiality of sand under rotational shear. The larger the stress ratio, the lower degree of non-coaxiality between the directions of the strain increment and stress was induced. However, the effects of the particle shape and material density on the non-coaxial behaviour of granular materials under rotational shear were found to be less significant.

7.1.3 Influence of intermediate principal stress on soil response

- Both the major principal stress direction α and the intermediate principal stress parameter b, has significant effects on the stress-strain and volume change behaviour of anisotropic sands under monotonic shear. In general, at constant α-values, the stiffness and shear strength of sands reduces and the volumetric compressibility increases with increasing values of b. The soil exhibits its highest strength at $b = 0.2$ and $\alpha = 0^{o}$ and the lowest at $b = 1.0$ and $\alpha = 75^{o}$.

- The strength parameter in the form of the peak friction angle (φ_p) also depended

strongly on the value of α and b. The peak friction angle is the highest for b = 0.5 and α = 0º, whereas the lowest friction angle is noted under the condition with b = 1.0 and α = 75º. The influence of the b-value on the non-coaxial behaviour of dense Leighton Buzzard sands under monotonic shear was evident: the lower the b-value is the higher the degree of non-coaxiality is induced.

- Apparent shear band was developed in the monotonic shear tests with different b-values. As the value of b increased, shear bands developed quicker and were more pronounced. Under b = 0.2 and 0.5, shear band inclinations were developed in the z-θ plane and the inclinations of the shear bands at different loading directions can be predicted well by taking account of the relative direction of the mobilized planes (Coulomb's theory) to the bedding plane. However, in the case with b = 1.0, shear band inclinations were seemed to be developed in the non-typical r-θ plane or the combination of r-z and r-θ planes, due to possible effects of strength anisotropy.

- The parameter b was also not a negligible factor for the sand deformation during rotational shear, but had significant impact. The amount of the accumulated volumetric strain increases at the same number of cycles with the increase in b-value under otherwise identical conditions. Meanwhile, although the size of the strain trajectories in the deviatoric strain space in the first few cycles tended to be larger for test under higher b-values, the final shape of the trajectories are almost the same size and their long axis are coincide with each other. Moreover, the effects of b on the non-coaxiality of dense Leighton Buzzard sand appeared to be less pronounced in rotational shear with the increase in rotation cycles.

7.2 Recommendations for Future Work

Based on the findings of this study the main recommendations for future work are given as follows:

- This study focuses mainly on the anisotropic behaviour of fully saturated Leighton Buzzard sand and much experimental data has also been published on the cross-anisotropy of saturated sand samples. However, less data is published on clays and undisturbed samples as well as partially saturated soils. There still remains a need to establish the independent effects of α and b values on the behaviour of a wider range of sedimentary soils with various degree of saturation.

- The test results clearly indicated that the preloading history to the peak stress has significant effects on the subsequent mechanical behaviour of anisotropic sands. However, the current tests were only carried out with preloading history in the deposition direction up to the peak stress. Experimental tests involving preshearing the specimen along different loading directions to various stress levels are recommended, in order to systematically investigating the influence of induced anisotropy.

- Loading paths involving not only the rotation of principal stress axes but also to the variation of the deviatoric stress are frequently encountered in engineering practice. Examples include pavement and railway foundations under traffic loading. Therefore, in order to get profound understanding of soil deformation under such complex stress regimes, laboratory combined loading test with the variation of both α and q is very much needed.

- In order to get in depth understanding of the anisotropic behaviour of granular

soils, the relationship between the macro and microscale responses of granular soils should be established. However, due to the limitation of the physical experiments, detailed data on particle-scale information cannot be acquired in the laboratory. To overcome this difficulty, numerical modelling using Distinct Element Method (DEM) provides an easy access to micro mechanical response of particulate assemblies. Therefore, a parallel study includes both experimental and numerical investigation is highly recommended in order to developing fundamental insight into the anisotropic behaviour of granular soils under generalized stress conditions.

References

Albert, C., Zdravkovic, and Jardine, R.J., (2003), 'Behaviour of Bothkennar clay under rotation of principal stresses'. Int. Workshop on Geotechnics of Soft Soils-Theory and Practice. Vermeer, Schweiger, Karstunen and Cundny , eds. VGE, pp.1-6.

Arthur, J. R. F., Bekenstein, S., Germaine, J. T., and Ladd, C. C., (1981), 'Stress path tests with controlled rotation of principal stress direction', Laboratory Shear Strength of Soil, American Society for Testing and Materials STP 740, pp. 516-540.

Arthur, R. F., and Menzies, B.K., (1972), 'Inherent anisotropy in sand', Géotechnique, Vol. 22, No. 1, pp. 115-131.

Arthur, R. F., and Phillips, A.B., (1975), 'Homogeneous and layered sand in triaxial compression', Géotechnique, Vol. 25, No.4, pp. 799-815.

Arthur, R. F., Chua K.S., Dunstan T., (1977), 'Induced anisotropy in sand', Geotechnique, Vol. 27, No.1, pp.13-30.

Arthur, R. F., Chua, K.S., Dunstan, T. and Rodriguez del Camino, J.I., (1980), 'Principal stress rotation: a missing parameter', Journal of the Geotechnical Engineering Division, ASCE, GT4, pp. 419-433.

Baldi, G., and Nova, R., (1984), 'Membrane penetration effects in triaxial testing. Journal of Geotechnical Engineering', ASCE, Vol. 110, No.3, 403-420.

Bishop, A. W., (1966), 'The strength of soils as engineering materials', 6th Rankine Lecture. Geotechnique, Vol. 16, No.2, pp. 91-128.

Bjerrum, L. and Kummeneje, O., (1961), 'Shearing resistance of sand samples with circular and rectangular cross sections', Norwegian Geotechnical Institute Publication, Vol. 44, No. 1.

British Standards, (1990), 'BS 1377-4: Compaction-Related Tests. Determination of maximum and minimum dry densities for granular material'' B.S.I, London,.

Broms, B. B., and Casbarian, A. O., (1965), 'Effects of rotation of the principal stress axes and of the intermediate stress on shear strength', Proc., 6th Int. Conf. Soil Mechanics, Vol. 1, pp. 179–183.

Cai, Y.Y., (2010), ‘An experimental study of non-coaxial soil behaviour using hollow cylinder testing’ PhD thesis submitted to the department of civil engineering, the University of Nottingham.

Cai, Y.Y., Yu, H. S., Wanatowski, D., and Li, X. (2012), ‘Non-coaxial behavior of sand under various stress paths’. Journal of Geotechnical and Geoenvironmental Engineering.

Cambou, B., Dubujet, P., Emeriault, F. and Sidoroff, F., (1995), ‘Homogenization for granular materials’, Eur. J. Mech. A, Solids, Vol. 14, No. 2, pp. 225–276.

Casagrande, A. and Carrillo, N., (1944), ‘Shear Failure on Anisotropic Materials’, Proc. Boston. Soc. of Civil Eng., Vol. 31, pp. 74-87.

Cornforth, D. H., (1964), ‘Some experiments on the influence of strain conditions on the strength of sand’, Geotechnique, Vol. 14, No. 2, pp. 143–167.

Cundall, P A, Drescher, A and Strack, O D L., (1982), ‘Numerical experiments on granular assemblies: measures andobservations’, Deformation and Failure of Granular Materials, Balkema, 355-370.

Cundall, P. A., and Strack, O. D. L., (1979), ‘A Discrete Numerical Model for Granular Assemblies’, Geotechnique, Vol. 29, pp. 47-65.

Darwin, G. H., (1918) ‘On the horizontal thrust of a mass of sand’, Minut. Proc. Instn Civ. Engrs, Vol. 71, pp. 350-378.

Desai, C. S., Janardahanam, R., and Sture, S., (1982), ‘High capacity multiaxial testing apparatus’, Geotechnical Testing J., GTJODJ, 5(1/2), pp. 26-33.

Donald, M.E., (1985), ‘stress-strain-strength behaviour of very soft soil sediment’ PhD thesis submitted to the Department of Civil Engineering, the University of Oxford.

Drescher, A., (1976), ‘An experimental investigation of flow rules for granular materials using optically sensitive glass particles’, Géotechnique, Vol. 26, pp. 591-601.

Drescher, A., and de Josselin de Jong. G., (1972), ‘Photoelastic verification of a mechanical model for the flow of a granular material’, J. Mech. Phys. Solids, Vol. 20, pp. 337-351.

Duncan, J.M. and Seed, H.B., (1965), ‘Errors in strength tests and recommended corrections’, Report, University of California, Berkeley.

Ergun, M. U., (1981), 'Evaluation of three-dimensional shear testing', Proc. of 10th International Conference on Soil Mechanics and Foundation Eng., Stockholm, pp. 593- 596.

Gens, A., Potts, D.M., (1984), 'Formulation of quasi-axisymmetric boundary value problems for finite element analysis', Engineering Computations, Vol.1, pp. 144-150.

Gutierrez, M., and Ishihara, K., (2000), 'Non-coaxiality and energy dissipation in granular materials', Soils and Foundations, Vol. 40, No.2, pp. 49-59.

Gutierrez, M., Ishihara, K. and Towhata, I. (1991), 'Flow theory for sand during rotation of principal stress direction', Soils and Foundations, Vol. 31, No. 4, pp. 121-132, .

Habib, P., (1953), 'Influence de la variation de la contrainte principale moyenne sur la résistance au cisaillement des sols', Proc. Third ICSMFE 1, pp. 131–136.

Hambly, E. C. and Roscoe, K. H., (1969), 'Observations and predictions of stresses and strains during plane strain of wet clays', Proc. 7th Int. Conf. Soil Mech., pp. 173-181.

Hight, D.W., Gens, A., Symes, M.J., (1983), 'The development of a new hollow cylinder apparatus for investigating the effects of principal stress rotation in soils', Geotechnique, Vol. 33, No. 4, pp. 355-383.

Hosseininia, E. S., (2012) 'Discrete element modelling of inherently anisotropic granular assemblies with polygonal particles', Particuology, Vol. 10, Issue 5, Pages 542-552.

Ibraim, E., Lanier, J., Muir Wood, D. and Viggiani, G. (2010), 'Strain path controlled shear tests on an analogue granular material', Géotechnique, Vol. 60, No. 7, pp. 545-559.

Ishihara, K., (1993) 'Liquefaction and flow failure during earthquakes', Géotechnique, Vol. 43, No. 3, pp. 351–415.

Ishihara, K., and Li S.-I., (1972), 'Liquefaction of Saturated Sand in Triaxial Torsion Shear Test', Soils and Foundations, Vol.12, No.3, pp. 19-39.

Ishihara, K., and Towhata, I., (1983), 'Sand response to cyclic rotation of principal stress directions as induced by wave loads', Soils and Foundations, Vol. 23, No. 4, pp. 11-26.

Joer H.A., Lanier J., Fahey M., (1998), 'Deformation of granular materials due to rotation of principal axes', Geotechnique, Vol. 48, No.5, pp. 605–619.

Kallstenius, T. and Bergau, W., (1961), 'Research on the texture of granular masses', Proc. 5th Int. Conf. on Soil Mechanics and Foundation Engineering, Vol. 1, pp. 165-170.

Kirkgard, M. M., and Lade, P. V. , (1993), 'Anisotropic three-dimensional behavior of a normally consolidated clay', Can. Geotech. J., 30, pp. 848–858.

Ko, H.-Y., and Scott, R. F., (1968), 'Deformation of Sand at Failure', Journal of the Soil Mechanics and Foundations Division, ASCE, Vol. 94, No. SM4, Proc. Paper 6028, pp. 883-898.

Kramer, S. L., Sivaneswaran, N. and David, R. O., (1990), 'Analysis of membrane penetration in triaxial test', Journal of Geotechnical Engineering, ASCE, 1990, Vol. 116, pp. 773-789.

Kramer, S.L. and Sivaneswaran, N., (1989), 'A stress path dependent correction for membrane. penetration', Journal of Geotechnical Engineering, ASCE, Vol. 115, No. 12, pp.1787-1804.

Kurukulasuriya, L.C., Oda, M. and Kazama, H., (1999), 'Anisotropy of undrained shear strength of an over consolidated soil by triaxial and plain strain tests', Soils and Foundations, Vol. 39, No. 1, pp. 21-29.

Kuwano, R., (1999), 'The stiffness and yielding anisotropy of sand', PhD thesis submitted to the Department of Civil Engineering, the University of London.

Lade, P. V. (2006), 'Assessment of test data for selection of 3-D failure criterion for sand', Int. J. Numer. Anal. Methods Geomech., 30 (4), pp. 307–333.

Lade, P. V., Nam, Y., and Hong, W. P., (2009), 'Interpretation of strains in torsion shear tests', Comp. Geotech., 36(1-2), pp. 211-225.

Lade, P.V., Duncan, J.M., (1973), 'Cubical triaxial tests on cohesionless soil', Journal of the Soil Mechanics and Foundation Division, ASCE, 99(SM10), pp. 793-811.

Lade, P.V., Nam, J., and Hong, W.P., (2008), 'Shear banding and cross-anisotropic behaviour observed in laboratory sand tests with stress rotation', Canadian Geotechnical Journal, Vol.45, pp. 74-84.

Li, X. and Yu H.S., (2009), 'Influence of loading direction on the behaviour of anisotropic granular materials', International Journal of Engineering Science 47 (2009), 1284-1296.

Li, X. and Yu H.S., (2010), 'Numerical investigation of granular material behaviour under rotation shear', Geotechnique 60, No.5, pp. 381-394.

Mahmood, Z. and Iwashita, K., (2010), 'Influence of inherent anisotropy on mechanical behavior of granular materials based on DEM simulations', International Journal of Numerical and Analytical Methods in Geomechanics, Vol. 34, No. 8, pp. 795–819.

Matsuoka, H., and Ishizaki, H., (1981), 'Deformation and strength of anisotropic soil', Proc., 10th Int. Conf. on Soil Mechanics and Foundation Engineering, Balkema, Rotterdam, the Netherlands, Vol. 1, pp. 699–702.

Matsuoka, H., and Nakai, T., (1974), 'Stress-deformation and strength characteristics of soil under different principal stresses', Proc., Japan Society of Civil Engineers (JSCE), Japan Society of Civil Engineers, Vol. 232, pp. 59-70.

Matsushima, T. and Konagai, K., (2001), 'Grain-shape effect on peak strength of granular materials', Computer Methods and Advances in Geomechanics, Proc. 10ACMAG, Vol. 1, pp. 361-366.

Menkiti, C.O., (1995), 'Behaviour of clay and clayey-sand, with particular reference to principal stress rotation', Msc. Dissertation, Imperial College of Science, Technology and Medicine, University of London.

Miura, S. and Toki S., (1984), 'Anisotropy in mechanical properties and its simulation of sands sampled from natural deposits', Soils and Foundations, Vol. 24. No. 3, pp. 69-84.

Miura, S. and Toki S., (1986), 'Deformations prediction for anisotropic sand during the rotation of principal stress axes', Soils and Foundations, Vol. 26, No.3, pp. 42-56.

Miura, S., and Kawamura, S., (1996), 'A procedure minimizing membrane penetration effects in undrained triaxial test', Soils and Foundations, Vol. 36, No.4, pp. 119-126.

Miura, S., and Toki, S., (1982), 'A sample preparation method and its effect on static and cyclic deformation-strength properties of sand', Soils and Foundation, Vol. 22, No. 1, pp. 61–77.

Molenkamp, F., and Luger, H.J., (1981), 'Modeling and minimization of membrane penetration effects in tests on granular soils', Geotechnique, Vol. 31, No. 4, pp. 471-486.

Mould, J. C., (1979), 'Multiaxial testing and analytical constitutive characterization of granular materials', Master Thesis, Virginia Polytechnical Institute and State University, pp. 50-82.

Nabil, S.E., (1976), 'Shear strength of a cohesionless soil under plane strain and triaxial conditions', Open Access Dissertations and Theses. Paper 484.

Nakata, Y., Hyodo, M., Murata, H., and Yasufuku, N., (1998), 'Flow deformation of sands subjected to principal stress rotation', Soils and Foundations, Vol. 38, No.3, pp. 115-128.

Nakata, Y., Hyodo, M., Murata, H., Itakura, S. and Yamada, Y., (1997), 'Flow deformation of sands subjected to principal stress rotation', Memoirs of the Faculty of Engineering, Yamaguchi University, Vol. 48, No. 1, pp. 57-64.

Naughton, P.J., and O'Kelly, B.C., (2003), 'The anisotropy of Leighton Buzzard Sand under general stress conditions', Proceedings Third International Symposium on Deformation Characteristics of Geomaterials, Vol. 1, pp. 285–291.

Naughton, P. J. and O'Kelly B. C., (2007), 'Stress non-uniformity in a hollow cylinder torsional sand specimen', Geomechanics and Geoengineering, Vol. 2, No. 2, pp. 117-122.

Newland, P. L. and Allely, B. H., (1959), 'Volume change during undrained traxial tests on saturated dilatant granular materials', Géotechnique, Vol. 9, No. 4, pp. 174-182.

Ochiai, H., and Lade, P. V., (1983), 'Three-dimensional behavior of sand with anisotropic fabric', J. Geotech. Eng., Vol. 109, No. 10, pp. 1313-1328.

Oda, M. and Iwashita K., (1999), 'Mechanics of granular materials: an introduction', Balkema, Rotterdam/Brookfield.

Oda, M., (1972a), 'Initial fabrics and their relations to the mechanical properties of granular materials', Soils and Foundations, Vol. 12, No.1, pp. 17-36.

Oda, M., (1972b), 'The mechanics of fabric changes during compressional deformation of sand', Soils and Foundations, Vol. 12, No.2, pp. 1-18.

Oda, M., (1981), 'Anisotropic strength of cohesionless sands', Journal of the Geot. Eng. Div., ASCE, Vol. 107, No. GT9, pp. 1219-1231.

Oda, M., Isao K. and Toshio H., (1978), 'Experimental study of anisotropic shear strength of sand by plane strain test', Soils and Foundations, Vol. 18, No. 1, pp. 25-38.

Oda, M., Nemat-Masser S. and Konishi J., (1985), 'Stress-induced anisotropy in granular masses', Soils and Foundations, Vol. 25, No. 3, pp. 85-97.

Oda, M. and Konishi J., (1974), 'Microscopic deformation mechanism of granular material in simple shear'. Soils and Foundations, Vol.14, No. 4, pp. 25–38.

Ohara, S., and Yamamoto, T., (1991), 'Practical method for obtaining correction factor of liquefaction resistance for membrane penetration', Soils and Foundation, Vol. 31, No.2, pp.188-196.

Parkin, A. K., Gerrard, C. M., and Willoughby, D. R., (1968), 'Deformation of sand in hydrostatic compression. Soil mechanics. Found. Div. 94, No. SM 1, pp. 336-340.

Phillips, A. B. and May, P. H., (1967), 'A form of anisotropy in granular media.' Special Task Report , Dept. of Civil and Municipal Engineering, Univ. College, London.

Porovic, E., (1995), 'Investigation of soil behaviour using a resonant column torsional shear hollow cylinder apparatus', PhD thesis submitted to the Department of Civil Engineering, University of London.

Pradhan, B.S., Tatsuoka, F. and Horii, N., (1988), 'Simple shear testing on sand in a torsional shear apparatus', Soils and Foundations, Vol. 28, No. 2, pp. 95-112.

Reinaldo, R., (2003), 'The anisotropic stress-strain-strength behaviour of brittle sediments', PhD thesis submitted to the Department of Civil Engineering, the University of London.

Rodriguez, N.M., (2012), 'Experimental Study of 3D failure surface for cross-anisotropic sand deposits during stress rotation', PhD thesis submitted to the Department of Civil Engineering, The Catholic University of America.

Roscoe, K. H., Bassett, R. H., and Cole, E. R. L., (1967), 'Principal axes observed duringsimple shear of a sand', Proc. 4th Eur. Conf. Soil Mech. Found. Eng., Oslo, pp. 231-237.

Rothenburg, L. and Bathurst, R. J., (1989), 'Analytical study of induced anisotropy in idealized granular materials', Géotechnique, Vol. 49, pp. 601-614.

Rudnicki, J. W. and Rice, J. R., (1975) 'Conditions for the localisation of deformation in pressure-sensitive dilatant materials', Journal of Mechanics and Physics of Solids 1975, Vol. 23, pp. 371–394.

Saada, A.S. and Townsend, F.C., (1981), 'State of the art: laboratory strength testing of soils', ASTM Spec. Tech. Publ., No. 740, pp. 7-77.

Saada, A.S., (1988), 'State of the art: Hollow cylinder torsional devices: their advantages and limitations', Advance triaxial testing of soil and rock. ASTM STP 977, American Society for Testing and Materials, Philadelphia, pp.766-795.

Sadrekarimi, A. and Olson, S.M.., (2012), 'Effect of sample preparation method on critical state behavior of sands', Geotechnical Testing Journal, ASTM, Vol. 35, No. 4.

Sayao, A.S.F.J., (1989), 'Behaviour of sand under generalised stress paths in the hollow cylinder torsional device', PhD Thesis, University of British Columbia, Vancouver, Canada.

Sayao, A.S.F.J., and Vaid, Y.P., (1991), 'A critical assessment of stress nonuniformities in hollow cylinder test specimens', Soils and Foundations, Vol. 31, No. 1, pp. 60-72.

Sayao, A.S.F.J., and Vaid, Y.P., (1996), 'Influence of intermediate principal stress on the deformation response of sand', Canadian Geotechnical Journal, Vol.33, pp. 822-828.

Sayao, A.S.F.J., and Vaid, Y.P., (1997), 'Effect of intermediate principal stress on the deformation response of sand', Geomechanics Abstracts, Vol. 1997, No. 2, p. 70.

Sazzad, M.M. and Suzuki, K., (2010), 'Micromechanical behavior of granular materials with inherent anisotropy under cyclic loading using 2D DEM', Granular Matter, Vol. 12, No. 6, pp. 597-605.

Serra, J. P. B., and Patrick Hooker, (2003), 'A New Computer Controlled Hollow Cylinder Torsional Shear Apparatus', 13th European Conference on Soil Mechanics and Geotechnical Engineering.

Shibuya, S. (1985), 'Undrained behaviour of granular materials under principal stress rotation', PhD. Thesis, Imperial College of Science, Technology and Medicine, University of London.

Sivathayalan, S. & Vaid, Y.P., (1998), 'Truly undrained response of granular soils with no membrane penetration effects', Canadian Geotechnical Journal, Vol. 35, pp. 730-739.

Surachat, S., (1977), 'Stress-strain-strength anisotropy of varved clays', Sc.D. thesis submitted to the Department of Civil Engineering, Massachusetts Institute of Technology.

Symes, M. J., (1983), 'Rotation of principal stresses in sand', PhD. Thesis, Imperial College of Science, Technology and Medicine, University of London.

Symes, M. J., Gens, A. and Hight, D.W., (1984), 'Undrained Anisotropy and Principal Stress Rotation in Saturated Sand', Géotechnique, Vol. 34, No. 1, pp. 11-27.

Symes, M. J., Gens, A., and Hight, D. W., (1988), 'Drained principal stress rotation in saturated sand', Géotechnique, Vol. 38., No. 1, pp. 59-81.

Symes, M.J., Hight, D.W and Gens, A., (1982), 'Investigation anisotropy and the effects of principal stress rotation and of the intermediate principal stress using a hollow cylinder apparatus', IUTAM Conference on deformation and failure of granular materials. Delft, pp. 441-449.

Tatsuoka, F., (1980), 'Stress-strain behavior of an idealized anisotropic granular material', Soils and Foundations, Vol. 20, No. 3, pp.75-90.

Tokimatsu, K. and Nakamura, K., (1986), 'A liquefaction test without membrane penetration effects', Soils and Foundations, Vol. 26, No. 4, pp. 127-138.

Tong, Z. X., Zhang J-M, Yu Y. L., Zhang G., (2010), 'Drained deformation behavior of anisotropic sands during cyclic rotation of stress principal axes', J. Geotchanical and Geoenviromental Engineering. ASCE. Vol. 136, No.11.

Towhata, I., and Ishihara, K., (1985), 'Undrained strength of sand undergoing cyclic rotation of principal stress axes', Soils Found., Vol. 25, No.2, pp: 135–147.

Uthayakumar, M., and Vaid, Y. P., (1998), 'Static liquefaction of sands under multiaxial loading', Can. Geotech. J., Vol. 35, No. 2, pp. 273-283.

Vaid, Y. P., Sivathayalan, S., and Stedman, D., (1999), 'Influence of Specimen-Reconstituting Method on the Undrained Response of Sand', Geotech. Test. J., Vol. 22, No. 3, pp. 187-195.

Vaid, Y.P., and Campanella, R.G., (1974), 'Comparison of Triaxial and Plane Strain Behaviour of an Undisturbed Clay', ASCE, Geotech. Eng. Div., Vol. 100, GT3, pp. 207-225.

Vaid, Y.P., Sayao, A.S.F, Hou, E. and Negussey, D., (1990), 'Generalised stress-path dependent behaviour with a new hollow cylinder torsional apparatus', Canadian Geotechnical Journal, Vol. 27, pp. 601-616.

Van Dyck, E.J., (2012), 'Effects of Principal Stress direction and the intermediate principal stress on the stress-strain-strength behavior of a cross-anisotropic fine sand deposit' PhD thesis submitted to the Department of Civil Engineering, The Catholic University of America.

Wang, Q., and Lade, P.V., (2001), 'Shear banding in true triaxial tests and its effect on failure in sand', Journal of Engineering Mechanics, ASCE, Vol. 127, No.8, pp. 754-761.

Wijewickreme, D. and Vaid. Y. P., (1993), 'Behavior of Loose Sand under Simultaneous Increase in Stress Ratio and Principal Stress Rotation', Canadian Geotechnical Journal, Vol. 30, No. 6, pp. 953-964.

Wijewickreme, D., Vald, Y. P., (1991), 'Stress nonuniformities in hollow cylinder torsional specimens', ASTM, Geotechnical Testing Journal, Vol. 14, pp. 349-362.

Wong, R.C.K., (2003), 'Strain-induced anisotropy in fabric and hydraulic parameters of oil sand in triaxial compression', Canadian Geotechnical Journal, Vol.40, No.3, pp. 489-500.

Wong, R.K.S. and Arthur, J.F.R., (1985), 'Induced and inherent anisotropy in sand', Géotechnique, Vol. 35, No. 4, pp. 471-481.

Yamada, Y., and Ishihara, K., (1979), 'Anisotropic deformation characteristics of sand under three dimensional stress conditions', Soils and Foundations, Vol. 19, No. 2, pp. 79–94,.

Yamamuro, J. A. and Wood, F. M., (2004), 'Effect of depositional method on the undrained behavior and microstructure of sand with silt', Soil Dynamic Earthquake Eng., Vol. 24, Nos. 9–10, pp. 751–760.

Yang, D.S., (2013), ' Numerical study of 3D granular material behaviour using DEM', PhD thesis submitted to the department of civil engineering, the University of Nottingham.

Yang, Y. and Yu, H. S., (2006), 'A non-coaxial critical state soil model and its application to simple shear simulations', International Journal for Numerical and Analytical Methods in Geomechanics, Vol. 30, No.13, pp. 1369-1390.

Yang, Z.X., Li X.S., Yang J., (2007), 'Undrained anisotropy and rotational shear in granular soil', Géotechnique 57, No. 4, 371-384.

Yang, Z.X., Li X.S., Yang J., (2008), 'Quantifying and modelling fabric anisotropy of granular soils', Géotechnique 58, No. 4, pp. 337-348.

Yin, J.H., and Kumruzzaman, M., (2008), 'The stress-strain-strength behaviour of a completely decomposed granite soil using a new advanced true triaxial testing system', Proc. of the 12th Int. Conf. of Int. Assoc. Comp. Meth. Adv. Geom. (IACMAG), Goa, India, pp. 1571-1579.

Yu, H. S., Yang, Y., Yuan, X., (2005) 'Application of non-coaxial plasticity models in geotechnical analysis', Proceedings of the16th International Conference on Soil Mechanics and Geotechnical Engineering, Vol. 2, Osaka, pp. 993–996.

Yu, H.S., Yuan, X., (2005), 'The importance of accounting for non-coaxial behavior in modeling soil–structure interaction', Proceedings of the 11th IACMAG, Invited Issue Paper, Vol. 4, pp. 709–718.

Yu, H. S., (2006) 'Plasticity and geotechnics', Springer.

Yu, H. S., and Yuan, X., (2006), 'On a class of non-coaxial plasticity models for granular soils', Proc. Royal Soc. A, 462, pp. 725-748.

Yu, H. S., (2008), 'Non-coaxial theories of plasticity for granular materials', Proc. 12th Int. Conf. of Int. Assoc. Comp. Meth. Adv. Geom. (IACMAG), Goa, India, pp. 361-378.

Zhang, K.Y., Yin Z.Z., Mei G.X., (2003), 'Development of the study on soil anisotropy', Journal of Rock and Soil Mechanics, Vol. 25. No. 9.

Zlatovic, S., and Ishihara, K., (1997), 'Normalized behaviour of very loose non-plastic soils: effects of fabric', Soils and Foundation, Vol. 37, No. 4, pp. 47-56.